IR-07-02

Feasibility of Externally Bonded FRP Reinforcement for Repair of Cracked Prestressed Concrete Girders, I-565, Huntsville, Alabama

Kyle S. Swenson
Robert W. Barnes

June 2007

ACKNOWLEDGEMENTS

DISCLAIMER

The opinions and conclusions expressed or implied in this report are those of the authors. They are not necessarily those of the funding agencies.

EXECUTIVE SUMMARY

After construction of Interstate 565 in Huntsville, Alabama, was completed, bridge inspectors discovered cracks in numerous prestressed concrete bulb-tee bridge girders made continuous for live load. Alabama Department of Transportation (ALDOT) personnel performed several different types of repairs, though none of them were successful in providing a long-term solution to the cracking in the prestressed concrete bulb-tee girders. The research presented in this thesis explores the use of external fiber reinforced polymer (FRP) reinforcement to repair and strengthen the cracked girders.

Current bridge design specifications were used to determine the factored ultimate load effects induced by dead and live loads on the bridge structure. The design shear and moment capacities of the cracked prestressed concrete bridge girders were calculated and compared to the factored ultimate load effects to determine if strength deficiencies exist. The tensile capacity of the longitudinal reinforcement was also calculated and compared to factored ultimate forces determined with a strut-and-tie analysis of the cracked end region of a typical bulb-tee girder. The results of the analytical procedures revealed that the cracks at the continuous ends of the bridge girders have caused multiple strength deficiencies.

Strut-and-tie modeling and a sectional analysis method were used to design an external FRP strengthening system. The external FRP reinforcement was designed such that its use will correct all strength deficiencies that exist in the cracked bulb-tee girders. Anchorage of the external FRP reinforcement was examined analytically. It was recommended that the continuous end of all girders in spans that contain cracked prestressed concrete bulb-tee girders should be strengthened with external FRP reinforcement. The external FRP reinforcement will be wrapped around the bottom flange of the girders and extended toward midspan, beyond the cracking in the end region of the girders.

TABLE OF CONTENTS

LIST OF TABLES

LIST OF FIGURES

CHAPTER 1: INTRODUCTION

1.1 PROJECT BACKGROUND

Construction of the Interstate 565 bridge structures in downtown Huntsville, Alabama, began in January 1988 and was completed in March 1991. The 2.45 miles (3.94 km) of interstate highway was constructed during a five-part project that cost the state of Alabama $91,045,779 (ALDOT 1994d). Both simply supported and continuous bridge structures were constructed. The bridges are composed of either steel or prestressed concrete girders and a cast-in-place reinforced concrete deck slab. For bridges composed of prestressed concrete bulb-tee girders, continuity was often established between adjacent spans to create two-, three-, and four-span continuous structures. A two-span continuous bridge composed of prestressed concrete bulb-tee girders made continuous for live load is shown in Figure 1.1.

During an inspection of the Huntsville I-565 bridge structures conducted in 1992, hairline cracks were found in the continuous ends of prestressed concrete bulb-tee girders. A second inspection of the bridges was conducted in the spring of 1994 and revealed that many of the cracks in the continuous ends of the prestressed concrete bulb-tee girders had propagated and widened. The most severe cracks had widths of 0.25 in. (6.4 mm) and were easily visible from the ground. Bridge inspectors completed a thorough survey of the I-565 bridge structures, documenting and mapping cracks in the prestressed concrete bulb-tee girders and continuity diaphragms.

After the survey of the I-565 bridge structures had been completed, the Alabama Department of Transportation (ALDOT) began to monitor the structures and repair girders affected by the cracking. False supports were installed near bents supporting the cracked end of bulb-tee girders so that a total collapse of the structure would be prevented if girders did fail. The false supports will remain in place until a permanent and reliable repair of the cracked girders has been completed. Epoxy injection was used to seal existing cracks and prevent their growth, though new cracks formed adjacent to those that were epoxy injected. Load tests were performed on spans containing cracked girders to evaluate the performance of the structure and the behavior of the cracked girders. Cracked girders were monitored to determine the effects of wind and thermal loads.

Monitoring of the cracked girders revealed that a large temperature gradient exists between the bridge deck and the prestressed concrete girders. The elevated temperatures on the bridge deck cause the superstructure to deflect upward. Because continuity was

established between spans, the girders are restrained from rotating or deflecting at interior supports. As a result, positive moments form near the interior supports. ALDOT determined that the positive moments induced by the thermal gradient caused the cracks in the prestressed concrete bulb-tee girders. This conclusion was later verified through analytical research performed by Auburn University personnel.

1.2 OBJECTIVES

The primary goal of this research program was to develop and design an external fiber-reinforced polymer (FRP) strengthening system to be used on the cracked prestressed concrete bulb-tee girders. In order to achieve this goal, multiple objectives were completed. The objectives were related to the analysis of the existing structure, evaluation of the strength of the cracked prestressed concrete bulb-tee girders, and the design of external FRP reinforcement.

The following list outlines the major objectives of the research program.

1. Develop envelopes for the factored ultimate moments and shear forces in the cracked prestressed concrete bulb-tee girders.

2. Calculate the design shear and moment capacities of the cracked prestressed concrete bulb-tee girders.

3. Compare the factored ultimate load effects to the design strength of the cracked prestressed concrete bulb-tee girders to determine if strength deficiencies exist.

4. Determine the amount of external FRP reinforcement required to adequately strengthen the affected girders. After strengthening, the ultimate strength limit state should be satisfied for both shear and flexure.

5. Determine a practical longitudinal and transverse configuration for the external FRP reinforcement.

6. Present final design recommendations for the external FRP strengthening system. Discuss the necessity of future experimental and analytical research.

2

1.3 SCOPE

Chapter 2 contains a thorough review of pertinent literature. Four major topics are covered in the literature review:

1. Bridges composed of prestressed concrete girders made continuous

2. Cracking in the transfer region of prestressing tendons in prestressed concrete

   flexural members

3. Shear strengthening of reinforced concrete flexural members

4. Shear strengthening reinforced concrete flexural members with FRP composites

A detailed description of the downtown Huntsville I-565 bridge structures and the cracks in the prestressed concrete bulb-tee girders is presented in Chapter 3. Geometric details of the structure and prestressed concrete bulb-tee girders are discussed and presented in Section 3.1. Constitutive materials are discussed in Section 3.2. Details of the cracking in the continuous ends of the bulb-tee girders are presented in Section 3.3.

In Chapter 4, a description and discussion of all analytical procedures is presented. The elastic structural analysis of the bridge structure is discussed in Section 4.1. Methods used to calculate the shear and moment capacities of the bridge girders are presented in Section 4.2. A description of the strut-and-tie analysis is presented in Section 4.3. The results of the analytical procedures are presented and discussed in Chapters 5 and 6.

The design of the external FRP reinforcement is presented and discussed in Chapter 7. Analytical methods used to design the external FRP reinforcement are presented in Section 7.2. Results of the analytical procedures are presented in Section 7.3. Section 7.4 outlines the analytical and experimental methods used to evaluate the anchorage of the external FRP reinforcement.

The adhesion tests performed on the cracked prestressed concrete bulb-tee girders in Huntsville, AL, are outlined in Appendix A. Test preparation, testing procedure, and test results are all presented. Symbols and other notation used in this document are defined in Appendix B.

Figure 1.1 – Two-span Continuous Bridge Structure in Huntsville, Alabama

CHAPTER 2: LITERATURE REVIEW

A review of literature pertaining to relevant research topics is presented in this chapter. The topics covered include the behavior of prestressed concrete girders made continuous, cracking in the transfer region of prestressed concrete girders, shear strengthening of reinforced concrete (RC) and prestressed concrete flexural members, and shear strengthening of concrete flexural members with fiber reinforced polymer (FRP) composites. The last topic has been covered in more detail because it was the main focus of the research.

2.1 BRIDGES COMPOSED OF PRESTRESSED CONCRETE GIRDERS MADE CONTINUOUS

Many states have used precast prestressed concrete girders in the construction of continuous highway bridges (Freyermuth 1969). The establishment of continuity between adjacent spans results in some major advantages. Midspan deflections are reduced in continuous structures, improving both the riding quality of the bridge and its appearance to motorists. Continuous bridges have fewer joints in the bridge deck, reducing the maintenance required at such locations as well as limiting the amount of

drainage onto the substructure (Freyermuth 1969; Mirmiran et al. 2001). Continuity also provides a degree of redundancy, which may be important for overloads or during extreme events (Mirmiran et al. 2001).

Bridges composed of prestressed concrete girders made continuous also have some significant disadvantages. Their analysis and design are more complex than that for simple span structures. Time-dependent effects such as creep and shrinkage must be carefully considered for continuous structures because they often induce restraint moments at interior supports and cause cracking. Thermal loadings and effects must be carefully considered in continuous structures. The construction sequence of bridges composed of prestressed concrete girders made continuous must also be considered in design. Failure to do so can reduce the degree of continuity achieved and cause serviceability problems over the life of the structure.

The following sections outline two factors affecting the behavior and performance of bridges composed of prestressed concrete girders made continuous: the construction sequence and the design of the continuity diaphragm. The construction sequence affects the times at which dead and live loads are applied to the structure. Design of the continuity diaphragm affects the degree of continuity established and the resulting behavior of the structure. Consideration of these issues is imperative if strength and serviceability problems are to be minimized for this type of bridge.

2.1.1 Construction Sequence

The construction sequence of bridges composed of prestressed concrete girders made continuous plays a vital role in their behavior because it affects the loads applied to the structure and the means by which the structure resists loads. The construction sequence of the structure begins with the fabrication of the prestressed concrete girders and ends with the application of traffic loads to the completed structure. Consideration of the construction sequence at early ages is extremely important, due to the time-dependent behavior exhibited by prestressed concrete girders.

Oesterle et al. (1989) have found that time-dependent effects must be considered in the design and evaluation of bridges composed of prestressed concrete girders made continuous. The time-dependent material properties of structural concrete, namely creep and shrinkage, affect the strength and behavior of concrete structures. Major construction events are also considered to be time-dependent effects because they often cause changes in the way a structure resists loads. Construction events may also result in the application of permanent dead loads, such as the weight of the reinforced concrete deck or the barrier rails. If time-dependent effects are not considered, the actual strength and behavior of the structure may be grossly different from that predicted analytically.

Creep and shrinkage occurring in the prestressed concrete girders routinely result in magnified deflections and losses of prestressing force in simple span structures. In

5

continuous structures, creep and shrinkage can cause increased bending moments and bending stresses. These effects are a result of the restraint moments that develop at continuous supports when continuity is established between adjacent spans. Formation of large restraint moments may cause cracking in the prestressed girder, cracking in the continuity diaphragm, or a reduction of the degree of continuity achieved at the continuous supports.

For prestressed concrete girders that are simply supported, rotation at the girder ends is unrestrained, and creep causes the camber to be magnified. When girder ends are restrained, as they would be in a continuous structure, the member is not able to freely deflect upward and the creep effect induces a positive restraint moment at the continuous supports. In many cases, the positive restraint moment induced at a continuous support results in cracking of the continuity diaphragm and a partial loss of continuity (Oesterle et al. 1989; Mirmiran et al. 2001). In some cases cracking may occur in the girder end as a result of the positive restraint moment. The location of the cracking will depend on the relative bending stiffnesses of the continuity diaphragm and the girders and the reinforcement details at the continuity connection.

In order to minimize the effects of creep in the prestressed girder, Mirmiran et al. (2001) and Oesterle et al. (1989) recommend that the deck and continuity diaphragm be cast as late as possible. This is not always practical and will depend on time constraints and project budgets. Delaying the casting of the deck and continuity diaphragm may result in the formation of negative restraint moments at continuous supports, eliminating cracking in the continuity diaphragm. Formation of negative restraint moments may cause cracks in the bridge deck. Cracking in the bridge deck may lead to more serious problems during the service life of the bridge.

The times at which major construction events occur are also important when considering the performance of bridges composed of prestressed concrete girders made continuous. Major construction events affecting the behavior of the structure include casting of the deck, casting of the continuity diaphragm, and fabrication of the prestressed concrete girders. Casting of the deck will increase the dead loads on the structure. Casting of the continuity diaphragm will make the structure continuous for all subsequent loads, namely live loads due to traffic. The age of the prestressed concrete girders at the time of deck and diaphragm casting is important because it affects the formation of restraint moments at the continuity diaphragm.

Oesterle et al. (1989) have found that casting the deck before the continuity diaphragm results in increased midspan moments because continuity has not been established. Casting the diaphragm before the deck only slightly reduces the midspan moments. If continuity diaphragms are cast before the deck, restraint moments forming at the continuity diaphragms may become very large and result in the formation of cracks. No major economic or structural advantage is obtained from sequencing the casting of the deck and continuity diaphragm, so simultaneous casting is recommended for simplicity

(Oesterle et al. 1989). By delaying the casting of the deck and continuity diaphragm, positive restraint moments developing over interior supports will be minimized or even eliminated (Mirmiran et al. 2001; Oesterle et al. 1989).

Ma et al. (1998) performed an analytical study that examined the effects of construction sequence and continuity connection type on the restraint moments that form over interior supports. Ma et al. conclude that the construction sequence does affect the magnitude and orientation of restraint moments. Ma et al. also discuss the need to provide continuity for negative moments at the interior support. Cracking at the girder-diaphragm joint has been shown to occur frequently when the negative moment continuity provided at the interior support is not adequate. Ma et al. recommend several options for reinforcement details to be used at continuity connections between prestressed concrete girders.

2.1.2 Design of the Continuity Diaphragm

In order for continuity to be established between adjacent simple span prestressed concrete girders, a continuity diaphragm must be constructed such that it restrains rotation of the girder ends at the support. According to Mirmiran et al. (2001), full continuity may only be achieved in theory. Oesterle et al. (1989) have determined that full continuity may be achieved in practice, though it is highly dependent on concrete material properties and the construction sequence. Regardless of the degree of continuity achieved initially, cracking of the continuity diaphragm will result in a reduced rotational stiffness and a partial loss of continuity. Designing continuity diaphragms to minimize cracking will help to preserve continuity and prevent serviceability problems.

In most cases, cracking in the continuity diaphragm is a result of the formation of a positive moment that exceeds the cracking moment of the diaphragm. Positive moments can form at continuous supports as a result of restraint moments, loading alternate spans in structures that contain three or more continuous spans, shrinkage and creep, or thermal effects. The magnitude and orientation of the moment formed at interior supports is dependent on the construction sequence, the geometry of the continuity diaphragm, and the flexural reinforcement ratio in the continuity diaphragm. Casting the deck and diaphragm at early girder ages may result in the formation of large positive restraint moments at the continuity diaphragm (Oesterle et al. 1989). Positive restraint moments may also become large if the stiffness of the continuity diaphragm is much greater than the stiffness of the prestressed concrete girders. Increases in the diaphragm bending stiffness are usually a result of high reinforcement ratios.

When a crack develops in the continuity diaphragm, a portion of the diaphragm's rotational stiffness is lost. As a result, prestressed concrete girders affected by the diaphragm cracks are forced to carry a portion of the applied loads as though they were simply supported. Simply supported behavior of the affected girders will continue until

the crack in the continuity diaphragm closes under applied loads (Oesterle et al. 1989). Once the crack closes under applied loads, the continuity diaphragm regains its capacity to resist negative moments and all subsequent loads are carried by the continuous structure (Oesterle et al. 1989). For bridges designed to carry live loads as a continuous structure, it is critical that the cracking in the continuity diaphragm be minimized or eliminated. Failure to do so may cause serviceability problems, such as the formation of flexural cracks in the midspan region of the prestressed concrete girders and increased girder deflections.

A seemingly obvious way to reduce cracking in the continuity diaphragm is to increase the amount of positive moment reinforcement. As a result, the flexural resistance and bending stiffness of the diaphragm are increased (Oesterle et al. 1989). Oesterle et al. (1989) found that the effects of over-reinforcing the continuity diaphragm in order to reduce cracking were offset by the increase in the positive restraint moment formed at the continuity diaphragm. Oesterle et al. (1989) concluded that the inclusion of positive moment reinforcement in continuity diaphragms was a wasteful practice and that such reinforcement should not be included in future structures.

Mirmiran et al. (2001) recommend that a minimum amount of reinforcement be provided in continuity diaphragms to resist positive moments. This should be done to keep crack widths to a minimum, to retain a reasonable degree of continuity, and to minimize serviceability problems. Mirmiran et al. (2001) suggest that reinforcement be provided such that the design moment capacity of the continuity diaphragm, ϕM_n, is twenty percent greater than the diaphragm cracking moment, M_{cr}. Analytical studies have shown that over-reinforcing the continuity diaphragm has little effect on the moments developed in the prestressed concrete girders and provides no structural advantage (Mirmiran et al. 2001).

In most bridges composed of prestressed concrete girders made continuous, the positive moment reinforcement in the continuity diaphragm is provided by steel reinforcement that protrudes from the girder ends. Mild steel reinforcement in the form of bent bars has been used as positive moment reinforcement for continuity diaphragms. Prestressing tendons have also been extended from the end of the girder and bent vertically such that they are anchored into the continuity diaphragm. The detailing of such reinforcement varies, depending on bridge geometry and the specifications used for design. Figure 2.1 shows the end detail of a prestressed concrete girder that utilized extended bent prestressing tendons to provide positive moment reinforcement at a continuity connection.

Mild steel bent bars have been shown to fail in a brittle manner at the bar bend when subjected to repeated loading (Freyermuth 1969; Oesterle et al. 1989). Noppakunwijai et al. (2002) performed pullout tests on extended bent prestressing tendons in order to determine their capacity at various embedment lengths. Recommendations are provided

8

for the minimum embedment length of extended bent prestressing tendons used as positive moment reinforcement for continuity diaphragms (Noppakunwijai et al. 2002). Extended bent prestressing tendons can provide adequate positive moment reinforcement for continuity diaphragms if detailed properly. When extended bent prestressing tendons are used to create continuity at girder ends, the anchorage of the tendons is improved at the girder end (Noppakunwijai et al. 2002). This results in an increased shear capacity for cross sections near the end of the girder (Noppakunwijai et al. 2002).

2.2 CRACKING IN THE TRANSFER REGION OF PRESTRESSING TENDONS IN PRESTRESSED

CONCRETE BRIDGE GIRDERS

Prestressed concrete flexural members are often designed such that they will not crack under service level loads. Cracking of the concrete may result in durability and serviceability problems, as well as losses in the effective prestressing force transferred to the concrete. If the prestressing tendons are unable to transfer the prestressing force to the concrete, the flexural and shear capacity of the member will be greatly reduced.

Tests performed on prestressed concrete flexural members have shown that when cracks propagate through areas where prestressing tendons are located, anchorage failure of the tendons becomes possible. Anchorage failure is more likely when cracks occur near the ends of prestressed concrete members where the prestressing tendons are transferring the prestressing force to the concrete (Russell et al. 1994; Barnes et al. 1999). Barnes et al. (1999) describes the mechanism causing the anchorage failure of a prestressing tendon by examining a portion of a prestressed concrete member containing cracks that cross the prestressing tendons.

When a crack forms, the prestressing tendons at the cracked section must resist a sharp increase in tensile force because the cracked concrete no longer carries tensile forces. The additional tension resisted by the prestressing tendons causes them to contract, reducing their diameter and cross-sectional area. This behavior is known as the Poisson effect. The radial compressive stress exerted on the tendon by the surrounding concrete decreases as the tendon diameter decreases. As a result, the effective bond provided by the concrete is reduced and the effective prestressing force transferred to the concrete on either side of the crack decreases (Barnes et al. 1999).

If the strength of the bond provided by the concrete surrounding the prestressing tendon is not large enough to adequately anchor the tendon, the tendon may slip. Slippage will occur until the bond provided by the surrounding concrete is sufficient. The effective prestressing force transferred to the concrete by the prestressing tendon is lost when the tendon slips, resulting in a translation of the transfer region along the length of the member (Barnes 2000). Slippage of the tendons may result in a partial or total loss

of prestressing force and a corresponding reduction of the shear and flexural capacities of the member.

Anchorage failure of prestressing tendons is highly dependent on the location of the cracking. Russell et al. (1994) found that cracks occurring within the transfer region of partially debonded prestressing tendons caused anchorage failures of the debonded tendons to occur. Results of other tests have shown that the crack causing the anchorage failure need not be within the transfer region so long as it occurs in close proximity to the transfer region (Barnes et al. 1999). If the crack occurs close enough to the transfer region of the prestressing tendons, the heightened stresses in the tendons resulting from the presence of the crack extend into the transfer region, causing an anchorage failure. The length over which the stresses in the prestressing tendon are increased due to the presence of the crack is called the "crack influence length" (Barnes et al. 1999).

Russell et al. (1994) recommend that prestressed concrete flexural members be designed such that cracking does not occur in the transfer region of the prestressing tendons under factored ultimate loads. If prestressed concrete flexural members are designed with such a recommendation in mind, the concept of the crack influence length proposed by Barnes et al. (1999) should be included. The resulting recommendation would be to design prestressed concrete flexural members such that cracks crossing prestressing tendons do not occur within one crack influence length of the transfer region. By designing prestressed concrete flexural members in such a way, it may be possible to avoid anchorage failures of the prestressing tendons at the ultimate strength limit state.

Proper anchorage of tendons is especially important when partially debonded tendons are used because they have been shown to be more susceptible to anchorage failures than fully bonded tendons (Barnes et al. 1999). Russell et al. (1994) recommend that partially debonded tendons be designed such that they become effective at different points along the length of the member. This type of design for partially debonded tendons is commonly referred to as staggered debonding. The use of staggered debonding among partially debonded tendons has been shown to minimize stress concentrations that may cause crack formation and propagation.

2.3 SHEAR STRENGTHENING OF REINFORCED CONCRETE FLEXURAL MEMBERS

It is not uncommon for concrete structures to require strengthening during their service lives. Mistakes in design calculations, improper detailing of reinforcement, construction faults, poor construction practices, changes in the use of the structure, changes in applied loading, damage caused by vehicular impact, and corrosion of the reinforcement may require reinforced or prestressed concrete members to be strengthened (Khaloo 2000). Members affected by these factors may have significant strength deficiencies or experience serviceability problems.

For existing members that are deficient in shear capacity, there exist multiple strengthening options. The method of shear strengthening best suited to a particular member depends on the geometry of the member, the magnitude of the required increase in shear capacity, the severity of the environmental and chemical exposure, and the available resources. It is extremely important that the shear strengthening method chosen be capable of adequately enhancing the shear capacity of the member while remaining economically feasible. The following sections give a brief overview of several different shear strengthening methods used for reinforced and prestressed concrete flexural members.

2.3.1 External Post-tensioning

External post-tensioned stirrups and composite straps have been used to enhance the shear capacity of RC and prestressed concrete flexural members (Khaloo 2000; Emmons 1993; Norris et al. 1997). The procedure used to implement these two strengthening methods is slightly different, though the result is much the same. By post-tensioning with external reinforcement, the section is compressed in the vertical direction. This vertical compression of the cross section acts to close existing shear cracks and provide confinement of the concrete. The result is a member that has an increased shear capacity and more ductility. The increase in the ductility of the member is a result of the confinement of the concrete provided by the external post-tensioning (Khaloo 2000).

Khaloo (2000) performed tests on 24 RC beams containing varying amounts of internal shear reinforcement. Portions of the beams were strengthened by externally post-tensioning in the vertical direction. Beams were then instrumented and loaded to failure. The capacity of the strengthened members was compared to that of unstrengthened control specimens. Khaloo (2000) states that a vertical compressive stress of $0.04 f_c'$ applied to shear critical regions of RC beams resulted in an increase in shear capacity and ductility. Crack widths were decreased in strengthened members. The improvement in shear and flexural capacity of the strengthened members was more significant for those members that contained small amounts of internal shear reinforcement. Khaloo (2000) also recommends the use of externally post-tensioning as a means to control shear cracks with widths of 0.375 in. (10 mm) or less.

The use of externally post-tensioned stirrups is rather difficult to implement for most members. External stirrups must be anchored for post-tensioning to be possible. For members supporting a slab, holes must be drilled through the slab for installation of the external reinforcement. Thus, strengthening with externally post-tensioned stirrups is difficult because portions of the bridge must be closed while repairs to the girders are made. Due to the intrusive nature of the repair, serviceability of the bridge deck is also a concern for this strengthening method. A concrete flexural member strengthened with externally post-tensioned stirrups is shown in Figure 2.2.

The use of externally post-tensioned composite straps is highly dependent on the geometry of the members that require strengthening. For post-tensioning to be possible, straps must be continuously wrapped around the web of the member. Lees et al. (2002) used external post-tensioned composite straps to strengthen reinforced concrete T-beams. The shear capacity of the strengthened members was over thirty percent larger than that of the control beams. Strengthening the beams with the external post-tensioned straps also changed the failure mode from a non-ductile shear failure to a ductile flexural failure. Though the use of this strengthening method has been shown to be effective for reinforced concrete flexural members, its use on actual bridge structures is not very practical. A concrete flexural member strengthened with external post-tensioned composite straps is shown in Figure 2.3.

2.3.2 Enlargement of the Cross Section

The shear capacity of RC flexural members has also been improved by enlarging the cross section (Khaloo 2000; Emmons 1993; Norris et al. 1997). In some cases, the cross section may be enlarged by means of casting concrete around the existing cross section with the aid of formwork. Shotcreting is also used to increase the cross-sectional area because it can be performed rapidly and does not require the use of formwork.

The applicability of this shear strengthening method relies on the geometry of the member that requires strengthening. Members being strengthened with this procedure must have a geometry such that the cross section can be sufficiently enlarged. The additional dead load of the built-up cross section increases the shear and moment demand on the member and may result in increased midspan deflections and bending stresses. If the effects of enlarging the cross section of the member will cause strength or serviceability problems in the future, alternative shear strengthening methods should be considered.

2.3.3 Shear Strengthening by Plate Bonding

Bonded steel and FRP plates have been used effectively to enhance the shear strength of both reinforced and prestressed concrete flexural members (Khaloo 2000; Norris et al. 1997; Colotti and Spadea 2001). Steel plate bonding was first used in the late 1960's to improve the flexural strength of RC beams. Research on the use of FRP composite plates began in the early 1980's. Shear strengthening by plate bonding is an attractive strengthening option because it has little effect on the geometry and loading of the structure and limits disruptions to the usage of the structure.

Swamy et al. (1999) tested RC beams strengthened with both steel and FRP plates on the beam sides and soffit to examine the effects of plate bonding on member shear capacity. Results indicate that the use of externally bonded plates can significantly increase the shear capacity of flexural members with little to no internal shear

reinforcement. The magnitude of the increase in shear capacity was dependent on the amount and distribution of externally bonded steel and FRP plates. Mechanical anchorage of the externally applied plates helped to prolong their effectiveness by delaying a peeling failure (Swamy et al. 1999). Mechanical anchorage was provided by epoxy bonding high-strength bolts into holes that were drilled through the external plates and into the RC beam (Swamy et al. 1999).

As the acceptance of FRP as a structural repair material has increased, the use of steel for shear strengthening by plate bonding has decreased. The advent of FRP composite materials is not the only reason that the use of steel plates has been abandoned, though. The bond between the externally bonded steel plate and the concrete has been shown to deteriorate over time, due to corrosion of the steel plate at the plate/adhesive interface. As the corrosion of the steel at the plate/adhesive interface progresses, the steel plate may become debonded from the concrete member. Because FRP is non-corrosive, this problem is eliminated. Steel plates used for plate bonding, although thin, are heavy and difficult to install. Lifting equipment and temporary shoring are necessary to install steel plates and keep them in place while the epoxy adhesive cures. FRP composites are lightweight and flexible, eliminating the need for shoring and lifting equipment.

2.3.4 Additional Shear Strengthening Methods

The addition of supports into existing spans has been used in the past to shorten span lengths and reduce shear forces induced by dead and live loads (Khaloo 2000). Insertion of a support into an existing span will change the way the span behaves, making a single span act as though it were a two-span continuous structure. The changes in the behavior of the member will depend on the span length, location of the support relative to the member ends, and the applied loading. If the existing member was not designed to have significant shear and negative moment capacity near the location of the additional support, this procedure is not feasible. Construction of additional supports may also restrict the usage of the structure or be overly expensive.

The introduction of passive internal shear reinforcement has been used to increase the shear capacity of existing concrete flexural members (Emmons 1993). Holes are drilled from the top of the member downward, into the web. Holes are drilled at an angle so that they cross shear cracks in a perpendicular orientation. Mild steel reinforcement is inserted into the drilled holes, which are later filled with grout or epoxy. The passive steel reinforcement acts to control crack widths and increases the shear capacity of the member. Placement of the drilled holes is extremely difficult, especially for members that are heavily reinforced. The nature of this repair method often results in a temporary closure of the structure to allow for installation of the reinforcement and time for the grout or epoxy to harden. Passive internal shear reinforcement used to increase the shear capacity of an existing RC flexural member is shown in Figure 2.4.

Epoxy injection of existing cracks in reinforced and prestressed concrete flexural members has been shown to help improve shear capacity (Khaloo 2000). This method is often used in conjunction with other strengthening procedures as a means to seal and control the growth of existing shear and flexural cracks. When epoxy injection is used as the sole method of repair, cracks often reopen under applied loads. Inspections of epoxy-injected cracks have shown that new cracks tend to form adjacent to the injected cracks.

2.4 SHEAR STRENGTHENING OF CONCRETE FLEXURAL MEMBERS WITH FRP

COMPOSITES

Strengthening RC flexural members with externally bonded FRP composites has become an increasingly popular trend in the past decade. FRP has been successfully used as external reinforcement for concrete structures, both in laboratory experiments and in practice. The ability of FRP composites to increase the shear capacity of existing RC flexural members has been shown through laboratory experimentation (Khalifa et al. 1999). Experimental studies on FRP shear strengthening compose a small percentage of the current research on FRP strengthening. This is due to the large amount of research dedicated to the study of flexural strengthening and column wrapping with FRP composite materials (Triantafillou 1998a).

Multiple cross-sectional and longitudinal FRP configurations have been used to strengthen RC flexural members in shear. Figure 2.5 shows the three most typical cross-sectional FRP configurations: the fully wrapped configuration, the U-wrap configuration, and the web-bonded configuration. Typical longitudinal FRP configurations are shown in Figure 2.6. The continuously bonded configuration is the most commonly used longitudinal configuration.

The success of external FRP shear reinforcement has been to shown to be dependent on multiple parameters. Consideration of all relevant parameters is necessary to determine whether or not strengthening with external FRP reinforcement will be beneficial. Norris et al. (1997) feel that design criteria will become available as research continues on this subject. Proper design criteria should enable engineers to design FRP strengthened members so that they possess both adequate strength and ductility. Until such design specifications are made available, external FRP shear reinforcement must be use with caution.

A discussion of the various parameters that affect the strength and ductility of FRP strengthened RC members is presented in the following sections. Preliminary design guidelines provided by researchers and the design guidelines currently recommended by ACI Committee 440 (2002) are also discussed. Additional concerns stemming from the use of external FRP shear reinforcement are presented.

2.4.1 Effects of External FRP Shear Reinforcement on Member Strength and

Ductility

The strength, or capacity, of a member refers to its ability to resist a particular load effect, such as shear, moment, torsion, or axial load. In order for the strengthening of an existing member to be effective, the additional reinforcement must increase the capacity of the member such that it is able to resist all factored ultimate loads. The final design must also satisfy serviceability limit states.

Members with adequate ductility are able to sustain large deflections and curvatures before failure. Ductile failures are more appealing because they display signs of impending failure while retaining the capacity to carry loads. Members that fail in a brittle fashion will show few signs of distress prior to failure. When strengthened with external FRP reinforcement, the ductility of RC flexural members is often significantly decreased. The primary reason for the decrease in ductility is related to the purely elastic behavior of FRP until failure. Decreases in the ductility of strengthened RC flexural members may also be due to a non-ductile failure mode controlled by debonding of the external FRP reinforcement.

The load-carrying capacity and ductility of RC members strengthened with external FRP reinforcement are dependent on many parameters, such as member geometry, material properties, relative amounts of internal and external reinforcement, cross-sectional and longitudinal placement of the FRP composite material, and the pre-existing condition of the member. The relationship between these parameters affects the magnitude of the improvement in load-carrying capacity and the controlling failure mode. If designed and detailed correctly, RC flexural members strengthened with external FRP shear reinforcement have been shown to retain an adequate amount of ductility while gaining a significant amount of shear capacity (Khalifa and Nanni 2000; Chajes et al. 1995; Chaallal et al. 2002).

2.4.1.1 FRP Reinforcement Ratio

The FRP shear reinforcement ratio, ρ_f, directly affects the shear capacity of strengthened RC flexural members. The FRP reinforcement ratio is as shown in Equation 2.1, where t_f is the thickness of the FRP reinforcement and b_w is the width of the web.

$$\rho_f = \frac{2t_f}{b_w} \qquad \text{Eq. 2.1}$$

Researchers have found that the relationship between the FRP shear reinforcement ratio and the magnitude of the increase in shear capacity are not linearly related (Adhikary and

Mutsuyoshi 2000; Micelli et al. 2002; Chaallal et al. 2002; Khalifa et al. 1998). Another way to express this idea is to say that an increase in the FRP reinforcement ratio may not result in a comparable increase in shear capacity. The exact reasons for the nonlinear relationship between the FRP reinforcement ratio and the magnitude of the increase in shear capacity are not totally clear.

Khalifa and Nanni (2000) and Khalifa et al. (1998) report that there exists a threshold value for the FRP reinforcement ratio beyond which no appreciable gains in shear capacity can be obtained. Pellegrino and Modena (2002) express a similar idea, having concluded that the effectiveness of external FRP shear reinforcement is reduced as the relative stiffness of the FRP increases. The relative stiffness of the external FRP reinforcement is expressed as the product of the FRP reinforcement ratio and the elastic modulus of the FRP composite material. The use of a relative FRP stiffness parameter was adopted by ACI Committee 440 (2002) and used in their design guidelines.

For RC flexural members requiring significant increases in shear capacity, high FRP reinforcement ratios may be required to satisfy the ultimate strength limit state. The use of high FRP reinforcement ratios has been shown to cause FRP debonding failures among strengthened members, resulting in significant decreases in member ductility (Li et al. 2001a; Micelli et al. 2002). Triantafillou and Antonopoulos (2000) conclude that there exists some threshold value for the FRP reinforcement ratio below which debonding of the FRP reinforcement will not be the controlling failure mode. When that threshold value is exceeded, mechanical anchorage of the FRP reinforcement must be provided in order to prevent FRP debonding and preserve the load-carrying capacity of the member. It is possible that the threshold value for debonding of the external FRP reinforcement is very low for some members and may severely limit the amount of FRP that can be used for strengthening.

The use of multiple layers of external FRP shear reinforcement is also suggested when high FRP reinforcement ratios are required. Layers of external FRP reinforcement can be oriented in such a way that each successive layer confines those layers below it. Premature failure caused by FRP debonding may be delayed or prevented if the layers of FRP are detailed correctly. Multiple layers of external FRP shear reinforcement are also able to resist tearing more effectively than a single sheet (Adhikary and Mutsuyoshi 2000).

2.4.1.2 Anchorage of Externally Bonded FRP Reinforcement

The anchorage of external FRP shear reinforcement directly affects the shear capacity and failure mode of strengthened members. If adequate anchorage is not provided, the external FRP reinforcement may fail prematurely by debonding from the concrete surface to which it is bonded. The shear capacity of a strengthened member that fails prematurely as a result of FRP debonding may be significantly lower than predicted by

analytical means. If the anchorage of the external FRP reinforcement is adequate, the strengthened member should be able to develop its maximum theoretical load-carrying capacity. The failure mode of the member will be controlled by flexure, shear, or rupture of the external FRP reinforcement.

Anchorage of external FRP shear reinforcement may be provided in a number of ways. The most efficient way to provide anchorage is through the bond between the FRP reinforcement and the concrete surface. Adequate anchorage can often be provided in this manner through proper design and installation of the FRP strengthening system. Anchorage has also been provided through the use of FRP bar end anchors, by bolting the FRP reinforcement to the member, and with mechanical fasteners.

Three typical cross-sectional configurations have been used in experimental studies of shear strengthening with FRP composites: the fully wrapped configuration, the U-wrap configuration, and the web-bonded configuration. The three configurations are shown in Figure 2.5. The amount of anchorage provided by each strengthening configuration varies, though each is dependent on the quality of the bond between the FRP composite material and the concrete member. De Lorenzis et al. (2001) believe that the condition of the concrete surface may have a significant effect on the strength of the bond between the FRP and the concrete member.

Khalifa et al. (2000) have shown that the fully wrapped configuration provides significant increases in shear capacity and is not susceptible to the debonding failure observed in many experimental tests of RC members strengthened with external FRP reinforcement. Triantafillou and Antonopoulos (2000) recommend that external FRP shear reinforcement be applied in the fully wrapped configuration whenever possible. Because the majority of existing members have geometries that prevent the use of the fully wrapped configuration, its use is not usually feasible for actual practice.

The U-wrap configuration of external FRP shear reinforcement has also been shown to increase the shear capacity of RC beams (Khalifa and Nanni 2000; Adhikary and Mutsuyoshi 2000; Chajes et al. 1995; Micelli et al. 2002). Because the external FRP shear reinforcement is not wrapped around the entire cross section, the bonded area of FRP is less than that for a fully wrapped configuration. Experimental results suggest that the anchorage of a U-wrapped FRP system is improved by applying the external FRP shear reinforcement over the full depth of the beam web (Adhikary and Mutsuyoshi 2000). The anchorage characteristics of U-wrapped external FRP shear reinforcement have been improved for RC T-beams by using FRP bar end anchors (Khalifa and Nanni 2000; Triantafillou and Antonopoulos 2000; Micelli et al. 2002; Khalifa et al. 2000). A typical FRP bar end anchor assembly is shown in Figure 2.7.

The web-bonded configuration has not been as widely used as the other two strengthening configurations. When the web-bonded configuration is used, debonding of the external FRP shear reinforcement occurs more often than when other FRP

configurations are used. The resulting behavior of the strengthened member is often characterized by premature failure due to FRP debonding while little to no improvement in shear capacity is obtained. The use of a U-wrap or fully bonded configuration is preferable to the web-bonded configuration for both strength and ductility (Khalifa and Nanni 2000; Khalifa et al. 1998).

If adequate anchorage cannot be provided through the bond between the concrete and external FRP shear reinforcement, mechanical anchorage of the FRP is necessary. Prevention of premature failures of strengthened members is possible if properly designed mechanical anchorage is provided. Lamanna et al. (2001) examined the feasibility of using mechanical fasteners for the application of external FRP reinforcement to RC members. Though this method has been effective when used with external FRP reinforcement applied to the soffit of RC flexural members, Lamanna et al. do not discuss the efficacy of mechanical fasteners when used to anchor external FRP reinforcement to the web of RC flexural members. According to Lamanna et al., the use of the mechanical fasteners resulted in the formation of cracks at each fastener location. The external FRP reinforcement was observed to slip when fasteners were not driven into the concrete properly, which resulted in less strengthening (Lamanna et al. 2001). Khalifa and Nanni (2000) used steel bolts to anchor externally bonded FRP plates to RC beams. This method of providing anchorage was shown to be effective, though it is time consuming and often very expensive.

The use of FRP bars as end anchors for U-wrapped external FRP shear reinforcement, shown in Figure 2.7, has been shown to be effective for delaying or preventing debonding of the FRP composite material (Micelli et al. 2002; Khalifa et al. 2000; Khalifa and Nanni 2000; Triantafillou and Antonopoulos 2000). This form of mechanical anchorage is dependent on the geometry of the member being strengthened. Thus far, its use has been limited to research and experimentation. The installation of FRP bar end anchors is labor intensive and time consuming. Once installed, FRP bar end anchors are often susceptible to environmental and chemical exposure.

2.4.1.3 FRP Composite Placement and Fiber Orientation

As discussed in the previous section, the cross-sectional configuration of external FRP reinforcement can significantly affect the capacity of a strengthened RC flexural member. The longitudinal FRP configuration also affects the capacity of strengthened members. Li et al. (2001a) have concluded that bonding external FRP shear reinforcement to the entire length of a flexural member is not necessary to achieve significant increases in shear capacity. The use of transverse FRP strips has been proposed as an alternative method to strengthen RC flexural members in shear. Multiple researchers have investigated the use of FRP strips to increase the shear capacity of RC flexural members. ACI Committee 440 (2002) gives design recommendations for externally bonded FRP strip reinforcement used to increase the shear capacity of RC flexural members.

Khalifa and Nanni (2000) performed tests on RC beams strengthened in shear with external FRP strips. Although increases in shear capacity were observed when the FRP strips were used, debonding of individual FRP strips occurred before the member reached its maximum load-carrying capacity (Khalifa and Nanni 2000). According to ACI Committee 440 (2002) recommendations, discrete strips of external FRP shear reinforcement may be used for strengthening, though the spacing of the strips must meet the spacing requirements for transverse shear reinforcement set forth in "Building Code Requirements for Structural Concrete (ACI 318-02) and Commentary (ACI 318R-02)" (ACI Committee 318 2002). ACI Committee 440 (2002) states that experimental specimens should be tested to evaluate the actual contribution of the FRP strips and validate the effectiveness of such a strengthening system until more reliable design guidelines are provided.

Despite the inefficiency and expense, Khalifa and Nanni (2000) recommend the use of continuous sheets or plates for external FRP shear reinforcement. Results of experimental testing performed on RC flexural members strengthened with external FRP shear reinforcement show that continuously bonded external FRP shear reinforcement is capable of increasing the load-carrying capacity of the member. Sudden failures are less likely when continuously bonded external FRP shear reinforcement is used, due to the larger bonded area of FRP (Khalifa and Nanni 2000). Li et al. (2001a) found that crack formation is delayed and the ductility of the strengthened member is slightly enhanced when continuously bonded external FRP shear reinforcement is used. Adhikary and Mutsuyoshi (2000) also found that cracking was significantly delayed for strengthened members when the FRP is continuously bonded.

FRP composite fiber orientation significantly affects the shear capacity of strengthened RC beams (Li et al. 2001b; Malek and Saadatmanesh 1998b). Because FRP is an orthotropic material, the contribution of external FRP shear reinforcement depends on the orientation of the fibers with respect to the longitudinal axis of the member. The performance of the FRP strengthening system can be maximized with proper orientation of the fibers. Bakis et al. (2002) believe that FRP composites can be used successfully as external shear reinforcement for RC members if the material is epoxy bonded to the member with the fibers aligned parallel to the direction of principal tensile concrete stresses.

When a single layer of unidirectional external FRP shear reinforcement is used for strengthening, larger increases in shear capacity have been gained by using a 90° orientation (perpendicular to the beam axis) as opposed to using a 0° orientation (Khalifa and Nanni 2000; Adhikary and Mutsuyoshi 2000; Norris et al. 1997). Providing external FRP reinforcement with fibers oriented at 90° is analogous to providing additional stirrups because the fibers carry force in the vertical direction. Although the 90° fiber orientation provides a more significant increase in shear strength, the use of external FRP

19

reinforcement with fibers oriented at 0° also increases the shear capacity of strengthened members (Adhikary and Mutsuyoshi 2000; Chajes et al. 1995).

Research has shown that the strengthening effect of external FRP shear reinforcement is improved with the use of multiple layers of reinforcement with different fiber orientations (Adhikary and Mutsuyoshi 2000; Chajes et al. 1995; Khalifa et al. 2000). Greater increases in shear capacity have been observed when two layers of external FRP reinforcement with 0° and 90° fiber orientations are used (Adhikary and Mutsuyoshi 2000; Khalifa et al. 2000). It is believed that the use of a secondary (topmost) layer of external FRP reinforcement provides restraint to the primary (bottommost) layer of FRP, thereby increasing the shear capacity of the member (Khalifa et al. 2000; Adhikary and Mutsuyoshi 2000). This result was observed when the orientation of the fibers was 90° and 0° for the primary and secondary layers, respectively. The restraint provided by the secondary layer of external FRP reinforcement also controls crack widths, which allows more shear force to be resisted by aggregate interlock along shear cracks.

2.4.1.4 Steel Reinforcement Ratio

Experiments performed by multiple researchers have shown that the transverse and longitudinal steel reinforcement ratios influence the ability of external FRP shear reinforcement to increase the shear capacity of RC flexural members. As the transverse reinforcement ratio increases, the external FRP shear reinforcement becomes less effective for increasing the shear capacity of the member (Pellegrino et al. 2002; Khalifa et al. 1998; Khalifa et al. 2000; Li et al. 2001b). Thus, an RC flexural member with a low transverse reinforcement ratio is capable of more significant increases in shear capacity with the use of external FRP shear reinforcement. Members with high transverse reinforcement ratios will show less significant increases in shear capacity. Chaallal et al. (2002) concluded that the optimum amount of external FRP shear reinforcement is directly related to the transverse steel reinforcement ratio.

Li et al. (2001a) recognize that the amount of internal longitudinal reinforcement affects the ability of external FRP reinforcement to increase the shear capacity of RC flexural members. The longitudinal reinforcement in a reinforced concrete flexural member provides the tension tie needed to form the truss mechanism that transfers shear forces to the member supports. Because the longitudinal reinforcement is a fundamental part of the shear transfer mechanism for an RC flexural member, its effectiveness will directly affect the shear capacity of the member. For a member that is under-reinforced in flexure, the longitudinal reinforcement ratio is low and the capacity of the tension tie is small. Shear strengthening with FRP may not provide a significant increase in shear capacity for under-reinforced members unless additional longitudinal reinforcement is provided.

20

The longitudinal reinforcement ratio is an important topic when considering the cracking in the end region of the prestressed concrete bulb-tee girders in Huntsville, Alabama. The position and width of the cracks in the bulb-tee girders suggests that the prestressing tendons may not be fully effective in the end region of the member. As a result, portions of the bulb-tee girder may have a very low longitudinal reinforcement ratio, making it difficult for shear forces to be transferred to the member supports. The tensile capacity of the longitudinal reinforcement in the bottom flange will be critical in the analysis and repair of the cracked bulb-tee girders. This subject is addressed in more detail in Chapters 3 and 6.

2.4.1.5 Pre-existing Condition of Concrete Member

The ability of an existing RC flexural member to be strengthened in shear is somewhat dependent on the condition of the member prior to strengthening. Many existing RC members have cracks that formed under the action of shear, flexure, torsion, shrinkage, creep, or thermal effects. Concrete may also deteriorate over time due to the effects of environmental and chemical exposure. These conditions may adversely affect the quality of the bond that can be achieved between the FRP composite and the concrete. Poor bond quality may compromise the effectiveness of the external FRP reinforcement.

Norris et al. (1997) fabricated nineteen RC beams and repaired them with external FRP shear reinforcement. Some of the beams were loaded prior to application of the external FRP reinforcement so that cracks would form. The presence of the flexural cracks was thought to more accurately reflect the condition of actual members that would be strengthened. The beams were then tested to evaluate the performance of the FRP strengthening system. Norris et al. (1997) concluded that the addition of external FRP shear reinforcement was effective for RC flexural members, regardless of whether they were cracked or uncracked before strengthening. The behavior and capacity of the cracked and uncracked beams was indistinguishable at the ultimate load level (Norris et al. 1997).

Vogel and Ulaga (2002) tested girders from a 90-year-old bridge in Switzerland to verify whether or not external FRP composites could be applied to concrete members that were severely deteriorated. The girders had discolored concrete, concrete spalling, honeycombing, exposed internal steel reinforcement, and other signs of aging on surfaces where external FRP reinforcement was bonded. External FRP reinforcement was shown to be effective in increasing both the shear and flexural capacity of the bridge girders when compared with an unstrengthened control specimen. The authors concluded that external FRP reinforcement is a viable repair option for severely deteriorated concrete flexural members as long as surfaces to which external FRP reinforcement is bonded are prepared correctly.

De Lorenzis et al. (2001) performed experimental tests on concrete members strengthened with externally bonded FRP composites in order to examine the effects of multiple parameters on the strength of the bond between the external FRP reinforcement and the concrete. Results of the experimental program revealed that the preparation of the surface to which the FRP is bonded greatly affects the strength of the bond and the capacity of the strengthened member. Greater bond strengths were recorded for surfaces that had been roughened by chiseling than for sandblasted surfaces. Chiseling of the surface is not a common practice and may not be practical for field applications where large amounts of FRP must be installed. Chiseling of the surface is not advisable for members that have limited concrete cover or are in areas subjected to severe chemical exposure. Micelli et al. (2002) concluded that the strength of the bond between external FRP reinforcement and concrete is weakened by poor concrete quality and improper surface preparation. ACI Committee 440 (2002) provides recommendations on surface preparation procedures in their report, *Guide for the Design and Construction of Externally Bonded FRP Systems for Strengthening Concrete Structures*. This report will be referred to as the *Guide* from this point forward.

2.4.2 Design and Analysis of RC Flexural Members Strengthened with External

FRP Shear Reinforcement

Shear strengthening with external FRP reinforcement will not be a standard practice for RC members until a simple and conservative design procedure is developed. In order for a design procedure to be developed, an analytical model capable of accurately predicting the contribution of the external FRP reinforcement to the shear capacity of the strengthened member must be developed. Many researchers have developed analytical models that calculate the shear capacity of FRP strengthened RC members. Most analytical models work well for specific data subsets but are generally unconservative when applied to the whole of the data contained in the FRP shear strengthening database (Triantafillou 1998b).

2.4.2.1 Failure Mode and its Effect on FRP Reinforcement Strains

Three unique modes of failure have been recognized by researchers and used in the development of existing analytical methods. A strengthened RC flexural member may fail in flexure or shear while the FRP remains effective as shear reinforcement, by debonding of the FRP, or by rupture of the FRP. Each of the three failure modes can be subdivided to more accurately describe a range of failures observed in experimental specimens. Because rupture of the FRP is rarely the controlling failure mode, it may be disregarded for practical design (Triantafillou 1998b).

The three modes of failure are all closely related to the anchorage of the external FRP reinforcement. If the anchorage of the external FRP reinforcement is inadequate, either debonding of the FRP or delamination of the concrete cover at the level of the longitudinal reinforcement is likely to be the controlling failure mode. Significant strains in the external FRP reinforcement cannot be attained when this type of failure controls the behavior of the strengthened member. As the anchorage of the FRP reinforcement is improved, strains in the external FRP reinforcement increase and the ductility of the strengthened member increases.

Malek and Saadatmanesh (1998a) have shown that the strains in external FRP shear reinforcement are consistently less than the ultimate FRP strain when strengthened RC flexural members fail. Malek and Saadatmanesh (1998a) reached this conclusion using analytical methods to perform a parametric study of FRP strengthened RC beams. Experimental evidence of the FRP strain at failure has been provided by multiple researchers and supports the conclusions of Malek and Saadatmanesh (1998a) (Norris et al. 1997; Chajes et al. 1995; Micelli et al. 2002; Khalifa et al. 2000).

Triantafillou (1998b) states that many researchers have arbitrarily chosen a maximum allowable FRP strain for use in their analytical methods. Although the use of a limiting FRP strain for design is consistent with the findings of many researchers, arbitrarily choosing a maximum allowable FRP strain may not be conservative. Using an allowable FRP strain that is too large results in an overestimation of the force carried by the FRP shear reinforcement and the shear capacity of the strengthened member. According to ACI Committee 440 (2002), the actual strain level reached in the FRP shear reinforcement at failure depends on many parameters, such as member geometry, FRP composite material properties, FRP reinforcement ratio, and the controlling failure mode. Harmon et al. (2003) believe that the maximum FRP strain reached before failure of the member is dependent on many more parameters related to the stiffness of the resin layer and the concrete to which the FRP is bonded. ACI Committee 440 (2002) recommends an upper limit of 4000 $\mu\varepsilon$ (0.4 percent elongation) for FRP shear reinforcement. Chaallal et al. (2002) report that the Japan Concrete Institute (JCI) recommendations allow an FRP strain of 7000 $\mu\varepsilon$ for design. Bakis et al. (2002) suggest limiting the strain in external FRP shear reinforcement to 4000 $\mu\varepsilon$–5000 $\mu\varepsilon$ in order to preserve aggregate interlock along cracks.

2.4.2.2 Calculation of Strengthened Member Capacity

Multiple researchers have developed analytical models for determining the nominal amount of external FRP shear reinforcement required for strengthening. Some controversy exists regarding the accuracy and conservatism of existing analytical models, due in part to poor correlation between analytical and empirical results (Triantafillou 1998a). Existing analytical models have made use of laminate theory, plasticity theory,

and nonlinear stress-strain relationships in order to more accurately reflect the behavior of strengthened members. Though the constant-angle truss analogy is most often used to develop expressions for the shear resistance of RC flexural members, variable-angle truss models and strut-and-tie models have also been used.

The sectional shear capacity of reinforced concrete flexural members is often represented as the sum of two terms: the shear resistance provided by the concrete and that provided by shear reinforcement. This relationship is expressed as shown in Equation 2.2, where V_n is the nominal sectional shear capacity, V_c is the shear resistance provided by the concrete, and V_s is the shear resistance provided by the transverse mild steel reinforcement.

$$V_n = V_c + V_s$$
<div align="right">Eq. 2.2</div>

For an RC flexural member strengthened with external FRP shear reinforcement, Equation 2.2 must be modified to account for the shear resistance provided by the external FRP reinforcement. If superposition of the shear contributions of the concrete, steel reinforcement, and external FRP reinforcement is allowable, then the nominal shear resistance of an RC member strengthened with external FRP shear reinforcement can be represented as shown in Equation 2.3. The final term in Equation 2.3, V_f, is the shear resistance provided by the external FRP shear reinforcement.

$$V_n = V_c + V_s + V_f$$
<div align="right">Eq. 2.3</div>

Researchers have proposed multiple expressions to calculate the contribution of the external FRP shear reinforcement to the shear capacity of a strengthened member, V_f. Despite the effort to determine an accurate expression for V_f, experimental results suggest that the contribution of the external FRP shear reinforcement cannot be calculated by using simple superposition (Li et al. 2001b). A complex interaction between the concrete, the internal shear reinforcement, and the external FRP shear reinforcement exists for strengthened members (Li et al. 2001b). This makes the determination of the shear resistance of any one of the three components extremely difficult.

Triantafillou (1998a) feels that attempting to quantify the shear resistance provided by the FRP reinforcement is impossible through rigorous analysis. Instead, a simplified method to estimate the contribution of the external FRP shear reinforcement should be used for design. Triantafillou has developed a simple function that describes the relationship between the relative stiffness of the FRP and the effective strain in the FRP at failure. As more experimental results are added to the FRP shear strengthening database, the relationship proposed by Triantafillou will undergo slight changes.

Because the superposition method does not seem to be capable of predicting the shear capacity of strengthened RC flexural members, alternative analytical models have been proposed. Malek and Saadatmanesh (1998a) developed an analytical model that utilizes modified compression field theory (MCFT) to calculate the shear capacity of FRP strengthened RC flexural members. The Malek and Saadatmanesh model also accounts for the orthotropic behavior of FRP composite reinforcement. Deniaud and Cheng (2001) report that the model developed by Malek and Saadatmanesh tends to slightly overestimate the contribution of the FRP shear reinforcement when the transverse steel reinforcement ratio is small. The model is also incapable of providing any insight into the failure mode of the strengthened member (Deniaud and Cheng 2001).

Deniaud and Cheng (2001) report that strut-and-tie models are a lower-bound solution and always produce conservative results. Using the strut-and-tie model proposed by Al-Nahlawi and Wight (1992), Deniaud and Cheng showed that the predicted capacity of experimental specimens was far less than their actual capacity. The conservatism of the Al-Nahlawi and Wight model became greater as member sizes increased (Deniaud and Cheng 2001).

Deniaud and Cheng (2001) also used an analytical model based on shear friction to predict the strength of RC beams strengthened with external FRP shear reinforcement. The shear friction method accurately predicted the contribution of external FRP shear reinforcement for experimental RC beams tested to failure. The capacity of strengthened members was overestimated for two of the sixteen members tested, so conservative predictions of member capacity are not always obtained with this model. In order to avoid over-estimating the capacity of strengthened RC members, all potential crack paths must be evaluated to determine where failure is most likely to occur (Deniaud and Cheng 2001). This model was able to predict the path of the crack causing failure with a reasonable amount of certainty.

2.4.2.3 ACI Committee 440 FRP Shear Strengthening Design Method

ACI Committee 440 (2002) presents general design recommendations for FRP-strengthened RC members in the *Guide*. Recommendations for the design of RC flexural members strengthened with external FRP shear reinforcement are located in Chapter 10 of the document. General design philosophy and design guidelines are presented in Chapter 8 of the *Guide*.

The ACI Committee 440 design procedure for RC flexural members strengthened with external FRP shear reinforcement is based upon a limit-states approach. ACI Committee 440 recommends that those load factors specified in ACI 318-02 should be used for design where applicable. Additional strength reduction factors related to the contribution of the external FRP reinforcement are specified in Chapter 10 of the *Guide*.

In the design method presented, ACI Committee 440 uses superposition to calculate the design shear capacity of the FRP strengthened member, as expressed in Equation 2.3.

$$\phi V_n = \phi_s \left(V_c + V_s + \Psi_f V_f \right)$$
Eq. 2.3

The term Ψ_f is a strength reduction factor placed on the contribution of the external FRP shear reinforcement. The value of Ψ_f is dependent on the FRP configuration used for strengthening. The term ϕ_s is the strength reduction factor for shear.

The terms V_c and V_s in Equation 2.3 are calculated as they are for general reinforced concrete design. Equations for V_c and V_s can be found in Chapter 11 of ACI 318-02. The shear capacity contribution of the external FRP shear reinforcement, V_f, is dependent upon the fiber orientation, the FRP material properties, the cross-sectional configuration of the FRP, the spacing and width of the FRP strips, and the stiffness of the FRP reinforcement. The maximum allowable FRP strain used in the design is based upon the material properties of the FRP and the stiffness of the external FRP reinforcement. The equations used to calculate V_f are not presented here, due to their length and complexity.

2.4.3 Additional Considerations for RC Flexural Members Strengthened with

External FRP Shear Reinforcement

The addition of external FRP shear reinforcement to existing RC flexural members greatly affects the formation and propagation of cracks. For uncracked RC flexural members, external FRP shear reinforcement has been shown to delay the formation of diagonal shear cracks (Khalifa and Nanni 2000). External FRP shear reinforcement also acts to control the width of cracks, even if the member is cracked before strengthening (Adhikary and Mutsuyoshi 2000; Li et al. 2001a). By reducing crack widths, aggregate interlock along crack faces is preserved and the member shear capacity is increased.

Experimental evidence suggests that the shear span to effective depth ratio, $\dfrac{a}{d}$, may significantly affect the contribution of external FRP shear reinforcement to the shear capacity of strengthened RC flexural members (Khalifa et al. 2000). Based upon tests performed on RC beams strengthened with external FRP shear reinforcement, Khalifa et al. report that the efficacy of the FRP shear reinforcement decreases as $\dfrac{a}{d}$ decreases. Based upon tests conducted on cracked T-beams, Micelli et al. (2002) concluded that strengthened members with low $\dfrac{a}{d}$ ratios are not capable of significant increases in shear

26

capacity. Failure of strengthened members with low $\dfrac{a}{d}$ ratios is often due to peeling of the FRP or failure of the mechanical anchorage.

Strengthening of RC flexural members that are subjected to negative moments is another concern that must be addressed in the use of external FRP shear reinforcement. Khalifa et al. (2000) concluded that the use of external FRP shear reinforcement is effective in regions of both positive and negative moment. This conclusion is based on the results of tests performed on two-span continuous RC beams strengthened with external FRP reinforcement and tested to failure. Khalifa et al. performed tests on a series of 27 RC beams, 19 of which were strengthened with external FRP shear reinforcement. The investigators concluded that the external FRP shear reinforcement is effective in regions of positive and negative moment, though its efficacy in negative moment regions may be reduced by flexural cracks that propagate from the top of the member. Such cracks are not restrained by the FRP shear reinforcement when the U-wrap or web-bonded configurations are used. The use of fully wrapped FRP shear reinforcement has been suggested where stress reversals and plastic hinge formation are expected in strengthened RC members (ACI Committee 440 2002).
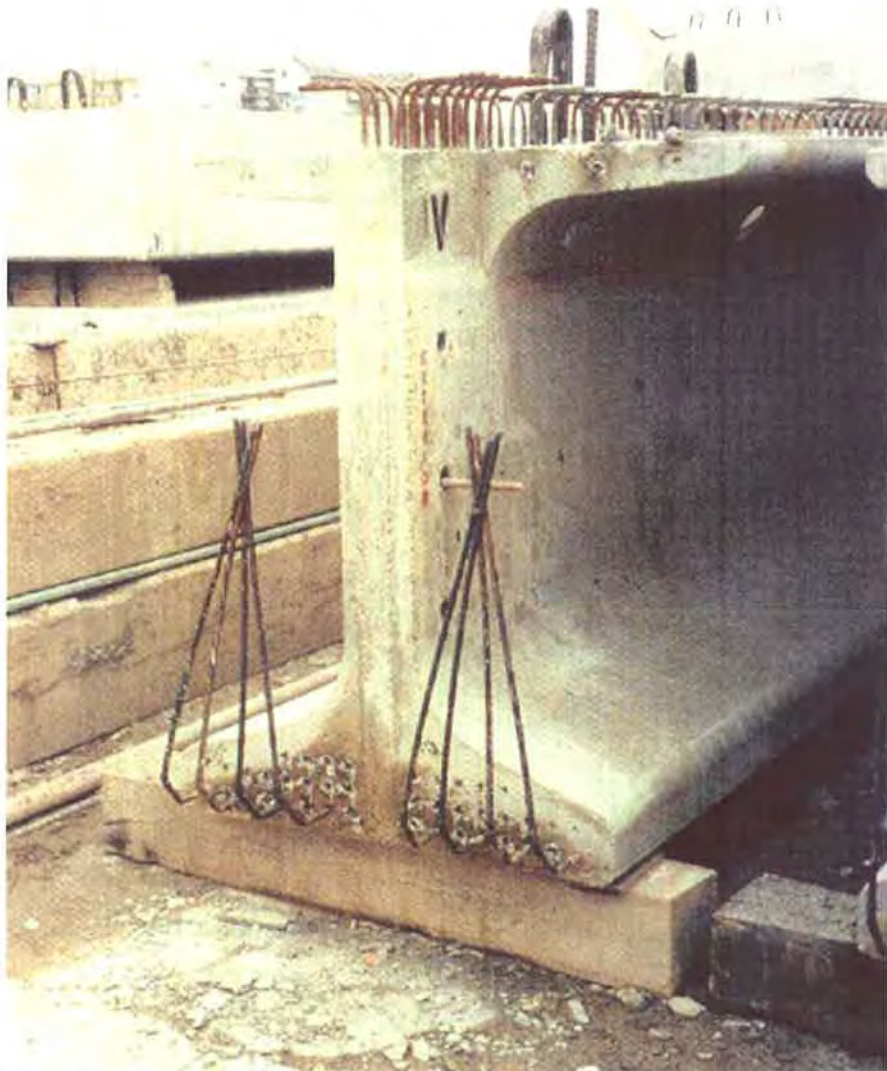
Figure 2.1 - Extended Bent Prestressing Tendons at the end of a Prestressed Concrete Girder (Noppakunwijai et al. 2002)
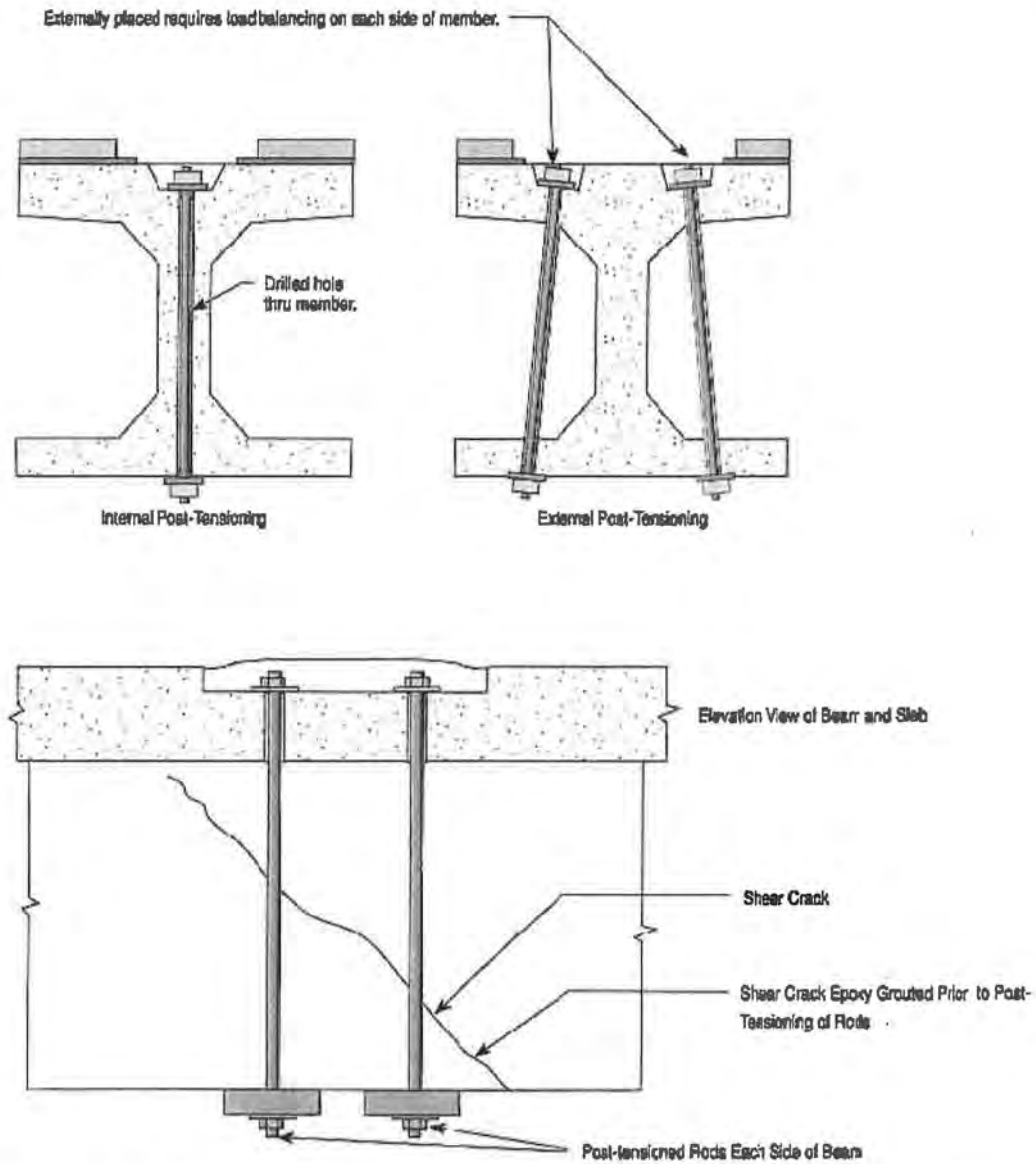
Figure 2.2 – Shear Strengthening with Post-tensioned Stirrups (Emmons 1993)

Tensioned Banding Strap

Concrete Beam Section View

Corner Load Transfer Assembly

Half Round Bar Stock

Lubricant between Half-Round and Strap

Shear Cracking

Beam

see section above

External Post-Tensioned Strap Shear Strengthening

Cracks Pressure Grouted with Epoxy Prior to Stressing of Straps

Column
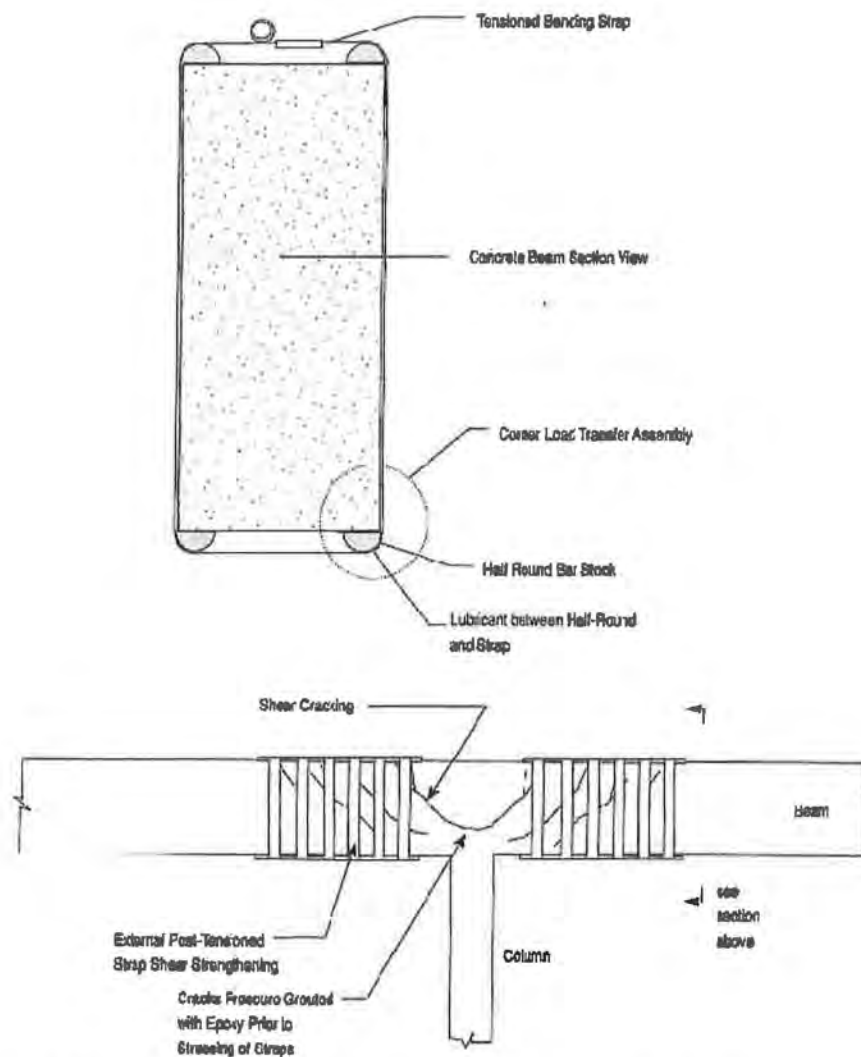
Figure 2.3 – External Post-tensioning with Composite Straps (Emmons 1993)
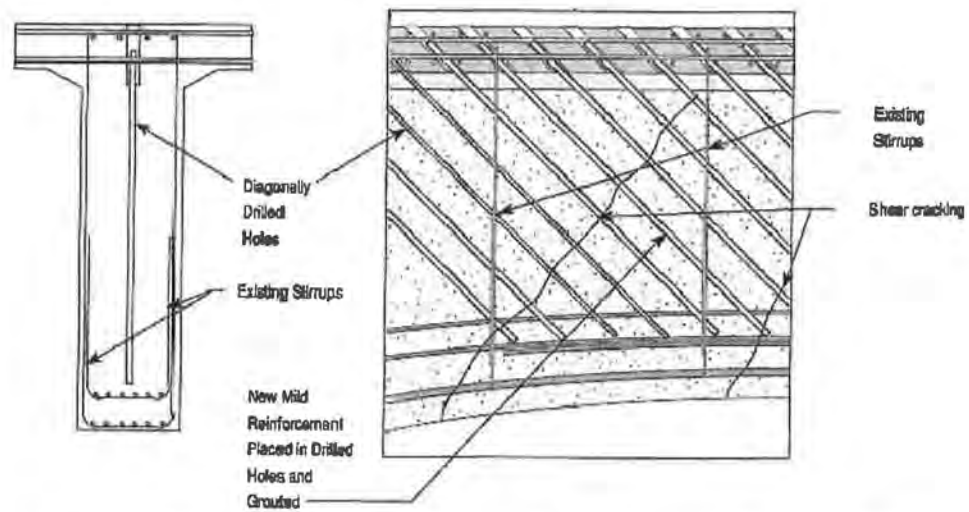
Figure 2.4 – Passive Internal Shear Reinforcement (Emmons 1993)

Fully Wrapped   U-Wrap   Web-Bonded
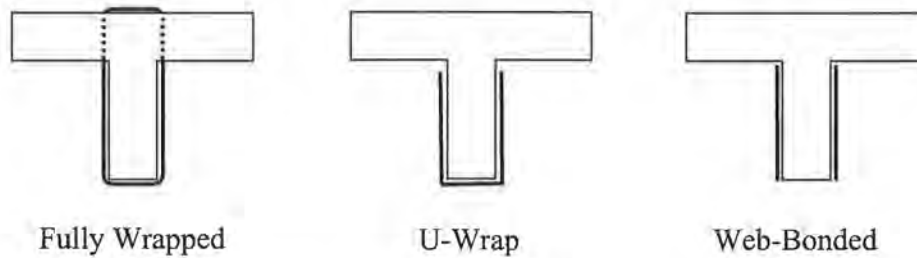
Figure 2.5 – Cross-sectional Configurations for External FRP Shear Reinforcement

(a) Continuously Bonded

(b) Discrete Strips
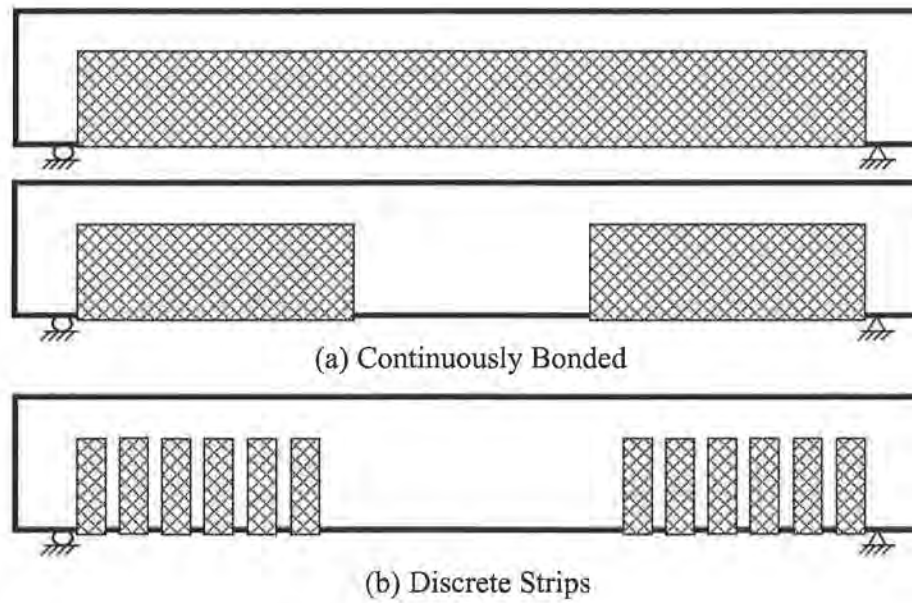
Figure 2.6 – Longitudinal Configurations for External FRP Shear Reinforcement

FRP Reinforcement

FRP Bar

Paste
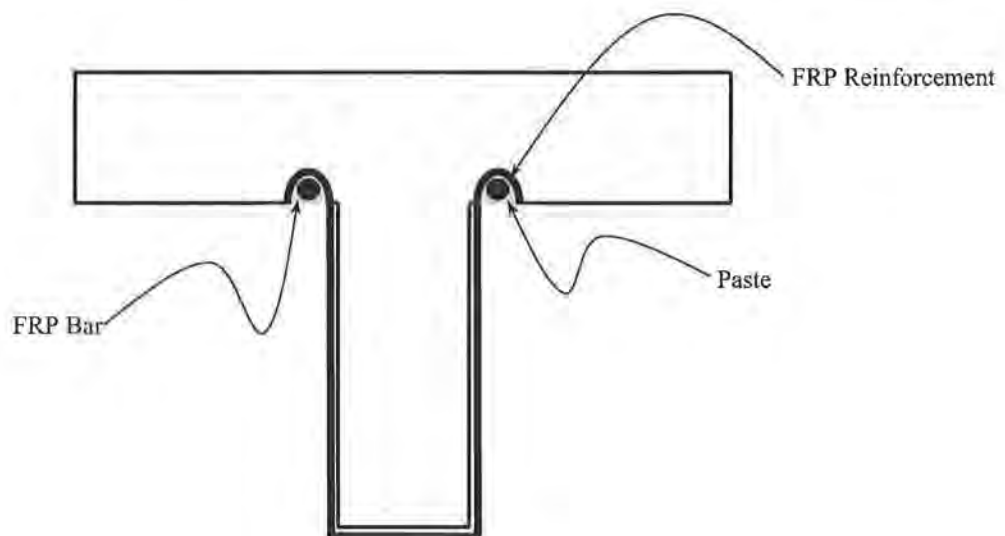
Figure 2.7 – FRP Bar End Anchor Detail

CHAPTER 3: PROJECT BACKGROUND

The Interstate 565 bridge structures in downtown Huntsville, Alabama, were erected during a five-part construction project that cost the state of Alabama $91,045,779. Construction of the 2.45 miles (3.94 km) of bridge structures began in January 1988 and was completed in March 1991 (ALDOT 1994d). Single span and multispan bridges were built in both the northbound and southbound directions. Bridges are composed of either steel girders or prestressed concrete girders and a cast-in-place composite RC bridge deck. The majority of the prestressed concrete girder bridges utilize bulb-tee girders made continuous for live load. Continuity was established to create two-, three-, and four-span continuous structures.

Fine, hairline cracks were discovered in some of the prestressed concrete bulb-tee girders during a routine bridge inspection in 1992. Hairline cracks are often seen at early ages in prestressed concrete girders and do not necessarily signify serious distress. Another inspection of the bridge was conducted 18 months later, during late March and early April of 1994. The second inspection revealed that many of the cracks discovered earlier had propagated and widened. Cracked girders were found at ten different sites between Eighth Street and Oakwood Avenue (ALDOT 1994d). Portions of I-565 affected by cracked girders are shown in Figure 3.1.

Cracks were typically located near the continuous ends of prestressed concrete bulb-tee girders made continuous. At the time of the 1994 inspection, the widest cracks had propagated through the bottom flange of the bulb-tee girder and extended into the girder web. The extent of the crack propagation varied, though some cracks extended as far as the intersection of the web and upper flange. Web-shear cracks were also present in some girders. Typical crack widths ranged from 0.002 in. (0.05 mm) to 0.25 in (6.4 mm).

ALDOT personnel felt that the affected bridges should be monitored to determine what had caused the cracks in the girder ends to become so large. Bridges were instrumented so that ALDOT personnel could monitor movements due to traffic, wind, and thermal loading. After several weeks, ALDOT personnel determined that traffic and wind loads were not a probable cause of the cracks. However, the difference in temperature between the bridge deck and the lower portion of the superstructure was causing a large upward deflection at midspan. The upward deflection sometimes exceeded the downward midspan deflection due to live loads.

Cracked girders at northbound Bent 52 were instrumented to examine if the cracks were significantly widening as a result of thermal loads. Results showed that the cracks

33

in the ends of the prestressed concrete bulb-tee girders moved both horizontally and vertically when a temperature differential of 13 °F (7.2 °C) existed between the deck slab and the underside of the superstructure. Crack movements were 0.039 in. (1 mm) or less in all cases (ALDOT 1994b). ALDOT personnel concluded that the cracks in the girders were a result of a temperature gradient between the bridge deck and the underside of the superstructure. The temperature gradient caused the superstructure to deflect upward. The upward deflection was restrained at interior supports, which resulted in the formation of positive moments at the girder ends. This phenomenon is known as "sun cambering."

During the second inspection of the bridges in 1994, face cracks in the continuity diaphragms were discovered. ALDOT personnel felt that cracks in the face of continuity diaphragms were a result of girders pulling away from the continuity diaphragm. Figure 3.2 shows the end of a prestressed concrete girder that has pulled out of the continuity diaphragm. Many of the continuity diaphragms also contained end cracks. A typical diaphragm end crack is shown in Figure 3.3.

Shortly after the inspection conducted in 1994, all of the Huntsville I-565 prestressed concrete bridges were surveyed. The inspectors performing the survey located cracks and documented their size and location relative to the girder end. The survey revealed that 3.2 percent of prestressed concrete girders made continuous contain cracks near their continuous end (ALDOT 1994c). All of the cracked girders are bulb-tee girders, either BT54 or BT63. None of the standard AASHTO girders have experienced such cracking. The results of the girder survey performed by ALDOT personnel are shown in Table 3.1.

Face cracks in the continuity diaphragms occurred more often at bents supporting bulb-tee girders. Approximately 57 percent of bents supporting bulb-tee girders have cracked diaphragm faces while only one of four bents supporting standard AASHTO girders contains face cracks. End cracks in the continuity diaphragms are present at approximately 85 percent of the bent locations. End cracks are present at all interior bents in two-span continuous structures and at all bents supporting BT54 girders (ALDOT 1994c).

Table 3.1 – Summary of Cracking in Prestressed Concrete Girders Made Continuous (ALDOT 1994c)

	BT54		BT63		AASHTO Types I, III, IV	
	# Girders	# Cracked	# Girders	# Cracked	# Girders	# Cracked
Mainline	732	33	656	9	72	0
Ramp	560	24	140	8	174	0
TOTAL	1292	57	796	17	246	0

34

Based upon the number of cracks found in the girders, their location, and their width, ALDOT personnel decided that action was necessary and that cracks in the girders needed to be remedied. Temporary supports, or false supports, were installed under all spans containing cracked girders in order to prevent collapse of the structure. A gap was left between the top of the false supports and the prestressed concrete girders to allow for deflection of the girders. The supports were placed within 10 ft (3.0 m) of bents supporting cracked bridge girders. A typical false support is shown in Figure 3.4.

ALDOT personnel also epoxy injected cracks in the ends of the affected prestressed concrete girders. A girder with epoxy-injected cracks is shown in Figure 3.5. Subsequent inspections of the cracked bridge girders revealed that new cracks formed in the vicinity of the epoxy-injected cracks. The new cracks have widths of 0.002 in. (0.05 mm) to 0.030 in. (0.8 mm) and formed adjacent to the existing epoxy-injected cracks. The presence of the new cracks has discouraged ALDOT personnel from reusing epoxy-injection as a means of repair for the cracked prestressed concrete bridge girders.

An attempt was also made to release some of the prestressed girders from the continuity diaphragm. This was accomplished by sawing the continuity diaphragm around the girder, allowing the girder to pull away from the diaphragm and act as though it were simply supported. Engineers believed that this procedure would prevent growth of existing cracks and prevent new cracks from forming in the girder ends. Sawing of the continuity diaphragm was performed at one bent located just east of Derrick Street, between Clinton Ave. and Holmes Ave.

Construction and installation of false supports, epoxy injection of cracks, sawing of continuity diaphragms, and long-term monitoring of the structures was estimated to cost the state a total of $500,000. This figure included the cost of all labor and material required for the repairs and long-term monitoring. According to an article from the *Birmingham Post-Herald*, 19 April 1995, completed repairs, monitoring, and testing of the Huntsville I-565 bridge structures had already cost the state of Alabama $312,000.

3.1 STRUCTURAL GEOMETRY AND DETAILS

In the following sections, geometric details of the Huntsville I-565 bridge structures selected for this research are presented. Northbound Spans 4, 5, 10, and 11 were the main focus of the research. These four spans will be referred to as the critical spans from this point forward. Most of the girders in the critical spans showed similar crack patterns at their continuous ends.

3.1.1 Huntsville I-565 Bridge Structures

Northbound Spans 4 and 5 form a two-span continuous structure composed of prestressed concrete bulb-tee girders made continuous for live load and a cast-in-place composite reinforced concrete deck. The length of each span is 98.29 ft (29.96 m), as measured along the centerline of the bridge deck from the centerline of the interior bent to the joint at the simply supported end of the span. The two-span structure is slightly curved, having a radius of horizontal curvature of about 1950 ft (594 m). Each span has a central subtended angle of 2.87°. Each span has nine prestressed concrete bulb-tee (BT54) girders.

Northbound Spans 10 and 11 form a similar two-span continuous structure. Each span has a length of 101.40 ft (30.91 m) and zero horizontal curvature. Both spans are composed of nine prestressed concrete bulb-tee (BT54) girders. The span length and girder length are not the same in the critical spans, due to the presence of the continuity diaphragm and the position of the bearing pads at either end of the girder. Table 3.2 summarizes the actual length and clear span length of individual prestressed girders in the critical spans.

Continuity was established between adjacent spans by casting a continuity diaphragm to restrain the rotation of the girder ends. A portion of the deck slab was cast monolithically with the continuity diaphragm. Vertical reinforcement is provided in the continuity diaphragm in the form of #4 and #6 mild steel reinforcing bars. Mild steel bent bars protruding from the ends of the prestressed concrete bulb-tee girders were used to provide positive moment reinforcement for the continuity diaphragm. The longitudinal steel reinforcement in the deck slab acts as negative moment reinforcement. Details of the continuity connection created at the interior support are shown in Figure 3.6, though the vertical reinforcement provided in the continuity diagram is not shown.

Table 3.2 – Girder Lengths and Clear Span Lengths for Critical Spans

	Girder Length (feet)	Clear Span Length (feet)
Spans 4/5, Girder 1	96.08	95.17
Spans 4/5, Girder 5	97.69	96.77
Spans 4/5, Girder 9	99.30	98.38
Spans 10/11, All Girders	99.42	98.50

1 ft = 0.305 m

Figure 3.7 shows the cross section of a typical critical span. The girder spacing is 96 in. (2440 mm), measured between the centerline of adjacent girders. Additional dimensions are shown in the figure. Cast-in-place diaphragms exist at midspan, though they have not been shown in the figure.

3.1.2 Prestressed Concrete Bulb-tee Girders

All of the girders in the critical spans are standard prestressed concrete bulb-tee (BT54) girders with a depth of 54 in. (1321 mm). The use of bulb-tee girders was proposed as part of a value engineering redesign of the Huntsville I-565 bridge structures. Standard AASHTO girders had been chosen for use in the original design. Cross section dimensions and details for a BT54 girder are shown in Figure 3.8.

All girders in the critical spans have identical reinforcement details. All girders contain longitudinal prestressing tendons and mild steel shear reinforcement. Longitudinal mild steel bent bars protrude from the ends of some girders. Reinforcement details vary between cross sections, due to the harped prestressing tendons and variable stirrup spacing.

Each girder was reinforced with a total of 38 prestressing tendons. Thirty-four of the tendons are 0.5 in. (12.7 mm) special, low-relaxation, prestressing tendons jacked to a stress of 202.5 ksi (1400 MPa). Six of the 0.5 in. special prestressing tendons are harped. Harped tendons have a constant eccentricity within 120 in. (3050 mm) of the girder midpoint and a slope of 0.08134 radians elsewhere. The longitudinal layout of the 0.5 in. special prestressing tendons for a typical BT54 girder is shown in Figure 3.9. The other four tendons are 7/16 in. (11.1 mm) diameter low-relaxation prestressing tendons jacked to a stress of 69.6 ksi (480 MPa). The 7/16 in. tendons are located near the top of the cross section. Because these tendons were not fully stressed, they were not considered in the calculation of the girder shear and flexural capacities.

Cross sections of a typical girder are shown in Figure 3.10 (girder end) and Figure 3.11 (midspan). As shown in Figure 3.10, twelve of the 28 straight prestressing tendons are partially debonded. Two are partially debonded for a length of 168 in. (4270 mm), and ten are partially debonded for a length of 48 in. (1220 mm).

A total of eight mild steel bent bars exist at all girder ends made continuous for live load. The eight bent bars act as positive moment reinforcement for the continuity diaphragm. The bent bar reinforcement has a total length of 61 in. (1550 mm). They are embedded 41 in. (1040 mm) into the girder end and extend 8 in. (200 mm) into the continuity diaphragm. The remaining 12 in. (305 mm) forms the vertical leg. The location and dimensions of the eight bent bars are shown in Figures 3.6 and 3.12.

Spacing of the vertical shear reinforcement, or stirrups, varies along the length of a typical girder. Stirrup spacing varies from 3.5 in. (89 mm) at the girder ends to 12 in.

(305 mm) within the span. The size of the stirrups also varies along the length of the member. For stirrups within 24 ft (7.3 m) of midspan, #4 bars were used to create the vertical legs of the stirrups. Stirrups outside of this region have vertical legs made from #5 bars. Figure 3.13 shows the location of the vertical shear reinforcement in a typical BT54 girder.

Due to the complex shape of the BT54 girders used, the stirrups are composed of multiple pieces of mild steel reinforcement. Fewer bends are required when the stirrups are made from multiple pieces of mild steel reinforcement and the stirrups can be fabricated and tied more easily. The use of lap splices creates a closed stirrup. Table 3.3 shows the details of the various mild steel reinforcing bars used to make the stirrups. Figures 3.14 and 3.15 show the cross-sectional arrangement of the individual stirrup reinforcing bars at the girder ends and in the midspan region.

3.1.3 Bridge Deck Slab

The bridge deck slab is composed of cast-in-place reinforced concrete and is reinforced with mild steel reinforcement in both the longitudinal and transverse directions. The bridge deck slab was designed to act compositely with the girders below it. The composite action was created by extending the stirrups in the prestressed concrete girders into the slab and by roughening the top surface of the girder. The thickness of the slab is 6.5 in. (165mm), though a "build-up" exists over each girder. The thickness of the "build-up" varies from 1.75 in. (45 mm) at midspan to 4.00 in. (100 mm) at the supports. The "build-up" was assumed to be 1.75 in. thick in the determination of the girder shear and flexural capacities.

Longitudinal and transverse reinforcement in the deck slab is provided by mild steel reinforcing bars. The diameter of the reinforcing bars used in the deck slab ranges from 0.50 in. (12.7 mm) to 0.875 in. (22.2 mm). The transverse reinforcement does not contribute to the shear or flexural capacity of the structure and was disregarded during analysis. The longitudinal reinforcement acts as negative moment reinforcement and resists tension forces in the deck slab induced by shear. The longitudinal reinforcement in the deck slab is shown in Figure 3.16. The #7 (22.2 mm diameter) bars are not continuous throughout the entire two-span structure, though they are continuous over the interior support. The #7 bars extend a minimum of 15 ft (4.6 m) beyond the centerline of the continuity diaphragm toward midspan. Some of the #7 bars extend an additional 10 ft (3.0 m) toward midspan. All other longitudinal reinforcement is continuous throughout both spans.

3.2 MATERIAL PROPERTIES

Concrete used to make the prestressed concrete girders had a 28-day design compressive strength, f_c', of 6000 psi (41 MPa). The concrete used for the cast-in-place RC bridge deck had a 28-day design compressive strength of 4000 psi (28 MPa). All concrete used for the prestressed concrete girders and the bridge deck is of normal weight. Design properties of the concrete were used for all calculations.

Prestressing tendons are of various sizes, though they all have the same material properties. All tendons are seven-wire, low-relaxation prestressing tendons. The nominal ultimate tensile strength of the tendons is 270 ksi (1860 MPa). The elastic modulus of the tendons is assumed to be 28,500 ksi (200 GPa).

Mild steel reinforcement was also used throughout the prestressed concrete girders and cast-in-place RC bridge deck. The size of the mild steel reinforcing bars varies, though the material properties are the same. All mild steel reinforcing bars have an ultimate tensile strength of 40 ksi (275 MPa) and have an elastic modulus of 29,000 ksi (200 GPa).

3.3 CRACKS IN THE HUNTSVILLE I-565 PRESTRESSED CONCRETE BRIDGE GIRDERS

As stated previously, many of the girders in northbound Spans 4, 5, 10, and 11 show similar cracking near their continuous ends. The girders contain cracks through the bottom flange that have propagated into the web. Web-shear cracks are also present in some girders, though the width of web-shear cracks tends to be much smaller. Figure 3.17 shows the extent of the cracking in northbound Spans 4 and 5. Figure 3.18 shows the cracking in northbound Spans 10 and 11. Two girders in northbound Span 5 had the most severe cracking near the continuous girder end, Girders 4 and 5. An elevation view of Girders 4 and 5 is shown in Figure 3.19.

The presence of the cracks in the girder ends gives reasonable cause to think that the effective prestressing force may have been reduced in the end of the girder. Evidence to support this hypothesis is provided by the position and width of the cracks, as well as the behavior of the girders under live loads. If the cracks have caused a loss of the effective prestressing force, the shear and moment capacities of the cracked girders may have been significantly reduced. Some potential scenarios regarding the amount of effective prestressing force remaining in the girder end are presented in this section.

For cracks as wide as 0.25 in. (6.4 mm) to remain open, a large positive moment would have to exist at the cross section containing the crack. Even if all continuity at the interior support is lost, the greatest positive moment induced at the cracked section by service loads has a magnitude of 2800 kip-in. (3800 kN-m). A moment with that magnitude will not cause cracks with widths exceeding 0.125 in. (3.2 mm) to form.

Positive moments forming at the cracked cross section as a result of thermal loads may be large enough to cause cracks with such widths to open temporarily. The wide cracks will only stay open as long as the thermal loads are imposed on the bridge structure, though. Thus, the cracks in the girder ends must remain open as a result of inelastic behavior at the cross section caused by slippage of the prestressing tendons.

An alternative theory suggests that inelastic behavior at the cracked cross section resulted from yielding of the prestressing tendons. If yielding was possible, a portion of the strain in the prestressing tendon would be lost upon removal of the applied loads. This would result in a reduction of the effective prestressing force transferred to the end region of the girder, the magnitude of which would depend on the amount of plastic strain developed in the tendons during yielding. Once they have yielded, the prestressing tendons may remain bonded and provide strength as passive reinforcement, but they would no longer transfer a significant amount of prestressing force into the girder end region.

The development of yield level stresses in prestressing tendons is possible, though it requires that the tendons be adequately anchored on both sides of the crack. The development length of a 0.5 in. (12.7 mm) special prestressing tendon is 80 in. (2030 mm), as calculated by Article 5.11.4.2 of the "AASHTO LRFD Bridge Design Specifications" (AASHTO 2002). Cracking in the girders occurs within 41 in. (1040 mm) of the continuous girder end, which is much less than a full development length. Because the tendon is anchored over such a short distance, development of such high stresses in the prestressing tendons is not likely.

The width of a flexural crack in a concrete member is related to the stress in the steel reinforcement crossing the crack. Knowing this, it can be assumed that the width of the crack is equal to the elongation of the reinforcement over some effective length. Thus, a crack with a width of 0.25 in. (6.4 mm) acting over a 60 in. (1520 mm) effective length (30 in. on either side of the crack) results in a reinforcement strain of about 0.004. A strain of this magnitude is equivalent to a stress of 114 ksi (790 MPa). If this stress is added to the prestressing force already present in the tendon, which is conservatively estimated to be 160 ksi (1100 MPa), the theoretical total stress in the tendon approaches or exceeds the ultimate strength of the prestressing tendons.

The hypothesis that the effective prestressing force in the end region of the girder has been lost was further validated with a simple analytical method. The amount of slippage experienced by the tendons if all prestressing force was lost was estimated by integrating the strain change in a single prestressing tendon from the girder end to the crack location, as shown in Equation 3.1. The strain in a single prestressing tendon is plotted for the cracked end region of the girder in Figure 3.20.

40

$$w_c = \int_a^b \varepsilon_{ps} dL = \int_0^{l_t} \left(\frac{f_{pe}}{l_t E_{ps}} x \right) dx + \int_{l_t}^{l_{crack}} \left(\frac{f_{pe}}{E_{ps}} \right) dx \qquad \text{Eq. 3.1}$$

It was shown that by assuming a transfer length of 30 in. (760 mm), a total slip of 0.150 in. (3.8 mm) is expected. This correlates well with the width of the large cracks in the girders, which range from 0.125 in. (3.2 mm) to 0.25 in. (6.4 mm). Thus, it may be concluded that the prestressing tendons have slipped as a result of the cracks in the girder end and all of the prestressing force in the tendons has been lost.

3.4 CURRENT RESEARCH ON THE HUNTSVILLE I-565 CRACKED BRIDGE GIRDERS

Auburn University has previously been engaged in research concerning the time-dependent behavior and cracking of the Huntsville I-565 bridge girders. The research focused on the development of stresses in the prestressed concrete girders and the continuity diaphragm due to time-dependent and thermal effects. The effect of the construction sequence used to erect the structures was also examined. An analytical procedure was developed to calculate the stresses in the girder, deck slab, and continuity diaphragm using a finite time interval method. Stresses resulting from time-dependent effects and dead loads were superimposed with the stresses resulting from the thermal loads on the structure.

Results of the analytical study indicate that cracking near the continuous ends of the prestressed girders is a result of the temperature gradient between the bridge deck and the girders (Gao 2003). Time-dependent effects induce tensile stresses in the bottom flange of the continuous girder end, though by themselves they should not be able to cause cracking in the girder until the girders have reached an age of at least 10 years (Gao 2003). Positive moments forming in and near the continuity diaphragm as a result of the thermal gradient have been great enough to cause cracking in the girders since early girder ages. The relatively short embedment length of the mild steel bent bar reinforcing bars used to create the continuity connection at the interior support are thought to have contributed to the formation of cracks in the girder ends, due to the concentration of tensile stresses at the end of the bars in a region where the effective prestress force is not fully developed (Gao 2003).
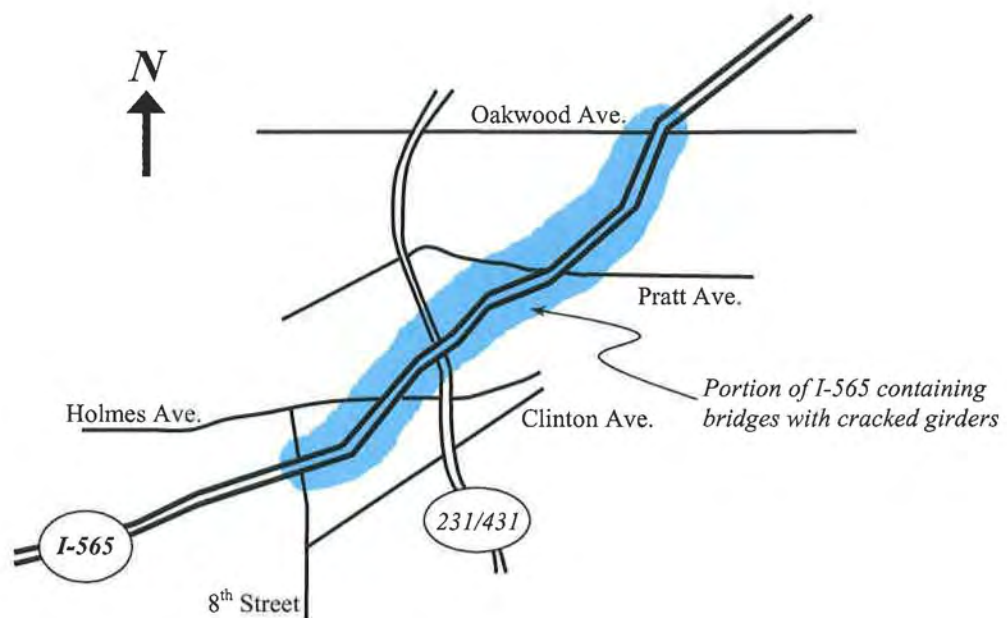
Figure 3.1 – Map of downtown Huntsville, Alabama

Figure 3.2 – Typical Pull-out Failure of a Prestressed Concrete Bulb-tee Girder

Figure 3.3 – Typical End Crack in a Continuity Diaphragm

Figure 3.4 – Typical False Support

Figure 3.5 – Typical Girder with Epoxy-injected Cracks

8"

3"

MK-651 bent bar (8 pcr
girder end made continuous)

MK-651 bent bar detail

12"

49"

Black – 9" x 24.5" x ¾" Elastomeric Bearing Pad
Checked – ¾" Premolded Bituminous Filler

¾" diameter dowel, 21" long
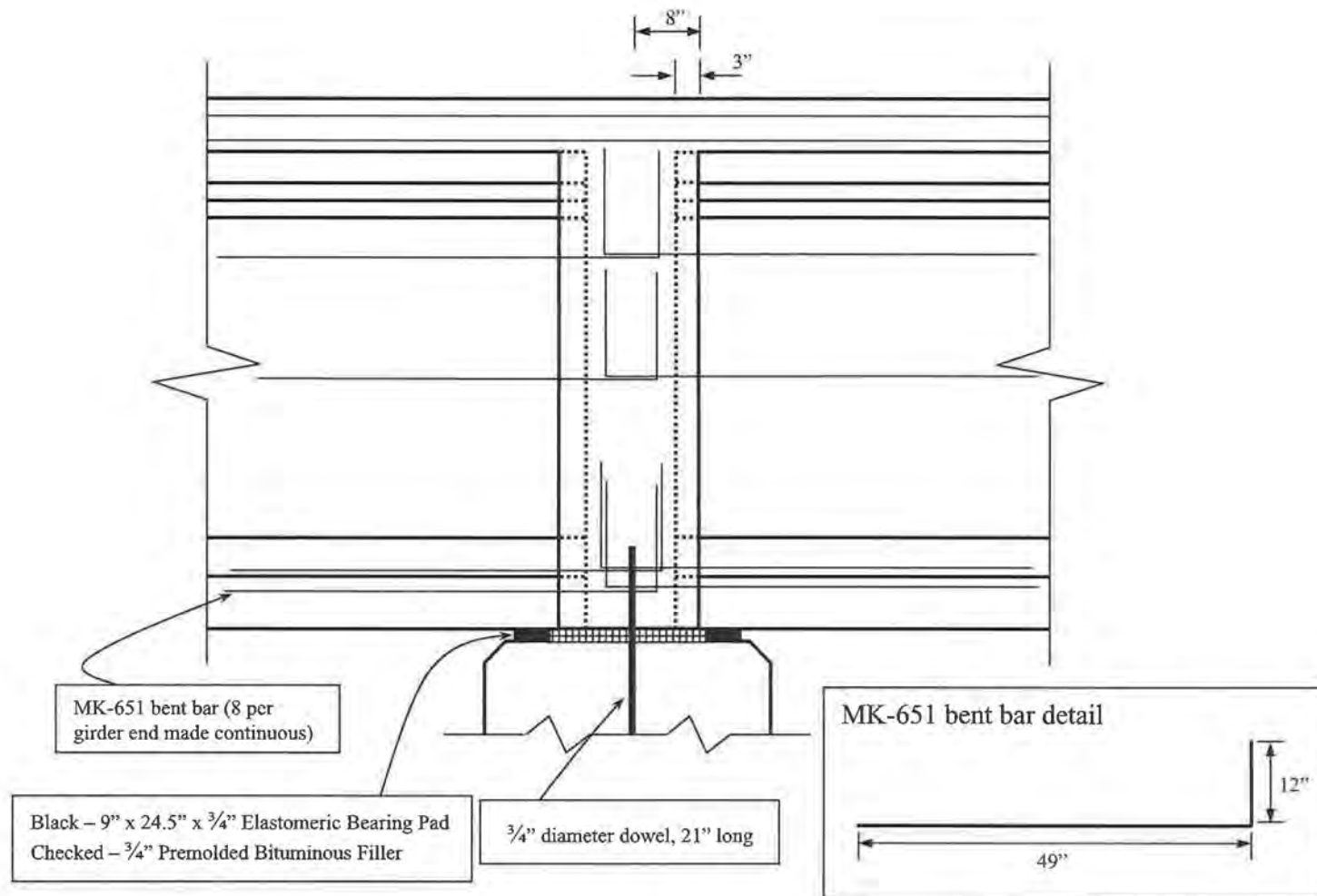
Figure 3.6 – Detail of Continuity Diaphragm at Interior Support

45
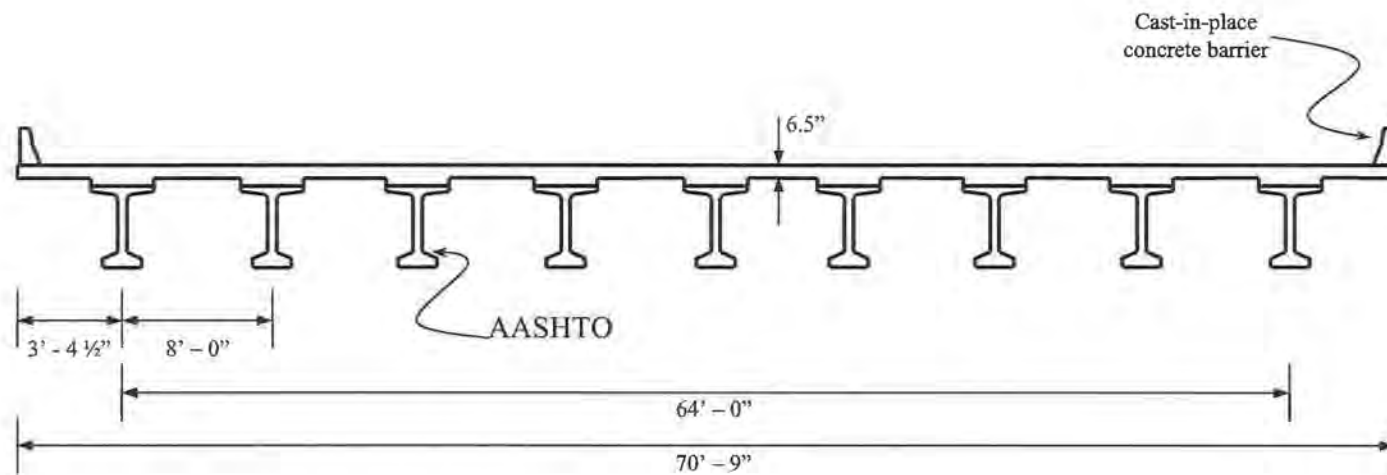
Figure 3.7 – Cross Section of a Typical Critical Span

42"

3.5"
2"
2"

2"

18"

6"

36"

54"

Cross Section
Properties

$A = 659$ in.^{2}
$I = 268077$ in.^{4}
$h = 54$ in.
$y_t = 26.37$ in.
$w = 686$ plf

10"

4.5"

6"

26"

¾" chamfer
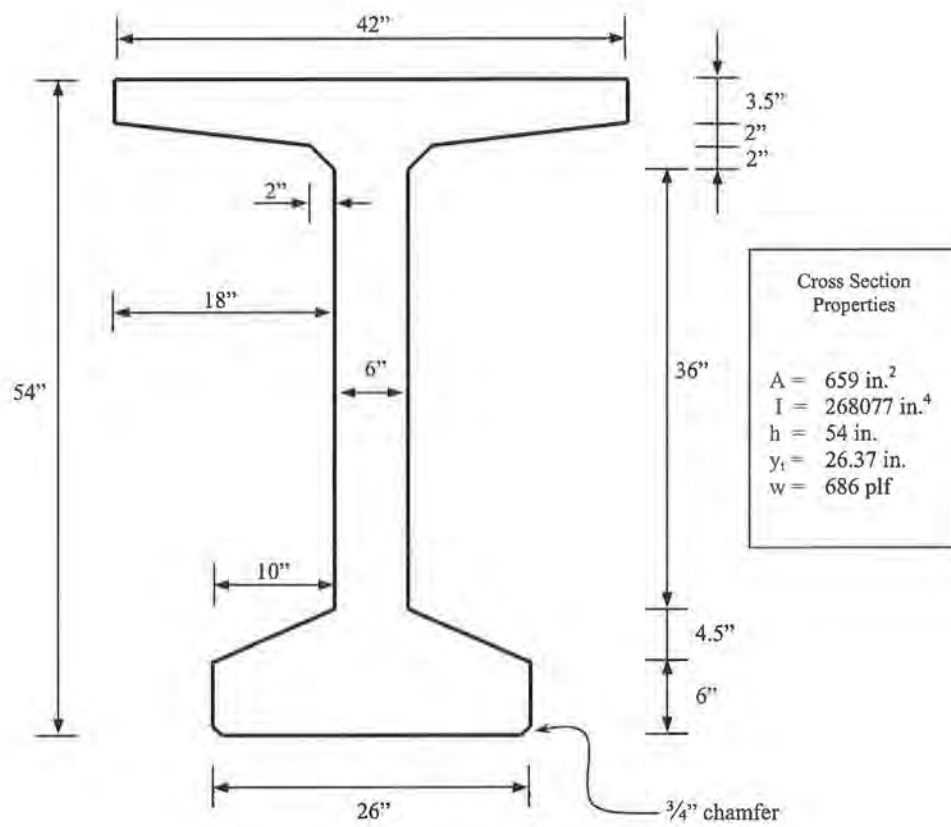
Figure 3.8 – Cross Section of a Typical BT54 Girder
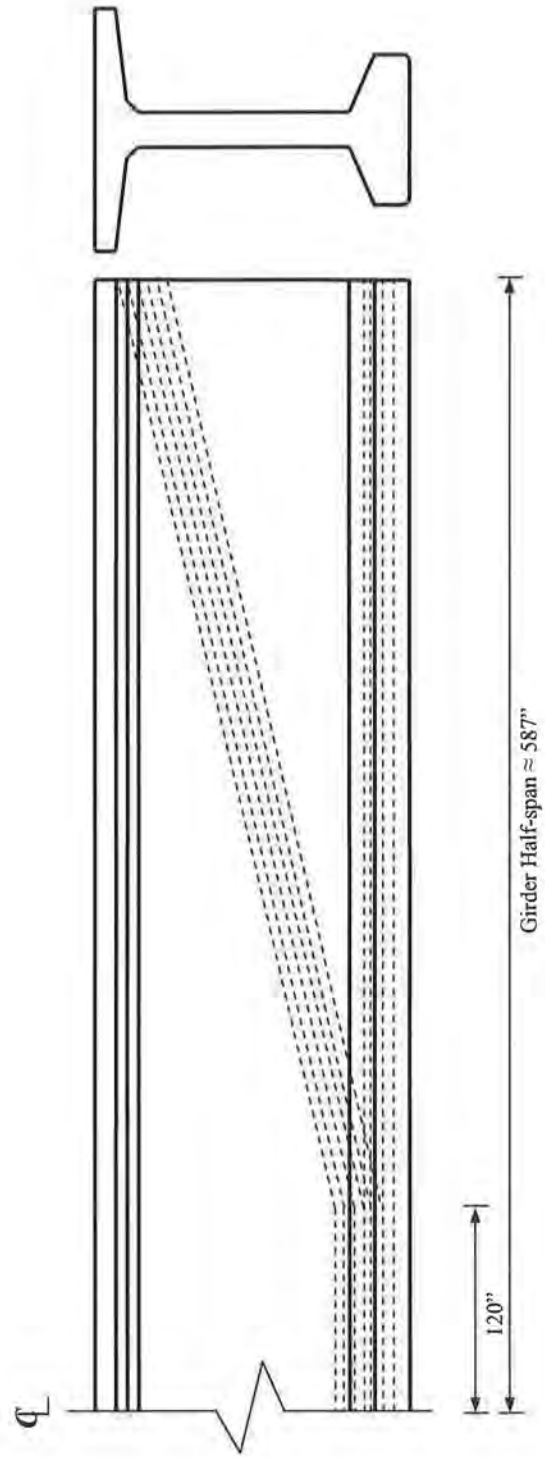
Figure 3.9 – Longitudinal Profile of Prestressing Tendons

Girder Half-span ≈ 587"

120"

℄

48
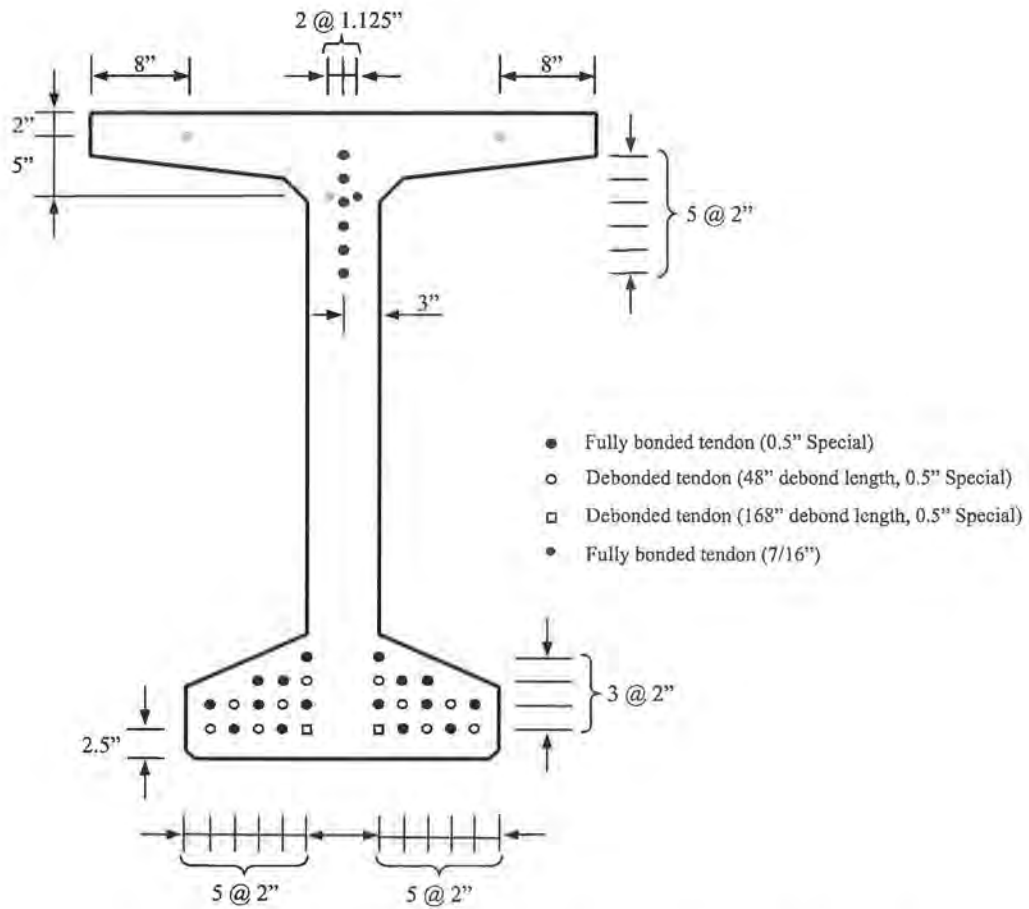
Figure 3.10 – Cross-sectional Prestressing Tendon Profile at Girder End
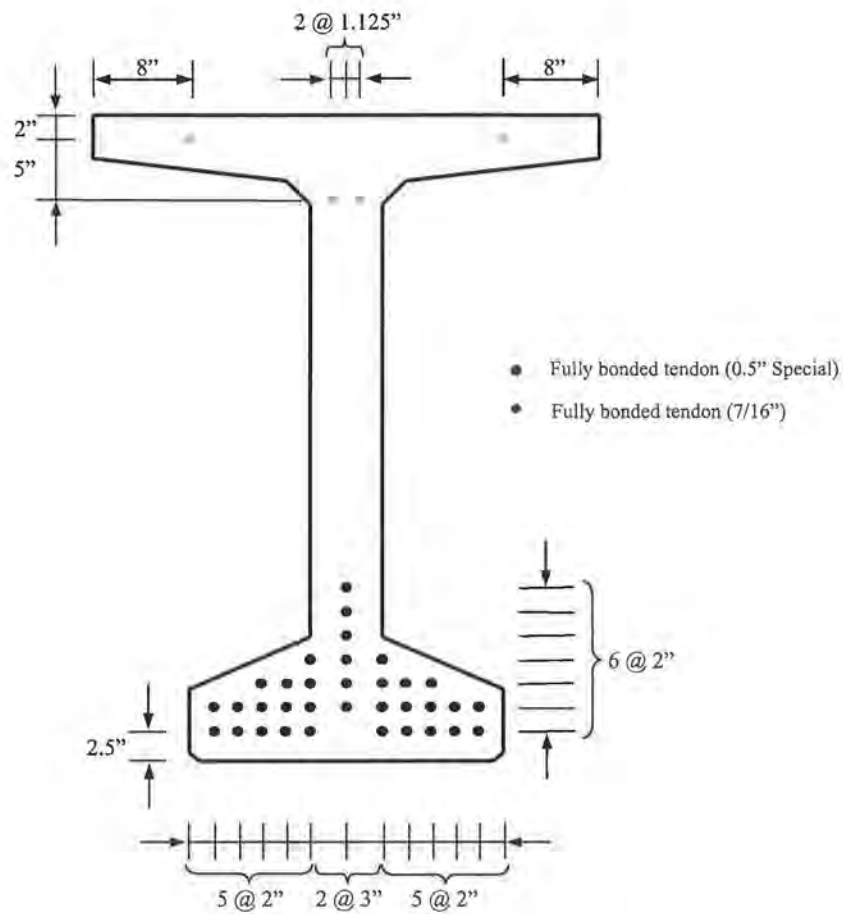
Figure 3.11 - Cross-sectional Prestressing Tendon Profile at Midspan
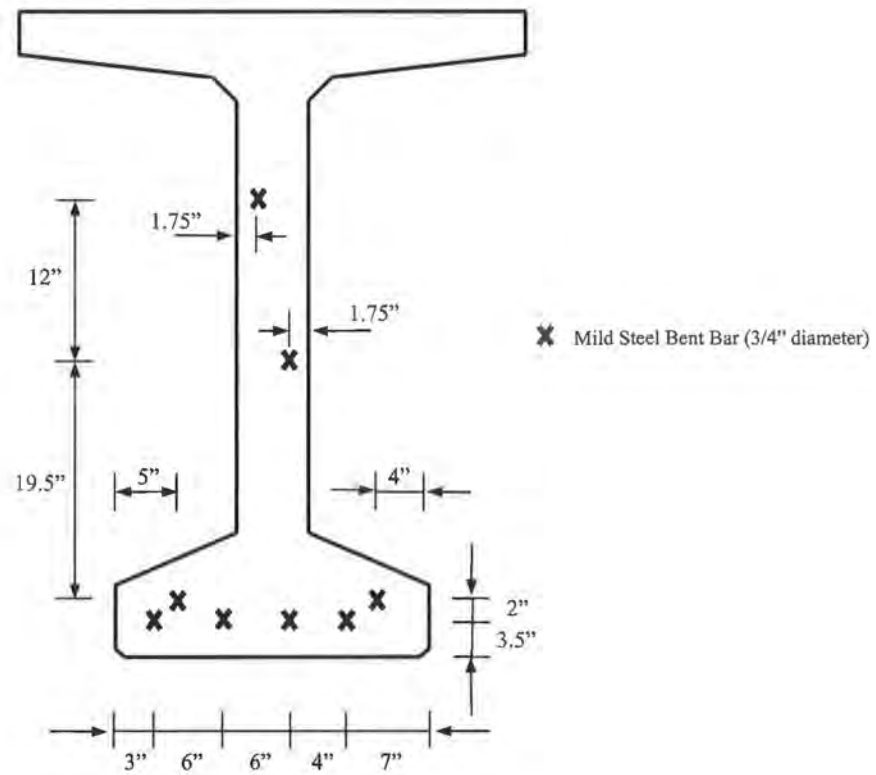
Figure 3.12 – Location of Mild Steel Bent Bars

1.5" clear spacing at girder end

Spaces @ 12" to midspan   7 spaces @ 6"   5 spaces @ 3.5"

-- All stirrups within 24' of midspan are #4 bars @ 12"
   spacing. All other stirrups are #5 bars, spaced as
   shown above.
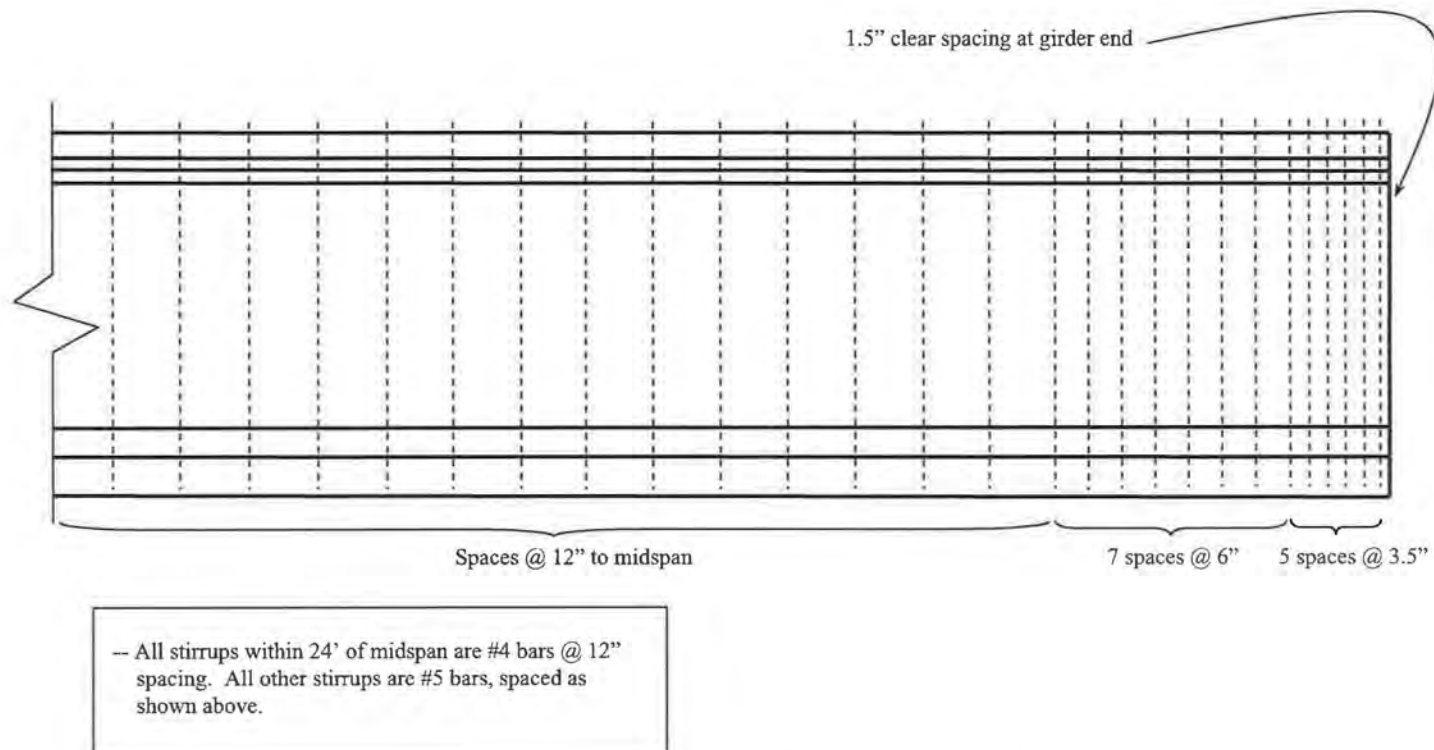
Figure 3.13 – Location of Vertical Shear Reinforcement in a Typical BT54 Girder

MK-451 stirrup,
1.25" cover

MK-352 stirrup,
1.125" cover

MK-553 stirrup,
2.125" cover

● Fully bonded tendon (0.5" Special)

○ Debonded tendon (48" debond length, 0.5" Special)

□ Debonded tendon (168" debond length, 0.5" Special)

● Fully bonded tendon (7/16")

MK-351 stirrup,
1.50" cover
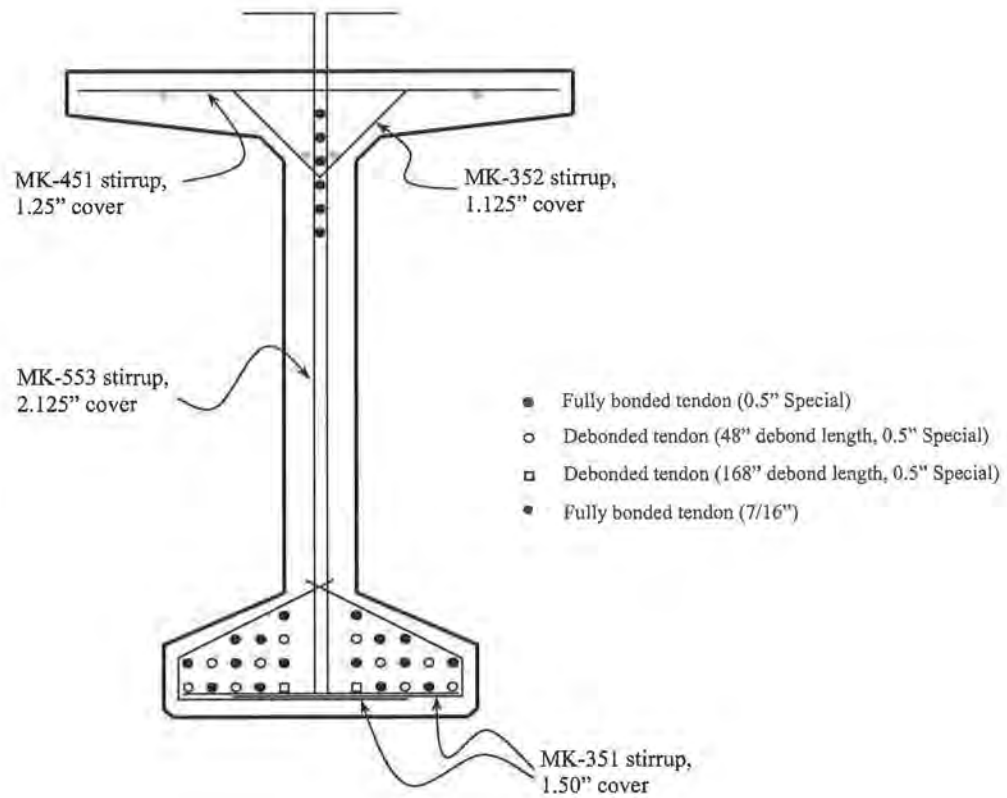
Figure 3.14 – Cross-sectional Configuration of the Vertical Shear Reinforcement at the Girder End
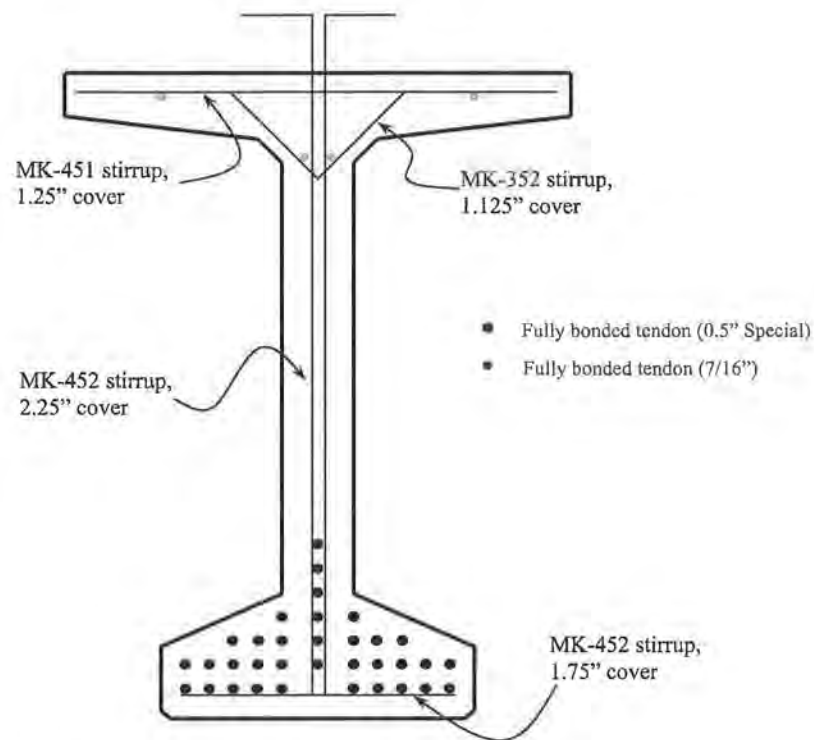
Figure 3.15 - Cross-sectional Configuration of the Vertical Shear Reinforcement at Midspan

2" clear cover on top of composite slab (typical)

■ #5 Bars, Bottom of Slab (E_1)
○ #4 Bars, Bottom of Slab (D_3)
● #4 Bars, Top of Slab (D_1)
△ #7 Bars, Top of Slab (F_1 and F_2)
▲ #7 Bars, Bottom of Slab (F_3 and F_4)

Transverse deck

1" clear cover on
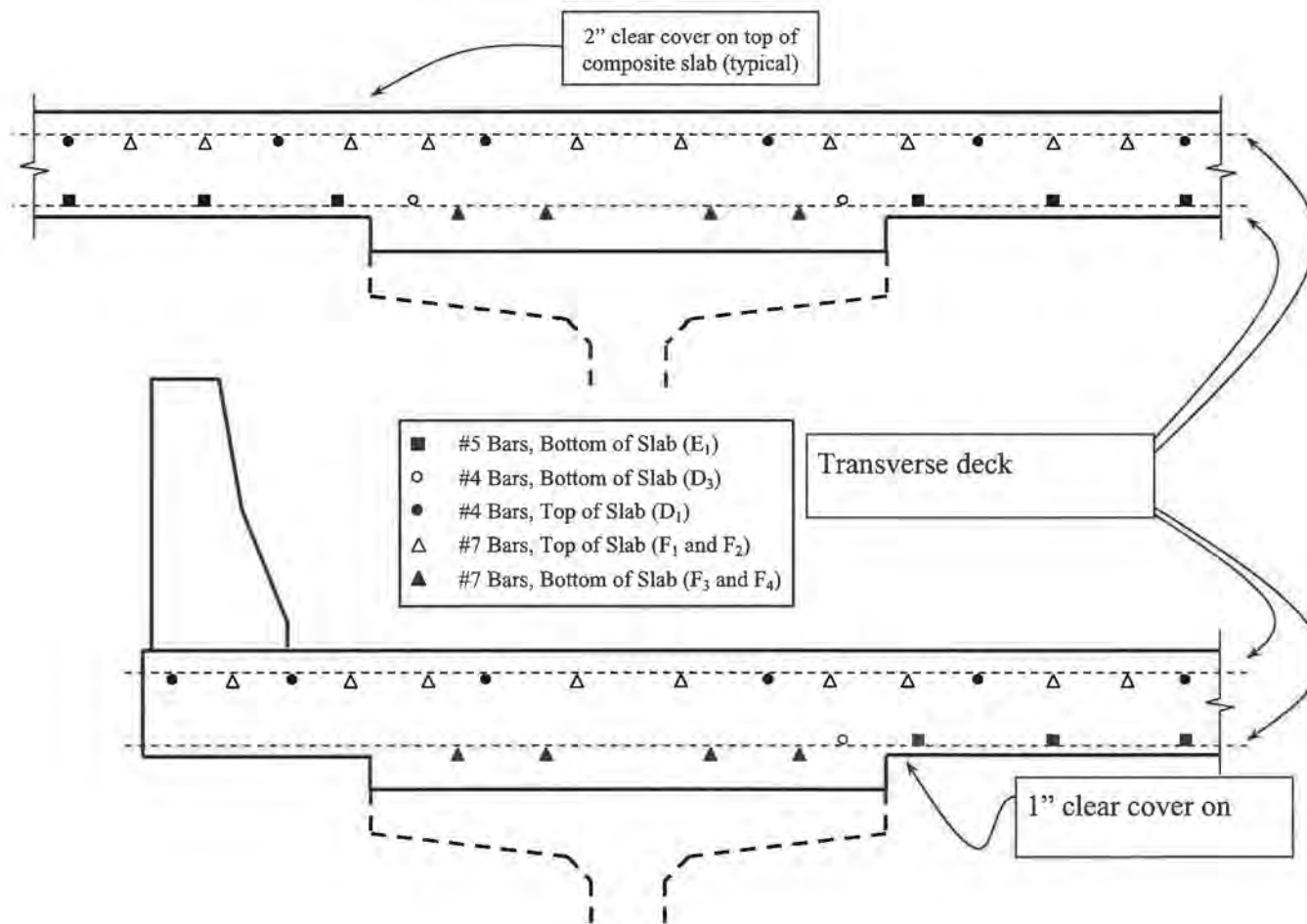
Figure 3.16 – Longitudinal Mild Steel Reinforcement in the Deck Slab

56

* Additional cracking was found to have occurred at these locations upon inspection of the bridge girders from 12/94 – 01/95.

CG = cracked girder
CDF = cracked diaphragm face

-- Markings in **bold face** were omitted in some reports
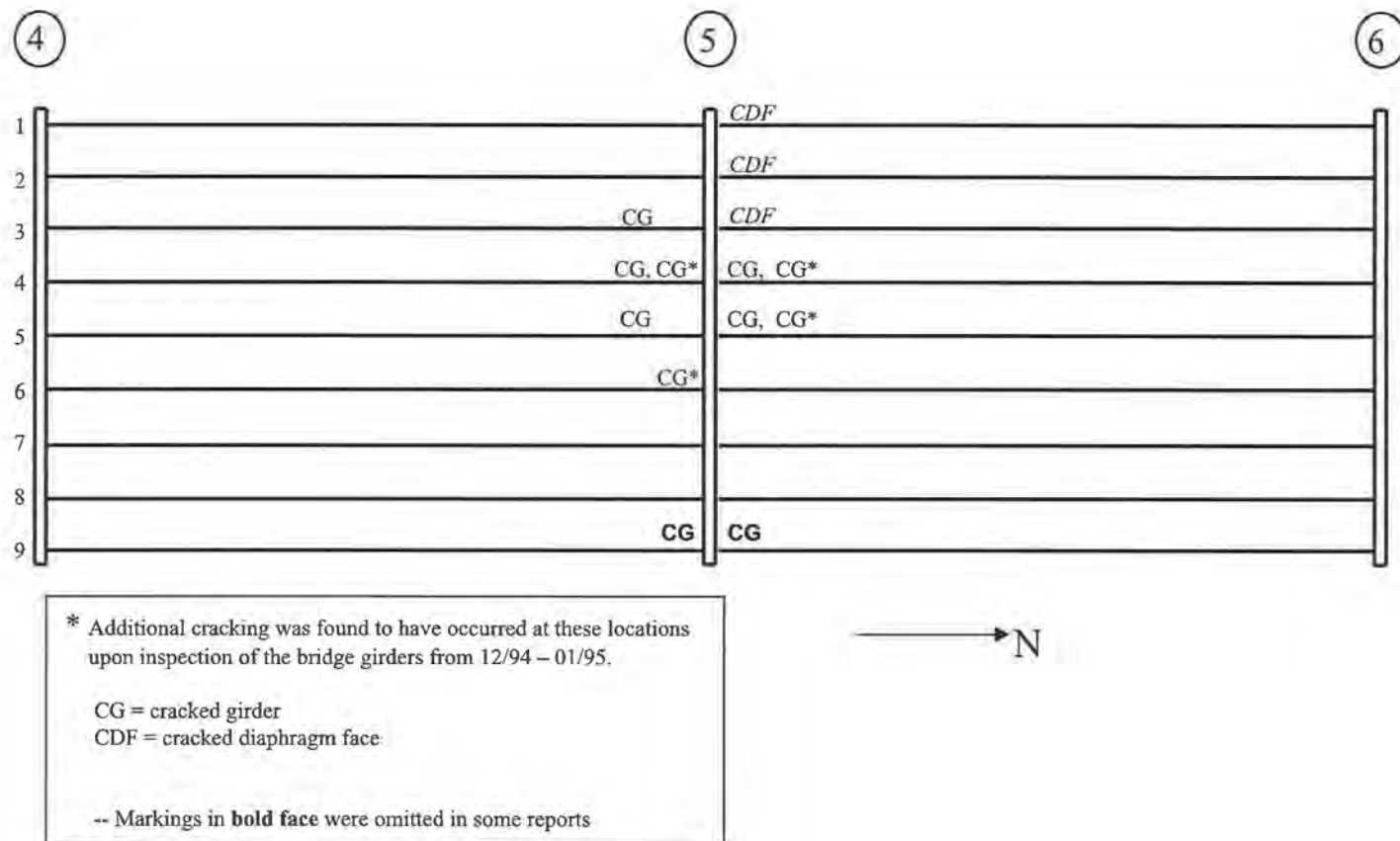
Figure 3.17 – Cracking in Bulb-tee Girders in Northbound Spans 4 and 5 (ALDOT 1994a)

57
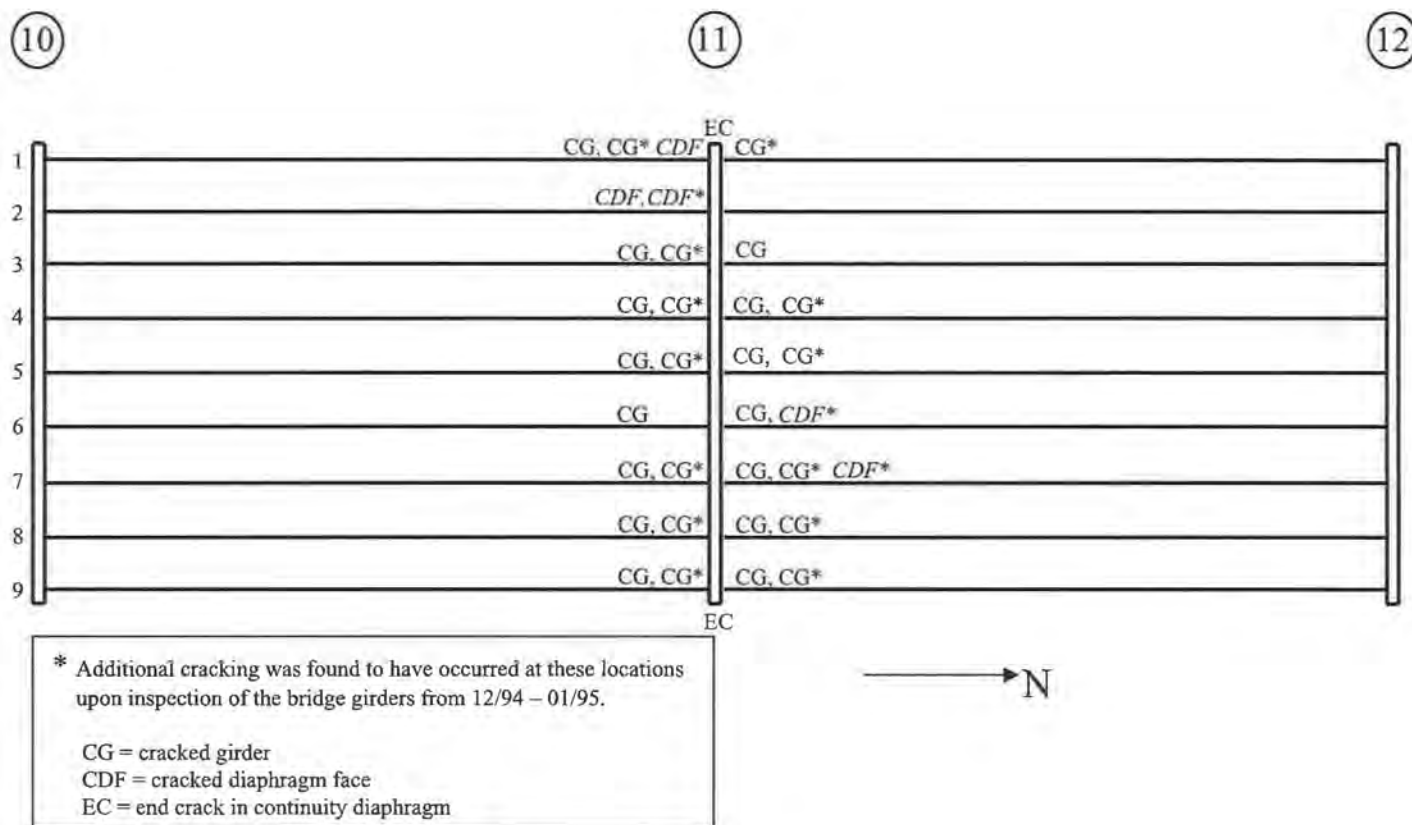
Figure 3.18 – Cracking in Bulb-tee Girders in Northbound Spans 10 and 11
(ALDOT 1994a)

Girder 4, Span 5, West View Crack Pattern

Girder 5, Span 5, West View Crack Pattern
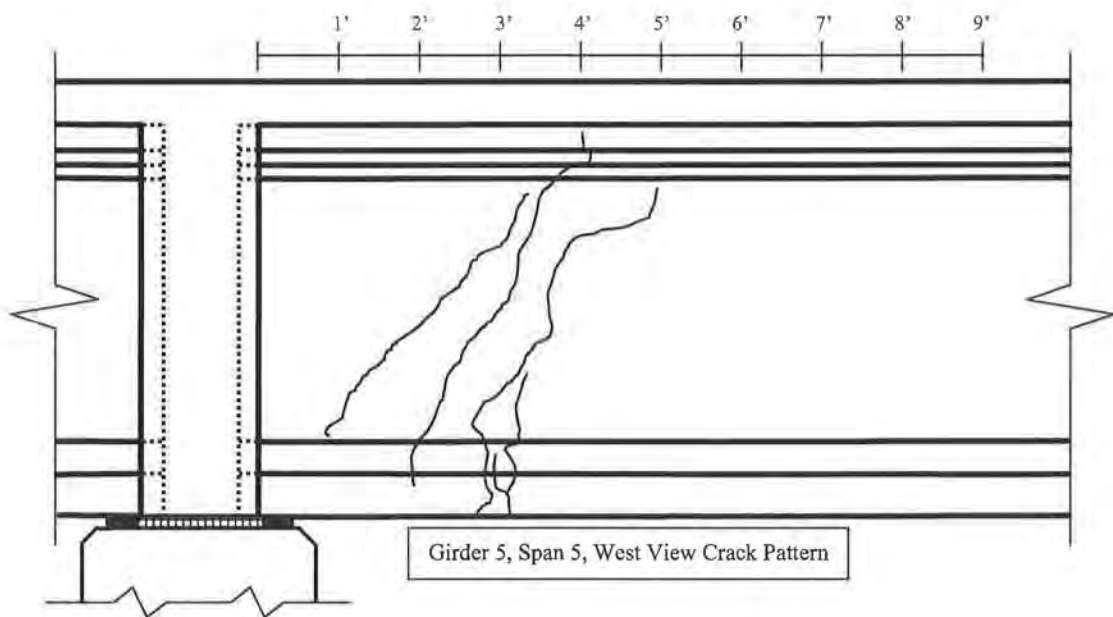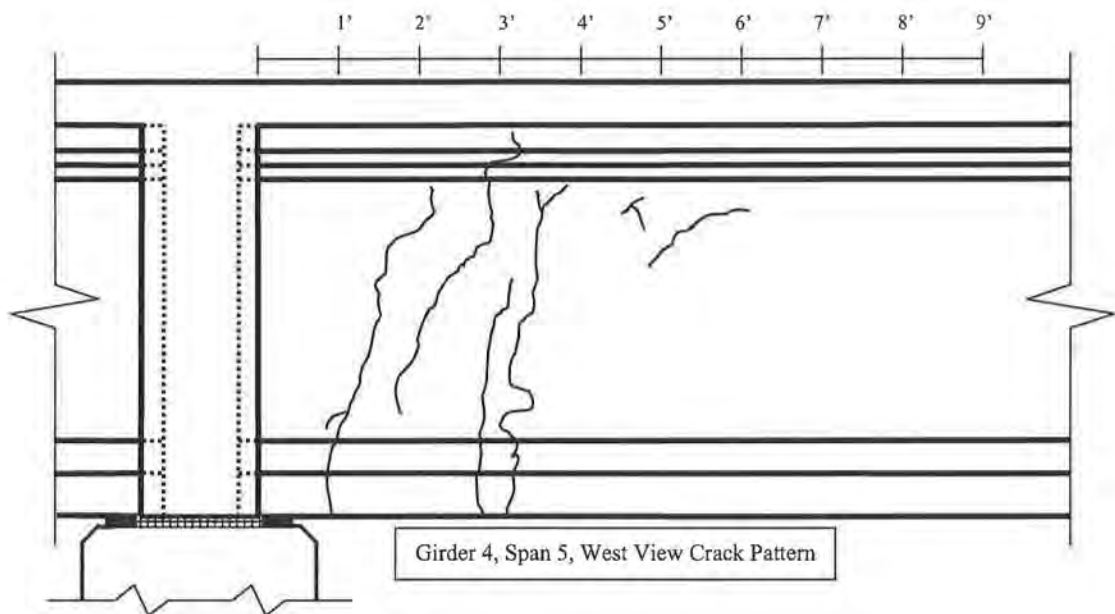
Figure 3.19 – Cracking in Girders 4 and 5 of Northbound Span 5
(ALDOT 1994a)

58
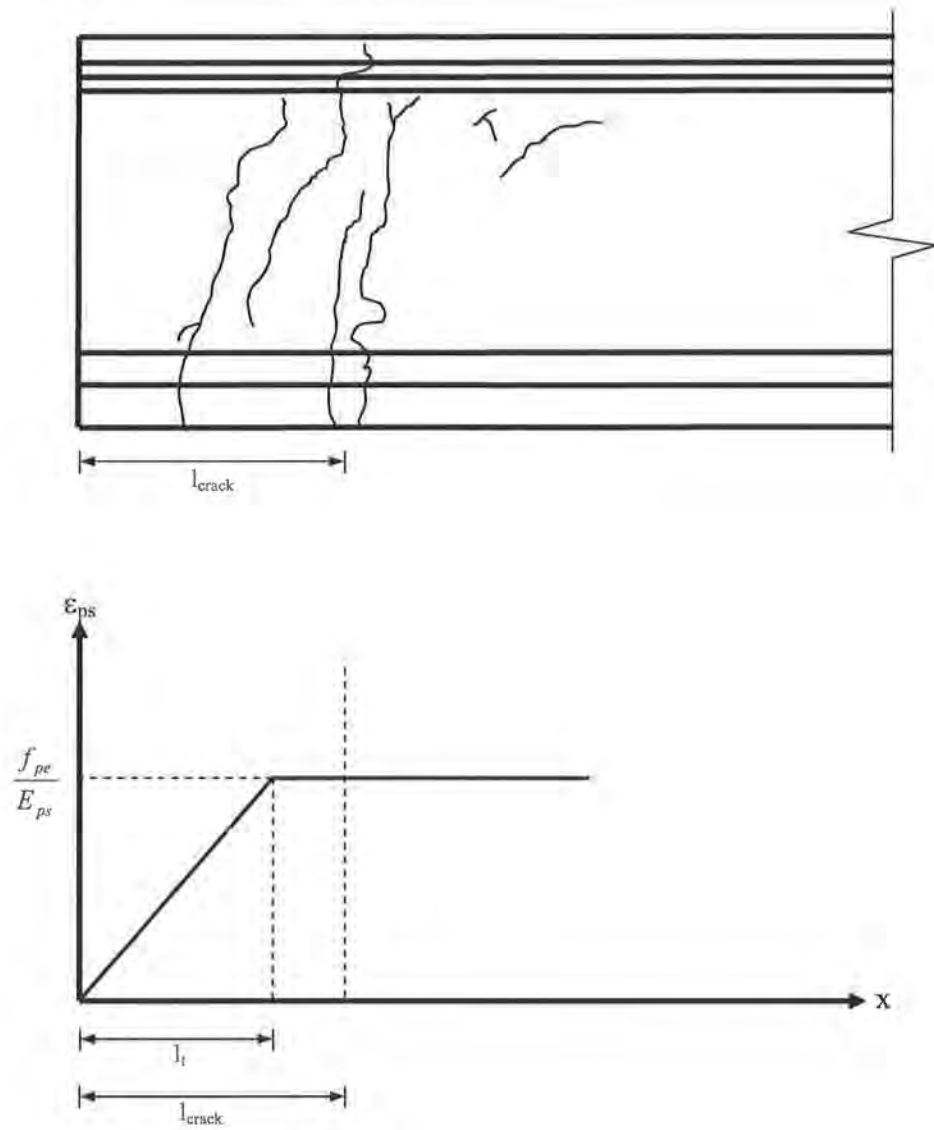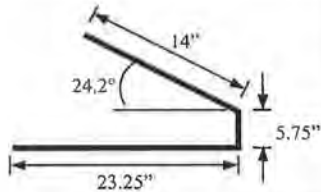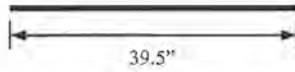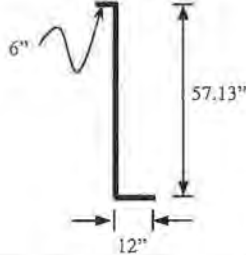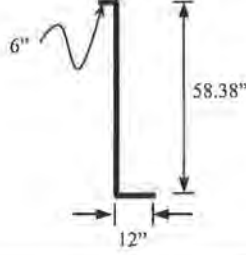
Figure 3.20 – Strain in a Single Prestressing Tendon in the End Region of a Cracked Bulb-tee Girder

Designation	Bar Size	Location	Shape
MK-351	#3	Lower Flange	
MK-352	#3	Upper Flange/ Web	
MK-451	#4	Upper Flange	
MK-452	#4	Web	
MK-553	#5	Web	

1 in. = 25.4 mm

Table 3.3 – Stirrup Summary

CHAPTER 4: ANALYTICAL METHODS

Three different analytical procedures were used in the examination of the Huntsville I-565 bridge structures. Preliminary results revealed that strength deficiencies exist in the cracked prestressed bulb-tee girders. Thus, the analytical methods were modified such that they could also be used in the examination of cracked girders repaired with external FRP reinforcement. Details regarding the strengthening of cracked bulb-tee girders with external FRP reinforcement are presented in Chapter 7.

The first analytical procedure used was an elastic structural analysis of a typical I-565 bridge structure. The elastic structural analysis was used to determine the factored ultimate load effects occurring in both interior and exterior girders. Factored ultimate shear and moment envelopes were created and used to locate strength deficiencies in the cracked prestressed concrete bulb-tee girders. The shear and moment envelopes were also used to determine whether or not strength deficiencies exist for cracked bulb-tee girders strengthened with external FRP reinforcement.

The second analytical procedure involved the use of a sectional model to calculate the shear and moment capacities of a typical cracked girder. Shear and moment capacities were calculated for cracked bulb-tee girders before and after repair with external FRP reinforcement. The capacities calculated with the sectional model were compared to the factored ultimate shear and moment envelopes to determine the location and magnitude of strength deficiencies. The comparison revealed that strength deficiencies do exist for unstrengthened cracked bulb-tee girders.

The third analytical procedure was a strut-and-tie analysis of a cracked prestressed concrete bulb-tee girder repaired with external FRP reinforcement. The strut-and-tie model allowed the flow of forces in the end region of a typical cracked bulb-tee girder to be examined more closely. The presence of external FRP reinforcement was included in the strut-and-tie models because the cracked bulb-tee girders were shown to be deficient in shear capacity in the cracked end regions of the girders. The forces that develop in the ties representing the prestressing tendons and external FRP reinforcement were of special interest. Although a strut-and-tie model of an unstrengthened cracked bulb-tee girder was not used, the results of the strut-and-tie analysis were helpful in assessing the strength of an unstrengthened cracked bulb-tee girder.

The results of the three analytical procedures are summarized and presented in Chapter 5. Discussion of the results of the analytical procedures is included in Chapter 6. Although all three analytical procedures were used to examine cracked bulb-tee girders

61

both before and after repair with external FRP reinforcement, only their application to the analysis of unstrengthened cracked bulb-tee girders is presented in this chapter. The use of the analytical procedures in the design of an external FRP strengthening system and the analysis of strengthened girders is discussed more thoroughly in Chapter 7.

4.1 ELASTIC STRUCTURAL ANALYSIS

An elastic structural analysis was completed to determine the factored ultimate load effects on a typical prestressed concrete bulb-tee girder. The factored ultimate load effects were compared to the capacity of a typical cracked girder to determine if strength deficiencies exist. Recommendations given in Chapter 4 of the AASHTO LRFD and several assumptions were utilized during the elastic structural analysis. The only structure considered in the elastic structural analysis was the two-span continuous structure composing northbound Spans 4 and 5.

GT STRUDL 7.0 software was used to perform the elastic structural analysis. The analysis was a very basic two-dimensional beam analysis. Each model was generated by creating nodes and connecting them with beam members. Load effects induced by applied loads were calculated with the stiffness method. Because deflections of the member were not of interest and linear-elastic behavior was assumed, material and cross-sectional properties were the same for each beam member.

4.1.1 Assumptions

In order to carry out the elastic structural analysis of the selected two-span structure, two major assumptions were necessary. The first of these assumptions concerned the horizontal curvature of the spans. Although northbound Spans 4 and 5 have a slight horizontal curvature, they were modeled as though they are straight. Table 4.6.1.2.1-1 of the AASHTO LRFD states that for multiple spans curved in the horizontal plane, straight spans may be assumed for analysis as long as the angle subtended by a single span is less than four degrees. Commentary within the specification states that a small horizontal curvature creates negligible differences in the calculated bending moments in the girders. Because northbound Spans 4 and 5 are slightly curved, the lengths of the girders are not all equal. The length of the spans was assumed to be equal to the length of the center girder for analysis purposes.

The second assumption related to the behavior of the structure at the interior support. It was assumed for analysis that no moments are transferred from the superstructure to the substructure at the interior bent. To model this appropriately in GT STRUDL, a single interior support was used. To make this possible, the length of each span in the model was increased. The length of the clear span is 1161.3 in. (29.50 m), but the clear span used in the model was 1173.3 in. (29.80 m). The 12 in. (305 mm) difference represents the distance between the assumed support location and the center of the

continuity diaphragm. Shear forces and moments obtained for model cross sections within the 12 in. region adjacent to the interior support were not used in the evaluation of the strength of the cracked bridge girders.

4.1.2 Models

Due to presence of the cracks in the girder ends, the response of the existing structure to applied live loads is not totally clear. Continuity at the interior support may have been reduced such that the spans act as though they are simply supported. The cracks in the girder ends may have resulted in the formation of an internal hinge, eliminating the ability of the girder to resist moments at the cracked cross section. The structure may also be acting as a two-span continuous unit for all live loads, as it was intended. The uncertainty of the behavior of the structure resulted in the need for multiple models to be used in the elastic structural analysis. The structure was modeled as two independent simply supported spans, a two-span continuous unit, and a two-span continuous unit with an internal hinge at the cracked cross section.

The first model used in the elastic structural analysis represented a single simply supported span. Performing the elastic structural analysis on two simply supported spans would not have changed the shear forces and moments occurring in the structure, so the second span was not included in the analysis. This model will be referred to as "Model #1" from this point forward. The clear span length was 1161.3 in. (29.50 m). Multiple nodes were used to subdivide the span. Nodes were placed every 100 in. (250 mm) and at member ends. Model #1 is shown in Figure 4.1. In the figure, black circles along the length of the member denote nodes.

The second model was a two-span continuous structure. This model will be referred to as "Model #2" from this point forward. The interior support was modeled as a pin, and the outer supports were represented with rollers. Each span had a clear span length of 1173.3 in. (29.80 m). The placement of nodes was not symmetric about the interior support. Model #2 is shown in Figure 4.2.

The third model was a two-span continuous structure containing an internal hinge in the left span. This model will be referred to as "Model #3" from this point forward. The hinge is located in the left span, 48 in. (1220 mm) from the interior support. The internal hinge was used to model the presence of cracks in the continuous end of one girder. The support conditions and clear span lengths used in this model were the same as those used in the second model. With the exception of an extra node at the crack location, the placement of nodes throughout the structure was the same as that in the second model. Model #3 is shown in Figure 4.3.

4.1.3 Loads

To simplify the analysis, each model was assumed to support a single design lane. The live load effects for an interior or exterior girder were calculated by multiplying the results of the elastic structural analysis by an appropriate distribution factor. Distribution factors for shear and moment were calculated according to Article 4.6.2.2 of the AASHTO LRFD and are presented in Section 4.1.6 of this chapter.

The dead loads applied to the structure were that which a single girder line must support. Dead loads on a single girder line include the self-weight of the prestressed concrete girders, the self-weight of the cast-in-place composite RC deck slab, and the self-weight of the barrier rails cast at the edges of the roadway. The self-weight of the barrier rails was distributed equally over the width of the bridge deck. The dead loads used in the analysis are shown in Table 4.1.

For analysis purposes, it was assumed that simply supported girders carry all dead loads. This assumption is not completely accurate, though. The barrier rails were cast after the entire deck slab had been cast, so it is more likely that their weight is carried by the continuous structure. Depending on the sequence in which the deck slab was cast, a portion of the weight of the deck slab may also be carried by the continuous structure.

Table 4.1 – Dead Loads on a Single Interior Girder Line

Prestressed Concrete Girders	686 lbs/ft	10.0 kN/m
Cast-in-Place Composite RC Deck Slab	727 lbs/ft	10.6 kN/m
Distributed Weight of Barrier Rails	91 lbs/ft	1.3 kN/m
TOTAL	1504 lbs/ft	21.9 kN/m

1 lb = 4.448 N, 1 ft = 0.305 m

Article 3.6.1.2.1 of the AASHTO LRFD designates the vehicular live load on the roadway of bridges as an HL-93 loading. This load combination involves a design truck or design tandem and a uniformly distributed lane load. In certain situations, a second design truck or design tandem may be used. This is discussed in more detail in Section 4.1.4.

The design lane load is 0.64 kips per linear foot (9.34 kN/m), as specified in Article 3.6.1.2.4 of the AASHTO LRFD. The design lane load should be distributed over a transverse width of 10.0 ft (3.0 m) that must be within the 12.0 ft (3.7 m) wide design

lane. The lane load is considered to be a live load, though it is not subject to dynamic effects.

Design truck and design tandem loads are prescribed within Article 3.6.1.2.2 of the AASHTO LRFD. A design truck has a front axle load of 8.0 kips (35.6 kN), and two rear axle loads of 32.0 kips (142.3 kN) each. The distance between the front axle and the leading rear axles is 14.0 ft (4.3 m). The spacing between the two rear axles may vary between 14.0 ft (3.7 m) and 30.0 ft (9.1 m), though 14.0 ft was used throughout the elastic structural analysis. The design tandem is described in Article 3.6.1.2.3 of the AASHTO LRFD. A design tandem is composed of two 25.0 kips (111.2 kN) loads spaced 4.0 ft (1.2 m) apart.

4.1.4 Load Placement and Load Combinations

In order to determine the most severe effects produced by the applied loads, the design truck and design tandem loads were moved longitudinally along the length of the span. By doing so, the shear forces and moments developed at specific cross sections along the length of the girder were determined for multiple vehicle positions. This allowed shear and moment envelopes to be developed for each model used in the elastic structural analysis.

Design trucks were oriented such that they could move in both the northbound and southbound direction, though the natural use of the selected two-span structure is for northbound traffic. Design truck and design tandem positions were varied along the length of the spans in increments of 100 in. (2540 mm) in order to obtain the most critical load effects for cross sections along the length of the structure. For Model #2 and Model #3, the placement of the design truck or design tandem near the interior support was not always consistent with the 100 in. increment.

The uniformly distributed dead loads and lane load were not varied during the analysis. It was judged that patterned loading of the dead loads and lane load would not significantly affect the shears and moments developed in the girders. Because the placement of the dead load and lane load were not varied, their effects were examined only once for each model.

The AASHTO LRFD gives recommendations for conservative, yet realistic, loading combinations for bridge structures. Article 3.6.1.3.1 states that the extreme load effect on the bridge should be determined by using the most critical of the following load combinations:

1. Dead load, design lane load, and design tandem load;

2. Dead load, design lane load, and design truck with variable axle spacing;

3. Dead load plus 90 percent of the effects of both the design lane load and two design trucks (AASHTO 2002).

The third combination may only be used to calculated negative moments between points of contraflexure and the reaction occurring at interior supports (AASHTO 2002). According to Article 3.6.1.3.1, the use of two design trucks requires that they be oriented in the same direction. There must be at least 600 in. (15.2 m) between the rear axle of the lead design truck and the front axle of the trailing design truck. The third load combination was only applicable to Model #2 and Model #3.

4.1.5 Load Factors

Once the load effects due to dead load, lane load, and design truck or design tandem live load had been determined, load factors were applied so that the ultimate load effects could be calculated. The load factors used were for the "STRENGTH I" load combination specified in Article 3.4.1 of the AASHTO LRFD. Equation 4.1 shows the equations used to calculate the ultimate load effects on the bridge girders.

$$V_u = 1.25 V_{Dead} + 1.75 \left(V_{Lane} + V_{Truck} (1 + IF) \right)$$

Eq. 4.1

$$M_u = 1.25 M_{Dead} + 1.75 \left(M_{Lane} + M_{Truck} (1 + IF) \right)$$

The term "IF" used in the above equations is the impact factor. The impact factor must be applied to all moving live loads to account for their dynamic effect on the structure. According to Table 3.6.2.1-1, for the "STRENGTH I" limit state, the impact factor is equal to 0.33.

4.1.6 Distribution Factors

Distribution factors are necessary to determine the live load effects on a single girder within a multi-girder bridge. The AASHTO LRFD gives equations for distribution factors for both shear and moment. The equations have been developed for various bridge types and account for multiple geometric parameters and the probability of multiple design lanes being loaded simultaneously. The selected two-span bridge structure falls into Category "k" in Table 4.6.2.2.1-1. The distribution factors for shear and moment for an interior girder were calculated with the Equation 4.2. Distribution factors for exterior girders were calculated with Equation 4.3.

$$DF_{int,SHEAR} = 0.2 + \frac{S}{12} - \left(\frac{S}{35}\right)^{2.00}$$

$$DF_{int,MOMENT} = 0.075 + \left(\frac{S}{9.5}\right)^{0.60} \left(\frac{S}{L}\right)^{0.20} \left(\frac{K_g}{12.0 L t_s^3}\right)^{0.10}$$

Eq. 4.2

$$DF_{ext,SHEAR} = \left(0.6 + \frac{d_e}{10}\right) DF_{int,SHEAR}$$

Eq. 4.3

$$DF_{ext,MOMENT} = \left(0.77 + \frac{d_e}{9.1}\right) DF_{int,MOMENT}$$

In Equations 4.2 and 4.3, S is the girder spacing in inches, L is the clear span length in inches, t_s is the thickness of the deck slab in inches, and d_e is the horizontal distance from the web of the exterior girder to the interior edge of the curb or traffic barrier in inches. The term, K_g, is expressed in Equation 4.4 below, where E_B is the elastic modulus of the beam material in kips per square inch, E_D is the elastic modulus of the deck slab material in kips per square inch, I is the moment of inertia of the cross section in in.[4], A is the cross-sectional area in square inches, and e_g is distance between the centroid of the girder cross section and the centroid of the deck slab cross section in inches.

$$K_g = \left(\frac{E_B}{E_D}\right)\left(I + A e_g^2\right)$$

Eq. 4.4

An additional equation for the moment distribution factor for exterior girders is given in equation C4.6.2.2.2d-1 of the AASHTO LRFD. The use of Equation C4.6.2.2.2d-1 is required for bridge types "a", "e", and "k" in Table 4.6.2.2.1-1. The use of Equation C4.6.2.2.2d-1, presented as Equation 4.5 below, is required because Equation 4.3 excludes the effects of diaphragms and cross frames within the span. The greatest distribution factor calculated from Equations 4.3 and 4.5 should be applied to the ultimate live loads.

$$R = \frac{N_L}{N_b} + \frac{X_{ext} \sum_1^{N_L} e}{\sum_1^{N_b} x^2}$$

Eq. 4.5

In Equation 4.5, N_L is the number of loaded design lanes, N_b is the number of girders in the span, X_{ext} is the horizontal distance from the centroid of the pattern of girders to the centroid of the exterior girder in inches, e is the eccentricity of the centroid of a design

67

truck or design lane load and the centroid of the pattern of girders in inches, and x is the horizontal distance from the centroid of the pattern of girders to the centroid of an individual girder in inches.

Table 4.2 – Distribution Factors

	Interior Girders	Exterior Girders
DF_{SHEAR}	0.814	0.652
DF_{MOMENT}	0.569	0.623

A range of applicability exists for the distribution factor equations given in Equations 4.2 and 4.3. The girder spacing, slab thickness, clear span length, and number of girders per span are all within the range of applicability of the equations. The distribution factors used to determine the factored ultimate load effects in the girders are shown in Table 4.2. Equation 4.5 resulted in the greatest moment distribution factor for an exterior girder when three design lanes were loaded and a multiple presence factor of 0.85 was used.

The factored ultimate loads were determined by applying the distribution factors to the ultimate loads. The equations used to calculate the factored ultimate load effects at a particular cross section are given in Equation 4.6.

$$V_u = 1.25 V_{Dead} + DF_{SHEAR}\left[1.75\left(V_{Lane} + V_{Truck}\left(1 + IF\right)\right)\right]$$

Eq. 4.6

$$M_u = 1.25 M_{Dead} + DF_{MOMENT}\left[1.75\left(M_{Lane} + M_{Truck}\left(1 + IF\right)\right)\right]$$

4.2 CALCULATION OF SHEAR AND MOMENT CAPACITIES FOR UNSTRENGTHENED

CRACKED BULB-TEE GIRDERS

The shear, positive moment, and negative moment capacities of a typical unstrengthened cracked bulb-tee girder were calculated for multiple cross sections along its length. All calculations were performed with the aid of a computer spreadsheet. Once the shear and flexural capacities of the unstrengthened cracked bulb-tee girder were calculated, they were compared to the factored ultimate load effects determined with the elastic structural analysis.

68

4.2.1 Assumptions

The first assumption made in the calculation of shear and moment capacities of the cracked bridge girders was related to the transfer of the prestressing force to the girder. Due to the width of the cracks at the girder ends, it was assumed that the effective prestressing force between the girder end and the crack location has been completely lost. Thus, the prestressing force in the concrete begins to build from the crack location and does so over the normal transfer length, l_t, as defined in equation 5.11.4.2-1 of the AASHTO LRFD. A reduction in the effective prestressing force typically reduces the shear and moment capacities of a prestressed concrete member. For this reason, the assumption that all the effects of prestressing have been lost in the cracked end of the girder is a conservative one.

A second assumption was made in order to more accurately determine the longitudinal strain at mid-depth of the cross section, ε_x, in the prestressed concrete girder. The equation given for ε_x in Article 5.8.3.4.2 of the AASHTO LRFD requires that the longitudinal steel reinforcement, A_s and A_{ps}, be on the flexural tension side of the member. For prestressed concrete members made continuous, this procedure is overly conservative in areas subjected to negative moment because the effects of prestressing are effectively ignored in the calculation of ε_x. The longitudinal strain at mid-depth of the cross section was calculated differently for sections subjected to negative moment. The modified procedure is described in Section 4.2.2.

4.2.2 Calculation of Shear Capacity

The nominal shear capacity of the prestressed concrete girders with cast-in-place composite RC slab was calculated with the procedure outlined in Section 5.8.3 of the AASHTO LRFD. Transfer of the prestressing force from the prestressing tendons to the concrete was considered, as well as the development of larger stresses in the prestressing tendons. The transfer length of a 0.5 in. (12.7 mm) special prestressing tendon was calculated as 60 times the tendon diameter, as recommended in Article 5.11.4.1 of the AASHTO LRFD. The development length was calculated with Equation 5.11.4.2-1 from the AASHTO LRFD. Partial debonding of tendons was considered in the calculation of shear capacity.

The procedure used to determine the nominal shear capacity of the cracked girders utilizes the modified compression field theory (MCFT). The MCFT is a sectional analysis and design method that is based on a variable-angle truss. The MCFT accounts for transverse tensile strains in the concrete struts and shear transfer across cracks in the member (ACI-ASCE Committee 445 2000). Shear design with the MCFT is recommended in the AASHTO LRFD. The following is a basic outline of the MCFT

sectional analysis procedure used to determine the design shear capacity of the cracked prestressed concrete girders. For the selected cross section:

1. Determine the factored ultimate shear force and moment, V_u and M_u, respectively.

2. Calculate the vertical component of the prestressing force, V_p.

3. Determine the width and depth of the web effective in resisting shear, b_v and d_v, respectively. The second term of the equation for b_v is an adjustment for the presence of post-tensioning ducts. The "k" term can be found in Table C5.7.3.1.1-1 or calculated with equation 5.7.3.1.1-2 of the AASHTO LRFD.

$$b_v = b_w - kd_d$$

$$d_v = MAX \begin{Bmatrix} 0.72h \\ 0.90d \\ d_e - \dfrac{a}{2} \end{Bmatrix}$$

<div align="right">Eq. 4.7</div>

In Equations 4.7, b_w is the width of the web in inches, d_d is the diameter of post-tensioning ducts in inches, h is the height of the member in inches, d is the distance from the extreme compression fiber to the centroid of the tension reinforcement in inches, and a is the depth of the rectangular stress block in inches.

4. Calculate v, the factored shear stress on the cross section, and v/f'_c. Because the web resists the greatest portion of the shear in the cross section, the value of f'_c used in determination of the shear capacity of the section should be the design compressive strength of the girder, determined 28 days after the concrete has been cast. The strength reduction factor used for shear, ϕ_s, was 0.90, as recommended in Article 5.5.4.2 of the AASHTO LRFD.

$$v = \frac{V_u - \phi_s V_p}{\phi_s b_v d_v}$$

Eq. 4.8

5. If M_u is a non-negative value, calculate the longitudinal strain at the mid-depth of the cross section, ε_x, with Equation 4.9a. If the resulting value of ε_x is negative, recalculate ε_x with Equation 4.9b. The initial θ value was obtained by using v, as calculated in Equation 4.8, and an assumed value of zero for ε_x.

$$\varepsilon_x = \frac{\dfrac{M_u}{d_v} + 0.5N_u + 0.5(V_u - V_p)\cot\theta - 0.7A_{ps}f_{pu}}{2(E_s A_s + E_{ps} A_{ps})}$$

Eq. 4.9a

$$\varepsilon_x = \frac{\dfrac{M_u}{d_v} + 0.5N_u + 0.5(V_u - V_p)\cot\theta - 0.7A_{ps}f_{pu}}{2(E_s A_s + E_{ps} A_{ps} + E_c A_c)}$$

Eq. 4.9b

In Equation 4.9a, N_u is the factored ultimate axial force in kips, θ is the angle of inclination of the diagonal compressive stress in the concrete, A_{ps} is the area of prestressing steel in square inches, f_{pu} is the specified tensile strength of the prestressing tendons in kips per square inch, E_s is the elastic modulus of the mild steel reinforcement in kips per square inch, A_s is the area of mild steel reinforcement in square inches, and E_{ps} is the elastic modulus of the prestressing tendons in kips per square inch. In Equation 4.9b, E_c is the elastic modulus of the concrete in the girder in kips per square inch, and A_c is the area of concrete on the flexural tension side of the cross section in square inches.

If M_u is a negative value, the value of ε_x must be calculated differently in order to take advantage of the effective prestressing force in the member. First, an initial mid-depth longitudinal strain, $\varepsilon_{x,initial}$, was calculated at mid-depth of the cross section. The effects of prestressing, girder self weight, and the weight of the deck slab were considered in the calculation of $\varepsilon_{x,initial}$. The initial mid-depth strain was then added to the mid-depth strain resulting from factored live load moments, factored ultimate shear forces, and factored

71

ultimate axial forces. The effects of factored dead load moments were omitted from the second term of the equation because they were accounted for in the first term. The initial mid-depth longitudinal strain was calculated with Equation 4.10. The actual longitudinal strain at mid-depth of the cross section was calculated with Equation 4.11. If the result of Equation 4.11a is negative, Equation 4.11b must be used. This is the modified procedure for calculation of ε_x mentioned in Section 4.2.1.

$$\varepsilon_{x,initial} = \left(\frac{1}{E_c}\right)\left(-\frac{F_e}{A} - \frac{F_e e y}{I} + \frac{M_{Dead} y}{I}\right) \qquad \text{Eq. 4.10}$$

$$\varepsilon_x = \varepsilon_{x,initial} + \frac{\dfrac{M_u - M_{Dead}}{d_v} + 0.5 N_u + 0.5\left(V_u - V_p\right)\cot\theta}{2\left(E_s A_s\right)} \qquad \text{Eq. 4.11a}$$

$$\varepsilon_x = \varepsilon_{x,initial} + \frac{\dfrac{M_u - M_{Dead}}{d_v} + 0.5 N_u + 0.5\left(V_u - V_p\right)\cot\theta}{2\left(E_s A_s + E_c A_c\right)} \qquad \text{Eq. 4.11b}$$

In Equation 4.10, F_e is the effective force in the prestressing tendons after losses in kips, e is the eccentricity of the prestressing tendons in inches, y is the distance from the centroid of the cross section to the mid-depth of the cross section in inches, and M_{Dead} is the moment due to dead loads in kip-inches.

6. Using the calculated values of v/f'_c and ε_x, calculate the strut inclination

angle, θ. The θ and β charts are a part of the AASHTO LRFD in the form of

Tables 5.8.3.4.2-1 and 5.8.3.4.2-2. If the calculated θ value is equal to the

initial θ value, determine β, which is a factor relating the effect of longitudinal

strain on the shear capacity of concrete. If the initial and final values of θ are

not equal, Steps 5 and 6 may be repeated iteratively until the procedure

converges on a value for θ. Once a θ value has been determined, determine the associated β value.

7. Determine the design shear capacity of the section, ϕV_n. The term f_c' should be in units of pounds per square inch (psi).

$$\phi_s V_n = \phi_s \left(V_c + V_s + V_p \right) \qquad \text{Eq. 4.12}$$

$$V_c = \frac{\beta \sqrt{f_c'} b_v d_v}{1000}$$

$$V_s = \frac{A_v f_y d_v \left(\cot \theta + \cot \alpha \right) \sin \alpha}{s} \qquad \text{Eq. 4.13}$$

In Equation 4.13, A_v is the cross-sectional area of the shear reinforcement in square inches, α is the angle of inclination of the stirrups, and s is the stirrup spacing in inches.

8. Check to see if the ultimate strength limit state is satisfied.

$$\phi_s V_n \geq V_u \qquad \text{Eq. 4.14}$$

4.2.3 Calculation of Longitudinal Reinforcement Capacity

Article 5.8.3.5 of the AASHTO LRFD recommends that the tensile capacity of the longitudinal reinforcement on the flexural tension side of the member be checked to ensure it has adequate capacity. This check is necessary because shear causes tension in the longitudinal reinforcement of a flexural member. The amount of tension induced by the shear in a member is dependent on the angle of inclination of the compressive stresses in the concrete and the amount of shear resisted by the concrete. Thus, longitudinal reinforcement must have enough capacity such that tension forces induced by both moment and shear can be resisted.

The equation given in Article 5.8.3.5, shown here as Equation 4.15a, was developed for a cross section subjected to shear and positive moment. The formulation of Equation 4.15a is based upon the equilibrium of forces shown in Figure 4.4. The AASHTO LRFD (2002) gives no guidance regarding the use of an equation for a combination of shear and negative moment. To address this deficiency, Equation 4.15b was developed using the

equilibrium condition shown in Figure 4.5. Equation 4.15b was used to determine the minimum required tensile capacity of the longitudinal mild steel reinforcement in the deck slab. Equation 4.15b was applied at all cross sections subjected to negative moments.

$$T = \frac{M_u}{\phi_f d_v} + 0.5\frac{N_u}{\phi_a} + \left(\frac{V_u}{\phi_s} - 0.5V_s - V_p\right)\cot\theta \qquad \text{Eq. 4.15a}$$

$$T = \frac{M_u}{\phi_f d_v} + 0.5\frac{N_u}{\phi_a} - \left(0.5V_s + V_p\right)\cot\theta \qquad \text{Eq. 4.15b}$$

The capacity of the longitudinal reinforcement must meet or exceed the magnitude of T calculated with Equation 4.15a or Equation 4.15b. The capacity of the longitudinal reinforcement was calculated assuming that the ultimate strength limit state controls. The strength reduction factors used for flexure, ϕ_f, and axial effects, ϕ_a, were 1.00 and 0.70, respectively. The strength reduction factor for shear, ϕ_s, was 0.90.

4.2.4 Calculation of Positive Moment Capacity

The nominal positive moment capacity of the prestressed concrete girders was calculated for multiple cross sections along the length of the cracked girder according to Section 5.7.3 of the AASHTO LRFD. As was the case for the shear capacity calculations, transfer and development lengths of the prestressing tendons were considered. Mild steel reinforcement in the deck slab was ignored. The following procedure was used to calculate the design positive moment capacity of the girders, $\phi_f M_n^+$.

1. Determine the factored ultimate moment, M_u, for the selected cross section.

2. Calculate the position of the neutral axis, c. The design compressive strength of the concrete, f_c', is that of the cast-in-place deck slab. If the result of Equation 4.17a results in a thickness greater than that of the slab, Equation 4.17b must be used.

$$c = \frac{A_{ps}f_{pu} + A_s f_y}{0.85 f_c' \beta_1 b_f + k A_{ps}\dfrac{f_{pu}}{d_p}} \qquad \text{Eq. 4.17a}$$

74

$$c = \frac{A_{ps} f_{pu} + A_s f_y - 0.85 f_c' \beta_1 t_s \left(b_f - b_w \right)}{0.85 f_c' \beta_1 b_w + k A_{ps} \dfrac{f_{pu}}{d_p}} \qquad \text{Eq. 4.17b}$$

In Equation 4.17a, f_y is the yield strength of the mild steel reinforcement in kips per square inch, β_1 is the ratio of the depth of the rectangular stress block to the depth of the neutral axis, b_f is the width of the flange in inches, and d_p is the distance from the extreme compression fiber to the centroid of the prestressing tendons in inches.

3. Calculate the average maximum stress in the prestressing tendons at the time for which the nominal flexural resistance of the member is required, f_{ps}.

$$f_{ps} = f_{pu} \left(1 - k \frac{c}{d_p} \right) \qquad \text{Eq. 4.16}$$

The term "k" can be found in Table C5.7.3.1.1-1 or calculated with equation 5.7.3.1.1-2 from the AASHTO LRFD.

4. Calculate the design positive moment capacity of the member, $\phi_f M_n^+$. The strength reduction factor used for flexure, ϕ_f, was 1.00, as recommended in Article 5.5.4.2 of the AASHTO LRFD. The term d_s is the distance from the extreme compression fiber to the centroid of the longitudinal mild steel reinforcement in inches.

$$\phi_f M_n^+ = \phi_f \left[A_{ps} f_{ps} \left(d_p - \frac{a}{2} \right) + A_s f_y \left(d_s - \frac{a}{2} \right) \right] \qquad \text{Eq. 4.18}$$

5. Check to see if the ultimate strength limit state is satisfied.

$$\phi_f M_n^+ \geq M_u \qquad \text{Eq. 4.19}$$

4.2.5 Calculation of Negative Moment Capacity

A procedure based on force equilibrium, strain compatibility, and constitutive material properties was employed to calculate the design negative moment capacity, $\phi_f M_n^-$, of the girders. The prestressed concrete girders were assumed to resist negative moments as though they are nonprestressed reinforced concrete members. Development of the mild steel reinforcement in the bridge deck slab was considered. The development length of mild steel deformed reinforcing bars in tension was calculated according to Equation 12-1 from ACI 318-02.

The following procedure was used to calculate $\phi_f M_n^-$.

1. Calculate the depth of the equivalent stress block, "a." In doing so, the ¾ in. (19 mm) chamfers at the bottom corners of the BT54 girder were neglected.

$$a = \frac{A_s f_y}{0.85 f_c' b} \qquad \text{Eq. 4.20}$$

2. Calculate the depth of the neutral axis, "c."

$$c = \frac{a}{\beta_1} \qquad \text{Eq. 4.21}$$

3. Check the strain in the tension steel, ε_s. If the strain in the tension steel is less than the steel yield strain, ε_y, an iterative method is necessary to locate the neutral axis of the cross section and to calculate the depth of the equivalent stress block.

$$\varepsilon_s = \varepsilon_{cu}\left(\frac{d-c}{c}\right) \qquad \text{Eq. 4.22}$$

4. Calculate the design negative moment capacity, $\phi_f M_n^-$. Two different strength reduction factors, ϕ_f, were used to determine the design negative moment capacity of the girders, 1.00 and 0.90. The reasons for using two different

strength reduction factors are discussed in more detail in Section 5.2.4 and

Section 6.1.

$$\phi_f M_n^- = \phi_f A_s f_y \left(d - \frac{a}{2} \right)$$

Eq. 4.23

5. Check to see if the ultimate strength limit state is satisfied.

$$\phi_f M_n^- \geq M_u$$

Eq. 4.24

4.3 STRUT-AND-TIE ANALYSIS

The flow of forces through a typical cracked prestressed concrete girder was examined more thoroughly by means of a strut-and-tie analysis. The results of the strut-and-tie analysis revealed the magnitude of the tension forces that must be resisted by the longitudinal tension reinforcement in the bottom flange. Because the elastic structural analysis and the calculation of the shear and flexural capacities of an unstrengthened cracked bulb-tee girder revealed that strength deficiencies exist, the presence of external FRP reinforcement was included in the strut-and-tie models.

Strut-and-tie analysis is permitted for structural concrete members or D-regions of such members (AASHTO LRFD 2002). A D-region, or disturbed region, is a portion of a structural concrete member adjacent to a cross sectional discontinuity or concentrated load. The flow of forces through a D-region is complex and is not governed by the assumptions that plane sections remain plane or that the distribution of shear stresses on the cross section is uniform across the depth of the member (ACI-ASCE Committee 445 2000).

Strut-and-tie models are plasticity-based models that allow the key force-resisting elements of a reinforced or prestressed concrete member to be represented as truss elements. Compression members are referred to as struts and tension members are called ties. Points of intersection between truss members within the strut-and-tie model are called nodes. The use of strut-and-tie models allows easier visualization of the forces in a structural concrete member and provides a lower-bound conservative design method (Schlaich et al. 1987).

According to Section 5.8 of the AASHTO LRFD (2002), D-regions are considered to control the behavior of cross sections within one effective member depth, d_v, from a concentrated force or abrupt geometric change. The D-region at the continuous end of a cracked prestressed concrete bulb-tee girder contains the large cracks shown in Figure 3.5

and is subjected to concentrated forces, both from the interior support reaction and vehicular live loads. The geometric discontinuity at the intersection of the girder and continuity diaphragm also contributes to the disturbed region at the continuous end of the girder. Multiple strut-and-tie models (STM) were developed in order to examine the forces within the member in the D-region at the continuous end of the girder.

4.3.1 Assumptions

The first assumption made in the strut-and-tie analysis involved the choice of load combinations. The critical load combinations were chosen such that a maximum tension force was induced in the ties in the bottom flange. The force in the ties will be most critical at or near the cracked cross section of the girder, due to the loss of prestressing effects at the cracked girder end. Load combinations inducing maximum shear and moment effects at the cracked cross section result in the largest forces being induced in the ties.

Inspection of the data from the elastic structural analysis revealed that there are a total of four critical load cases. Each load case causes a maximum shear or moment effect at the cracked cross section. The four critical load cases are:

1. Maximum shear force at cracked section (Model A)

2. Maximum positive bending moment at cracked section (Model A)

3. Maximum shear force at cracked section (Model B)

4. Maximum shear force at cracked section (Model C)

The first two critical load cases result from application of the same load configuration to Model A. Thus, three different strut-and-tie models were constructed: one representing the simple span (A), one representing the two-span continuous structure (B), and a third representing the two-span continuous structure with an internal hinge at the cracked cross section in the girder end (C). Details of the models are discussed in the following section.

The second assumption made during the strut-and-tie analysis related to the magnitude of the forces applied to the STM. The live load portion of the ultimate load effect on each girder was computed using a distribution factor, as described in Section 4.1.6. Because the distribution factors for shear and moment are not equal, the use of the factored ultimate load effects is not applicable to the strut-and-tie models. In order for equilibrium to be satisfied, a single distribution factor must be used.

The distribution factor for shear in an interior girder, the largest of the distribution factors, was used to determine the loads applied to the strut-and-tie models. The moment

78

distribution factor calculated with Equation 4.2 most accurately describes the distribution of *midspan* moments. The shear distribution factor more accurately describes the load distribution near support regions where shear forces are more critical than moments. Thus, the shear distribution factor is a better choice for use with the strut-and-tie analysis of the end region of a cracked bulb-tee girder.

A final assumption was made concerning the loading of the STMs. Because all loads applied to the STM must be located at joints, it was assumed that the distributed dead load and lane load could be discretized into point loads. The locations of the joints in each model were usually dictated by the placement of design truck loads on the structure.

4.3.2 Strut-and-Tie Model Geometry and Loading

Each of the three strut-and-tie models is unique and represents a specific load configuration on a specific type of structure. An example of a typical strut-and-tie model used to examine the flow of forces through the cracked end region of a bulb-tee girder is shown in Figure 4.6. All struts are shown as dashed lines. All ties are shown as solid lines. Nodes are located at the ends of all strut and tie members and are shown as small black dots.

Because all the girders have identical reinforcement details, the location of ties representing longitudinal reinforcement is consistent from one model to the next. All ties are located at the centroid of actual reinforcement. Ties representing straight, fully bonded prestressing tendons are located 8.75 in. (222 mm) from the bottom of the composite cross section. Ties representing the external FRP reinforcement are located 3.60 in. (91 mm) from the bottom of the composite cross section. Ties representing mild steel reinforcement in the deck slab, which are not shown in Figure 4.6, are located 3.75 in. (95 mm) from the top of the composite cross section. The location of ties representing stirrups varies because each tie represents the centroid of a group of stirrups. Harped tendons were disregarded in the strut-and-tie analysis.

The depth of the horizontal compression struts was consistent between all strut-and-tie models. The depth of the horizontal struts was based upon the position of the flexural neutral axis at the ultimate strength limit state. For compression in the deck slab resulting from positive bending moments, struts were assumed to be 5.00 in. (127 mm) deep. Thus, the centroid of the compressive force in the deck slab is located 2.50 in. (64 mm) from the top of the composite cross section. The centroid of the compressive force in the bottom flange is located 2.00 in. (51 mm) from the bottom of the composite cross section.

The depth of the overall strut-and-tie models was determined by horizontal strut and tie positions. The length of the girder represented by an individual STM was dependent on the position of the design truck loads on the span. All design truck loads applied within 23 ft (7.0 m) of the interior support were included in the analysis. Truss joints were created such that design truck loads could be placed on the span as they were in the

79

elastic structural analysis of the bridge structure. The length of each STM model was not seen as a critical factor in the analysis because D-regions resulting from concentrated axle loads applied far from the interior support were not considered to be of great importance. The strut-and-tie analysis concentrated on the forces developed in the D-regions at the interior support and at the curtailment of the external FRP reinforcement.

In each model, the region surrounding the curtailment of the external FRP reinforcement was refined. The area of refinement and the curtailment of the external FRP reinforcement are clearly indicated in Figure 4.6. By refining the area near the curtailment of the external FRP reinforcement, a better understanding of the forces that develop in the FRP and prestressing tendons was obtained. Refinement also aided in the comparison of factored ultimate tie forces to the tensile capacity of the reinforcement. If the tensile reinforcement in the bottom flange is not able to carry the factored ultimate tie forces, modification of the model geometry or the amount of external FRP reinforcement is necessary.

The overall length of the area of refinement near the curtailment of the external FRP reinforcement was based upon an estimation of the point at which the prestressing tendons have transferred the effective prestressing force to the concrete. Assuming that the effects of prestressing have been lost in the girder end, transfer of the prestressing force to the concrete starts at the cracked cross section. It was assumed that the prestressing tendons carry little to no tensile forces from the cracked cross section to a point 84 in. (2130 mm) from the girder end. Thus, the prestressing tendons should be able to transfer the effective prestressing force to the concrete over the 42 in. (1070 mm) gap between the cracked cross section and the point 84 in. (2130 mm) from the girder end. This distance is significantly greater than the transfer length of 30 in. (760 mm) used in the calculation of girder shear and moment capacities.

Between the points located 84 in. (2130 mm) and 130 in. (3200 mm) from the end of the girder, respectively, the whole of the tensile force carried by the FRP must be transferred to the prestressing tendons. The point at 130 in. was chosen as a conservative estimate of the curtailment of the external FRP reinforcement. At this point along the girder cross section, the prestressing tendons have been given nearly 90 in. (2290 mm) to become fully developed, which is greater than the development length assumed in the calculation of girder shear and moment capacities.
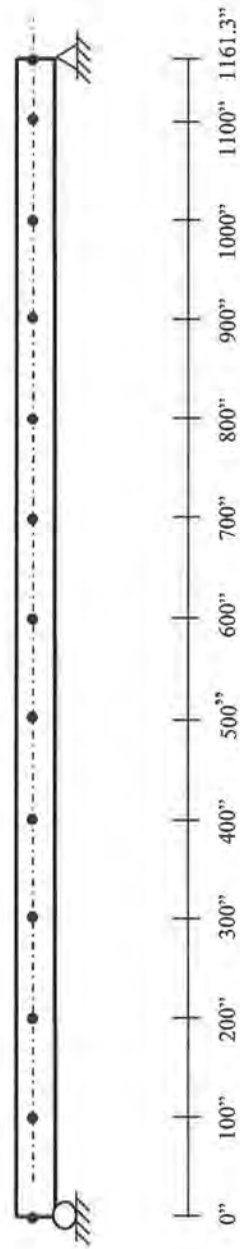
Figure 4.1 – Model #1 used in the Elastic Structural Analysis
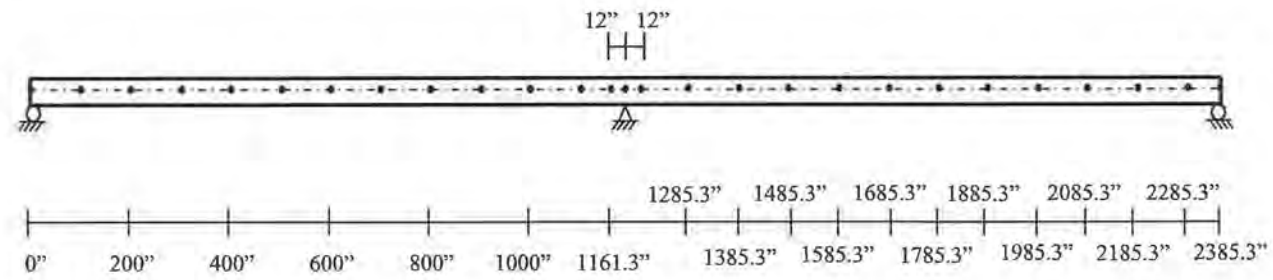
Figure 4.2 – Model #2 used in the Elastic Structural Analysis
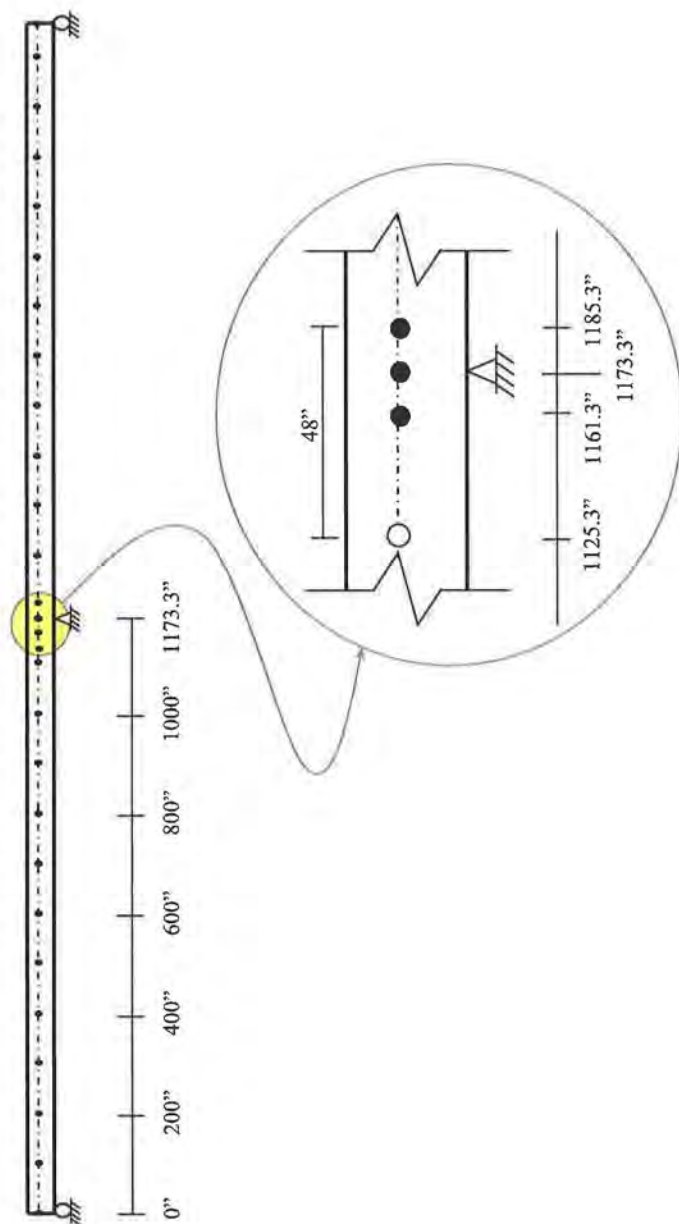
Figure 4.3 – Model #3 used in the Elastic Structural Analysis
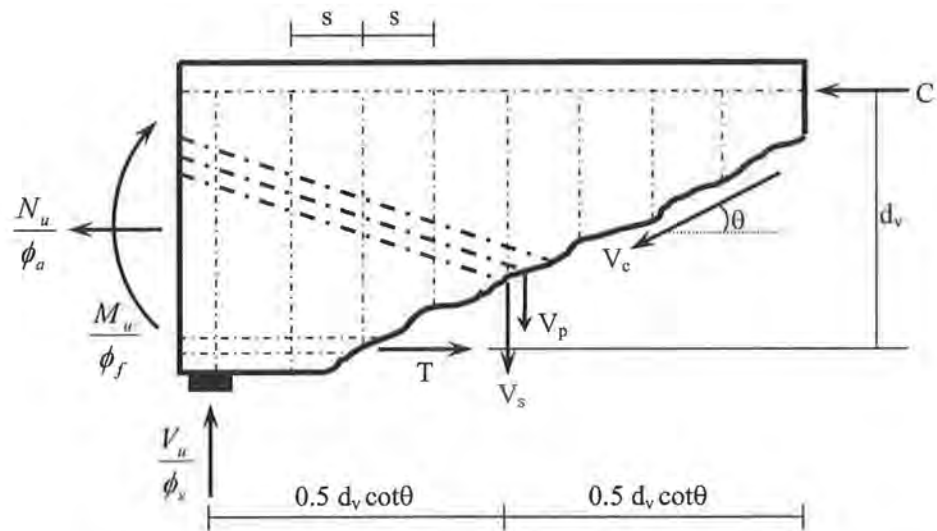
Figure 4.4 – Free-body Diagram of Girder End Region used to Formulate Equation 4.15a (AASHTO LRFD 2002)
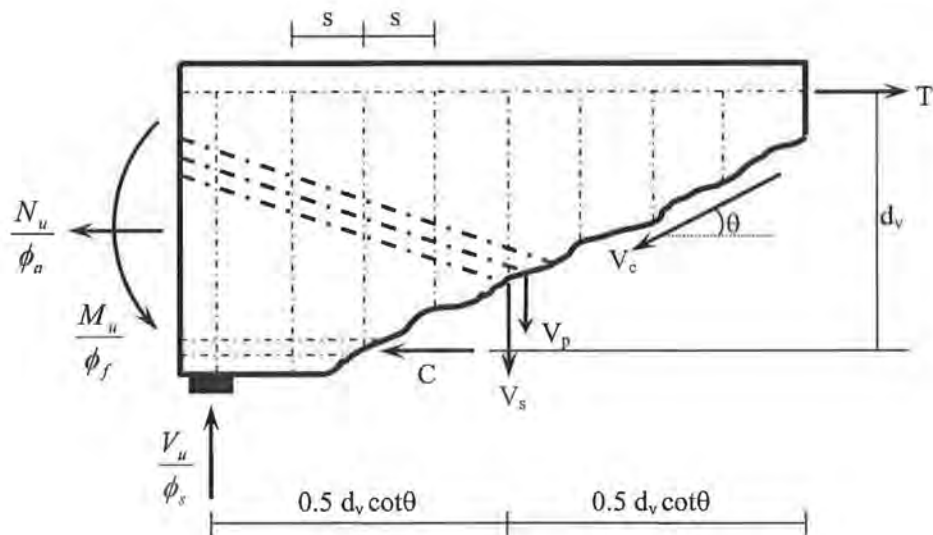
Figure 4.5 – Free-body Diagram of Girder End Region used to Formulate Equation 4.15b
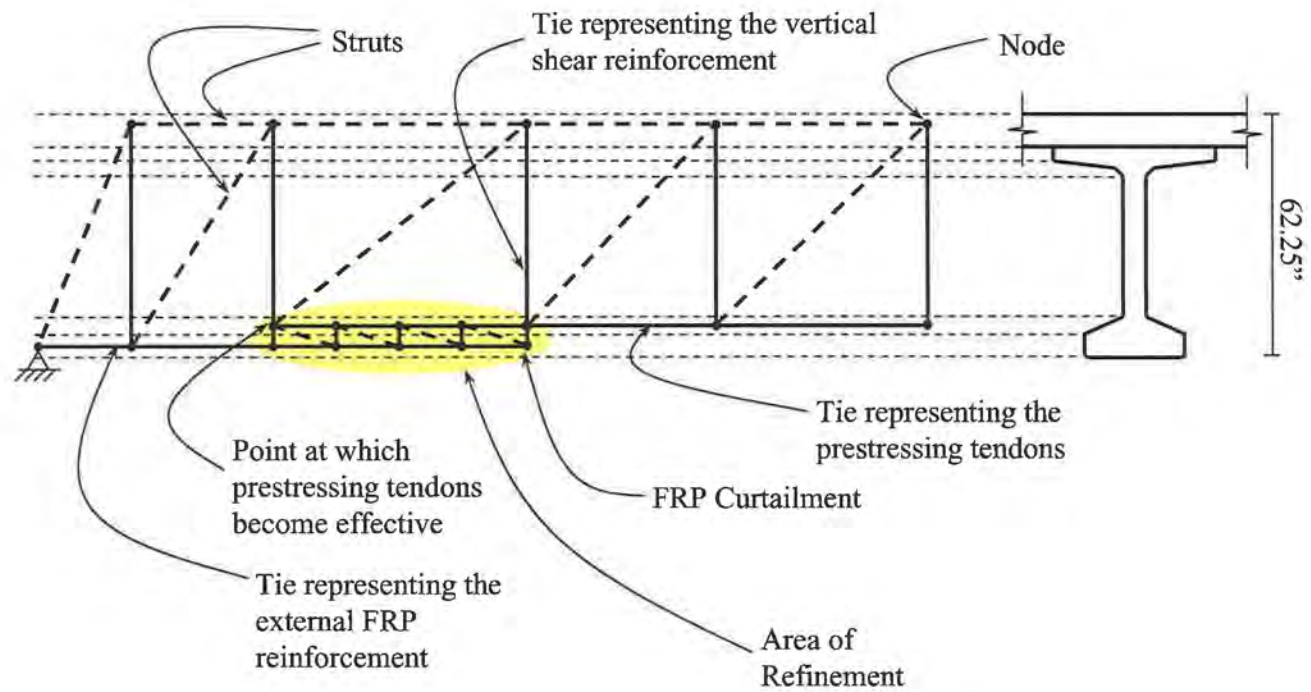
Figure 4.6 – Typical Strut-and-Tie Model

Struts

Tie representing the vertical shear reinforcement

Node

62.25"

Point at which prestressing tendons become effective

FRP Curtailment

Tie representing the prestressing tendons

Tie representing the external FRP reinforcement

Area of Refinement

CHAPTER 5: RESULTS OF ANALYTICAL PROCEDURES

The results of the analytical procedures described in Chapter 4 are presented in this chapter. The whole of the analytical results cannot be presented, due to the great volume of data obtained from the analysis of the Huntsville I-565 bridge structures. Only the most critical results from the elastic structural analysis, calculation of cracked girder shear and flexural capacities, and the strut-and-tie analysis have been presented. The results of the analytical procedures are discussed in Chapter 6.

5.1 ELASTIC STRUCTURAL ANALYSIS

The elastic analysis of the selected two-span structure was completed with the GT STRUDL 7.0 software. Three different models were utilized so that the behavior of the structure could be examined more closely. Two different types of vehicles, a design truck and a design tandem, were used to model the vehicular live load on the bridge structure. Vehicular live loads were moved longitudinally along the bridge in order to develop shear and moment envelopes. Dead loads and lane loads for a single girder line were also applied to the model.

A total of thirty live load shear and moment envelopes were created with the data from the elastic structural analysis. Each live load envelope is composed of maximum shear or moment effects and the corresponding moments or shear forces for a single design lane. For example, a maximum positive moment envelope includes the maximum positive moment and the corresponding shear force at discrete cross sections along the length of the girder. The simultaneous use of the maximum possible shear force and maximum possible moment at a cross section may be overly conservative.

5.1.1 Model #1: Simple Span Model

For Model #1, envelopes were created for shear and positive moment. Because Model #1 was a single simply supported span, negative moments were not induced in the girder. Corresponding moments and shear forces were determined, though they have not been shown. Figure 5.1 shows the live load shears for a simply supported girder. Figure 5.2 shows the live load moments for a simply supported girder. The meaning of the notation used in Figures 5.1-5.14 is given in Table 5.1. In each of these figures, the noncontinuous support is located at 1161.3 in. (29.50 m).

86

Table 5.1 – Notation used in Chapter 5 Figures

Symbol	Meaning
T	Design Tandem
LL	Lane Load
HL93	Design Truck
N	Northbound
S	Southbound

As can be seen in Figure 5.1, the maximum live load shear force occurs at the supports and has a magnitude of 96.0 kips (427 kN). The maximum live load shear force at midspan is 29.0 kips (129 kN). The single design truck and lane load (HL93) produces the maximum shear effects for Model #1. This result is not surprising because the design truck is much heavier than the design tandem.

In Figure 5.2, the maximum live load moment envelope is shown. Just like the shear envelope, the moment envelope is controlled by the placement of the design truck. The maximum live load moment at midspan is slightly greater than 26,000 kip-in. (35,300 kN-m).

The dead loads on the structure produce a linear shear diagram and a parabolic moment diagram. The maximum dead load shear force at the supports is 64.7 kips (288 kN). The maximum dead load moment occurs at midspan and has a magnitude of 18,750 kip-in. (25,400 kN-m). Dead load shear forces on the simple span are shown in Figure 5.3. Dead load moments are shown in Figure 5.4.

5.1.2 Model #2: Two-Span Continuous Model

For Model #2, three envelopes were created: shear, positive moment, and negative moment. The corresponding shear or moment effects were determined for each envelope, though they are not presented. Dead loads were assumed to be supported by simply supported girders. Thus, the dead load shear forces and moments in the girders are the same as that for Model #1.

Figure 5.5 shows the unfactored live load shears for a girder made continuous for live load. Cross sections located within 12 in. (305 mm) of the interior support are not of interest because they represent the continuity diaphragm. The maximum shear force at the simple support (noncontinuous end of girder) is 87.1 kips (387 kN), caused by a single design truck in the northbound direction. The maximum shear force at midspan is

15.0 kips (67 kN). The maximum shear force at the interior (continuous) support is 105.4 kips (469 kN), caused by a single design truck in the southbound direction. Although the greatest magnitude of shear force in the midspan region of the girder is produced by the dual design truck loading, Article 3.6.1.3.1 of the AASHTO LRFD states that such a loading should not be used to determine the maximum effects due to shear.

Figure 5.6 shows the live load moments for a girder made continuous for live load. Both positive and negative moments are shown in this figure. Live load combinations involving a single design truck or the design tandem control the positive moment envelope. When compared to the positive moment envelope for Model #1, positive moments from Model #2 are significantly smaller. The greatest live load positive moment from Model #2 occurs about 500 in. (12.7 m) from the simple support and has a magnitude of 19,200 kip-in. (26,000 kN-m).

Two different live load combinations control the negative moment envelope: the southbound orientation of a single design truck and dual design trucks. The dual design trucks control only a small portion of the envelope near the interior support. Negative moments due to live load begin to form 620 in. (15.7 m) from the simple support. The maximum live load negative moment occurs at the interior support and has a magnitude of nearly 22,000 kip-in. (29,800 kN-m).

5.1.3 Model 3: Two-Span Continuous Model with an Internal Hinge

It was not clear whether or not the use of Model #3 would be beneficial to the evaluation of the cracked prestressed concrete bridge girders. Before a full elastic structural analysis was performed with Model #3, a comparison was made between the results of an analysis for Model #2 and that for Model #3. The only difference between the two analyses would be the presence of the internal hinge in one span of Model #3. A uniformly distributed dead load and lane load were used on both spans. A single design truck was placed such that it was on the span containing the hinge, oriented in the southbound direction, with the rear axle at the internal hinge. Placement of the design truck in Model #2 was the same as that for Model #3, with the rear axle located 48 in. (1220 mm) from the interior support. Results of the comparison between Model #2 and Model #3 revealed that the shear forces and moments within the structure do not differ significantly as a result of the internal hinge.

A comparison of the factored ultimate load effects is shown in Table 5.2 for dead load, lane load, and a single design truck oriented in the southbound direction with the rear axle at the internal hinge location. The shear at the simple support in Model #3 is nearly 8.0 kips (35.6 kN) larger than that in Model #2. The small increase in shear at the simple support is insignificant because the factored ultimate shear forces at the simple support are significantly less than those at the interior support. The shear force at the interior support is less severe in Model #3. Positive moments forming in Model #3 are

88

considerably larger than in Model #2, though not as large as those forming in Model #1. Negative moments at the continuous support are less severe in Model #3.

In an attempt to verify this result, a second design truck was placed on the unhinged span of Model #3. The second design truck was oriented in the southbound direction. The front axle was placed at a distance of 552 in. (14.0 m) from the interior support, leaving the prescribed minimum distance of 600 in. (15.2 m) between the rear axle of the lead truck and the front axle of the trailing truck. The shear forces and moments induced in Model #3 were compared to those induced in Model #2 for an identical load configuration. The comparison revealed that shear forces and moments in the span containing the hinge in Model #3 are not significantly changed when a second truck is added to the adjacent span. In light of this result, Model #3 was not used to create shear and moment envelopes.

Table 5.2 – Comparison of Factored Ultimate Load Effects Induced in Models #2 and #3

for an Identical Load Configuration

	Model #2		Model #3	
	Location*	Magnitude	Location*	Magnitude
Shear	0.0 in.	29.4 kips	0.0 in.	37.2 kips
Shear	1161.3 in.	105.4 kips	1161.3 in.	96.8 kips
M^+_{MAX}	550.0 in.	8100 kip-in.	700.0 in.	13,000 kip-in.
M^-_{MAX}	1161.3 in.	12,200 kip-in.	1161.3 in.	3450 kip-in.

1 in. = 25.4 mm, 1 kip = 4.448 kN

* Measured from the simple support (x = 0 in.)

5.1.4 Factored Ultimate Load Effects

Equation 4.1 was used to determine the factored ultimate shear, V_u, and factored ultimate moment, M_u, at cross sections along the length of the bridge girders. The distribution factors calculated according to Equations 4.2–4.5 were then applied to determine the factored ultimate load effects on the girders. A total of thirty envelopes were developed from the elastic structural analysis of Model #1 and Model #2.

5.2 CALCULATION OF CRACKED GIRDER SHEAR AND MOMENT CAPACITIES

The shear, positive moment, and negative moment capacities of a typical unstrengthened cracked bulb-tee girder were calculated for multiple cross sections along the length of the girder. The capacities of the girder were then compared to the factored ultimate load effects to determine if the ultimate strength limit state is satisfied for shear and flexure. The tensile capacity of the longitudinal reinforcement on the flexural tension side of the girder was calculated and compared to the minimum required tensile capacity calculated with the appropriate version of Equation 4.15. The minimum required tensile capacity calculated with Equation 4.15 includes the effects of both shear and flexure on the tension developed in the longitudinal reinforcement.

Because all the cracked bridge girders in the selected two-span structure are precast prestressed concrete BT54 girders with identical reinforcement details, analysis of individual girders was not necessary. Thus, calculation of the shear and flexural capacities was performed for a typical cracked bridge girder. The worst cracking among the girders is in Girders 4 and 5 of northbound Span 5. Cracking occurs 38 in. (970 mm) from the face of the continuity diaphragm, or 41 in. (1040 mm) from the continuous end of the girder.

5.2.1 Shear Capacity

Examination of the procedure used to calculate the nominal shear capacity of the cracked girders reveals that the shear capacity of a concrete flexural member varies with the applied shear forces and moments. The nominal shear capacity of the cracked prestressed concrete bridge girders was calculated for each envelope developed with the elastic structural analysis. Shear capacity was calculated for both interior and exterior girders.

A plot of the design shear capacity of a cracked bulb-tee girder versus the factored ultimate shear demand from a single southbound design truck is shown in Figure 5.7 for a typical simply supported interior girder. The largest live load shear forces on a simply supported cracked girder result from a single design truck and lane load. Shear forces are at a maximum at the supports, regardless of the position or type of live loads on the bridge. The design shear capacity of the cracked girder is not adequate in a small region surrounding the cracked cross section. The factored ultimate shear demand exceeds the design shear capacity of a cracked interior girder by as much as 49.2 kips (219 kN), or 26.0 percent, for a single design truck oriented in the southbound direction. For a cracked exterior girder, the factored ultimate demand exceeds the design shear capacity in the same small region surrounding the cracked cross section, though the deficiency of shear capacity is only four kips.

Envelopes developed from the elastic structural analysis of Model #2 revealed that slightly larger shear forces develop near the continuous support when the structure acts as

90

a two-span continuous unit. A plot of the design shear capacity of a cracked bulb-tee girder versus the factored ultimate shear demand from a single southbound design truck is shown in Figure 5.8 for a typical interior girder made continuous for live load. The southbound orientation of the design truck induces the most severe live load shear forces at the interior support and at the cracked cross section. The design shear capacity of a cracked interior girder exceeds the factored ultimate shear demand by 18.3 kips (81 kN) in the region adjacent to the cracked cross section. At the cracked cross section, the factored ultimate shear demand is equal to 93 percent of the design shear capacity. The design shear capacity of the exterior girders is satisfactory for all factored ultimate load envelopes.

This significant reduction in the shear capacity of cross sections near the cracked cross section can be attributed to the slippage of the prestressing tendons. Because the effective prestressing force is not transferred to the concrete in the cracked end region of the girder, the longitudinal strain at mid-depth of the member is not compressive. As a result, the angle of inclination of the compressive concrete stresses in the cracked end region of the girder is much larger. This results in a sharp reduction in the concrete shear resistance, V_c, and the design shear capacity of the member, $\phi_s V_n$. The deficiency of shear capacity for cross sections in the cracked end regions of bulb-tee girders is addressed in the design of the external FRP reinforcement, which is presented and discussed in Chapter 7.

5.2.2 Longitudinal Reinforcement Capacity

The AASHTO LRFD requires that the longitudinal reinforcement on the flexural tension side of the member have a minimum capacity, T, calculated with Equation 4.15. For a simply supported cracked bulb-tee girder, the capacity of the longitudinal reinforcement is not adequate at either girder end. This is true for both interior and exterior cracked bridge girders. The capacity of the longitudinal reinforcement is unsatisfactory over a length of 14 in. (360 mm) at the uncracked end of the girder. At the continuous end of the girder, the capacity of the longitudinal reinforcement is unsatisfactory over a total length of 64 in. (1630 mm), which extends 23 in. (580 mm) beyond the location of the cracks.

Based upon shear and moment envelopes developed for the two-span continuous structure, positive moments form near the noncontinuous end of the girder and negative moments for near the continuous end of the girder. The tensile capacity of the longitudinal reinforcement is unsatisfactory over a length of 14 in. (360 mm) at the noncontinuous end of the girder, which is the same result obtained from the analysis of a simply supported girder. At the continuous end of the girder, the longitudinal tension reinforcement is in the deck slab. The tensile capacity of the longitudinal deck slab

reinforcement is satisfactory for all cross sections subjected to negative moments. These results are valid for both interior and exterior girders.

5.2.3 Positive Moment Capacity

The positive moment capacity of a typical cracked bridge girder was calculated for multiple cross sections along the length of the girder. Calculation of the flexural capacity of the member was performed according to Section 5.7.3 of the AASHTO LRFD. The design positive moment capacity of the girder was then compared to the factored ultimate moments from the elastic structural analysis. A strength reduction factor of 1.00 was used to calculate the design positive moment capacity of the girder, as recommended in the AASHTO LRFD.

As expected, the largest positive moments induced in the cracked girders are the result of loads applied to the simple span structure. A plot of the design positive moment capacity of a typical simply supported interior girder versus the factored ultimate demand from a single southbound design truck is shown in Figure 5.9. The design positive moment capacity of a typical interior cracked girder is not adequate for cross sections in the continuous end of the girder. Deficiencies of positive moment capacity occur for cross sections between the cracked cross section and the continuous end of the girder and are a result of the cracks in the girder end.

A plot of the design positive moment capacity of a typical simply supported exterior girder versus the factored ultimate demand from a single northbound design truck is shown in Figure 5.10. As was the case for an interior girder, the design positive moment capacity is not adequate for cross sections near the continuous end of the girder. The deficiency of positive moment capacity in the exterior girder is a result of the cracks in the girder end.

The positive moments induced in the two-span continuous structure are not as large as those that occur in the simply supported structure. For this reason, the positive moment envelopes developed for Model #2 are not presented here. The design positive moment capacity of the cracked girders is sufficient for both interior and exterior girders if the bridge behaves as a two-span continuous structure.

5.2.4 Negative Moment Capacity

The design negative moment capacity of the cracked bridge girders was calculated with a procedure that utilizes force equilibrium, strain compatibility, and constitutive material properties. Girders were assumed to act as non-prestressed reinforced concrete flexural members when subjected to negative moments. Two different flexural strength reduction factors were considered when the design negative moment capacity was calculated. The

effect of the strength reduction factor on the design negative moment capacity of a typical cracked girder is discussed in Section 6.1.

The largest negative moments form at the continuous end of a typical girder due to 90 percent of the effects of two design trucks oriented in the southbound direction. A plot of the design negative moment capacity of a typical interior girder made continuous for live load versus the factored ultimate moment demand is shown in Figure 5.11 for a strength reduction factor of 1.00. The factored ultimate moment demand only approaches the design capacity of the girder near the ends of the member. At the continuous support, the design negative moment capacity of the girder is 26,600 kip-in. (36,000 kN-m) and the factored ultimate demand is 25,900 kip-in. (35,100 kN-m).

The factored ultimate negative moments in a typical exterior girder exceed the design negative moment capacity of the girder when a strength reduction factor of 1.00 is used. A plot of the design negative moment capacity of a typical exterior girder made continuous for live load versus the factored ultimate moment demand is shown in Figure 5.12 for a strength reduction factor of 1.00. The deficiency of design negative moment capacity is over a length of 36 in. (910 mm) at the continuous end of the girder. The lack of moment capacity at the continuous end is not a result of the cracking in the girder end, though. The cracking observed in the bulb-tee girders is not symptomatic of excessively large negative moments being applied to the girder.

A smaller strength reduction factor was also considered in the calculation of the design negative moment capacity of the cracked girder. Article 5.5.4.2.1 of the AASHTO LRFD suggests a strength reduction factor of 0.90 for flexure in non-prestressed concrete members. The use of the smaller strength reduction factor results in a ten percent reduction in the design negative moment capacity of a typical cracked girder. A plot of the design negative moment capacity of a typical interior girder made continuous for live load versus the factored ultimate moment demand is shown in Figure 5.11 for a strength reduction factor of 0.90. Additional flexural strength deficiencies become apparent near the continuous end of the girder where negative moments are greatest. The deficiency of design negative moment capacity occurs over a distance of 16 in. (410 mm) at the continuous end of the girder. Figure 5.14 shows a plot of the design negative moment capacity of a typical interior girder made continuous for live load versus the factored ultimate moment demand for a strength reduction factor of 0.90. Flexural deficiencies exist over a distance of 48 in. (1220 mm) at the continuous end of the girder.

5.3 STRUT-AND-TIE ANALYSIS

Strut-and-tie models were developed to examine the flow of forces in the continuous end of a cracked girder for specific load configurations. The factored ultimate forces in the bottom flange ties were compared to the tensile capacity of the longitudinal tensile reinforcement that they represent, namely the external FRP reinforcement and the

prestressing tendons. The transfer of tensile forces from the external FRP reinforcement to the prestressing tendons in the region of the FRP curtailment was also examined using the strut-and-tie analysis.

Four critical load cases were chosen based upon their ability to induce maximum shear forces and moments at the cracked cross section. The load cases chosen necessitated the creation of three strut-and-tie models. The results of the strut-and-tie analysis of a typical cracked girder are presented as factored ultimate member forces, as shown in Table 5.3.

Model A, shown in Figure 5.15, is representative of the cracked end of a simply supported bulb-tee girder for the load configurations producing maximum shear and maximum positive moment effects at the cracked cross section. As expected, tensile forces develop in the ties representing the prestressing tendons and the external FRP reinforcement. The factored ultimate tension force in the external FRP reinforcement is 104.0 kips (463 kN) in Member 1 and 255.4 kips (1136 kN) in Member 2. Member 16, representative of the prestressing tendons, must carry a factored ultimate tension force of 300.1 kips (1335 kN). The factored ultimate tension force in the prestressing tendons increases away from the support, becoming as large as 631.5 kips (2809 kN) in Member 19.

Model B is shown in Figure 5.16 and is representative of the cracked end of a bulb-tee girder made continuous for live load. The load configuration used with the Model B produces maximum shear at the cracked cross section. Because negative moments exist in the region adjacent to the continuous support in the structure, compression forces exist in the bottom flange. The figure shows that the applied loading does not induce tension in members in the bottom flange near the support. The ties representing the prestressing tendons are required to carry some tension, though it is much less than that required as a result of other critical load cases. The factored ultimate tension force in Member 16 is only 177.1 kips (788 kN).

Model C, shown in Figure 5.17, is representative of the cracked end of a bulb-tee girder made continuous for live load that has an internal hinge at the cracked cross section. The load configuration used with Model C produces maximum shear at the cracked cross section. The applied loads induce tension in the ties representing the external FRP reinforcement and the prestressing tendons. A factored ultimate tension force of 6.0 kips (26.7 kN) exists in Member 1. Member 2 has a factored ultimate tension force of 140.0 kips (623 kN). Member 16 represents the prestressing tendons and has a factored ultimate tension force of 189.3 kips (842 kN). The factored ultimate tension force in the prestressing tendons increases to 552.4 kips (2457 kN) in Member 19.

The development of the forces in the ties is a critical subject that must be addressed. All ties must be capable of carrying the factored ultimate force from the strut-and-tie analysis along the entire length of the tie. Thus, for ties representing prestressing tendons or external FRP reinforcement, tensile forces must be fully developed at the end of the tie

94

closest to the support. For Member 1, the tie extending from the nodal zone at the member support, the tension force must be developed at the point where the centroid of the reinforcement extends beyond the extended nodal zone (ACI Committee 318 2002). For design and analysis purposes, the extended nodal zone was considered to end at the inside face of the bearing pad.

From the results of the strut-and-tie analysis, it is clear that the critical load cases for the simply supported girder (Model A) will control the required tensile capacity of the external FRP reinforcement and the prestressing tendons. Although the loading applied to Model C produces tension in the bottom flange ties, the magnitudes of the tensile forces are not as severe as those from Model A. The results from Model B are of little importance because tension forces were not induced in the bottom flange ties.

Although a strut-and-tie model of the existing cracked girder was not made, some conclusions can be made about the behavior and strength of an unstrengthened cracked bridge girder. Examination of the strut-and-tie models reveals that applied loads cause tensile forces in the bottom flange if the behavior of the girders is not that of a continuous structure. Because the prestressing tendons have been assumed to be ineffective between the girder end and the crack location, they are not capable of resisting the tension forces present in the bottom flange ties. Without the external FRP reinforcement, the cracked prestressed concrete girders are not capable of transferring loads to the supports by the mechanism assumed in Model A and Model C.

If the behavior of the structure is that of a two-span continuous structure, Model B is the most applicable of the three models presented. The validity of the Model B depends on whether or not compression forces are actually induced in Members 1 and 2. Even if the structure exhibits two-span continuous behavior, the width of the cracks in the end region of the girder may hinder the formation of compressive forces in the bottom flange of the member.
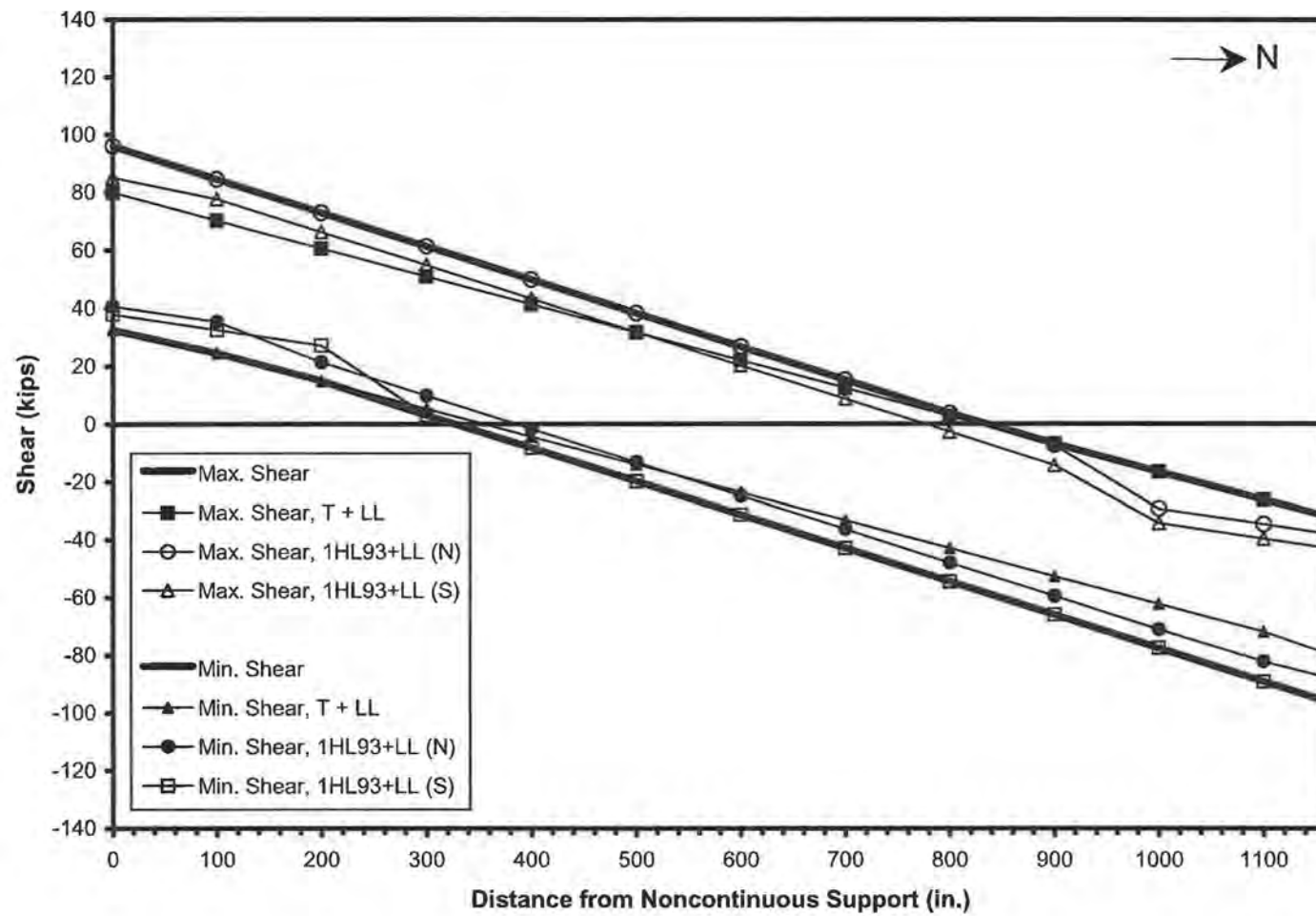
Figure 5.1– Unfactored Live Load Shears for Simply Supported Girder

96
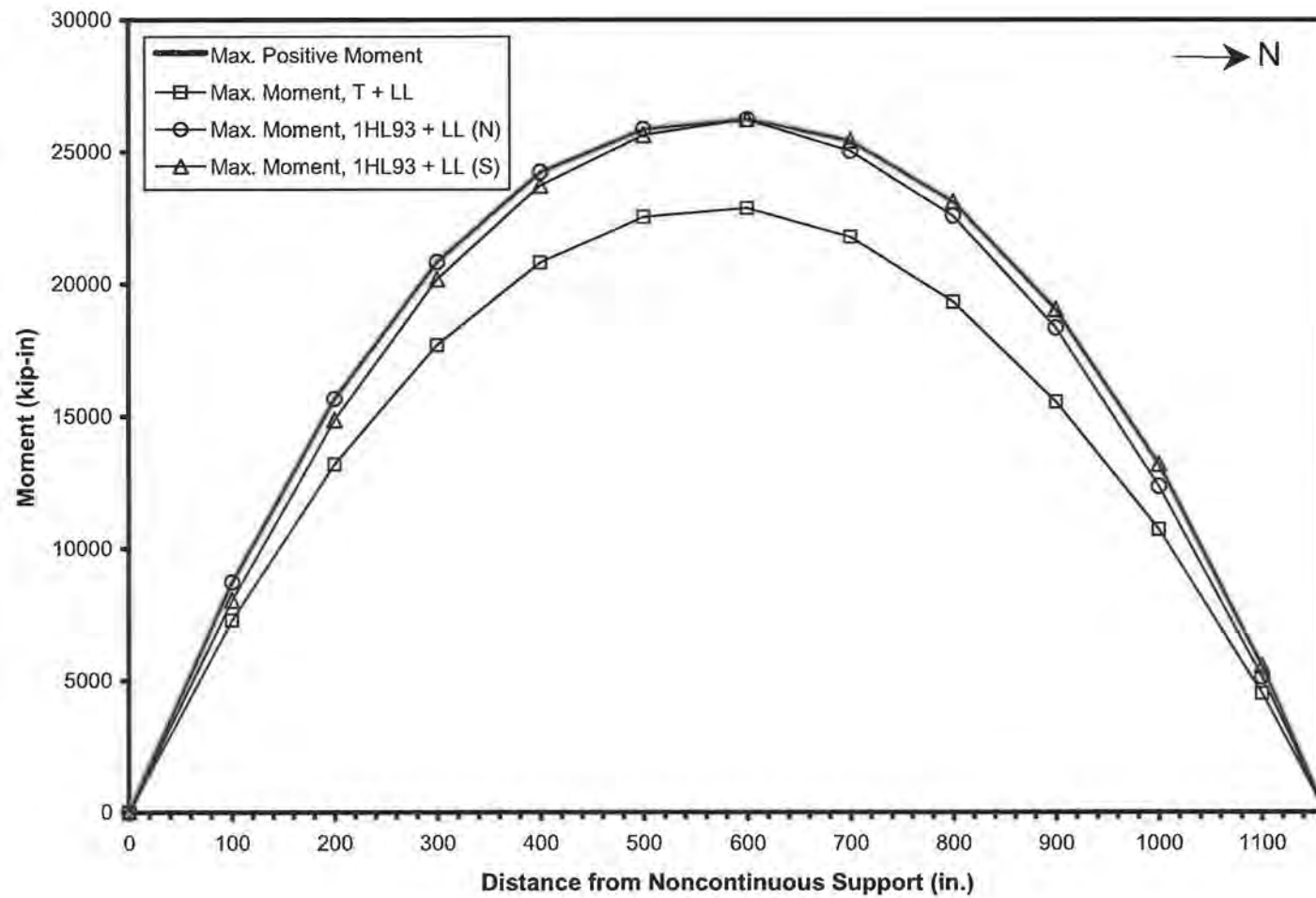
Figure 5.2– Unfactored Live Load Moments for Simply Supported Girder
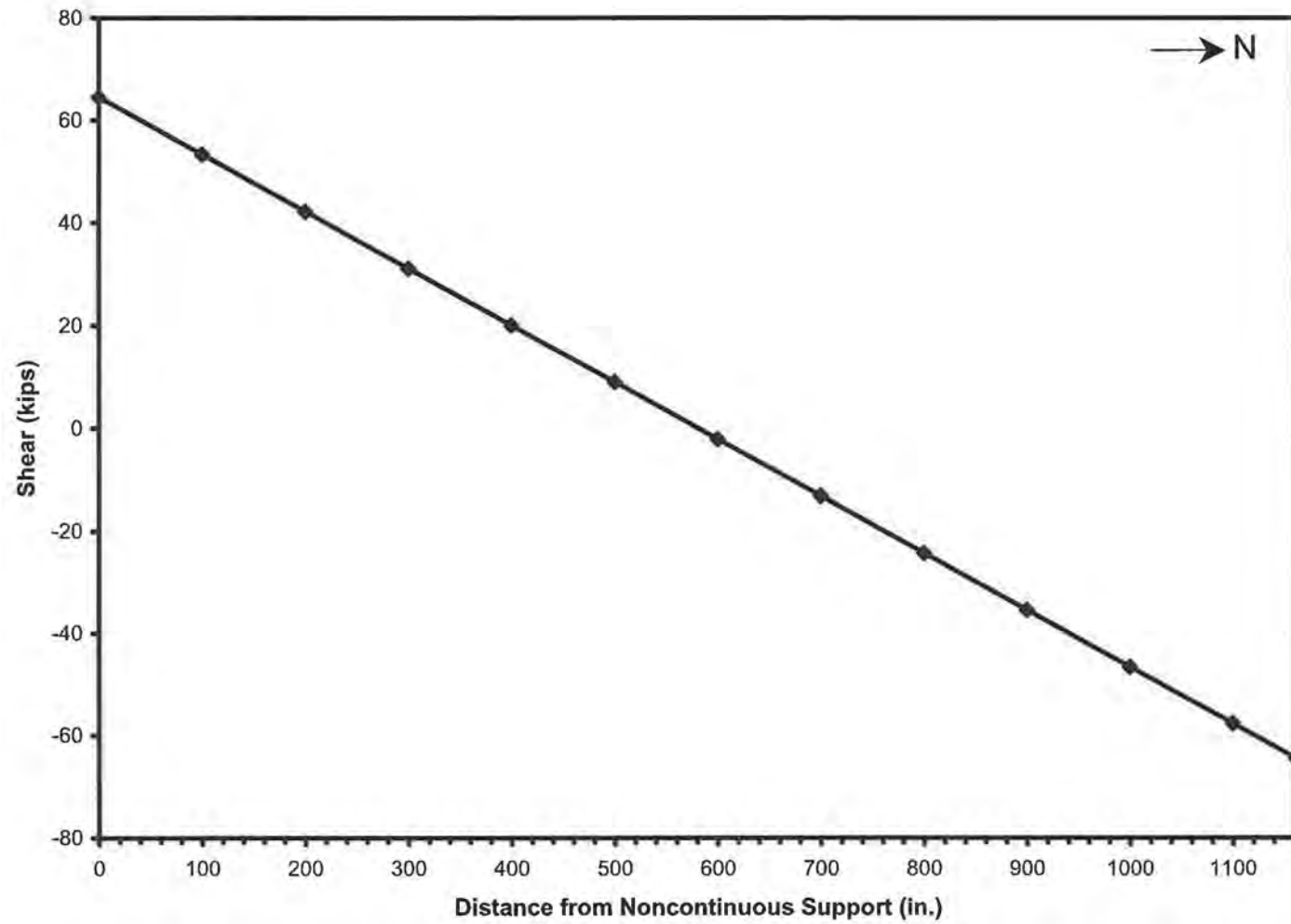
Figure 5.3– Unfactored Dead Load Shear Diagram

98
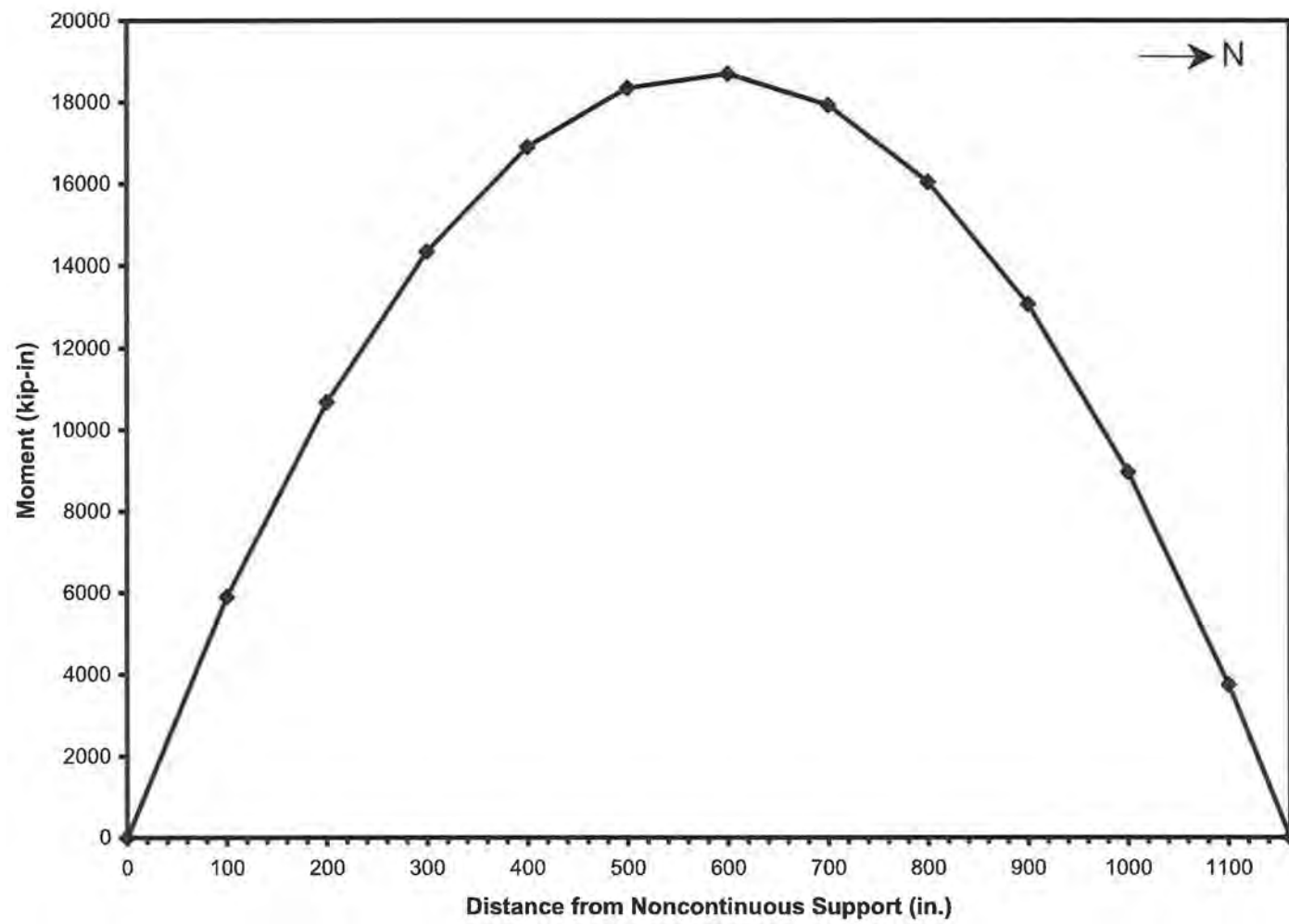
Figure 5.4– Unfactored Dead Load Moment Diagram

99
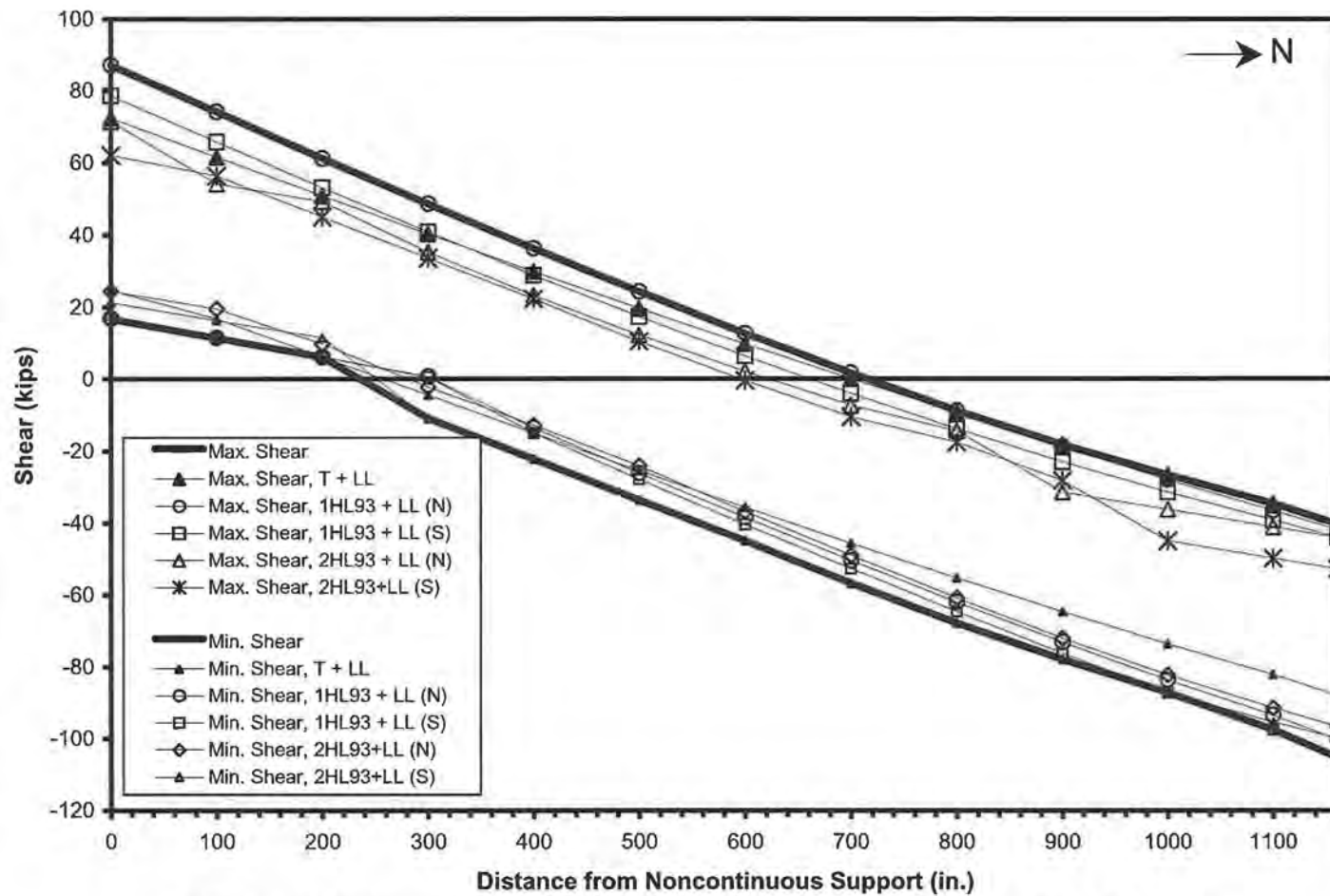
Figure 5.5– Unfactored Live Load Shears for Girder Made Continuous for Live Load
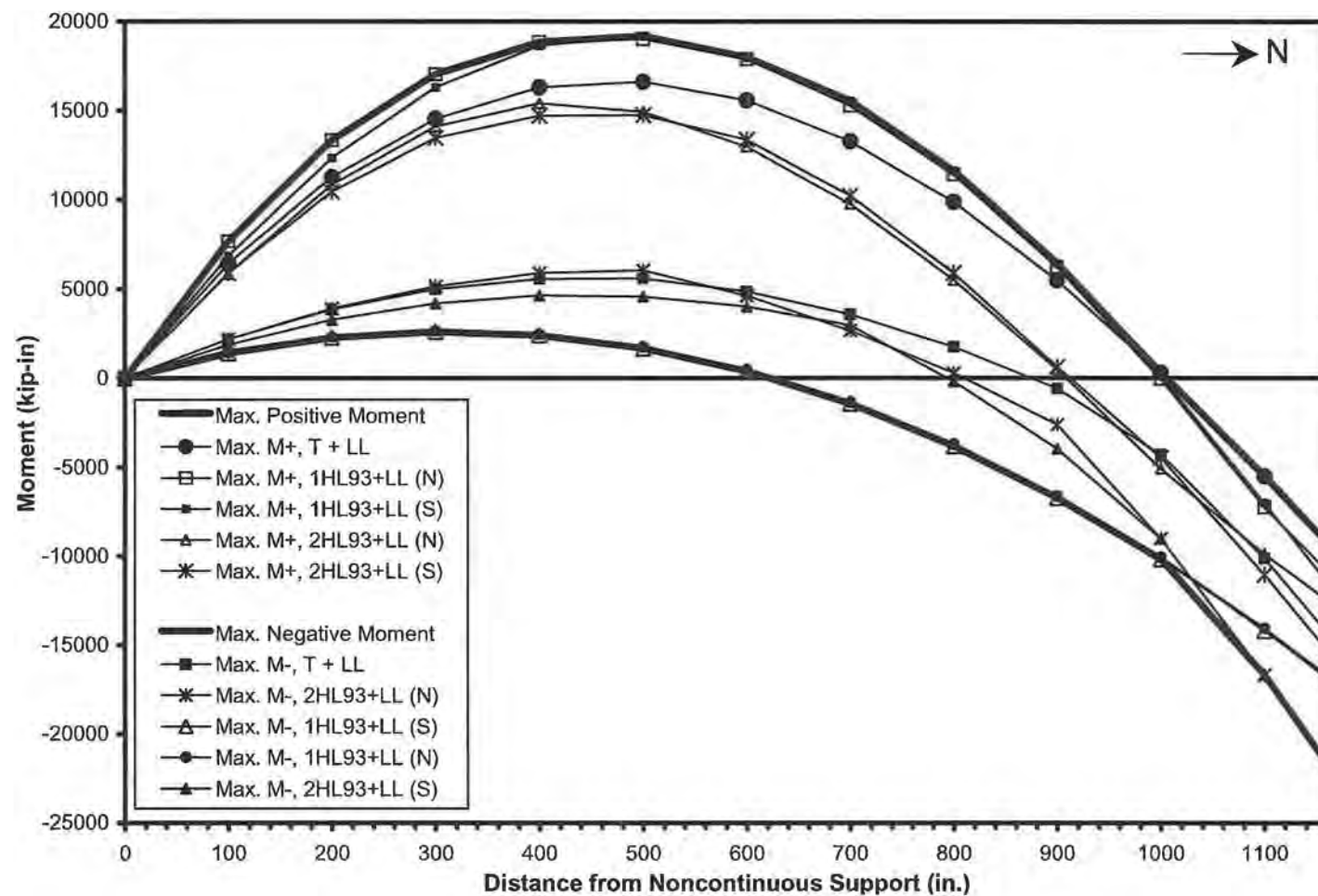
Figure 5.6– Unfactored Live Load Moments for Girder Made Continuous for Live Load
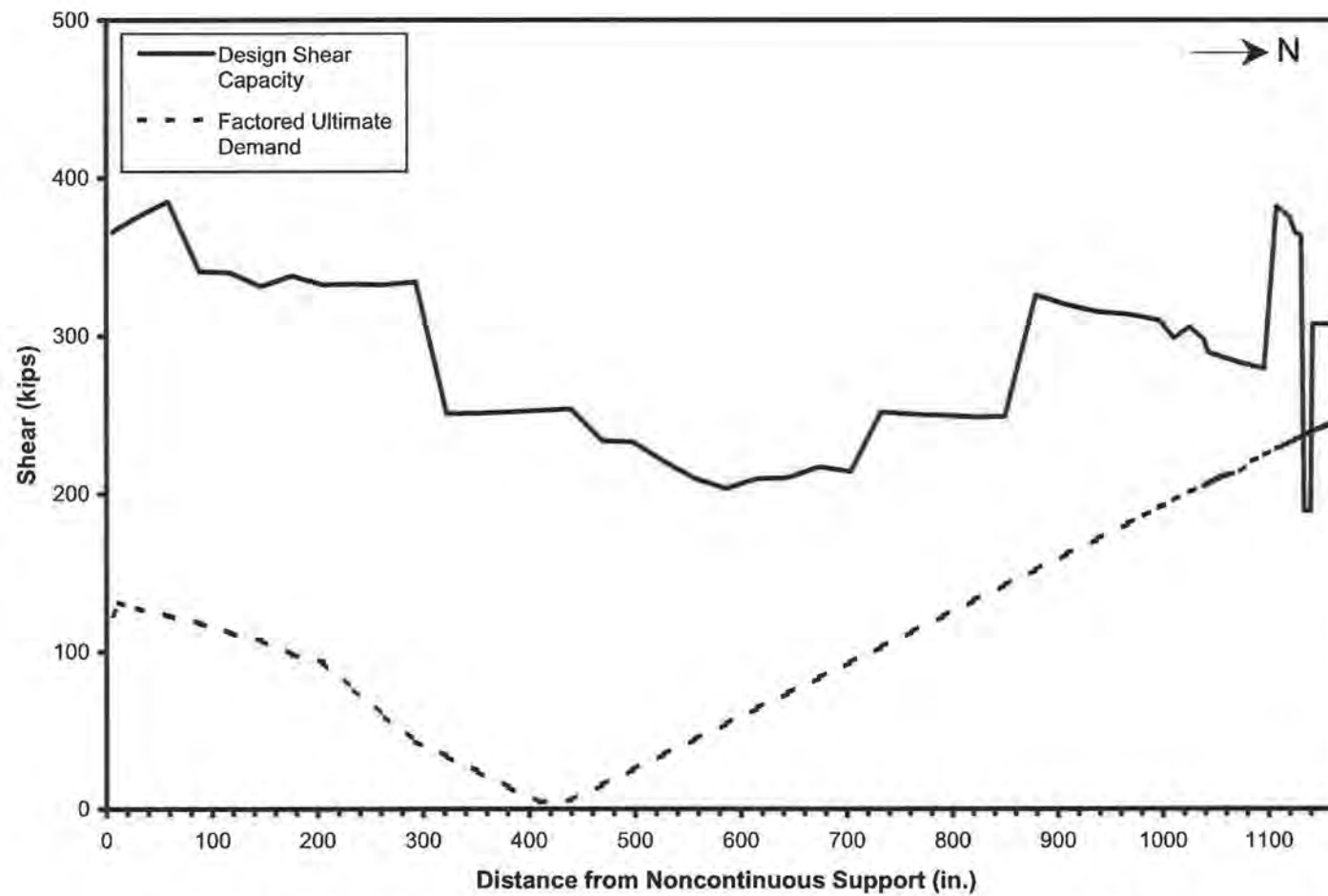
***Figure 5.7– Design Shear Capacity vs. Factored Ultimate Demand for a Simply Supported
Interior Girder (1 Design Truck, Southbound)***

102
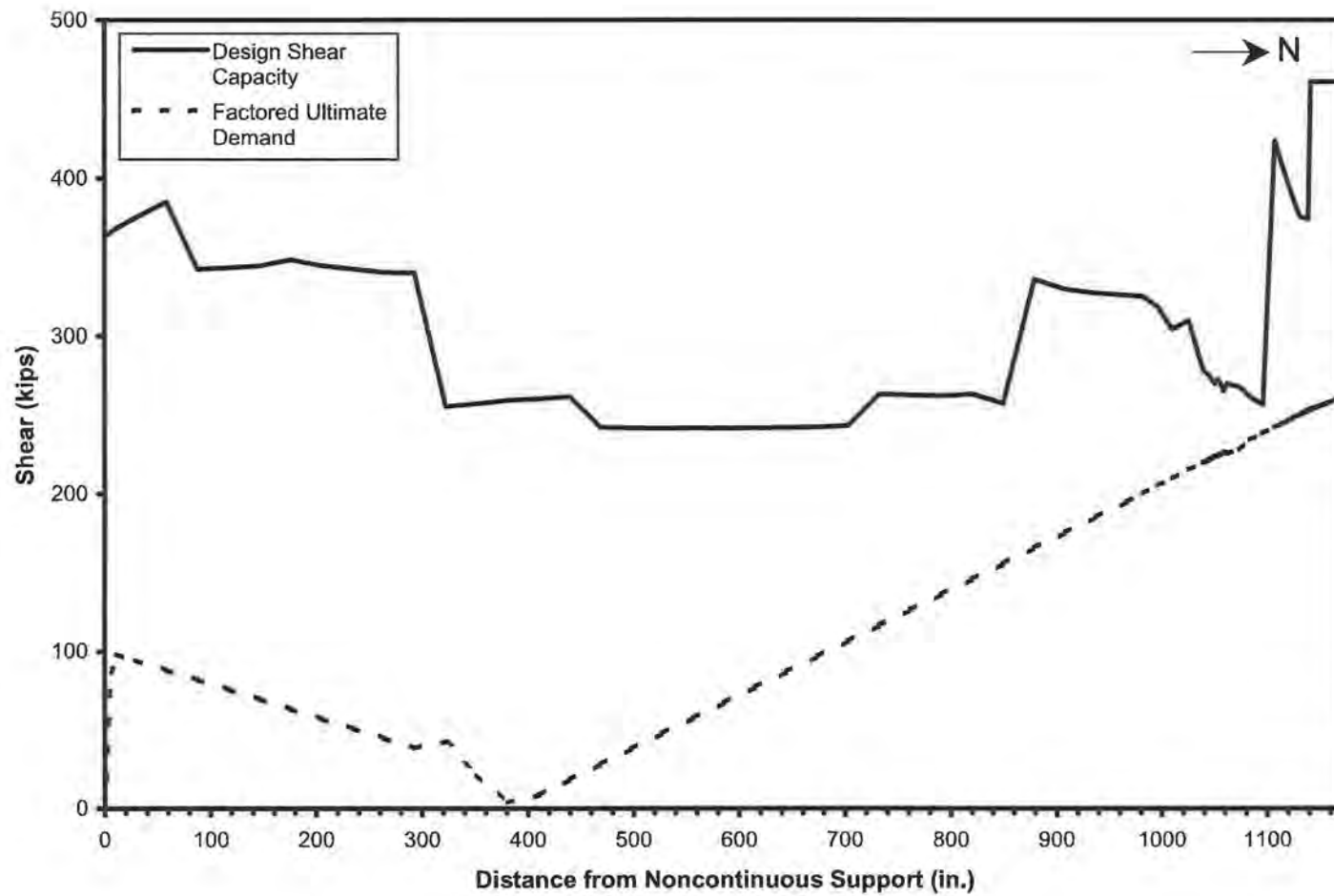
Figure 5.8– Design Shear Capacity vs. Factored Ultimate Demand for anInterior Girder Made Continuous for Live Load (1 Design Truck, Southbound)

103
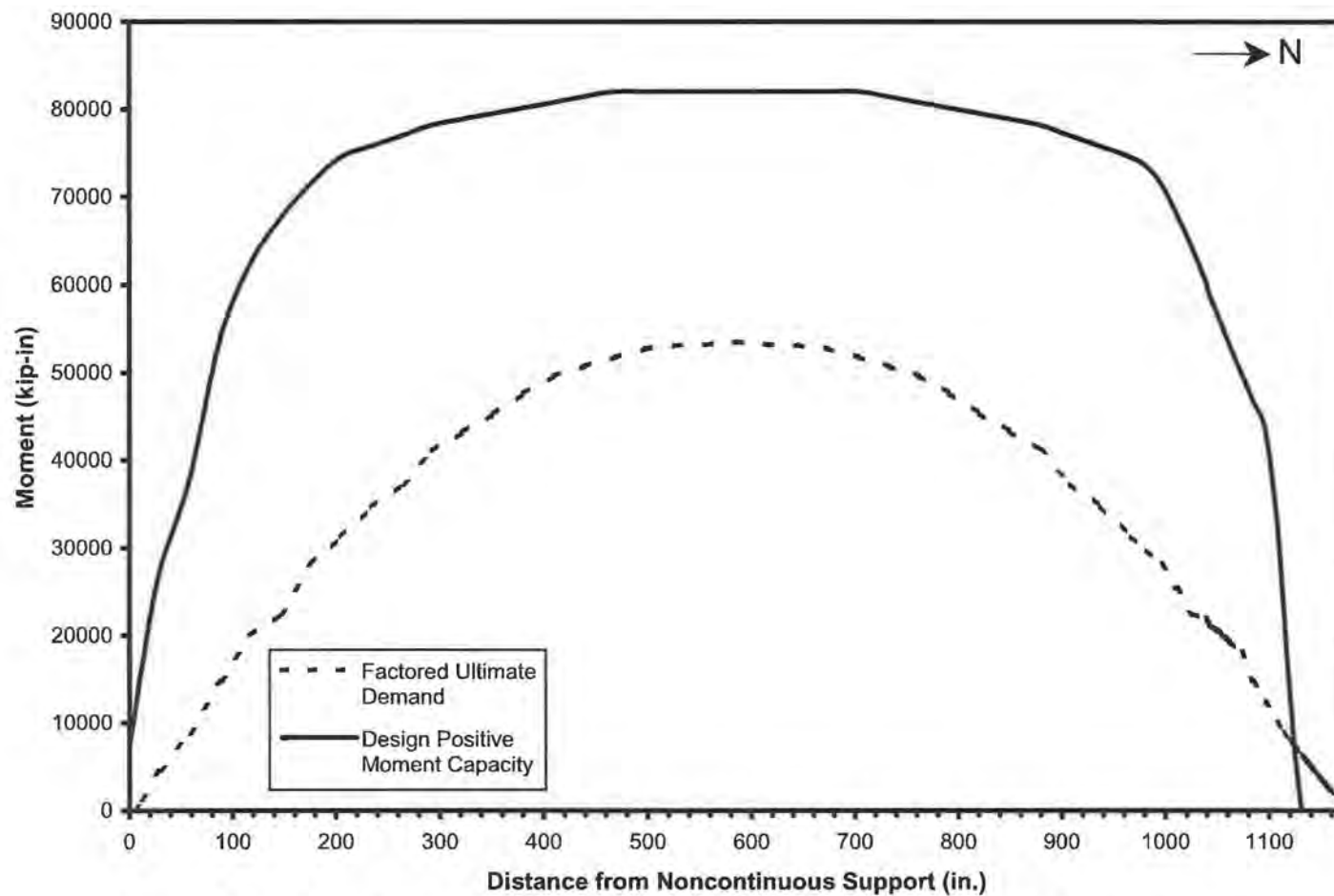
Figure 5.9– Design Positive Moment Capacity vs. Factored Ultimate Demand for a Simply Supported Interior Girder (1 Design Truck, Southbound)
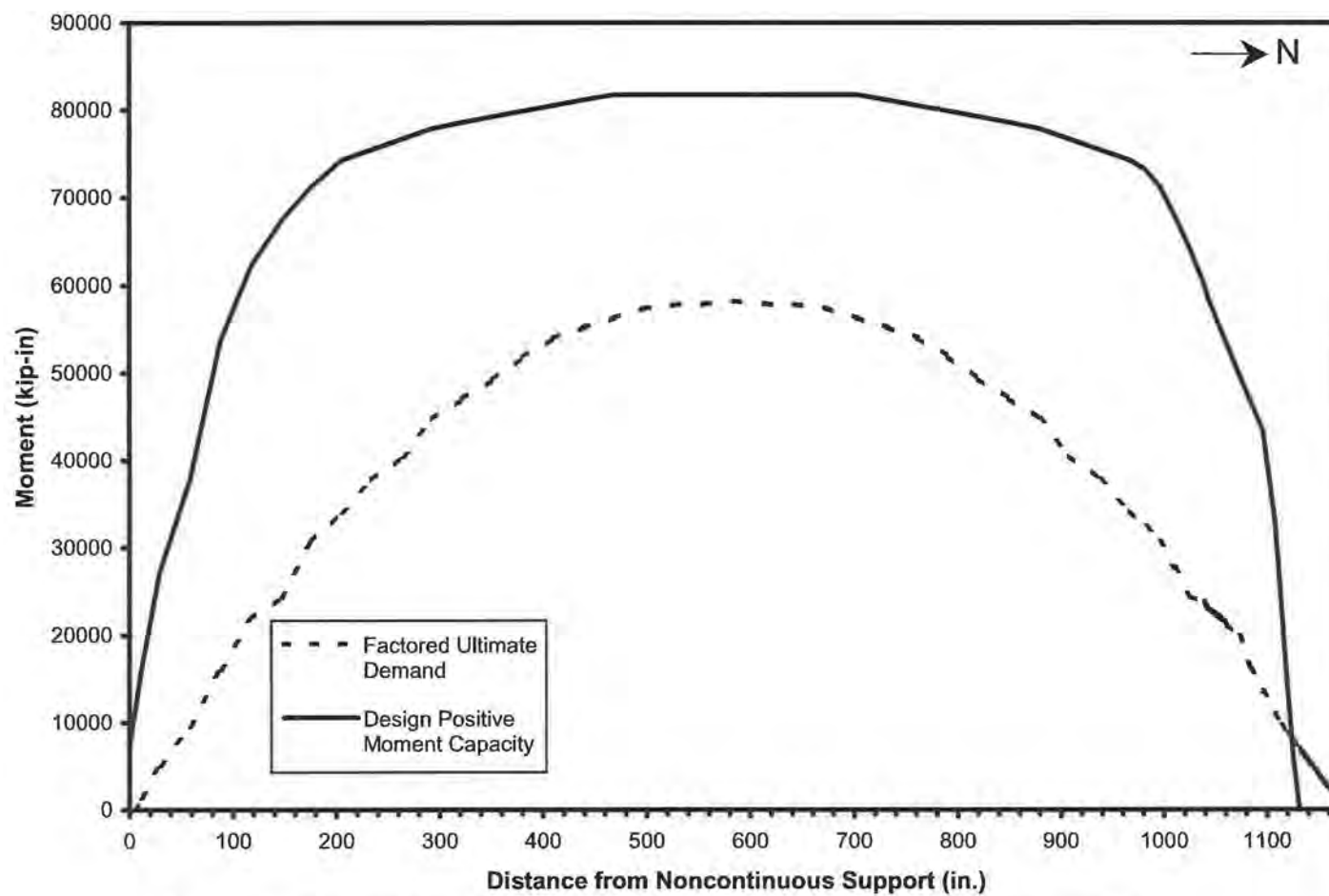
Figure 5.10– Design Positive Moment Capacity vs. Factored Ultimate Demand for a Simply Supported Exterior Girder (1 Design Truck, Northbound)
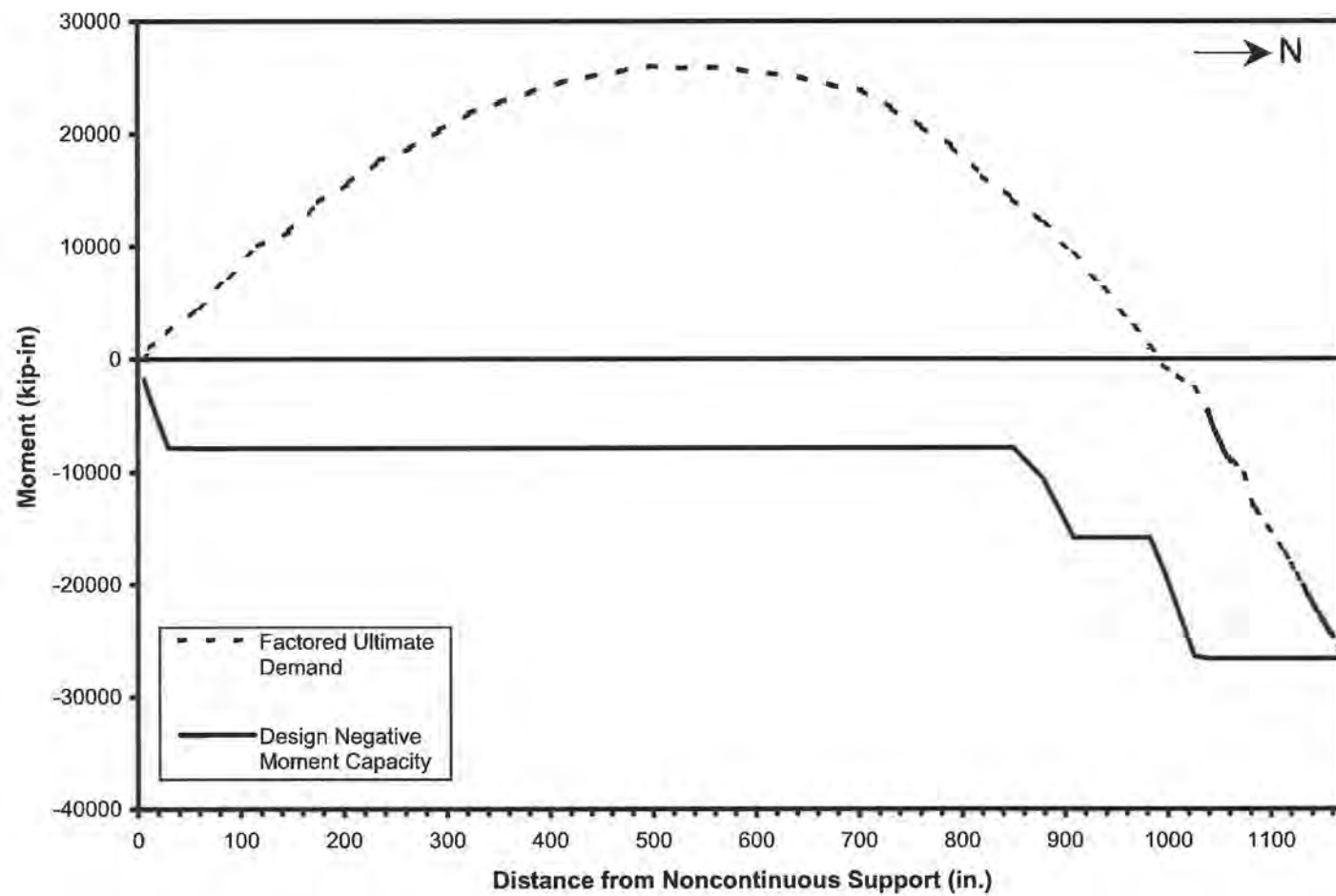
Figure 5.11– Design Negative Moment Capacity vs. Factored Ultimate Demand for an Interior Girder Made Continous for Live Load ($\phi_f = 1.00$)

106
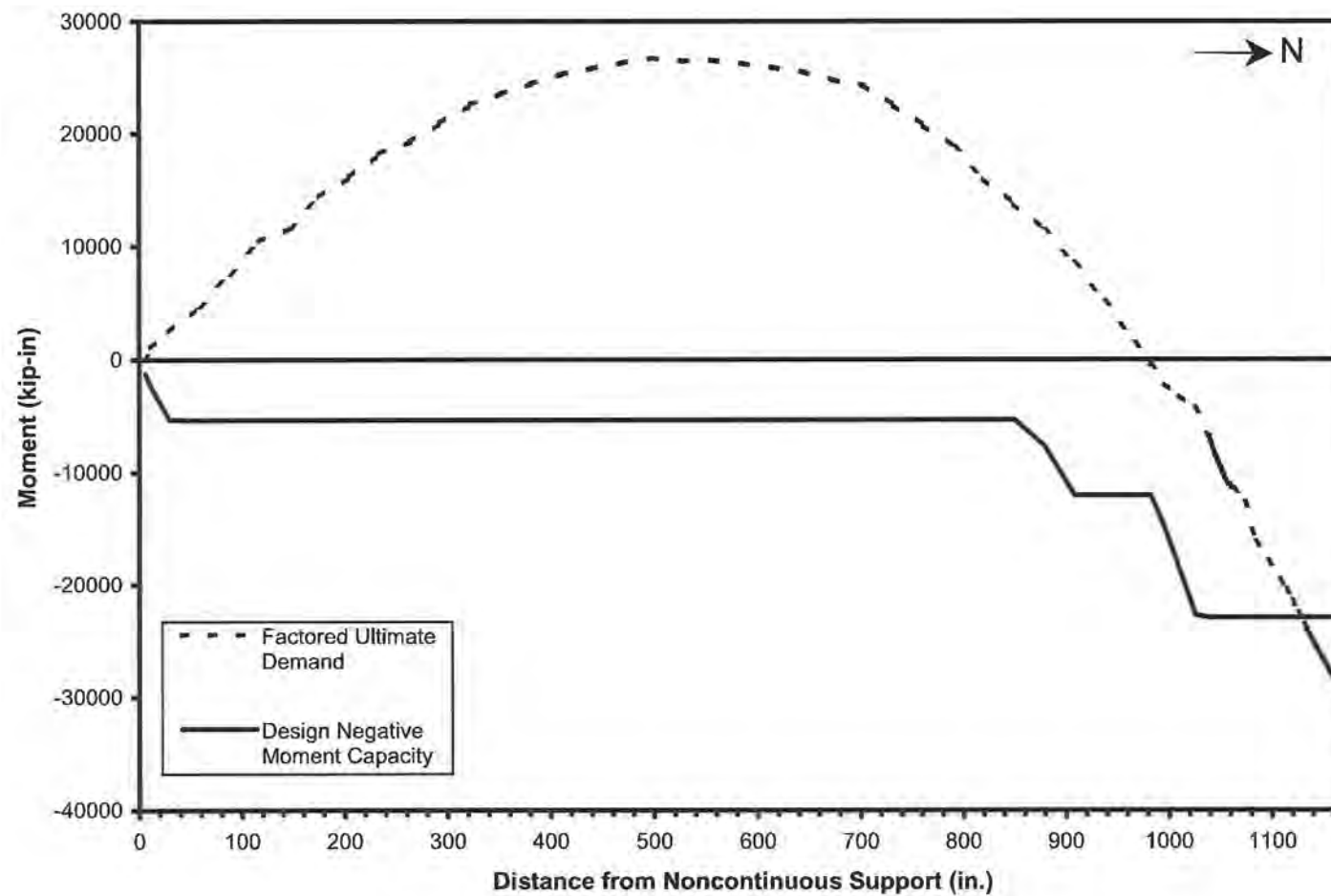
Figure 5.12– Design Negative Moment Capacity vs. Factored Ultimate Demand for an Exterior Girder Made Continuous for Live Load ($\phi_f = 1.00$)

107
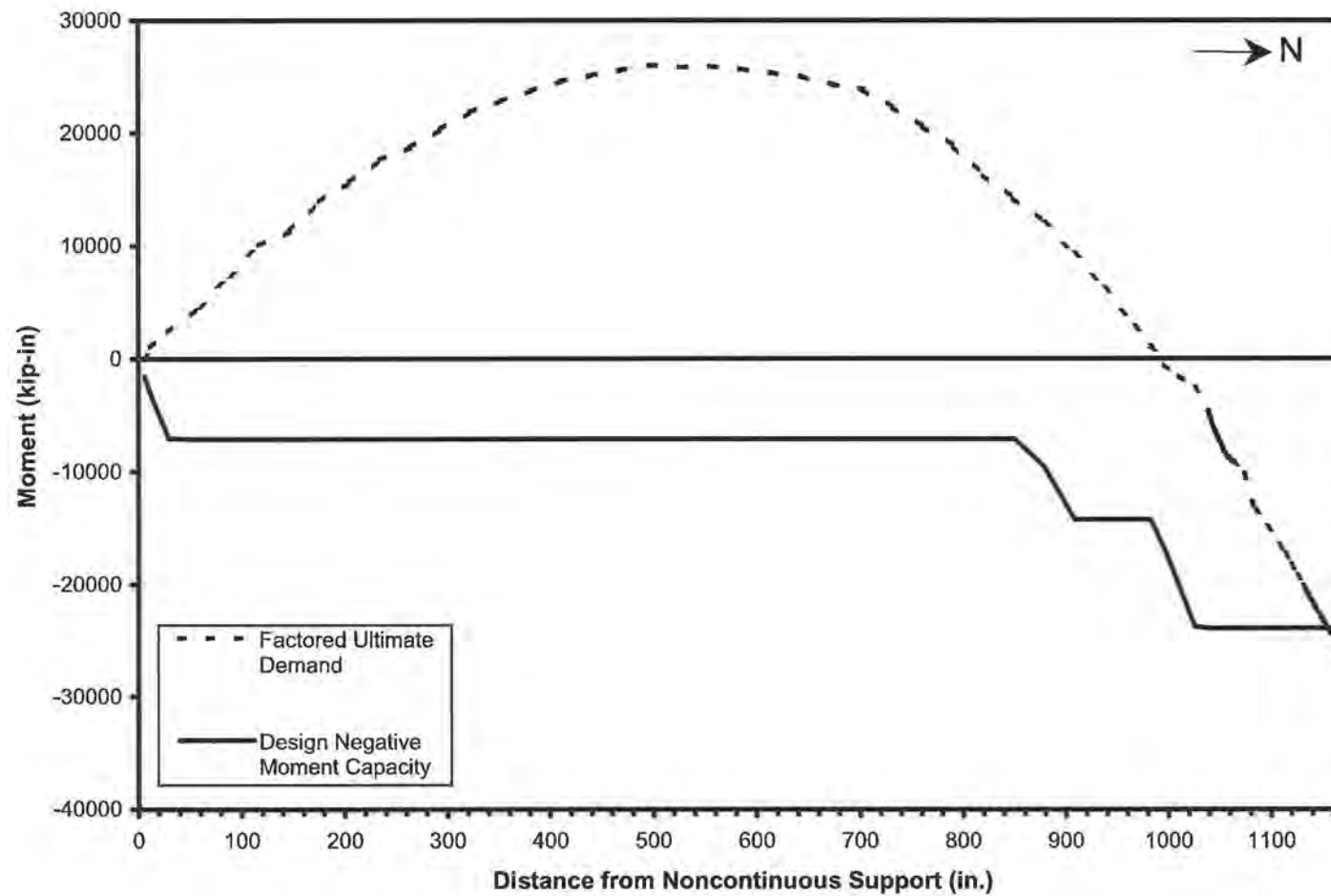
Figure 5.13– Design Negative Moment Capacity vs. Factored Ultimate Demand for an Interior Girder Made Continuous for Live Load ($\phi_f = 0.90$)

108
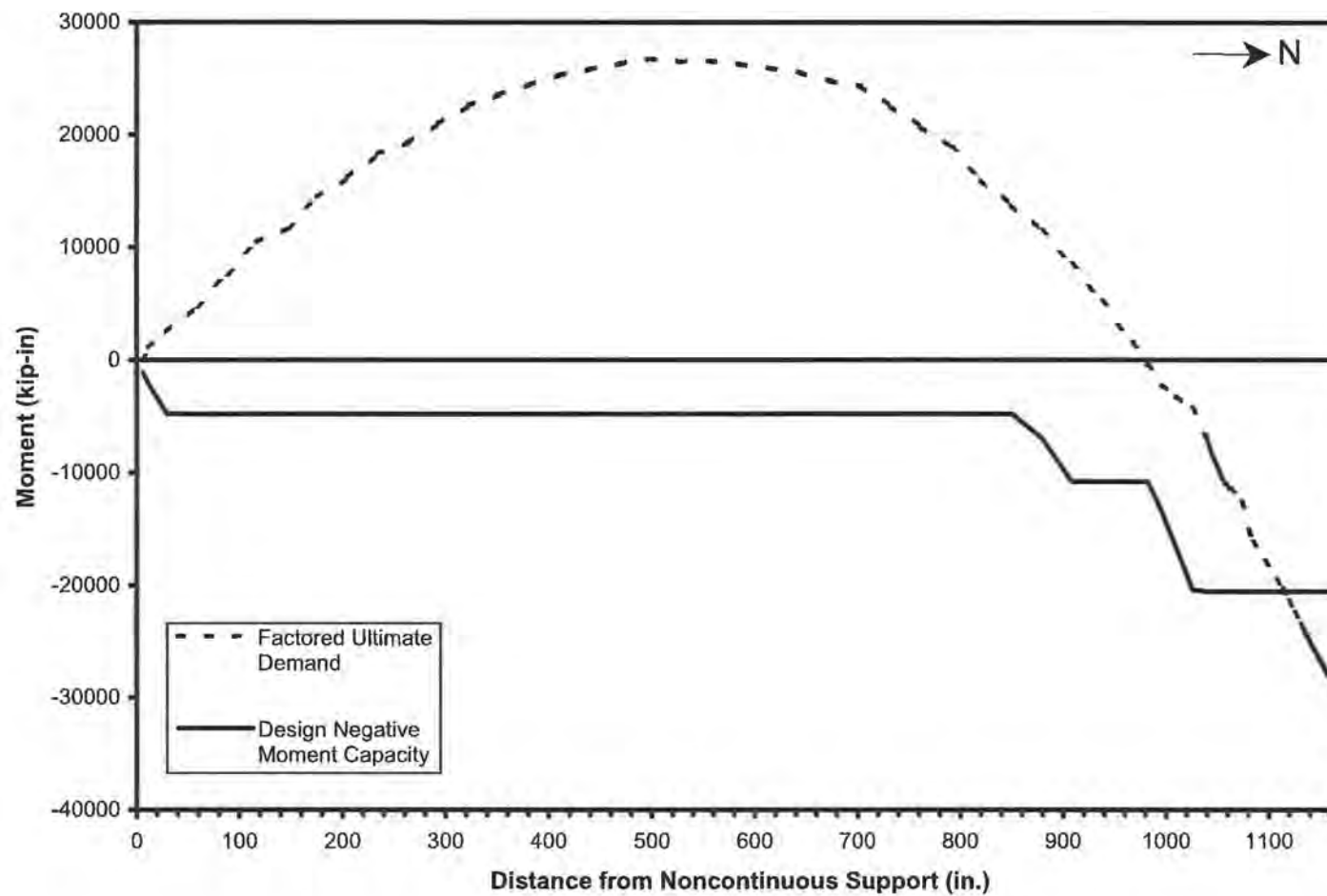
Figure 5.14– Design Negative Moment Capacity vs. Factored Ultimate Demand for an Exterior Girder Made Continuous for Live Load ($\phi_f = 0.90$)
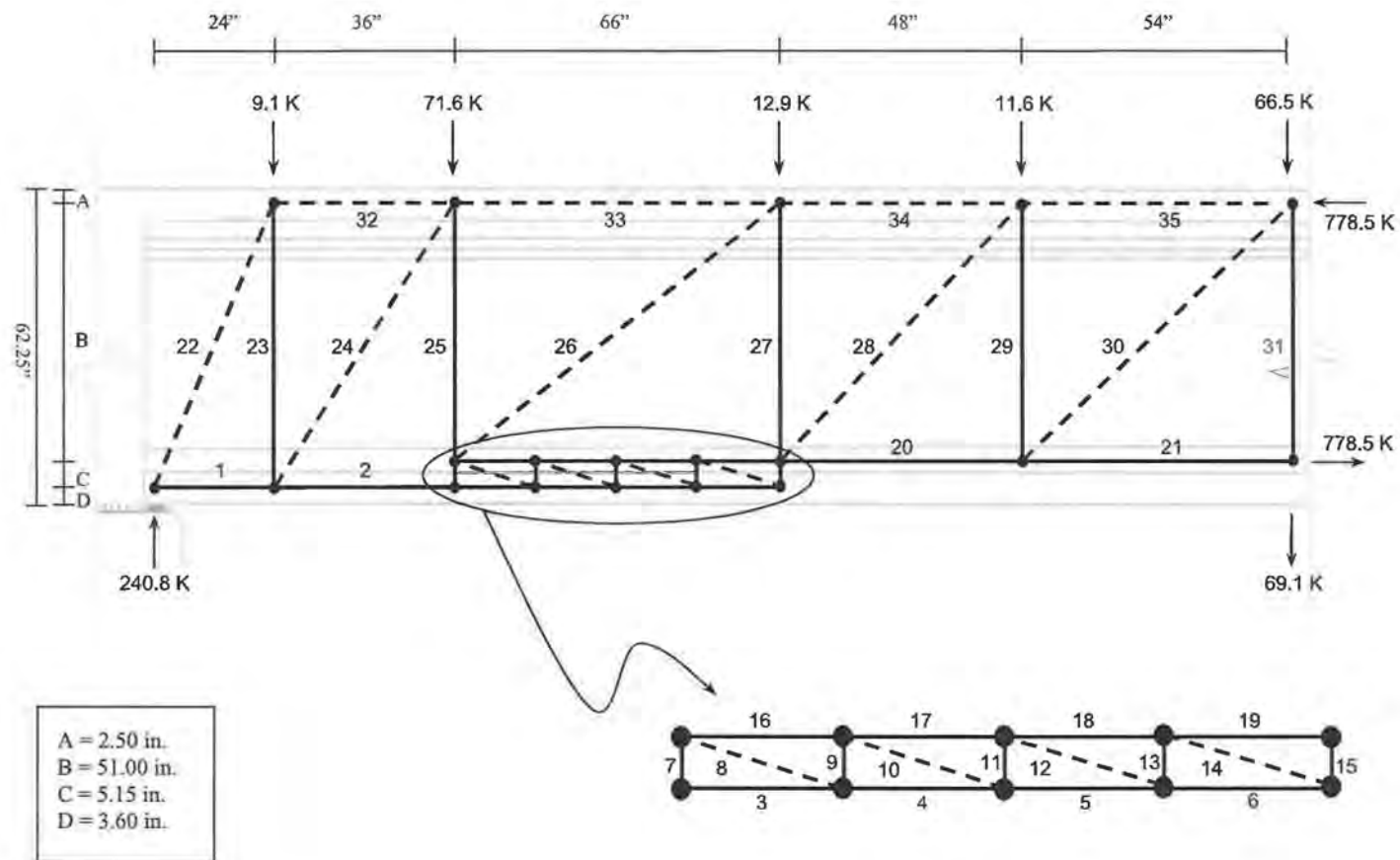
Figure 5.15 – Strut-and-Tie Model of Cracked End Region of a Simply Supported Girder (Model A)

110

Figure 5.16 – Strut-and-Tie Model of Cracked End Region of a Girder Made Continuous for Live Load (Model B)
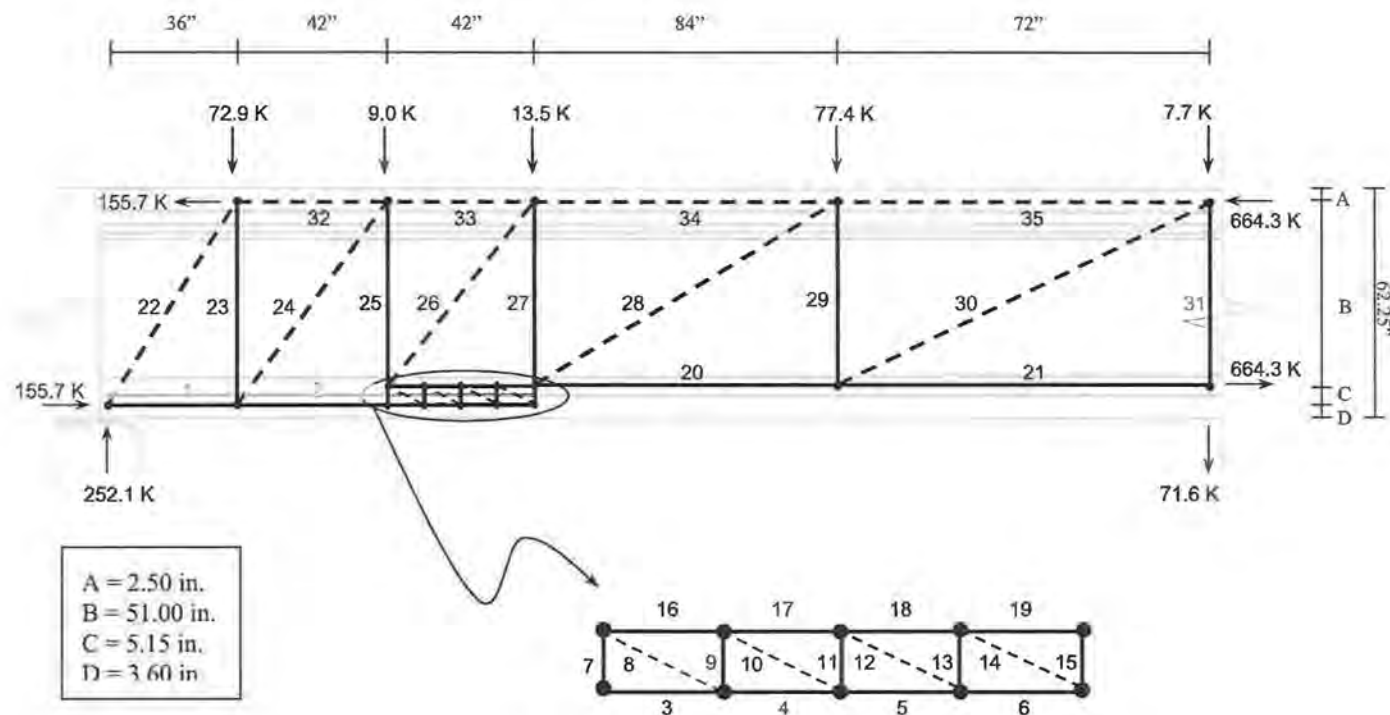
Figure 5.17 – Strut-and-Tie Model of Cracked End Region of a Girder Made Continuous for Live Load with an Internal Hinge at the Cracked Cross Section (Model C)

Table 5.3 – Strut-and-Tie Member Forces

Member #	Simple Span	Two-Span Continuous	Hinged
1	104.0 (T)	214.9 (C)	5.9 (T)
2	255.4 (T)	36.0 (C)	140.0 (T)
3	255.4 (T)	36.0 (C)	140.0 (T)
4	190.5 (T)	27.0 (C)	105.0 (T)
5	128.3 (T)	18.0 (C)	70.0 (T)
6	62.2 (T)	9.0 (C)	35.0 (T)
7	0 (T)	0 (T)	0 (T)
8	67.9 (C)	10.0 (C)	39.0 (C)
9	20.0 (T)	4.4 (T)	17.2 (T)
10	65.3 (C)	10.0 (C)	39.0 (C)
11	20.0 (T)	4.4 (T)	17.2 (T)
12	69.0 (C)	10.0 (C)	39.0 (C)
13	20.0 (T)	4.4 (T)	17.2 (T)
14	65.3 (C)	10.0 (C)	39.0 (C)
15	20.0 (T)	4.4 (T)	17.2 (T)
16	300.1 (T)	177.1 (T)	189.3 (T)
17	362.3 (T)	168.1 (T)	224.3 (T)
18	428.4 (T)	159.1 (T)	259.3 (T)
19	490.6 (T)	150.1 (T)	294.3 (T)
20	631.5 (T)	343.8 (T)	552.4 (T)
21	778.5 (T)	311.4 (C)	664.3 (T)
22	264.6 (C)	233.8 (T)	299.5 (C)
23	234.2 (T)	294.4 (C)	179.2 (T)
24	278.8 (C)	224.8 (T)	223.8 (C)
25	162.6 (T)	288.5 (C)	170.2 (T)
26	297.8 (C)	145.3 (T)	242.7 (C)
27	169.7 (T)	244.8 (C)	173.9 (T)
28	205.6 (C)	145.4 (T)	301.9 (C)
29	138.1 (T)	214.9 (T)	79.3 (T)
30	201.7 (C)	36.0 (T)	137.2 (C)
31	71.6 (T)	150.1 (C)	71.6 (T)
32	104.0 (C)	- - -	5.9 (T)
33	255.4 (C)	- - -	140.0 (C)
34	490.6 (C)	- - -	294.3 (C)
35	631.5 (C)	- - -	552.4 (C)

113

CHAPTER 6: DISCUSSION OF RESULTS

6.1 STRENGTH AND BEHAVIOR OF THE CRACKED PRESTRESSED CONCRETE GIRDERS

Three different models were used to complete the elastic structural analysis of the selected two-span bridge structure. The goal of using multiple models in the analysis was to determine how the damaged, or unrepaired, two-span bridge structure behaves under factored ultimate dead and live loads. Based upon the results of the elastic structural analysis and the evaluation of the shear and flexural capacities of the girders, some conclusions about the behavior of the structure under factored ultimate loads can be made.

6.1.1 Two-Span Continuous Behavior

Assuming that the dominating behavior of the bridge is that of a two-span continuous structure, all girders are subjected to negative moments near the interior support. Comparison of the factored ultimate load effects and the design negative moment capacity of the cracked bulb-tee girders revealed that flexural strength deficiencies exist for cross sections near the interior support. The magnitude of the strength deficiencies depends on the strength reduction factor used to calculate the design negative moment capacity of the girder.

When a strength reduction factor of 1.00 was used, a cracked exterior girder had a small deficiency of negative moment capacity at its continuous end. As shown in Figure 5.12, the factored ultimate demand exceeds the design negative moment capacity of the girder over a length of 36 in. (910 mm) at the girder end. Assuming that cross sections near the continuous end of the girder have adequate ductility, a plastic hinge will form near the girder end. It can be safely assumed that cross sections near the continuous end of the girder have adequate ductility because the member is very lightly reinforced at its ends. Any load applied after plastic hinge formation will be carried by the exterior girder as though it is simply supported.

The formation of a plastic hinge in the exterior girder is possible, but whether or not the girder will resist additional loads after development of a plastic hinge is not totally clear. Compatibility suggests that the deflection of two adjacent girders must not be grossly different if the girders behave elastically. Even though the exterior girder is able to deflect more easily as a result of the formation of the plastic hinge, the adjacent interior girder would restrain the deflection of the exterior girder. Because the loads

114

carried by a flexural member are directly proportional to the deflection of the member when behaving elastically, the exterior girder would not carry as much additional load as the adjacent interior girder. Additional analysis and experimentation would be required to determine the magnitude of the load redistribution from the exterior girder to the adjacent interior girder. The redistribution of loads between girders in multi-girder bridges is a complicated phenomenon and is not within the scope of this research.

The use of a smaller strength reduction factor results in more widespread flexural strength deficiencies. When a strength reduction factor of 0.90 was used, both interior and exterior girders were shown to be deficient in negative moment capacity at their continuous ends. The deficiency of negative moment capacity occurs over a length of 48 in. (1220 mm) for exterior girders and 16 in. (410 mm) for interior girders. Because both interior and exterior girders have flexural strength deficiencies at their continuous ends, the formation of plastic hinges in multiple girders is a possibility that must be considered. If multiple plastic hinges were to form in the girder ends, the behavior of the girders may be more like that of simply supported members. Simply supported behavior is discussed in more detail in Section 6.1.3.

The shear capacity of the cracked girders exceeds the factored ultimate demand if two-span continuous behavior controls the behavior of the structure. Figure 5.8 shows the most critical shear envelope for an interior girder in the two-span continuous structure. The gradual decrease in shear capacity in the cracked end of the girder is a result of the loss of effective prestressing force transferred to the concrete. The sharp increases in shear capacity are related to the spacing of stirrups in the member end.

The capacity of the longitudinal tension reinforcement is not satisfactory for the cracked girders. The tensile capacity of the prestressing tendons is not adequate at the simply supported girder end. Because the simply supported ends of the cracked girders have not shown any signs of cracking or distress, the lack of tensile capacity of the prestressing tendons is not considered to be a significant problem.

6.1.2 Continuous Behavior with an Internal Hinge at the Cracked Cross Section

A slight variation in the behavior of the two-span structure would result from the presence of an internal hinge at the cracked cross section. The internal hinge would be a result of the inability of the cracked cross section to resist moments. The behavior of such a structure was examined by means of an elastic structural analysis.

The formation of a plastic hinge at the interior support could create a collapse mechanism for a girder containing an internal hinge at the cracked cross section. Formation of a plastic hinge in the continuous end of a girder would be the result of negative moments exceeding the negative moment capacity of the girder. Based upon the results of the limited structural analysis performed on Model #3, factored ultimate negative moments at the continuous end of the cracked girders are much less severe when

115

an internal hinge is present. The design negative moment capacity of the cracked bulb-tee girders is much greater than the factored ultimate negative moments that form in the end of the girder containing the internal hinge. Thus, failure of the structure due to an instability created by two hinges in a single span is not a concern that must be addressed. The collapse mechanism may also be prevented through redistribution of loads to adjacent girders.

Both positive and negative bending moments occur in a cracked bulb-tee girder containing an internal hinge at the crack location. As stated earlier, the factored ultimate negative moments at the interior support do not exceed the design negative moment capacity of the girders. The design positive moment capacity of the girders exceeds the factored ultimate demand for all cross sections subjected to positive moments. Thus, the design flexural capacity of the girders is satisfactory for the hinged structure.

Shear and moment envelopes were not developed from the elastic structural analysis of Model #3, though a general trend can be seen in the results of the analysis performed. The shear forces in the uncracked girder end are greater in Model #3 than they are in the other two models used in the elastic structural analysis. Shear forces in the cracked girder end are smaller in Model #3 than in Models #1 and #2. Positive and negative moments in Model #3 are generally smaller in magnitude than those occurring in the other two models.

The shear capacity of cross sections in the small region between the cracked cross section and the continuous girder end is not significantly affected by the presence of an internal hinge at the cracked cross section. On the other side of the cracks, factored ultimate dead and live loads induce positive moments at each cross section. Because cracked girders have been shown to lack shear capacity when subjected to large shear forces and positive moments, cross sections on this side of the cracked cross section may be deficient in shear strength. It is noted, however, that the combination of shear force and moment is much less severe for cross sections in Model #3 than for those in Model #1. Any deficiencies in shear capacity for cross sections in a continuous girder containing an internal hinge will likely be smaller in magnitude than those occurring in a simply supported girder. The deficiency of shear capacity of simply supported cracked girders is addressed in the following section.

6.1.3 Simple Span Behavior

The behavior of the structure may also be that of two simply supported spans. This type of behavior would occur if the continuity at the interior support has been completely lost. Loss of continuity may be the result of a combination of factors, such as poor detailing of reinforcement, overload of the structure, time-dependent concrete effects in the prestressed concrete girders, or a poorly timed construction sequence.

Factored ultimate dead and live loads induce positive bending moments in simply supported girders. As shown in Figures 5.9 and 5.10, a deficiency of positive moment capacity exists for both interior and exterior cracked bulb-tee girders. The deficiency of positive moment capacity is the result of the loss of effective prestressing force in the tendons caused by the large cracks in the continuous end of the girder. As shown in Figures 5.9 and 5.10, a total loss of prestressing force at the girder end would result in a flexural failure of the girder if simply supported behavior controls. Because this has not occurred in any of the cracked bulb-tee girders, structures containing cracked bulb-tee girders must not be behaving as though they are simply supported. The deficiency of positive moment capacity will likely be corrected with the addition of external FRP reinforcement.

The design shear capacity of the cracked bulb-tee girders is unsatisfactory for both interior and exterior girders. Figure 5.7 shows the most critical shear demand envelope for an interior girder. Because the prestressing tendons have become ineffective in the cracked end region of the girder, there is not any effective longitudinal reinforcement on the flexural tension side of the member. As a result, the inclination of the compressive concrete struts is at a maximum for cross sections in the cracked end of the girder. This greatly reduces the shear capacity of cross sections on both sides of the cracked cross section.

The tensile capacity of the longitudinal reinforcement is less than that required by Article 5.8.3.5 of the AASHTO LRFD. The deficiency of tensile capacity provided by the prestressing tendons occurs at both ends of the girder. The slight deficiency of tensile capacity at the uncracked end of the girder is not a major concern and will not be addressed. A greater deficiency of tensile capacity exists in a 64 in. (1630 mm) wide region at the cracked end of the girder. This is discussed in more detail in the following section.

6.2 STRUT-AND-TIE ANALYSIS

The strut-and-tie analysis was performed to examine the flow of forces through a typical cracked bulb-tee girder, specifically the D-region at the continuous end of the member. The tensile forces developed in the ties representing the external FRP reinforcement and prestressing tendons were of special interest. The factored ultimate forces in the bottom flange tensile ties were compared to the design tensile capacity of the prestressing tendons and the external FRP reinforcement. The capacities of other members in the strut-and-tie models were not considered.

Because the prestressing tendons compose the only longitudinal reinforcement in the bottom flange of the bridge girders, their inability to carry tension between the cracked cross section and the girder end limits the means by which an existing cracked girder can resist factored ultimate loads. The flow of forces through the cracked bulb-tee girder

117

must be such that significant tension forces do not develop in the bottom flange. The results of the strut-and-tie analysis reveal that large tension forces develop in the bottom flange at the cracked girder end if simply supported behavior is assumed. Moderate to large tensile forces are induced in the bottom flange between the cracked cross section and the girder end when factored ultimate loads are applied to the Model B. Two-span continuous behavior results in compression forces in the bottom flange of the girder. Thus, it must be concluded that the existing structure can only dependably resist the factored ultimate loads if continuity has been preserved and the formation of an internal hinge at the cracked cross section does not occur.

6.3 CONCLUSIONS

The results of the analytical procedures revealed that only one of the three types of behavior considered in the analysis of the cracked bulb-tee girders is acceptable under factored ultimate loads: two-span continuous behavior. Acceptable behavior of the cracked girders is based upon ultimate strength considerations, namely flexure and shear, and factored ultimate tension forces in the longitudinal reinforcement. If the two-span bridge structure does not behave as though it is continuous, cracked girders lack adequate shear capacity. Alternative types of behavior also result in the formation of large tensile forces in the bottom flange between the cracked cross section and the girder end. The tensile forces in the bottom flange cannot be carried by the existing longitudinal reinforcement.

Cracked bulb-tee girders behaving as though they are continuous at the interior support are deficient of negative moment capacity near their continuous ends. Factored ultimate moments exceed the design flexural capacity of both interior and exterior girders when a strength reduction factor of 0.90 is used. The lack of negative moment capacity is not likely to be the cause of a structural failure, though it may result in plastic hinge formation at the continuous ends of the girders during extreme loading events.

Multiple strength deficiencies exist for cracked bulb-tee girders if two-span continuous behavior does not occur. The design shear capacity of the cracked bulb-tee girders is not satisfactory when simply supported behavior occurs. Although shear and moment envelopes were not developed for the two-span continuous structure with an internal hinge at the cracked cross section, the shear strength of the cracked girders is probably not adequate for cross sections near the cracked cross section. A deficiency of positive moment capacity exists at the cracked ends of the bulb-tee girders if simply supported behavior occurs. The tensile capacity of the prestressing tendons is unsatisfactory over a length of 64 in. (1630 mm). All strength deficiencies are a result of the cracking that has occurred in the ends of the bulb-tee girders.

118

Unfortunately, the behavior of the two-span structure at the factored ultimate load level cannot be determined using non-destructive experimentation. Load testing of the structure would be helpful in determining the behavior of the structure under service level loads but may not provide any other useful information. In order to ensure that factored ultimate loads do not cause a failure of individual girders or the structure as a whole, girders should be strengthened such that they are able to dependably resist factored ultimate loads for all three types of behavior. The design of a strengthening system utilizing external FRP reinforcement is presented and discussed in the next chapter.

CHAPTER 7: DESIGN OF THE EXTERNAL FRP STRENGTHENING SYSTEM

Analysis of the cracked prestressed concrete bridge girders revealed that deficiencies in shear capacity and tensile capacity of the longitudinal reinforcement exist at the continuous ends of the girders. Flexural deficiencies exist in a narrow region surrounding the cracked cross section in exterior girders. With the exception of the lack of tensile capacity provided by the longitudinal reinforcement at the uncracked ends of the girders, the strength deficiencies are a result of the cracks in the girder ends. The use of external FRP reinforcement may provide a means to strengthen the cracked bulb-tee girders within a reasonable budget and with minimal disruption to the use of the structure. If the external FRP reinforcement is designed to act as tensile reinforcement for the bottom flange, its presence should eliminate the strength deficiencies near the continuous end of cracked bulb-tee girders.

The use of external FRP reinforcement will also be advantageous for those girders that are yet uncracked at their continuous end. It is hoped that the installation of external FRP reinforcement on the bottom flange of uncracked girders will prevent future cracks from forming in the clear span of the girder. Cracks should be forced to occur behind the bearing pad or even within the continuity diaphragm. The formation and location of cracks that form after installation of the external FRP reinforcement will depend upon the magnitude of the thermal gradient, FRP material properties, FRP reinforcement ratio, the length of girder to which the FRP is applied, the relative flexural capacities of the girder and continuity diaphragm, and the behavior of adjacent girders.

An overview of the procedures used during the design of the external FRP strengthening system is presented in this chapter. During the design, the optimal configuration of the external FRP reinforcement, the amount of FRP reinforcement used for strengthening, and the means necessary to achieve adequate anchorage of the FRP reinforcement were determined. Section 7.2 outlines the procedures used during the design of the external FRP reinforcement. Results of the design procedures are presented

in Section 7.3. The anchorage of the external FRP reinforcement is discussed in Section 7.4.

7.1 FRP MATERIAL PROPERTIES

In order to simplify the design of the external FRP reinforcement, a single FRP product was chosen. The Tyfo SCH-41 composite manufactured by Fyfe Co. was used in all design and analysis procedures. The Tyfo SCH-41 composite is a wet lay-up system comprised of Tyfo SCH-41 reinforcing fabric and Tyfo S epoxy. The Tyfo SCH-41 composite fabric contains unidirectional carbon fibers and a glass veil backing to aid in fabric stability during installation. The Tyfo S epoxy is a two-part adhesive used to both saturate the composite fabric and bond the fabric to the concrete.

A single piece of the SCH-41 composite reinforcing fabric has a thickness of 0.011 in. (0.3 mm). The width of the composite fabric sheets can be specified when ordered, though it is typically produced and shipped in 24 in. (610 mm) wide rolls. The SCH-41 composite fabric should not come into contact with moisture before it has been saturated with Tyfo S epoxy and allowed to fully cure. The shelf life of the SCH-41 fabric is ten years. Tyfo S is a two-part epoxy adhesive used for bonding the SCH-41 composite to the concrete substrate. The two parts used to make the Tyfo S epoxy are sent in individual pre-measured five-gallon (18.9 L) buckets. Once mixed in appropriate portions, the Tyfo S epoxy has a pot life of two hours. The shelf life of the Tyfo S epoxy is two years. Both the Tyfo S epoxy and the SCH-41 fabric should be stored at temperatures between 40 °F and 90 °F (4 °C and 32 °C) to preserve the stated shelf life of the products. The material properties of the Tyfo SCH-41 composite and the Tyfo S epoxy are shown in Table 7.1.

Table 7.1 – Material Properties of SCH-41 Reinforcing Fabric and Tyfo S Epoxy

FRP – SCH-41 Reinforcing Fabric	Epoxy – Tyfo S
$f_{fiber,MAX}$ = 550 ksi $\varepsilon_{fiber,MAX}$ = 0.017 in/in E_{fiber} = 33,400 ksi	f_e = 10,500 psi $\varepsilon_{e,MAX}$ = 0.05 in/in E_e = 461,000 psi

1 in. = 25.4 mm, 1 ksi = 6.895 MPa

When the Tyfo S epoxy is used to saturate and bond the SCH-41 reinforcing fabric to a concrete substrate, a composite system is created. The composite system, composed of the reinforcing fabric and the epoxy adhesive, is a thin laminate whose behavior can be described with unique material properties. Material properties for the laminate are shown in Table 7.2. The design thickness of a single layer of the laminate is 0.04 in. (1.0 mm),

though the actual thickness may vary. In order to distinguish the laminate from the composite reinforcing fabric, a single layer of the laminate will be referred to as a "ply" from this point forward.

Table 7.2 – Material Properties of FRP Laminate Plies

Typical Test Values	Design Values
$f_{fu}^* = 127$ ksi $\varepsilon_{fu}^* = 0.012$ in/in $E_f^* = 10,500$ ksi	$f_{fu} = 108.0$ ksi $\varepsilon_{fu} = 0.012$ in/in $E_f = 8900$ ksi

1 in. = 25.4 mm, 1 ksi = 6.895 MPa

7.2 DESIGN METHOD FOR EXTERNAL FRP STRENGTHENING SYSTEM

The external FRP reinforcement is intended to provide longitudinal tensile reinforcement on the bottom flange of the bulb-tee girders at the cracked girder end where the existing prestressing tendons are ineffective. Use of the external FRP reinforcement on the bottom flange of the bulb-tee girders will increase the tensile capacity of the longitudinal reinforcement at the cracked end of the girder, increase the design shear capacity of strengthened cross sections, and ensure that factored ultimate shear forces can be transferred through the girders to the supports. Uncracked girders will also benefit from strengthening with external FRP reinforcement.

The procedure used to design the external FRP reinforcement is based on the sectional model used in the evaluation of the existing shear and flexural capacities of the cracked bridge girders. The sectional model was used to determine the tensile capacities of the external FRP reinforcement and the prestressing tendons along the length of the girder. The design tensile capacities of the external FRP reinforcement and prestressing tendons were then compared to the factored ultimate forces from the strut-and-tie analysis. The design flexural and shear capacities of the strengthened bridge girder were calculated to determine if the ultimate strength limit state is satisfied for a given design.

7.2.1 Assumptions

The anchorage of the external FRP reinforcement was determined to be a critical part of the design, due to the magnitude of the forces that must be carried by the FRP near the end of the girder. In the preliminary design of the external FRP reinforcement, it was assumed that the FRP is perfectly anchored at its ends. Although this condition is

difficult or impossible to achieve in practice, it simplified calculations. Anchorage of the external FRP was considered in a later portion of the design procedure.

The trial cross-sectional configuration of the external FRP reinforcement was based upon the material properties of the FRP composite strengthening system, which were provided by the manufacturer, and the geometry of the bottom flange of the girder. The width of a single ply of the FRP composite system was limited to 58 in. (1470 mm). Details of the bottom flange dimensions are shown in Figure 7.1. If a width greater than 58 in. is used, the FRP must be bonded to a re-entrant corner at the intersection of the bottom flange and web. Bonding external FRP reinforcement to re-entrant corners requires special detailing to ensure that the bond between the FRP and concrete is maintained (ACI Committee 440 2002). Fibers within the reinforcing fabric are unidirectional and were oriented such that they run parallel to the longitudinal axis of the girder.

The longitudinal distribution of the external FRP reinforcement is critical near the girder end. The external FRP reinforcement must be terminated at the inside face of the bearing pad on the bottom surface of the bottom flange. On the sides and upper surfaces of the bottom flange, FRP composite plies may be extended beyond the inside face of the bearing pad by 10 in. (25 mm) before reaching the face of the continuity diaphragm. Figures 7.2 and 7.3 show the cross-sectional FRP configuration for cross sections near the continuous end of a typical cracked bulb-tee girder. Extension of the external FRP reinforcement beyond the inside face of the bearing pad is necessary to transfer forces to the support.

The position of the FRP curtailment within the span was most influenced by the development of forces in the external FRP reinforcement and the prestressing tendons. Factored ultimate forces in the bottom flange ties were determined with the strut-and-tie analysis. Between the cracked cross section and the curtailment of the external FRP reinforcement, the factored ultimate tension in the FRP decreases from a maximum value to zero. In the same region, the factored ultimate tension force in the prestressing tendons increases dramatically. This is true for Models A and C, shown in Figures 5.15 and 5.17. The FRP curtailment position had to be chosen such that the growing forces in the prestressing tendons could be developed. In order to allow the full development of the prestressing tendons, the external FRP reinforcement was extended beyond the cracked cross section by a distance equal to the development length of a 0.5 in. (12.7 mm) special prestressing tendon. The development length was calculated with Equation 5.11.4.2-1 of the AASHTO LRFD and is equal to 79.2 in. (2010 mm). If this distance is used, the external FRP reinforcement must be extended by a minimum of 107 in. (2720 mm) from the inside face of the bearing pad. A conservative estimate of 120 in. (3050 mm) was used for design.

7.2.2 Calculation of the Tensile Capacity of the Longitudinal Reinforcement

The tensile capacity of the external FRP reinforcement and the prestressing tendons was calculated with the sectional model described in Section 4.2. The tensile capacity of the external FRP reinforcement was calculated as prescribed in Chapter 9 of the *Guide*. Transfer and development lengths of the prestressing tendons were considered in the calculation of their tensile capacity.

Because design guidelines in Chapter 9 of the *Guide* limit the strain in the external FRP reinforcement to prevent non-ductile debonding failures, the effect of external FRP reinforcement on the strains developed in the prestressing tendons was examined. Compatibility of strains suggests that the strain induced in the prestressing tendons by post-repair loads may not exceed the limiting strain for the FRP for strengthened cross sections. If the effective FRP strain at failure, ε_{fe}, is small, corresponding strains in the prestressing tendons may limit stresses to values that are significantly less than those calculated with Equation 4.16.

The following procedure was used to determine the tensile capacity of the external FRP reinforcement and the prestressing tendons.

1. Calculate the design rupture strain of the FRP, ε_{fu}, where C_E is the environmental factor for the FRP reinforcement, and ε_{fu}^* is the ultimate tensile strain of the FRP reported by the manufacturer.

$$\varepsilon_{fu} = C_E \varepsilon_{fu}^*$$

Eq. 7.1

2. Calculate the bond-dependent coefficient for flexure, κ_M, where ε_{fu} is the design ultimate tensile strain of the FRP, n is the number of FRP laminate plies, E_f is the modulus of elasticity of the FRP, and t_f is the thickness of a single FRP laminate ply.

$$\kappa_M = \begin{cases} \dfrac{1}{60\varepsilon_{fu}} \left(1 - \dfrac{nE_f t_f}{2{,}000{,}000}\right) \leq 0.90 & nE_f t_f \leq 1{,}000{,}000 \\ \\ \dfrac{1}{60\varepsilon_{fu}} \left(\dfrac{500{,}000}{nE_f t_f}\right) \leq 0.90 & nE_f t_f > 1{,}000{,}000 \end{cases} \quad \text{for}$$

Eq. 7.2

123

3. Calculate the effective limiting strain in the FRP, ε_{fe}, the effective limiting stress in the FRP, f_{fe}, and the tensile capacity of the FRP, F_{frp}.

$$\varepsilon_{fe} = \varepsilon_{fu} \kappa_M$$
$$f_{fe} = E_f \varepsilon_{fe} \qquad\qquad \text{Eq. 7.3}$$
$$F_{frp} = A_f f_{fe}$$

In Equation 7.3, κ_M is the bond-dependent coefficient for flexure and A_f is the cross-sectional area of the FRP in square inches.

4. Check to see if the ultimate strength limit state is satisfied for the ties that represent the external FRP reinforcement. The strength reduction factor used to calculate the design tensile capacity of the external FRP reinforcement, ϕ, was 0.70. The factored ultimate force in the tension tie, F_u, was determined with the strut-and-tie analysis.

$$\phi F_{frp} \geq F_u \qquad\qquad \text{Eq. 7.4}$$

5. Based upon the maximum FRP strain calculated with Equation 7.3, calculate an approximate maximum stress that may be developed in the prestressing tendons, $f_{p,MAX}$. The stress in the prestressing tendons after losses of prestressing force was assumed to be 160 ksi (1100 MPa), which is the same value that is used in calculation of girder shear and flexural capacities. Transfer and development of the prestressing force must be considered in the calculation of f_{ps}. The maximum force that may be developed in the prestressing tendons, $F_{p,MAX}$, is calculated as shown in Equation 7.5.

$$f_{p,MAX} = f_{pe} + \varepsilon_{fe} E_{ps} \leq f_{ps}$$
$$F_{p,MAX} = A_{ps} f_{p,MAX} \leq A_{ps} f_{ps}$$

<div align="right">Eq. 7.5</div>

6. Check to see if the ultimate strength limit state is satisfied for the ties that represent the prestressing tendons. The strength reduction factor used to calculate the design tensile capacity of the prestressing strands, $\phi F_{p,MAX}$, is equal to 0.90, in accordance with Article 5.5.4.2.1 of the AASHTO LRFD. The ultimate force in the tension tie, F_u, was determined with the strut-and-tie analysis.

$$\phi F_{p,MAX} \geq F_u$$

<div align="right">Eq. 7.6</div>

7.2.3 Calculation of Strengthened Member Shear and Flexural Capacities

The design shear capacity of the strengthened bridge girder was calculated and compared to the factored ultimate shear demand from each of the three models used in the elastic structural analysis. Calculation of the shear capacity of discrete cross sections was performed with the sectional model described in Section 4.2. The use of the external FRP reinforcement should increase the shear capacity of strengthened cross sections, eliminating the shear strength deficiencies in the cracked end of the bridge girder.

The positive moment capacity of a typical strengthened bulb-tee girder was evaluated through the strut-and-tie analysis. The strut-and-tie method of analysis is a lower-bound method. Therefore, the tensile forces induced in the longitudinal reinforcement in the strut-and-tie model will be of greater magnitude than those from a simple sectional analysis because the tension induced by shear is accounted for in the strut-and-tie method. Thus, if cross sections are capable of resisting the factored ultimate forces from the strut-and-tie models, the flexural capacity of the girder at those cross sections will be satisfactory.

Using the procedure outlined in Section 4.2.2, the shear capacity of a typical FRP strengthened bulb-tee girder was calculated. In doing so, changes were made to Equation 4.9 to account for the presence of the external FRP reinforcement. The modified equation, Equation 7.7, is shown below. The denominator in Equation 7.7 includes the term "$E_f A_f$," which is a relative stiffness parameter for the external FRP reinforcement.

This term was added to account for the increased stiffness of strengthened cross sections, which will result in a reduction of the longitudinal strain at mid-depth of the member, ε_x. The addition of external FRP reinforcement does not affect the calculation of shear capacity for cross sections subjected to negative moments. Thus, Equation 7.8 is identical to Equation 4.11. The initial mid-depth longitudinal strain, $\varepsilon_{x,initial}$, was calculated as shown in Equation 4.10. Reasons for the use of two terms to calculate ε_x are discussed in Section 4.2.2. Equation 4.14 was used to determine if the ultimate strength limit state is satisfied for shear.

$$\varepsilon_x = \frac{\dfrac{M_u}{d_v} + 0.5N_u + 0.5\left(V_u - V_p\right)\cot\theta - 0.7A_{ps}f_{pu}}{2\left(E_sA_s + E_{ps}A_{ps} + E_fA_f\right)} \qquad \text{Eq. 7.7a}$$

$$\varepsilon_x = \frac{\dfrac{M_u}{d_v} + 0.5N_u + 0.5\left(V_u - V_p\right)\cot\theta - 0.7A_{ps}f_{pu}}{2\left(E_sA_s + E_{ps}A_{ps} + E_cA_c + E_fA_f\right)} \qquad \text{Eq. 7.7b}$$

$$\varepsilon_x = \varepsilon_{x,initial} + \frac{\dfrac{M_u - M_{Dead}}{d_v} + 0.5N_u + 0.5\left(V_u - V_p\right)\cot\theta}{2\left(E_sA_s\right)} \qquad \text{Eq. 7.8a}$$

$$\varepsilon_x = \varepsilon_{x,initial} + \frac{\dfrac{M_u - M_{Dead}}{d_v} + 0.5N_u + 0.5\left(V_u - V_p\right)\cot\theta}{2\left(E_sA_s + E_cA_c\right)} \qquad \text{Eq. 7.8b}$$

The minimum required tensile capacity of the longitudinal reinforcement, calculated according to Article 5.8.3.5 of the AASHTO LRFD (2002), was not used for strengthened cross sections. Satisfaction of Equation 7.4 ensured that the capacity of the longitudinal tension reinforcement is adequate for strengthened cross sections subjected to positive moments. For cross sections subjected to negative moments, the tensile capacity of the longitudinal reinforcement is that of the deck slab reinforcement. The tensile capacity of the longitudinal reinforcement must exceed the magnitude of the tensile force calculated with the appropriate version of Equation 4.15.

126

7.3 RESULTS OF THE FRP DESIGN METHOD

Multiple designs of the strengthened bridge girder were performed to determine the minimum amount of external FRP reinforcement required for strengthening. The assumed configuration of the external FRP reinforcement was examined to determine if it was effective, practical, and economical. The FRP curtailment position was also examined to determine if the chosen position was satisfactory.

As described in Section 7.2.2, a maximum FRP strain criterion recommended by ACI Committee 440 (2002) was adopted. An additional criterion recommended by Breña (2000) was also used in the calculation of FRP tensile capacity. Breña (2000) suggests that the FRP design strain be limited to 0.007. The limit proposed by Breña is often lower than that obtained by following the procedure proposed in Chapter 9 of the *Guide*. Design results for both FRP strain criteria are presented in this section.

7.3.1 Design #1 – 1-ply System

The initial design of the external FRP reinforcement used a single laminate ply. The total cross-sectional area of external FRP reinforcement was 2.32 in^2 (1500 mm^2). The external FRP reinforcement was terminated 120 in. (3050 mm) from the inside face of the bearing pad. At the support, the FRP was extended beyond the inside face of the bearing pad by 10 in. (25 mm) on the side and top faces of the bottom flange. Details of the cross-sectional configuration of the FRP near the support are shown in Figures 7.2 and 7.3. The longitudinal configuration of the 1-ply FRP strengthening system is shown in Figure 7.4.

The design tensile capacity of the external FRP reinforcement is 133 kips (590 kN) when the ACI 440 criterion is used. Using the Breña criterion, the design capacity of the external FRP reinforcement is 101 kips (450 kN). The factored ultimate force in the tie representing the FRP in the strut-and-tie models is as large as 255 kips (1136 kN) at the location of the cracks in the girder end. Thus, the design tensile capacity of the 1-ply system is inadequate, regardless of the strain criterion used for design. A plot of the design tensile capacity of the 1-ply system versus the factored ultimate demand from the strut-and-tie analysis is shown in Figure 7.5.

7.3.2 Design #2 – 2-ply System

Two laminate plies were used in the second design of the strengthened bridge girder. The total cross-sectional area of external FRP reinforcement was 4.64 in^2 (3000 mm^2). The cut-off point for the second ply was located 114 in. (2900 mm) from the inside face of the bearing pad, 6 in. (150 mm) short of the first ply. The staggered curtailment of the FRP laminate plies is recommended in Chapter 9 of the *Guide* for members strengthened with multiple layers of external FRP reinforcement. By staggering the cut-off ends of the FRP

127

laminate plies, stress concentrations are minimized in the curtailment region. The longitudinal configuration of the 2-ply FRP strengthening system is shown in Figure 7.6. Details of the cross-sectional configuration of the FRP near the support are shown in Figures 7.2 and 7.3.

The design tensile capacity of the external FRP reinforcement exceeds the factored ultimate demand at all cross sections within the strengthened girder end region if the ACI 440 criterion is used. The design tensile capacity is 265 kips (1180 kN) where two plies are bonded to the bottom flange of the girder. The design tensile capacity in the small region between FRP cut-off points is 133 kips (590 kN).

Use of the Breña criterion results in a smaller design tensile capacity for the external FRP reinforcement. The design tensile capacity is 202 kips (900 kN) where two plies of FRP are bonded. The factored ultimate demand is 255 kips (1136 kN) at the crack location in the girder end. Thus, the 2-ply system does not have adequate tensile capacity when the Breña criterion is used. A plot of the design tensile capacity of the 2-ply system versus the factored ultimate demand from the strut-and-tie analysis is shown in Figure 7.7.

7.3.3 Design #3 – 3-ply System

The third design of the external FRP reinforcement utilized three laminate plies. The total cross-sectional area of external FRP reinforcement was 6.96 in^2 (4500 mm^2). The first FRP laminate ply was terminated 120 in. (3050 mm) from the inside face of the bearing pad. Each subsequent ply was terminated 6 in. (150 mm) short of the ply beneath it. The longitudinal configuration of the 3-ply FRP strengthening system is shown in Figure 7.8. Details of the cross-sectional configuration of the FRP near the support are shown in Figures 7.2 and 7.3.

The design tensile capacity of the external FRP reinforcement exceeds the factored ultimate demand at all strengthened cross sections for the 3-ply system. For cross sections with three plies, the design tensile capacity is 338 kips (1505 kN) when the ACI 440 criterion is used. When the Breña criterion is used, the design tensile capacity is 304 kips (1350 kN).

The tension tie extending from the nodal zone at the support must have a design tensile capacity of 104 kips (463 kN). The design tensile capacity of the FRP is nearly three times that required at the inside face of the bearing pad when the more conservative of the two strain criteria is used. The largest factored ultimate tension force from the strut-and-tie analysis occurs at the location of the cracks in the girder end and has a magnitude of 255 kips (1136 kN). The design tensile capacity of the external FRP reinforcement exceeds this value for both design criteria. A plot of the design tensile capacity of the 3-ply system versus the factored ultimate demand from the strut-and-tie analysis is shown in Figure 7.9.

Although the 3-ply FRP strengthening system has adequate tensile capacity, it does not resolve the deficiency of shear capacity at the cracked end of the bridge girder. For cross sections in a 15 in. (380 mm) long region surrounding the cracked cross section, factored ultimate shear forces exceed the design shear capacity of the girder. The design shear capacity remains deficient for cross sections near the cracks because the additional stiffness provided by the external FRP reinforcement is not adequate. Examination of Equation 7.7, which is used to calculate the mid-depth longitudinal strain in the girder, reveals that the only non-zero term in the denominator is the relative stiffness parameter of the external FRP reinforcement, "E_fA_f." If the external FRP reinforcement does not have an adequate stiffness, the mid-depth longitudinal strain will not be significantly reduced, and the design shear capacity of cross sections in the cracked end region of the girder will remain unsatisfactory. A plot of the design shear capacity versus the factored ultimate shear demand is shown in Figure 7.10 for a cracked bulb-tee girder strengthened with the 3-ply system.

7.3.4 Design #4 – 4-ply System

The fourth design of the external FRP reinforcement utilized four laminate plies. The total cross-sectional area of external FRP reinforcement was 9.28 in^2 (6000 mm^2). The first FRP laminate ply was terminated 120 in. (3050 mm) from the inside face of the bearing pad. Each subsequent ply was terminated 6 in. (150 mm) short of the ply beneath it. The longitudinal configuration of the 4-ply FRP strengthening system is shown in Figure 7.11. Details of the cross-sectional configuration of the FRP near the support are shown in Figures 7.2 and 7.3.

The tensile capacity of the external FRP reinforcement is satisfactory for all strengthened cross sections. Using the ACI 440 criterion, no improvement in the design tensile capacity is obtained by adding a fourth FRP laminate ply. This is a result of the κ_M factor used in the determination of the limiting FRP strain, which decreases as the stiffness of the external FRP reinforcement increases. However, the design tensile capacity of the external FRP reinforcement increases when the Breña criterion is used. For cross sections strengthened with four laminate plies, the Breña criterion results in a design tensile capacity of 405 kips (1800 kN), which is almost 20 percent larger than the tensile capacity calculated with the ACI 440 criterion. A plot of the design tensile capacity of the 4-ply system versus the factored ultimate demand from the strut-and-tie analysis is shown in Figure 7.12.

When the 4-ply FRP strengthening system is used, the design shear capacity exceeds the factored ultimate demand for all cross sections. The external FRP reinforcement increases the stiffness of strengthened cross sections, resulting in a reduction of the mid-depth longitudinal strain, ε_x. As a result, the inclined compression struts are able to form at a shallower angle, θ, and the shear capacity of the cross section is increased. Thus, the

129

design shear capacity of cross sections in the cracked end of the bulb-tee girder can be increased without adding transverse reinforcement. A plot of the design shear capacity of a cracked bulb-tee girder strengthened with the 4-ply FRP strengthening system versus the factored ultimate shear demand is shown in Figure 7.13.

The positive moment capacity of cross sections strengthened with external FRP reinforcement was examined with the strut-and-tie analysis. As stated earlier, the lower-bound nature of the strut-and-tie method of analysis results in much greater factored ultimate forces in the ties representing the FRP and prestressing tendons. If the distance between the forces in the bottom flange and top flange of the member has not been grossly overestimated, the positive moment capacity of the member should be more than adequate.

7.3.5 Discussion of FRP Design Procedure Results

Four different external FRP strengthening systems were examined to determine the minimum amount of external FRP reinforcement required for strengthening, to examine the FRP strengthening configuration, and to determine a conservative curtailment position for the external FRP reinforcement. The procedure used to design the external FRP reinforcement is based on the sectional model described in Section 4.2. Elastic structural analysis of the two-span bridge structure was used to determine the factored ultimate shear forces and moments in a typical cracked girder. The factored ultimate tensile forces in the prestressing tendons and external FRP reinforcement were determined through a strut-and-tie analysis of a strengthened bridge girder.

Of the four external FRP strengthening systems examined, only the 4-ply system is able to adequately strengthen the cracked bridge girders. The 4-ply system is capable of resisting the factored ultimate tension forces determined through the strut-and-tie analysis. If fewer than four FRP laminate plies are used, the design shear capacity of the strengthened bridge girder remains inadequate in a small region near the cracked cross section. Based upon the ability of the external FRP reinforcement and prestressing tendons to resist factored ultimate tension forces from the strut-and-tie analysis, the design positive moment capacity of cross sections in the cracked end region of the bulb-tee girder exceed the factored ultimate demand.

The curtailment of the external FRP reinforcement was positioned 120 in. (3050 mm) from the outside face of the bearing pad for the strut-and-tie analysis. The same curtailment location was used in the sectional model, though the FRP was extended by 10 in. (250 mm) so that it was terminated 120 in. (3050 mm) from inside face of the bearing pad. Examination of the results presented in Sections 5.2 and 5.3 reveals that the chosen FRP curtailment position is acceptable. The design tensile capacities of both the prestressing tendons and external FRP reinforcement exceed the factored ultimate tension

130

forces from the strut-and-tie analysis. Figure 7.14 shows a plot of tensile capacity versus factored ultimate demand for the prestressing tendons.

7.4 ANCHORAGE OF THE EXTERNAL FRP REINFORCEMENT

The analytical method used to determine the nominal amount of external FRP reinforcement for strengthening was based on an assumption of perfect anchorage at the ends of the FRP. This assumption was made to simplify design calculations and determine if strengthening of the cracked bulb-tee girders could be achieved for ideal conditions. As the results presented in the preceding section have shown, external FRP reinforcement can increase the tensile capacity of the longitudinal reinforcement and increase the shear capacity of cross sections near the cracks.

If external FRP reinforcement is to be used to strengthen the bulb-tee girders, the anchorage of the FRP must be examined. Anchorage of the external FRP reinforcement is most critical at the continuous end of the cracked girder. This is a result of the larger tension forces that occur near the support and the limited cross-sectional area of external FRP reinforcement on cross sections near the end of the girder. The examination of the anchorage of the external FRP reinforcement should also be helpful in determining the practicality of the FRP configuration chosen for strengthening.

The most basic means of providing anchorage for externally bonded FRP reinforcement is through the bond between the FRP and the concrete substrate. The strength of the bond between the FRP and concrete is dependent on the properties of the concrete and the adhesive material used. Failure of the bond may occur if the strength of concrete exceeds the strength of the adhesive used to bond the FRP to the concrete. Failure through the concrete is more likely when the strength of the adhesive exceeds the strength of the concrete. ACI Committee 440 (2002) reports that the soundness and tensile strength of the concrete near the concrete/FRP interface have a major impact on the effectiveness of the FRP strengthening system. De Lorenzis et al. (2001) arrived at a similar conclusion regarding the relationship between the condition of the concrete surface and bond strength. If adequate anchorage of the external FRP reinforcement cannot be achieved through bond strength, alternative methods of providing anchorage must be used.

The tensile strength of the concrete used in fabrication of the I-565 prestressed concrete bulb-tee girders was evaluated experimentally. Adhesion tests were performed in accordance with ASTM D 4541 – 95 in order to evaluate the tensile strength of the concrete to which the external FRP reinforcement will be bonded when continuous girder ends are repaired. Description of the test preparation, procedure, and results are presented in Appendix A. Results of the adhesion tests indicate that the concrete to which external FRP reinforcement will be bonded is of good quality and has an average tensile strength of at least 480 psi.

Mechanical fasteners have been used successfully by Lamanna et al. (2001) to enhance the anchorage of external FRP reinforcement. The fasteners may be used in conjunction with an epoxy adhesive or they may be used as the sole means of anchoring the external FRP reinforcement to the concrete member. The use of mechanical fasteners may create additional problems for FRP strengthened concrete members. The act of driving the fastener into the concrete causes cracking in the concrete surrounding the fastener. The extent of the cracking depends on the concrete strength, fastener diameter and depth, and edge distances. For unbonded external FRP reinforcement mechanically fastened to concrete members, improper driving of the fasteners may result in slippage of the FRP and a reduction in the effectiveness of the strengthening system (Lamanna et al. 2001). For systems that use an epoxy adhesive to bond the external FRP reinforcement to the concrete, fasteners can be used as a means to provide additional anchorage for the FRP. Triantafillou and Antonopoulos (2000) report that the JCI has made recommendations requiring the use of mechanical fasteners for externally bonded FRP shear reinforcement to minimize premature and brittle failures.

Improvements in the anchorage of external FRP reinforcement may also be obtained through optimization of the cross-sectional and longitudinal configuration of the FRP. Khalifa et al. (2000) have determined that wrapping the external FRP reinforcement around the cross section improves its effectiveness and minimizes the number of premature failures. For shear applications, it is recommended that the external FRP reinforcement be fully wrapped if possible. If not fully wrapped, the external FRP reinforcement should be bonded in a U-wrap configuration that extends as high as possible on the beam web (ACI Committee 440 2002). Annaiah et al. (2001) and Khalifa and Nanni (2000) suggest the use of end anchors when the anchorage of the external FRP reinforcement is critical. Increasing the longitudinal length over which external FRP reinforcement is bonded to the member has also been shown to affect the anchorage of the FRP. ACI Committee 440 (2002) recommends extending external FRP reinforcement beyond inflection points by a minimum of six inches or half of the effective member depth when it is used as flexural reinforcement.

After an examination of the 4-ply FRP strengthening system and the proposed FRP cross-sectional and longitudinal configurations, it was decided that the anchorage of the external FRP reinforcement should be solely provided by the strength of the bond between the FRP and concrete if possible. This decision was made for a number of reasons, though it was influenced by the inability of other anchorage devices to provide a substantial amount of anchorage for the external FRP reinforcement.

The presence of the prestressing tendons in the bottom flange prohibit driving mechanical fasteners more than 1.75 in. (44 mm) into the girder. The shallow embedment of the mechanical fastener results in a very low fastener shear capacity. Thus, a large number of fasteners would be required to satisfy minimum strength requirements. If too many fasteners are used, the holes made by the fasteners may

significantly reduce the tensile capacity of the external FRP reinforcement. The reduction in tensile capacity would be the result of a loss of net FRP cross-sectional area and the creation of stress concentrations throughout the FRP laminate plies.

The geometry of the girder and the usage of the external FRP reinforcement prevent the FRP configuration from being significantly changed. The trial cross-sectional configuration of the 4-ply FRP strengthening system already calls for the FRP to be extended beyond the inside face of the bearing pad by 10 in. (250 mm), which brings the FRP within 1 in. (25 mm) of the continuity diaphragm. Extending the FRP upward such that it is bonded to the girder web would not be an efficient way to provide anchorage at the inside face of the bearing pad and would require the FRP to be bonded at a re-entrant corner. The use of end anchors embedded within the continuity diaphragm was not considered, due to complicated installation and expense.

7.4.1 Analytical Evaluation of the Anchorage of External FRP Reinforcement

An analytical method proposed by Harmon et al. (2003) was used to examine the anchorage that could be provided by the strength of the bond between the FRP and concrete. The method proposed by Harmon et al. (2003) accounts for the presence of the external FRP reinforcement, the resin layer, and the concrete, and how the relative stiffness of each affects the strength of the system. The extent of flexural cracking is also considered, as well as shear forces and moments at critical sections in the strengthened member.

Harmon et al. (2003) present two different failures modes that cause non-ductile failures of FRP strengthened members: FRP delamination and concrete cover delamination. Within the FRP delamination failure mode, three distinct types of delamination failure are recognized. The first FRP delamination failure type is shown to occur at a flexural crack and is denoted by "A" in Figure 7.15. For failure type "A", a very long bonded length of FRP exists in a region where there are no flexural cracks. The second FRP delamination failure type is denoted by "B" in Figure 7.16. Failure type "B" is analogous to a development length failure for a mild steel reinforcing bar or a prestressing tendon. The third FRP delamination failure type is denoted by "C" in Figure 7.16. Failure type "C" occurs between flexural cracks that are spaced a distance, s, apart.

The second type of failure mode presented by Harmon et al. (2003) is concrete cover delamination. Harmon et al. (2003) state that additional testing and experimentation is required to validate the relationships developed to predict failures occurring by delamination of the concrete cover. For this reason, concrete cover delamination was not considered in the examination of the anchorage of the external FRP reinforcement.

Based upon the three different FRP delamination failure types considered by Harmon et al. (2003), two distinct regions of the cracked prestressed concrete bulb-tee girders were determined to be critical for anchorage of the FRP. Critical Zone #1 is the region at

the end of the external FRP reinforcement, specifically the 10 in. (250 mm) between the inside face of the bearing pad and the face of the continuity diaphragm. Critical Zone #2 is the region between the inside face of the bearing pad and the location of Node 2 in Model A. The width of Critical Zone #2 is 15 in. (380 mm). A detailed view of the cracked end region of a strengthened bulb-tee girder is shown in Figure 7.17 to illustrate the location of the two critical zones.

A FRP delamination failure in Critical Zone #1 will be controlled by failure type "B." The short length of external FRP reinforcement provided at the member end will make development of factored ultimate tension forces in the FRP critical. Cracking through the bottom flange in Critical Zone #1 is not likely because it is located over the bearing pad at the continuous support.

Failure type "B" or "C" will control a delamination failure in Critical Zone #2. If a crack forms at the inside face of the bearing pad, failure type "C" may be the controlling failure type. For a type "C" failure, the cross section located 15 in. (380 mm) from the inside face of the bearing pad would be analogous to the critical crack. A type "B" failure may be the dominating type of anchorage failure in Critical Zone #2 if a more conservative approach is taken. Conservatively assuming that the external FRP reinforcement is ineffective behind the inside face of the bearing pad, the force in the FRP will be equal to zero at the inside face of the bearing pad. All tensile forces in the FRP must be developed over the 15 in. (380 mm) region designated as Critical Zone #2. An anchorage failure in Critical Zone #2 will be due to an inadequate development length, similar to that which will occur in Critical Zone #1.

Regardless of the controlling failure type, the actual behavior of the external FRP reinforcement in Critical Zone #2 cannot be determined with a simple elastic analysis. If a significant amount of force develops in the FRP at the inside face of the bearing pad, failure type "C" may be a more accurate representation of the mechanism that controls an FRP delamination failure. Shear lag effects in the external FRP reinforcement may also be present, due to the configuration of the FRP on the cross section. For the cross section labeled "A" in Figure 7.17, no tension forces exist in the portion of the FRP bonded to the bottom surface of the bottom flange, yet the FRP bonded to the sides and top surfaces of the bottom flange are effective in resisting tensile forces.

The following method was used to determine if the anchorage of the external FRP reinforcement is adequate for the 4-ply strengthening system. The method presented does not include the effects of concrete flexibility. Because the flexural stiffness of the gross concrete section is so much larger than the axial stiffness of the external FRP reinforcement, ignoring the effects of concrete flexibility is conservative (Harmon et al. 2003).

134

1. Calculate the force per unit width that can be developed in the FRP, T_o. The equation used to calculate T_o depends on the controlling failure type. For a type "B" FRP delamination failure, T_o is calculated with Equation 7.9, where τ_{max} is the maximum allowable stress in the concrete, α is parameter used in the calculation of the anchorage of the external FRP reinforcement in in.$^{-1}$, and L is the bonded length of FRP in inches. The maximum allowable stress in the concrete, τ_{max}, is equal to $12\sqrt{f'_c}$.

$$T_o = -\frac{\tau_{max}}{\alpha}\frac{\left(e^{-2\alpha L}-1\right)}{\left(e^{-2\alpha L}+1\right)}$$

Eq. 7.9

For a type "C" FRP delamination failure, T_o is calculated with Equation 7.10, where T_s is the force per unit width of FRP at the non-critical crack in kips per inch.

$$T_o = \frac{\tau_{max}}{\alpha}\frac{\left(e^{\alpha s}-e^{-\alpha s}\right)}{\left(e^{\alpha s}+e^{-\alpha s}\right)} + \frac{2T_s}{\left(e^{\alpha s}+e^{-\alpha s}\right)}$$

Eq. 7.10

The force that can be developed in a unit width of FRP is dependent on the strength of the concrete, the properties of the resin layer, the bonded length of FRP, and the spacing of cracks when applicable. The term in the denominator, α, is a function of the properties of the bond layer and the external FRP reinforcement and is calculated as shown in Equation 7.11.

$$\alpha = \sqrt{\frac{G_b}{E_f t_f t_b}} = \sqrt{\frac{g_b}{E_f t_f}}$$

Eq. 7.11

In Equation 7.11, G_b is the shear modulus of the bond layer in kips per square inch, t_b is the thickness of the bond layer in inches, and g_b is the effective shear stiffness of the bond layer in kips per inch.

2. Calculate the force that can be developed in the FRP, F_{frp}, where w_f is the width of a single FRP laminate ply in inches.

135

$$F_{frp} = T_o w_f \leq A_f f_{fu}$$ Eq. 7.12

3. Check to see if the ultimate strength limit state is satisfied. The strength reduction factor used for this calculation is discussed in Section 7.4.3.

$$\phi F_{frp} \geq F_u$$ Eq. 7.13

7.4.2 Results of the Analytical Evaluation of FRP Anchorage

Inspection of Equations 7.9 and 7.10 revealed that the failure load calculated with 7.9 will always be more conservative than that calculated with Equation 7.10. This result was verified by examining how the force per unit width of FRP at the critical crack was affected by varying the FRP force per unit width at the non-critical crack, T_s. When T_s was set equal to zero, the failure load calculated with Equation 7.10 was the same as that calculated with Equation 7.9 for a bonded length equal to the crack spacing, s. Because Equation 7.9 results in more conservative estimates of the failure load, failure type "C" was not considered in the evaluation of the anchorage of the external FRP reinforcement.

For Critical Zone #1, failure type "B" was considered between the inside face of the bearing pad and the end of the FRP at the face of the continuity diaphragm. The force per unit width of FRP calculated with Equation 7.9 was 4.91 kips/in (0.86 kN/mm). When multiplied by the width of the FRP bonded to the girder at the inside face of the bearing pad, the total force in the FRP was determined to be equal to 147 kips (655 kN). The factored ultimate tension force that must be resisted by the external FRP reinforcement is equal to 104 kips (463 kN) at the inside face of the bearing pad, as determined in the strut-and-tie analysis. Thus, the anchorage of the external FRP reinforcement is adequate in Critical Zone #1 if the strength reduction factor used to calculate the design anchorage capacity is no less than 0.70.

For Critical Zone #2, failure type "B" was considered. The force per unit width of FRP calculated with Equation 7.9 was 5.14 kips/in (0.90 kN/mm). The total force in the FRP at a cross section 15 in. (380 mm) from the inside face of the bearing pad was determined to be equal to 298 kips (1326 kN). The factored ultimate tension force in the external FRP reinforcement at the same cross section is 255 kips (1136 kN), as determined in the strut-and-tie analysis. The anchorage of the external FRP reinforcement is adequate in Critical Zone #2 if the strength reduction factor used to calculate the design anchorage capacity of the FRP is no less than 0.85.

7.4.3 Conclusions

From the results of the analytical method proposed by Harmon et al. (2003), it can be concluded that the anchorage of the external FRP reinforcement is most critical in Critical Zone #2. This is evident by the necessity of a strength reduction factor no smaller than 0.85 for anchorage in Critical Zone #2. It is noted that the assumption of a type "B" failure in Critical Zone #2 is conservative and that the force already developed in the FRP bonded to the sides and top surfaces of the bottom flange may improve the overall anchorage of the external FRP reinforcement.

Current AASHTO and ACI specifications do not provide guidance on the choice of strength reduction factors for the anchorage of externally bonded FRP reinforcement. Specifications within the AASHTO LRFD (2002) were examined to justify the choice of 0.85 as the strength reduction factor to be used for the anchorage of externally bonded FRP reinforcement.

The AASHTO LRFD (2002) recommends strength reduction factors of 1.00 and 0.90 for flexure in prestressed and non-prestressed reinforced concrete, respectively. The strength reduction factor for shear and torsion in concrete members is 0.90. When compared to the strength reduction factors from ACI 318-02, those from the AASHTO LRFD (2002) are significantly larger. This is because the AASHTO LRFD (2002) resistance factors are calibrated for different load types, configurations, and factors. If the two specifications are to result in an equally conservative design for a given member, the methods used to determine the factored ultimate loads must be significantly more conservative in the AASHTO LRFD (2002). Thus, the factored ultimate forces used to assess the capacity of the strengthened cracked bulb-tee girders are most likely very conservative, and the use of a strength reduction factor of 0.85 for anchorage of the externally bonded FRP reinforcement should be acceptable for design for factored ultimate loads determined with the AASHTO LRFD (2002).

The conservatism of the choice of the strength reduction factor for anchorage of the external FRP reinforcement is also shown through an examination of strength reduction factors specified in ACI 318-02. The strength reduction factor for strut-and-tie models is equal to that for shear and torsion in reinforced concrete, 0.75. The strength reduction factor used to calculate the design anchorage capacity of the external FRP reinforcement was 0.85, which is less than the strength reduction factor for shear in the AASHTO LRFD (2002), 0.90. Thus, the strength reduction factor chosen for anchorage of the external FRP reinforcement is slightly more conservative than that used to calculate design shear capacity.

Based upon a strength reduction factor of 0.85 for anchorage of externally bonded FRP reinforcement, adequate anchorage can be provided through bond for the 4-ply strengthening system. Because the design anchorage capacity of the proposed FRP strengthening system satisfies ultimate strength requirements, changes to the amount or

137

distribution of the external FRP reinforcement need not be made on the basis of anchorage. Mechanical fasteners need not be used to improve the anchorage of the external FRP reinforcement to the girder. The cross-sectional and longitudinal FRP configurations described in Section 7.2.1 should be used for design.
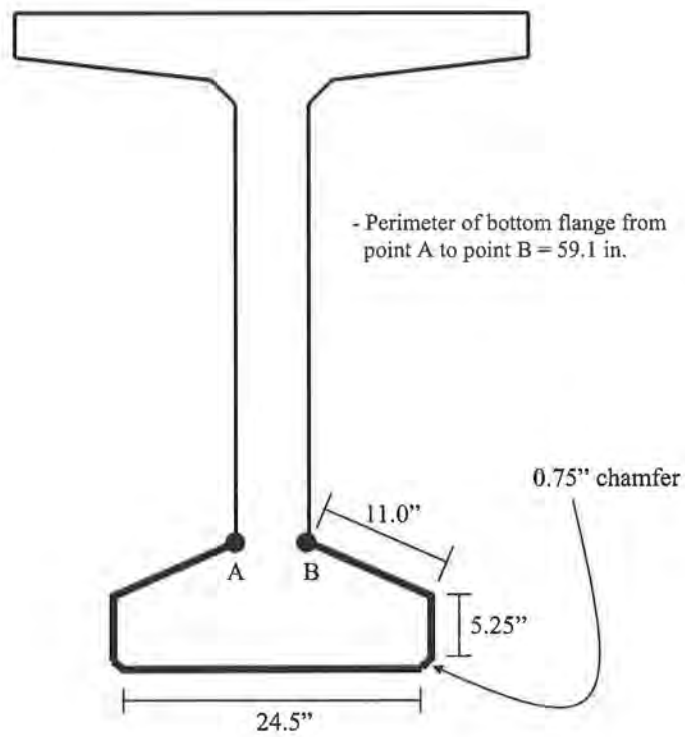
Figure 7.1 – Detail of Bottom Flange of BT54 Girder

1" 10"

Total effective width of
FRP reinforcement
bonded to girder = 30 in.

A

A

Inside face of
bearing pad

Face of continuity
diaphragm
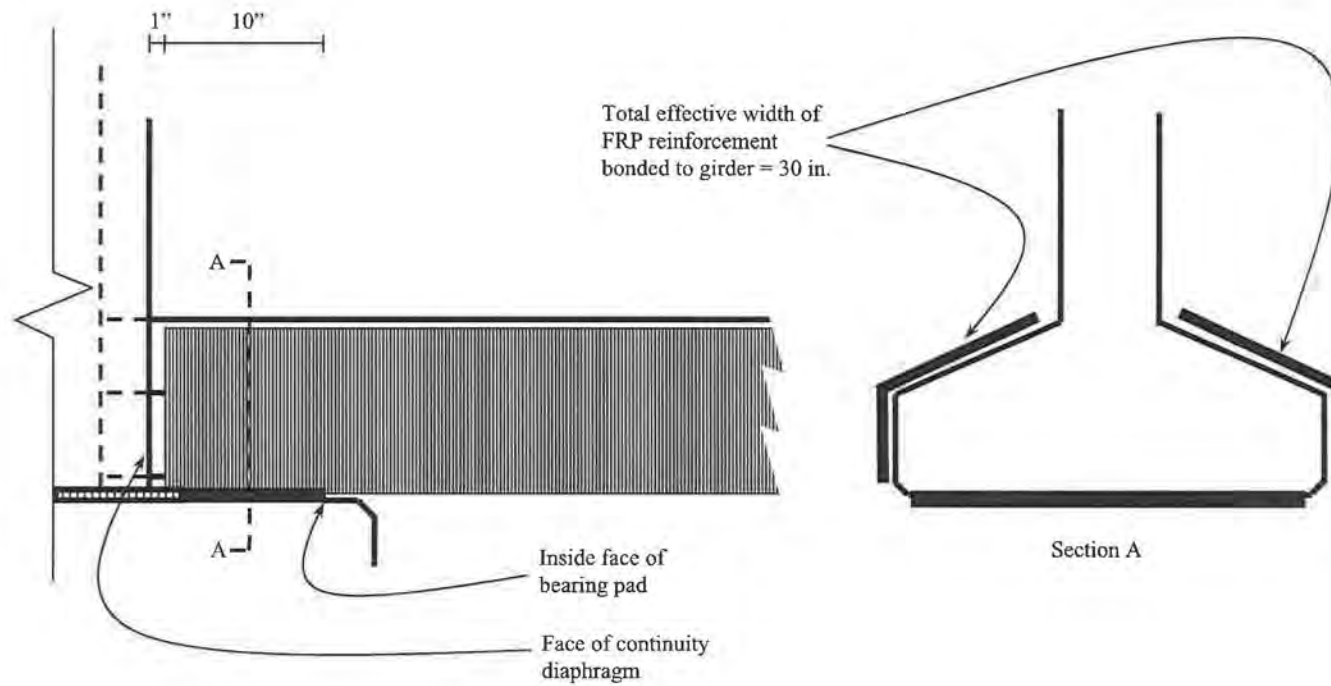
Section A

Figure 7.2 – Detail of Cross-sectional FRP Configuration for Cross Sections
Over and Behind the Bearing Pad at the Continuous Support

1"   10"

Total effective width of
FRP reinforcement
bonded to girder = 58 in.

B

B

Inside face of
bearing pad

Face of continuity
diaphragm
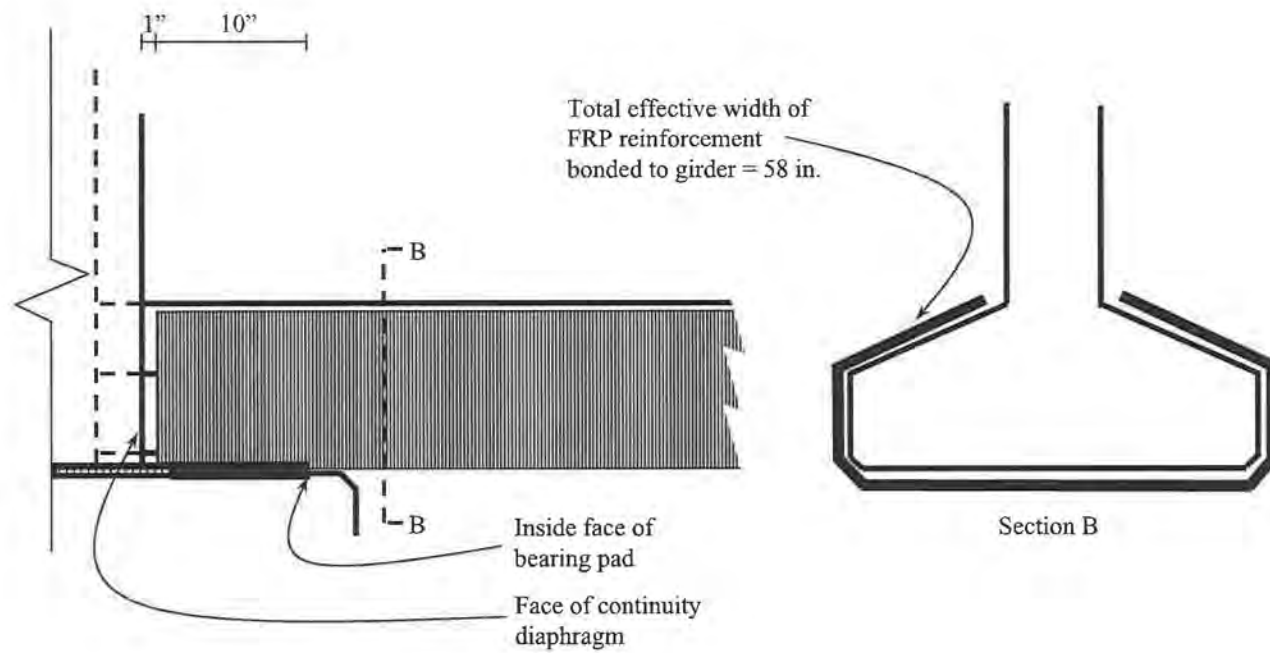
Section B

*Figure 7.3 – Detail of Cross-sectional FRP Configuration for Cross Sections
in the Clear Span of the Bulb-tee Girder*

Figure 7.4 – Longitudinal Configuration of the 1-Ply FRP Strengthening System
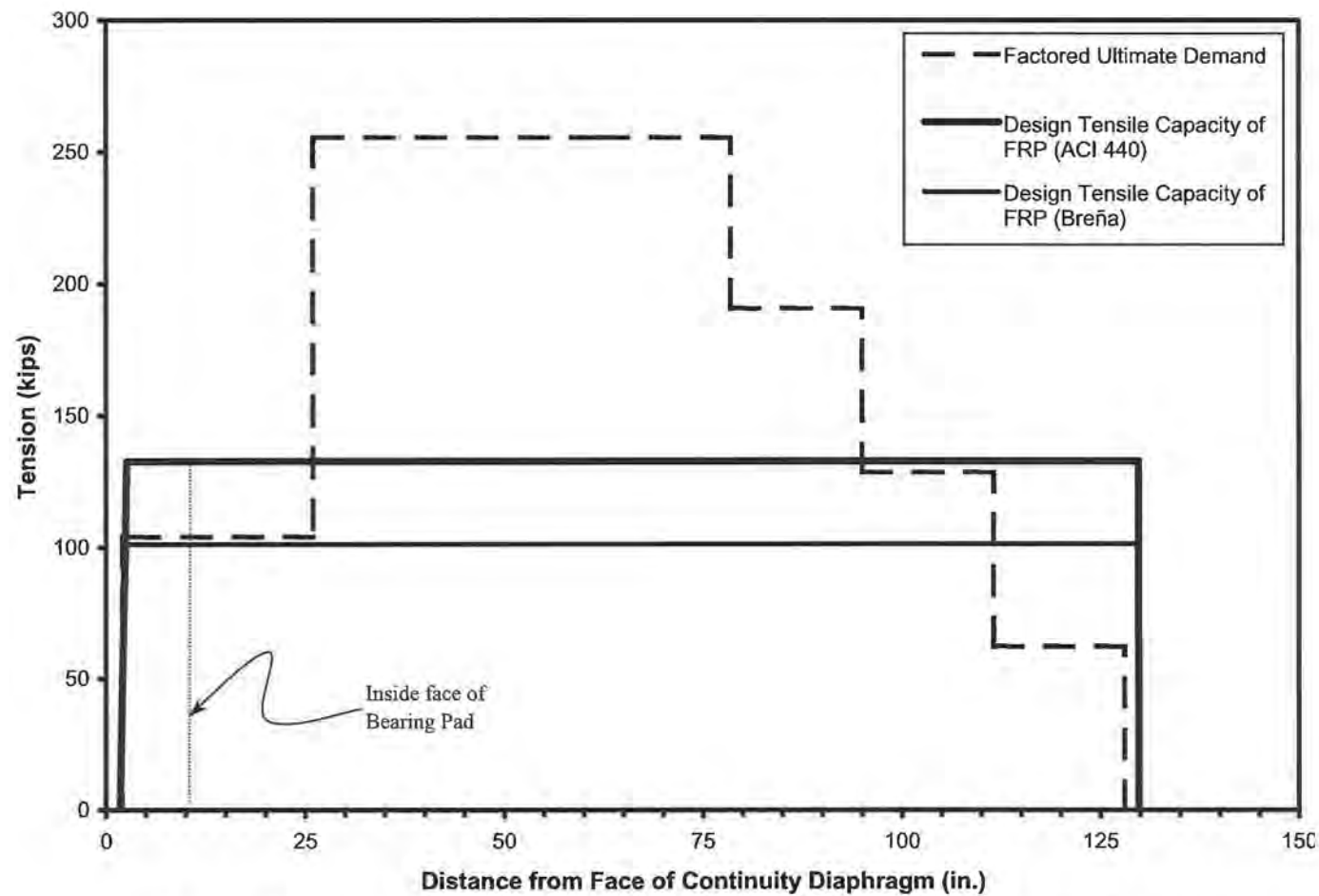
Figure 7.5 – Design Tensile Capacity vs. Factored Ultimate Demand for the 1-Ply FRP Strengthening System

143
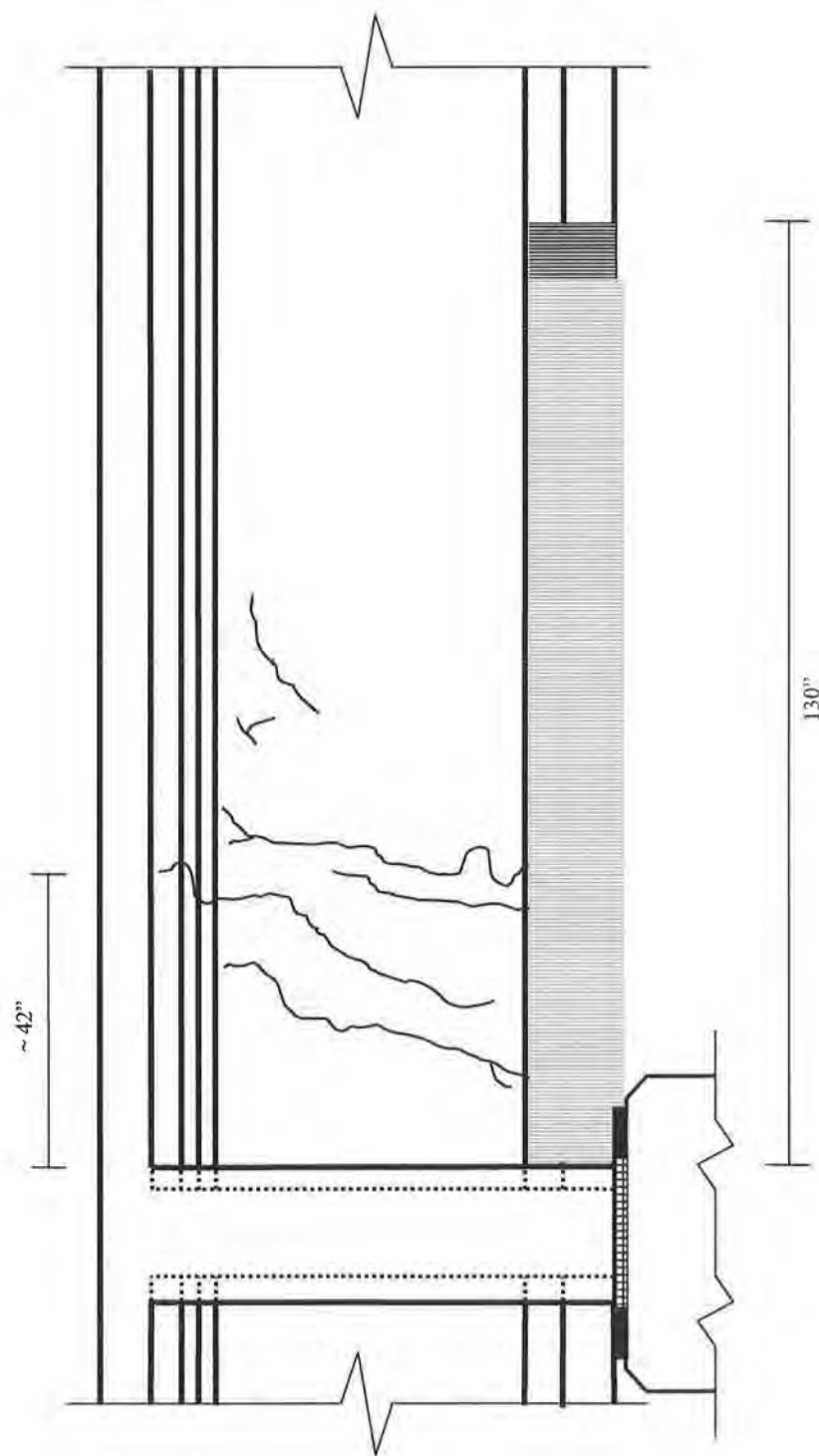
Figure 7.6 – Longitudinal Configuration of the 2-Ply FRP Strengthening System

144
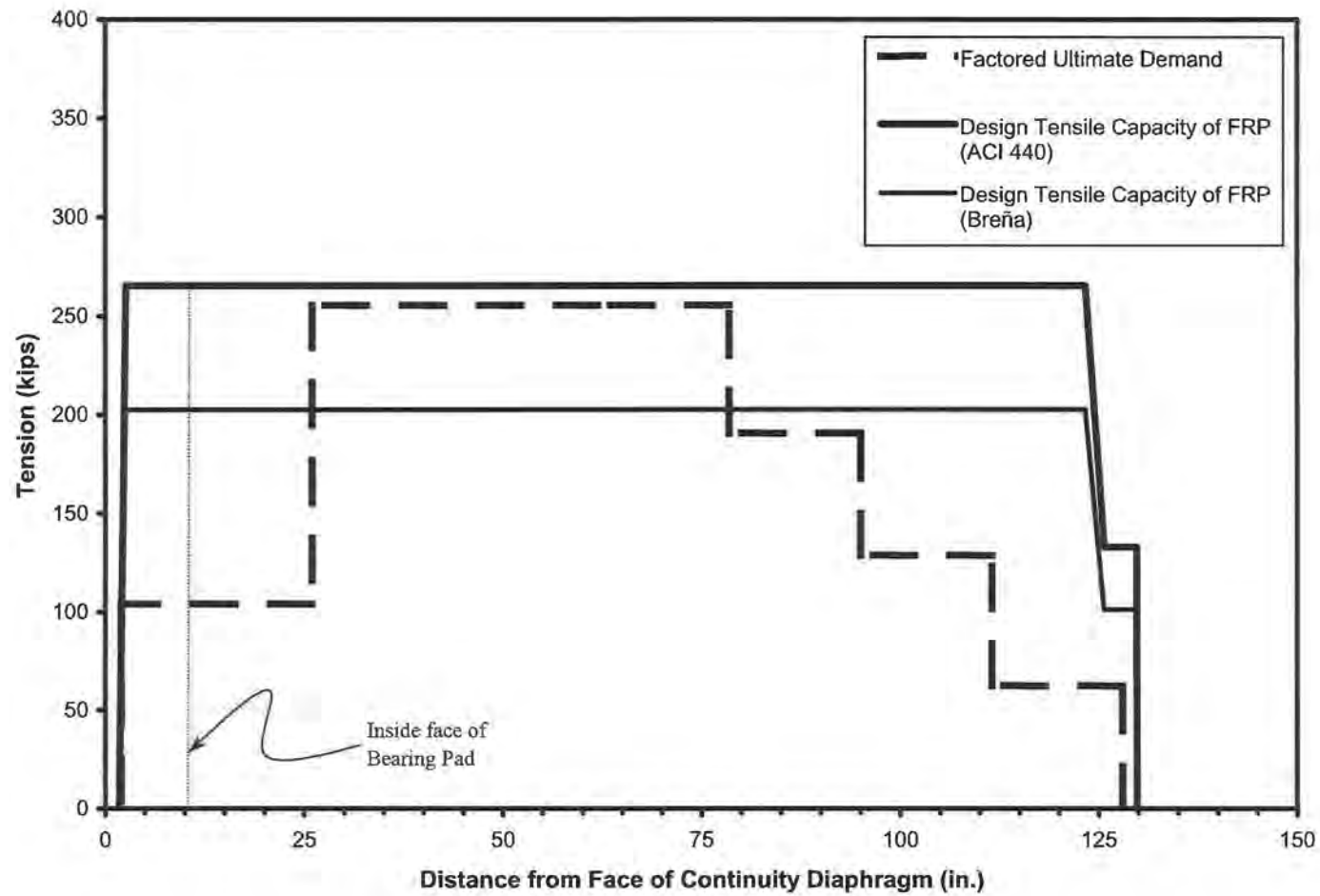
Figure 7.7 – Design Tensile Capacity vs. Factored Ultimate Demand for the 2-Ply FRP Strengthening System
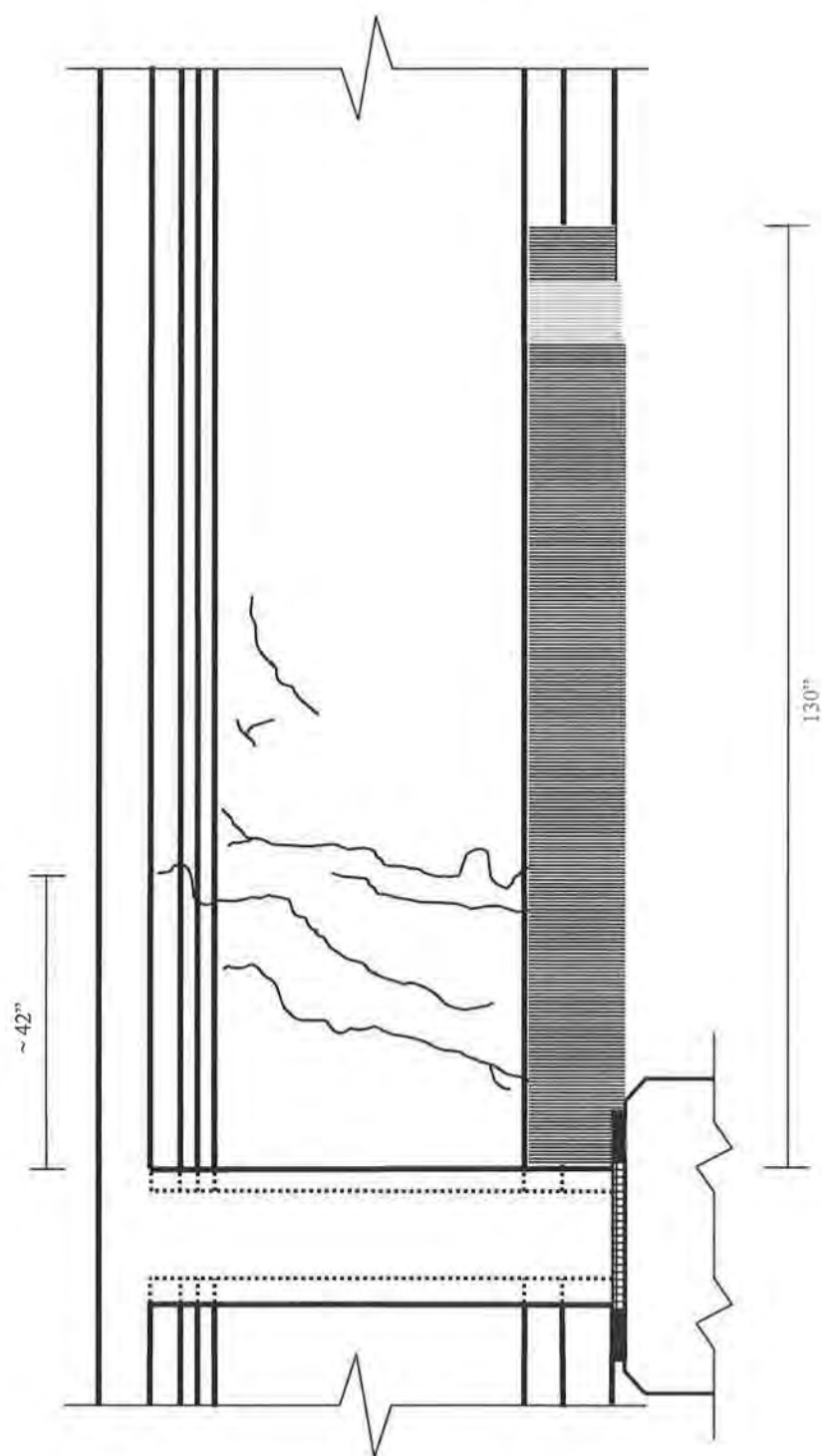
Figure 7.8 – Longitudinal Configuration of the 3-Ply FRP Strengthening System

~42"

130"

146
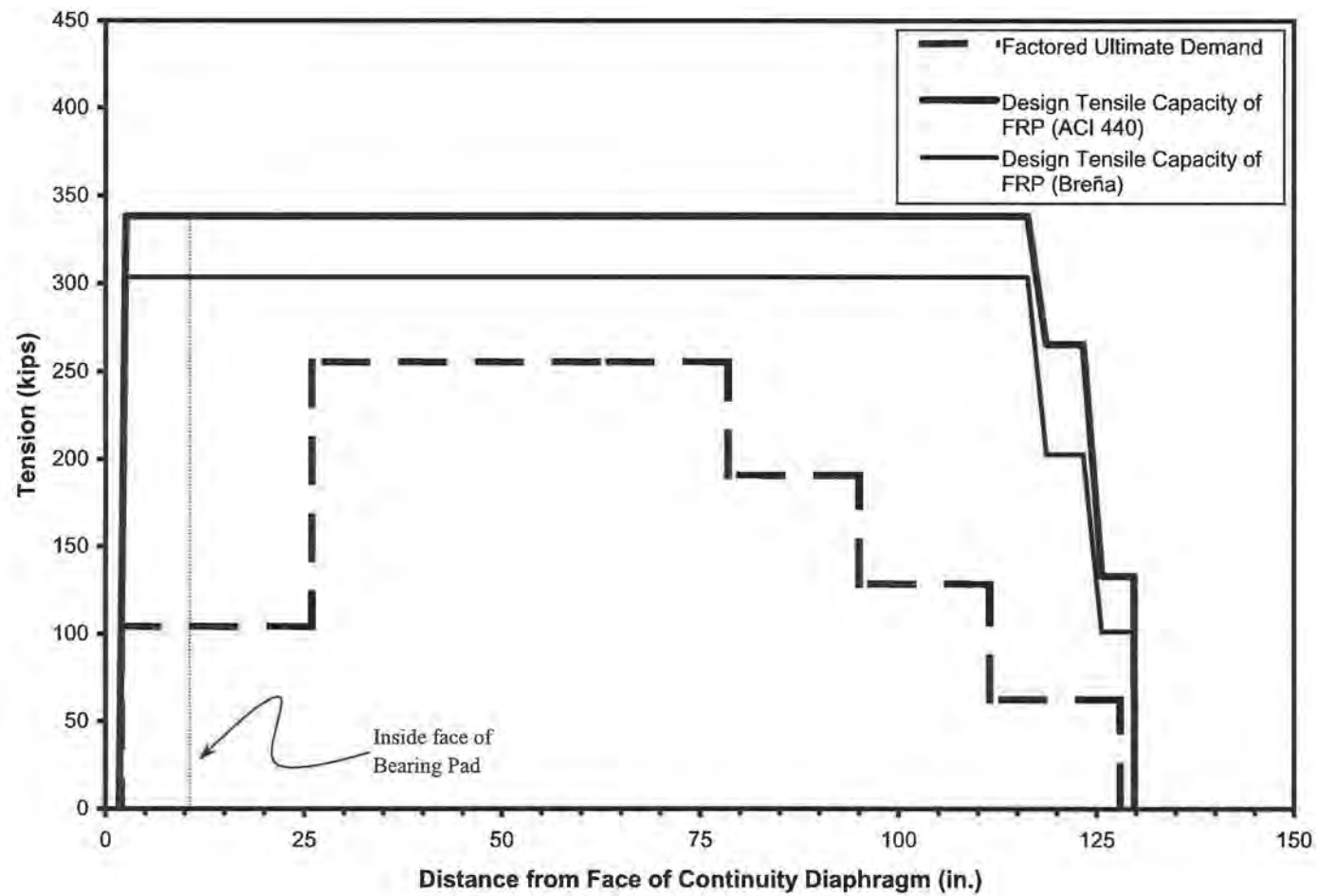
Figure 7.9 – Design Tensile Capacity vs. Factored Ultimate Demand for the 3-Ply FRP Strengthening System

147
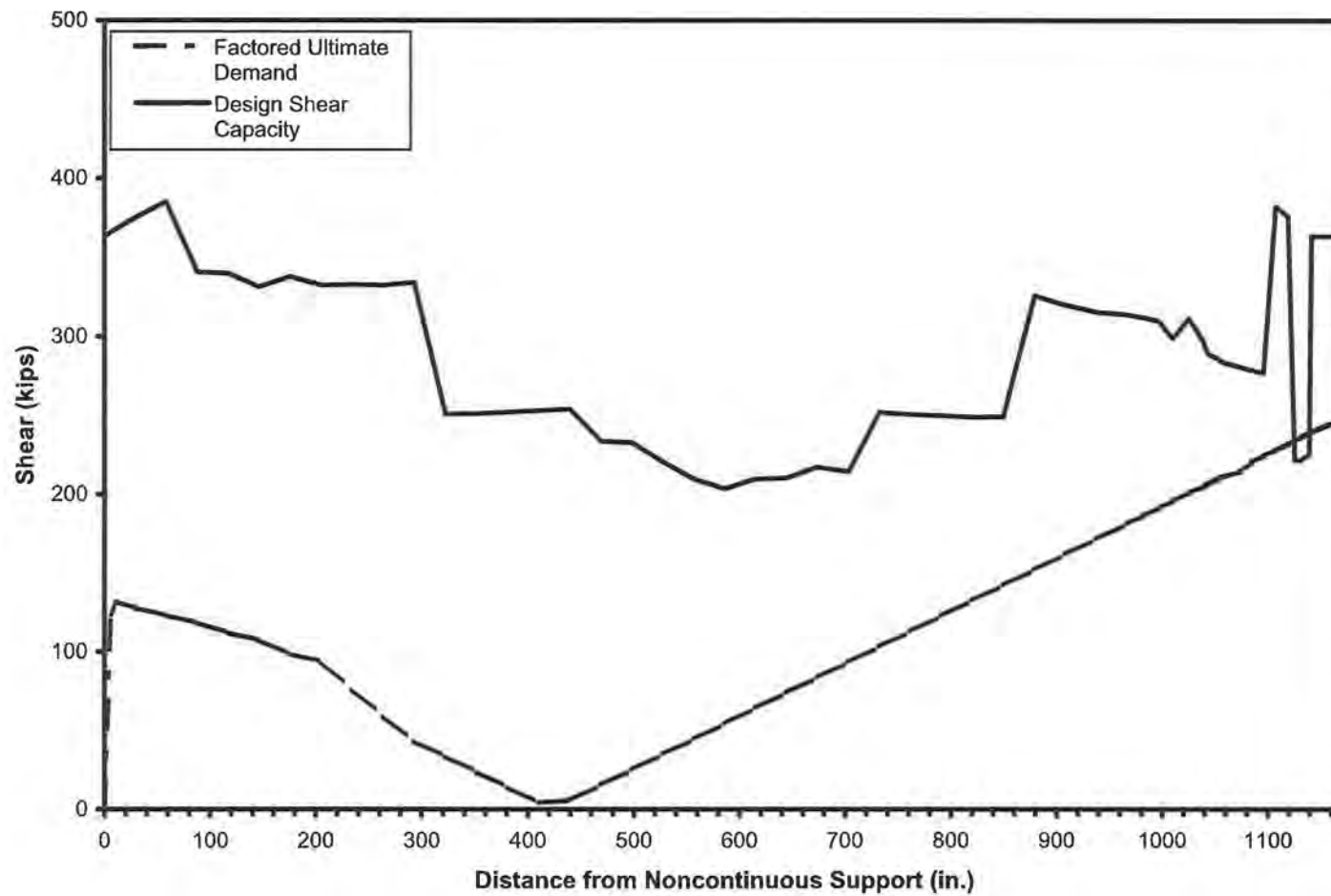
Figure 7.10 – Design Shear Capacity vs. Factored Ultimate Demand for the 3-Ply FRP Strengthening System on an Interior Girder

148

~42"

130"
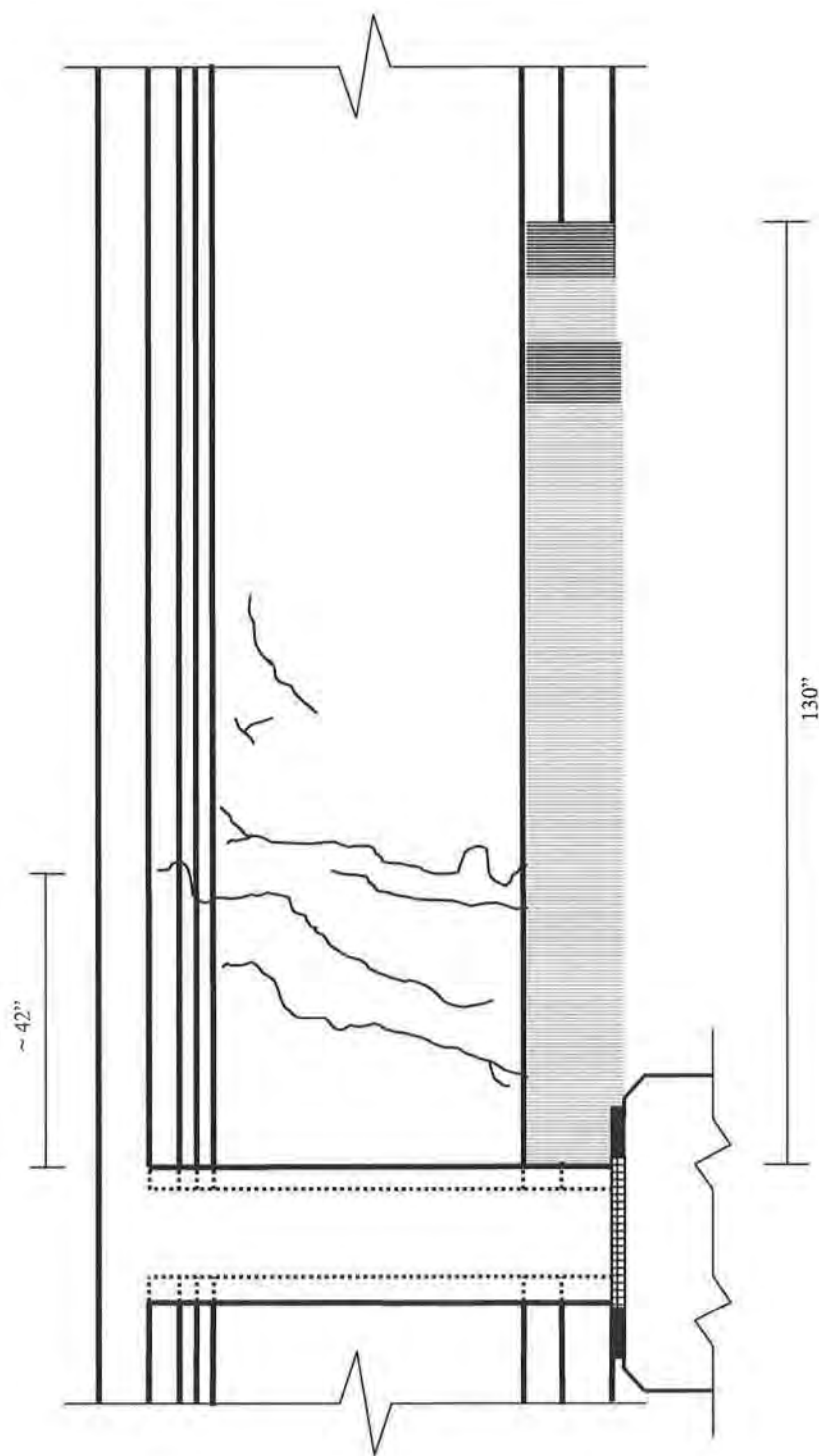
Figure 7.11 – Longitudinal Configuration of the 4-Ply FRP Strengthening System
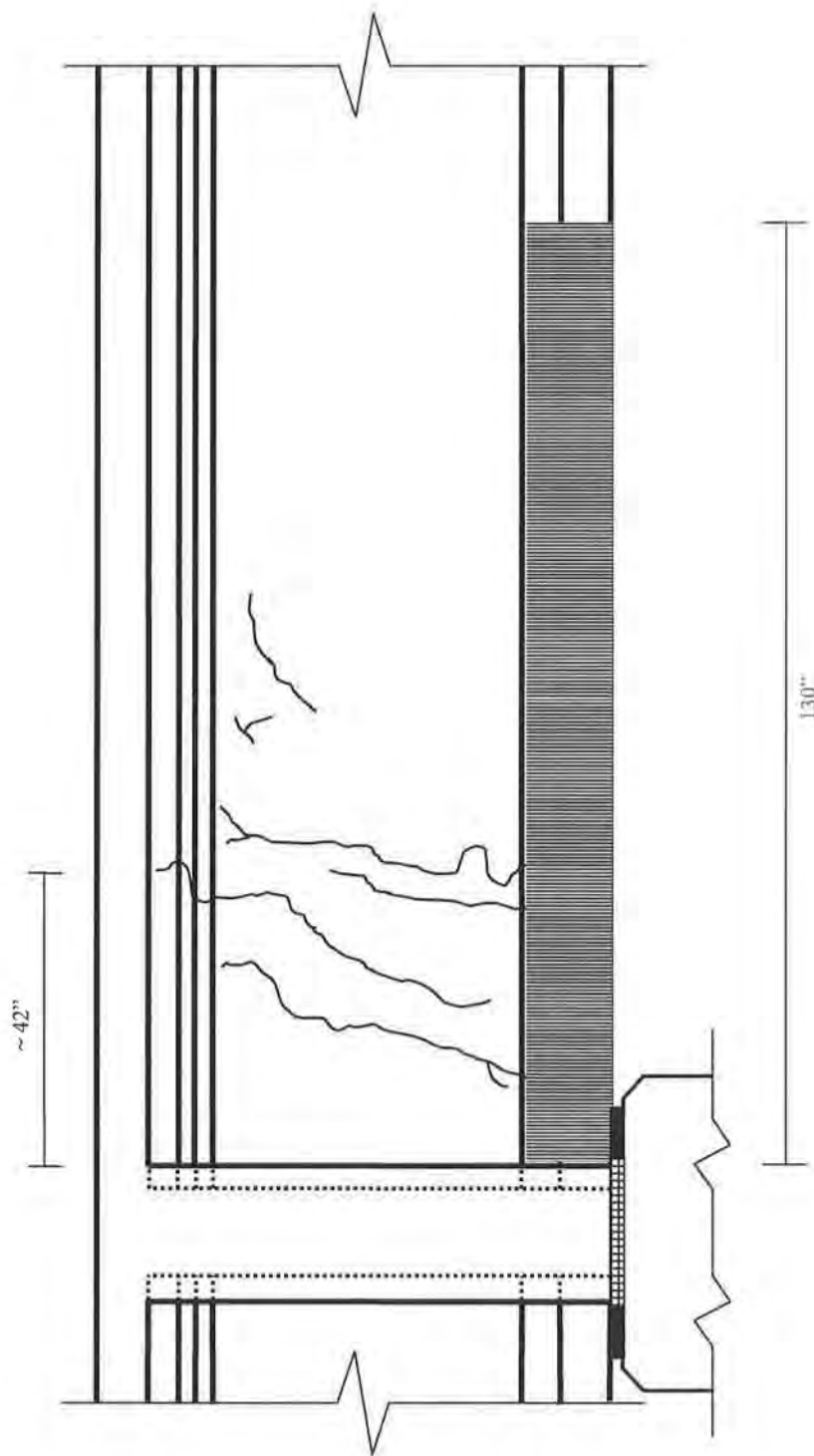
149
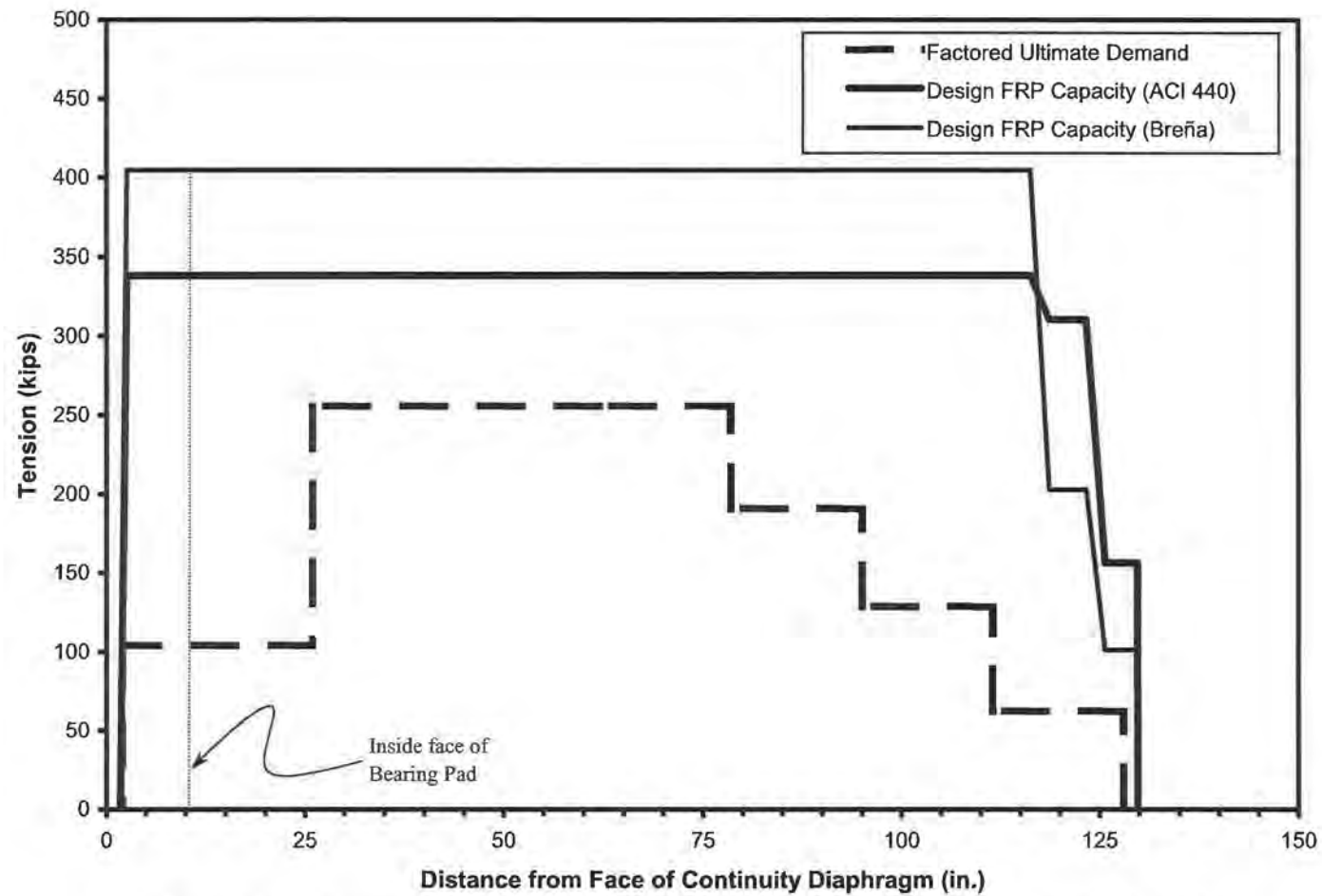
Figure 7.12 – Design Tensile Capacity vs. Factored Ultimate Demand for the 4-Ply FRP Strengthening System

150
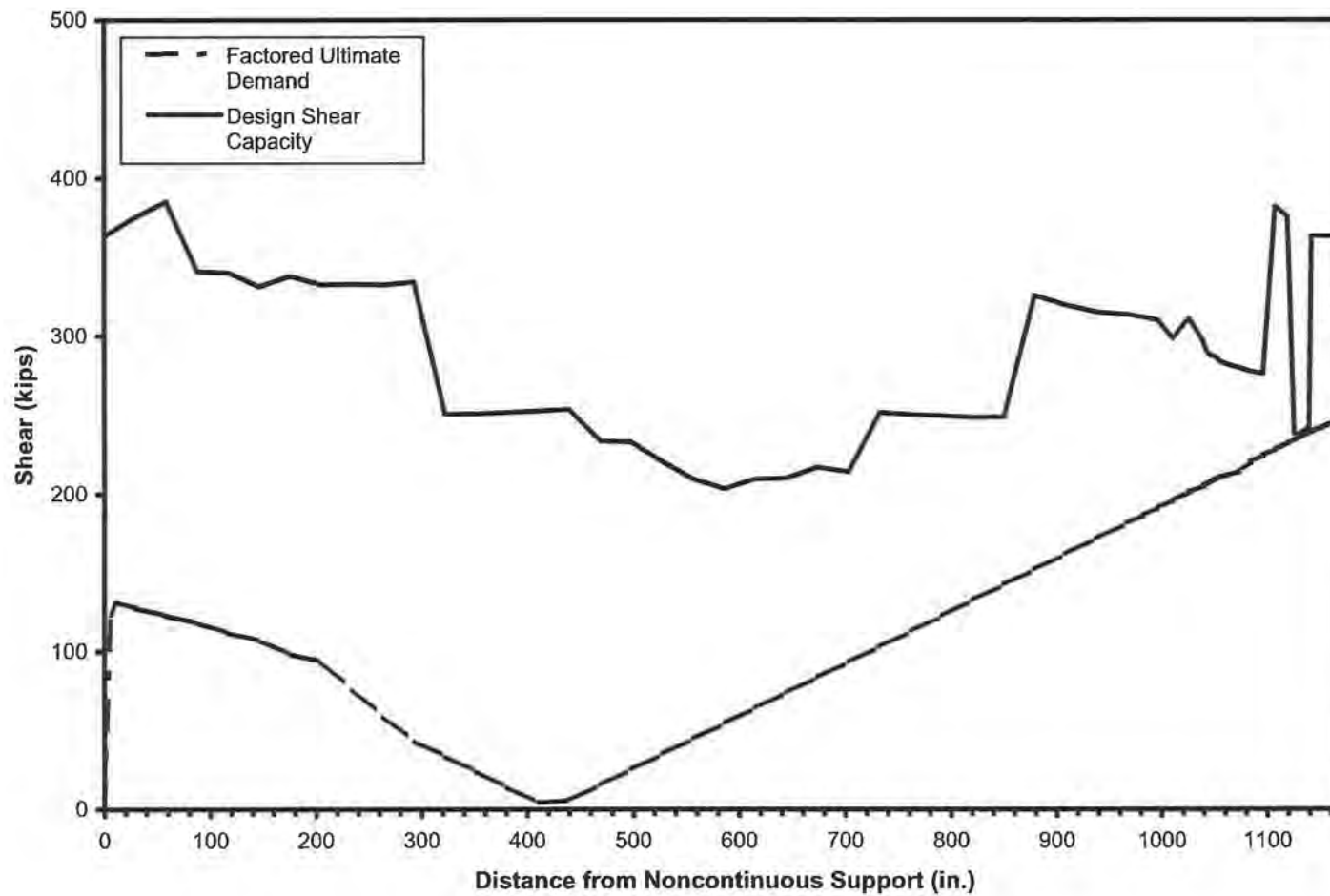
Figure 7.13 – Design Shear Capacity vs. Factored Ultimate Demand for the 4-Ply FRP Strengthening System on an Interior Girder

151

Figure 7.14 – Tensile Capacity vs. Factored Ultimate Demand for the Prestressing Tendons

152

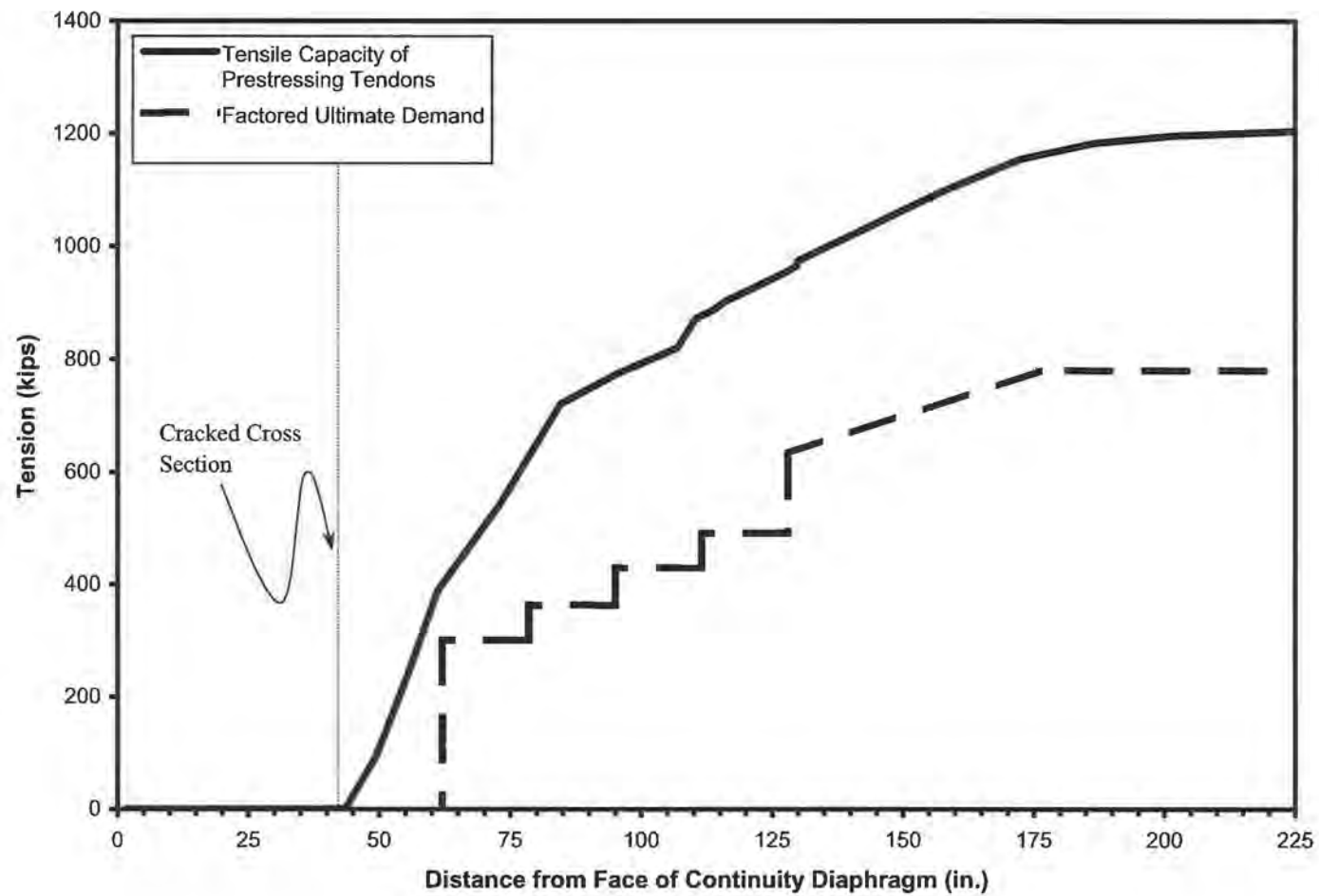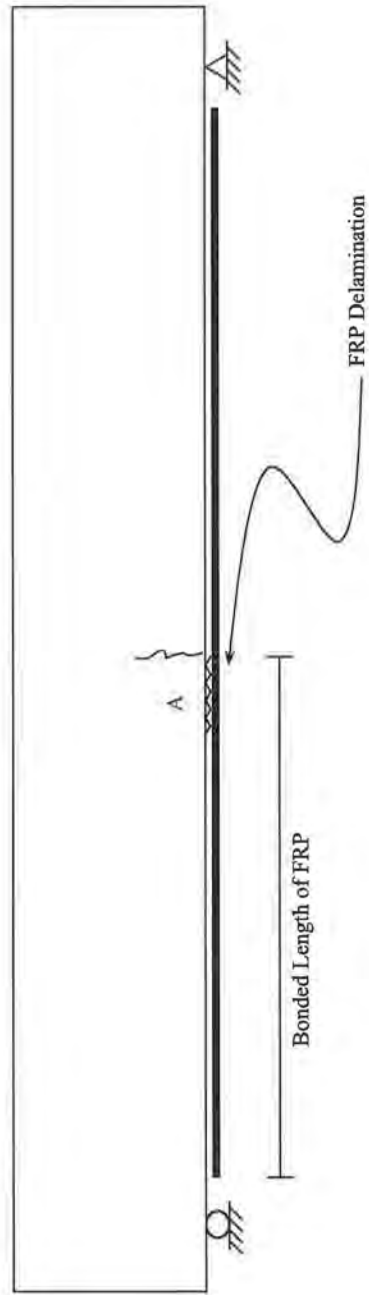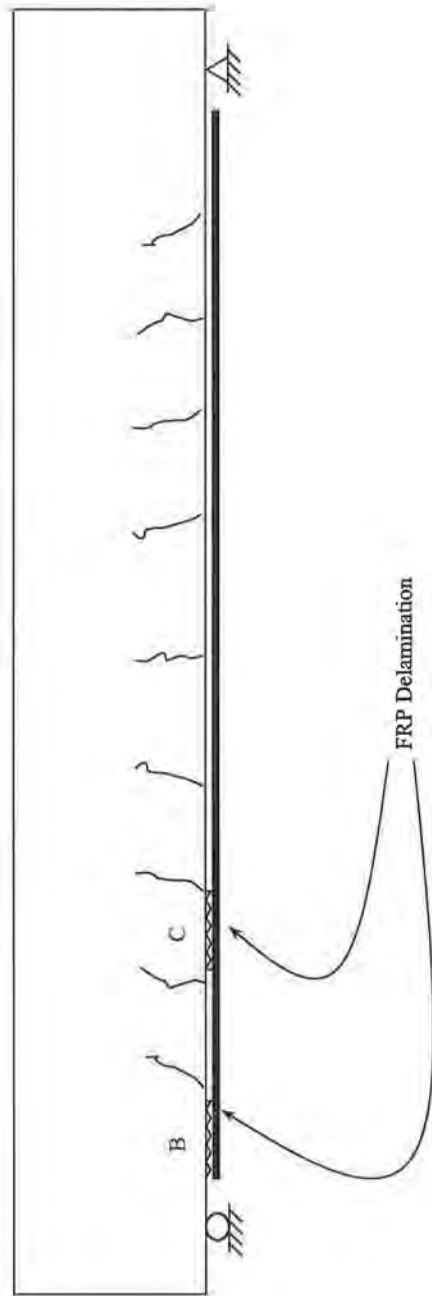*Figure 7.15 – FRP Delamination Type A*

Figure 7.16 – FRP Delamination Types B and C

154

Critical Zone #1   Critical Zone #2
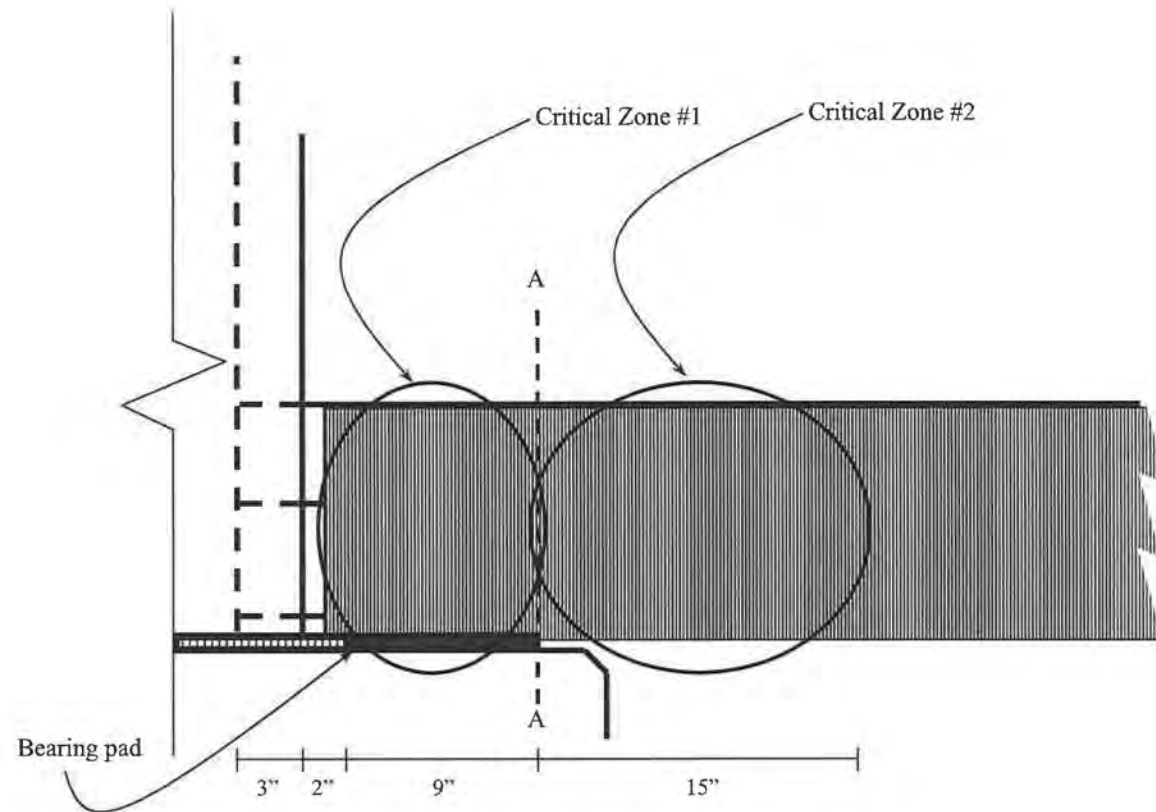
A

Bearing pad

3" 2" 9" 15"

Figure 7.17 – Detailed of the Cracked End Region of a Strengthened Bulb-tee Girder

CHAPTER 8: CONCLUSIONS AND RECOMMENDATIONS

The Interstate 565 bridge structures in Huntsville, Alabama, were constructed during a five-part project that began in January 1988 and ended in March 1991. Many of the bridge structures are composed of prestressed concrete bulb-tee bridge girders that were made continuous for live loads. More than three percent of the prestressed concrete bulb-tee bridge girders made continuous for live load contain cracks at their continuous ends. The cracks were discovered during bridge inspections conducted between the end of the construction process and the spring of 1994. When discovered, the width of the cracks varied between 0.002 in. (0.05 mm) and 0.25 in. (6.4 mm). Cracks formed at the bottom of the cross section and propagated through the bottom flange into the web.

ALDOT personnel performed several procedures aimed at preventing further cracking of the bulb-tee girders and repairing those girders that were cracked. False supports were installed near bents supporting cracked girders so that a total collapse of a span would not occur. Cracks at the continuous ends of the bulb-tee girders were sealed and epoxy injected. An attempt to free unaffected girders from the continuity diaphragm was made by sawing into the continuity diaphragm around the perimeter of the girder.

8.1 CRACKING IN THE PRESTRESSED CONCRETE BULB-TEE GIRDERS

ALDOT personnel monitored and tested spans that contain cracked bulb-tee girders to determine how traffic, wind, and thermal loads affect the cracked girders. Testing and monitoring of the cracked bulb-tee girders revealed that traffic and wind loads are not a likely cause of the cracks and do not significantly affect the width of the cracks. However, thermal loading of the girders induced by a temperature gradient between the top and bottom of the superstructure caused increases in the width of cracks and movement between crack faces. ALDOT personnel concluded that the cracks had formed as a result of a phenomenon called "sun cambering."

The width of the cracks suggests that the prestressing tendons may have slipped between the cracked cross section and the girder end. The strain relieved through slippage of the tendons was estimated using Equation 3.1. The amount of slip estimated with Equation 3.1 correlates well with the width of the cracks in the continuous girder ends. Because slippage of the prestressing tendons seemed to be likely for cracked bulb-tee girders, it was assumed that the effects of prestressing had been lost in all cross sections between the cracked cross section and the continuous end of the girder.

Some spans composed of cracked prestressed concrete bulb-tee girders made continuous for live loads contain girders that are uncracked at their continuous ends. The most likely explanation as to why some girders have cracked and others have not is related to the redistribution of loads and the restraint provided by the continuity diaphragm. The loads on the structure, namely the thermal loads, cracked girders individually, reducing the rotational stiffness of the structure each time new cracks

156

formed in the end of one girder. After the rotational stiffness at the interior support had been sufficiently reduced through cracking in the girder ends, the structure gained the ability to rotate more freely at the interior support under thermal loading. The presence of cracks in the face of the continuity diaphragm also aided in the reduction of the rotational stiffness of the structure by allowing girders adjacent to the face cracks to rotate more freely at the interior support.

8.2 ANALYSIS OF THE CRACKED PRESTRESSED CONCRETE BULB-TEE GIRDERS

Three different analytical procedures were used in the examination of the cracked prestressed concrete bulb-tee bridge girders. An elastic structural analysis was completed to determine the factored ultimate load effects on a typical cracked bulb-tee girder. The flexural and shear capacities of the cracked girders were evaluated with current AASHTO and ACI specifications and recommendations. Lastly, a strut-and-tie analysis was performed to examine the flow of forces through the cracked end of a typical cracked bulb-tee girder.

Factored ultimate shear forces and moments from the elastic structural analysis were compared to the design shear and flexural capacity of the girders. Comparisons showed that multiple strength deficiencies exist near the cracked ends of cracked girders. All deficiencies of positive moment capacity, shear capacity, and tensile capacity of the longitudinal reinforcement are the result of the cracks in the continuous ends of the girders. The deficiencies of shear and positive moment capacity exist for cross sections near the continuous end of the girder. The tensile capacity of the prestressing tendons is less than that required for shear resistance according to Article 5.8.3.5 of the AASHTO LRFD (2002). The deficiency of negative moment capacity at the continuous ends of the girders is not a result of the cracking in the girder end.

Results from the strut-and-tie analysis revealed that the magnitude and orientation of the forces that develop in the concrete and steel reinforcement are dependent on the behavior exhibited by the structure. Simple span behavior results in the largest tensile forces in the bottom flange tension reinforcement. Tensile forces are also induced in the bottom flange tension reinforcement if the behavior of the bridge is continuous with an internal hinge at the cracked cross section. Purely continuous behavior results in compression forces in the bottom flange.

The behavior of the structure at the factored ultimate load level is important in assessing whether or not strength deficiencies exist. Because the prestressing tendons have slipped between the cracked cross section and the continuous end of the girder, they cannot be depended on to resist tensile forces that develop in the bottom flange of a cracked girder. Thus, all tensile forces that are induced in the bottom flange near the cracked end of the member must be carried by external FRP reinforcement. If no external FRP reinforcement is used to strengthen the cracked bulb-tee girder, two of the three mechanisms assumed in the strut-and-tie models are not capable of transferring factored ultimate loads to the supports.

157

8.3 Design of the External FRP Strengthening System

The use of external FRP reinforcement was determined to be feasible to repair and strengthen cracked prestressed concrete bulb-tee girders. External FRP reinforcement bonded to the bottom flange of the cracked bulb-tee girders was designed to act as longitudinal reinforcement, correcting the strength deficiencies that have resulted from the cracking in the continuous ends of the girders. Longitudinal and cross-sectional FRP configurations, the cross-sectional area of FRP required for adequate strengthening, and detailing requirements for the external FRP reinforcement were the most important aspects of the design.

The longitudinal and cross-sectional FRP configurations used in the early stages of the design were based upon material properties of the FRP reinforcement and the dimensions of a typical BT54 girder. Analytical methods were used to determine the shear capacity of the strengthened bulb-tee girder and the tensile capacity of the external FRP reinforcement. The nominal amount of FRP was determined by increasing the amount of external FRP reinforcement used for strengthening until all strength deficiencies were eliminated.

Analysis revealed that four plies of the external FRP reinforcement would be necessary to adequately strengthen the cracked bulb-tee girders. If fewer than four plies are used, the design shear capacity of the strengthened member is inadequate for cross sections near the cracked cross section. A comparison of the design tensile capacity of the external FRP reinforcement and the factored ultimate tensile forces from the strut-and-tie models revealed that four plies of FRP were adequate. The positive moment capacity of a typical strengthened bulb-tee girder is satisfactory, as determined by examination of the results of the strut-and-tie analysis. The anchorage of the 4-ply FRP strengthening system was examined analytically. According to the results of the analytical examination of the anchorage of the external FRP reinforcement, adequate anchorage can be provided by the bond between the concrete and FRP. The tensile strength of the concrete was verified through experimental testing of cracked bulb-tee girders in Huntsville, Alabama, and is discussed in Appendix A.

8.4 Recommendations

Based upon the results of the analytical methods described in Chapter 4 and the design of the external FRP strengthening system described in Chapter 7, strengthening cracked and uncracked girders in northbound Spans 4 and 5 with external FRP reinforcement is recommended. Strengthening will eliminate strength deficiencies in cracked bulb-tee girders, prevent cracking in the clear span at the continuous end of uncracked bulb-tee girders, and ensure that all girders can resist factored ultimate loads for the three types of structural behavior considered. Details of the external FRP strengthening system are presented in the following sections.

8.4.1 Area of External FRP Reinforcement Required for Strengthening

Four plies of the SCH-41 composite laminate should be used to strengthen each bulb-tee girder. Once installed, each FRP laminate ply will have a thickness of 0.04 in. (1.0 mm).

The width of each ply should be 58 in. (1470 mm). The nominal area of the external FRP reinforcement will be 9.28 in.^{2} (6000 mm^2).

Cross sections located between the inside face of the bearing pad and the continuity diaphragm cannot accommodate FRP laminate plies that are 58 in. (1470 mm) wide. The presence of the bearing pad requires that each FRP laminate ply be notched such that external FRP reinforcement will fit around the bearing pad. For cross sections between the inside face of the bearing pad and the continuity diaphragm, the width of external FRP reinforcement will be limited to 30 in. (760 mm).

8.4.2 Longitudinal FRP Configuration

The longitudinal FRP configuration for a typical strengthened bulb-tee girder is shown in Figure 8.1. Each FRP laminate ply should be extended to within 1 in. (25 mm) of the face of the continuity diaphragm. Portions of the FRP laminate plies bonded to the bottom surface of the bottom flange should be extended to within 1 in. (25 mm) of the inside face of the bearing pad. The bottommost FRP laminate ply should be terminated 120 in. (3050 mm) beyond the inside face of the bearing pad. Each subsequent FRP laminate ply should be terminated 6 in. (150 mm) shorter than the ply beneath it. The staggered termination of FRP laminate plies should minimize stress concentrations formed at the curtailment of the plies. Each FRP laminate ply should be oriented such that the fibers in the SCH-41 reinforcing fabric are oriented in the longitudinal direction.

8.4.3 Cross-Sectional FRP Configuration

In order to make the most efficient use of the external FRP reinforcement, it should be wrapped around the bottom flange of the bulb-tee girder. The cross-sectional FRP configuration for a typical cross section is shown in Figure 8.2. Figure 8.2 corresponds with Section A shown in Figure 8.1. This cross-sectional configuration will maximize the bonded area of external FRP reinforcement and increase the anchorage developed through the bond between the FRP and the concrete.

A wrapped cross-sectional configuration will not be possible for cross sections between the inside face of the bearing pad and the continuity diaphragm. The cross-sectional FRP configuration for cross sections between the inside face of the bearing pad and the continuity diaphragm is shown in Figure 8.3. Figure 8.3 corresponds to Section B shown in Figure 8.1. For cross sections in this region, the external FRP reinforcement will only be bonded to the sides and top surfaces of the bottom flange.

8.4.4 Anchorage of External FRP Reinforcement

The anchorage of the external FRP reinforcement was examined by using an analytical method proposed by Harmon et al. (2003). Assuming that a strength reduction factor of 0.85 for anchorage of externally bonded FRP reinforcement to concrete is satisfactory, adequate anchorage of the FRP can be achieved through the bond between the concrete and FRP. Mechanical anchorage devices are not necessary.

8.4.5 Detailing of External FRP Reinforcement

Tasks related to the preparation of the concrete surface are necessary to ensure that the bond between the FRP and concrete is adequate. Before any other procedures can begin, cracks in the continuous ends of the girder must be sealed and epoxy injected. It is recommended that cracks with widths of 0.010 in. (0.25 mm) or more be epoxy injected. After cracks have been epoxy injected, surfaces on the bottom flange of the girder between the continuity diaphragm and the FRP curtailment location must be sandblasted or grinded. The finished surface should be relatively smooth and free of protruding objects. For best results, Fyfe Co. recommends that a tolerance of 1/32 in. (0.8 mm) be used when determining if sandblasted or grinded surfaces have been prepared correctly.

All corners of the bottom flange must be ground such that the radius of any corner turned by the external FRP reinforcement is no less than 0.5 in. (12.7 mm). Grinding of the corners on the bottom flange must be performed for cross sections located between the face of the continuity diaphragm and the FRP curtailment location. Rounding the corners will reduce stress concentrations in the external FRP reinforcement. After this step is fulfilled, dust and laitance should be removed with compressed air or a water cannon. Surfaces on the bottom flange must be allowed to dry before the external FRP reinforcement can be installed.

8.4.6 Installation of External FRP Reinforcement

The installation of the external FRP reinforcement should be performed in accordance with manufacturer specifications. Tyfo S epoxy, used to bond the SCH-41 reinforcing fabric to the concrete, should be mixed in a 100 to 42 ratio by weight of parts A and B. Mixing should be done with a low-speed mixer for five minutes or until the epoxy is uniformly blended. Once mixed, the pot life of Tyfo S epoxy is two hours.

The SCH-41 reinforcing fabric must be saturated with Tyfo S epoxy before it can be bonded to the girders. Saturation with Tyfo S epoxy may be completed with specialized equipment, though hand saturation is acceptable given that the epoxy is applied uniformly on the surface of the fabric. Saturation of the SCH-41 reinforcing fabric must not be performed at temperatures less than 40 °F (4.4 °C). The manufacturer should be consulted on the cure time of the Tyfo S epoxy.

8.5 FURTHER RESEARCH

Additional research is recommended to evaluate the effectiveness of the proposed external FRP strengthening system. Load testing of the two-span bridge structure should be performed before and after repair to examine changes in the behavior of the structure and the forces developed in the external FRP reinforcement. An examination of the anchorage of the proposed FRP configuration may also be worthwhile. Because the anchorage of the FRP cannot be evaluated in a non-destructive manner, test specimens strengthened with a FRP configuration similar to that used to strengthen the cracked bulb-tee girders would be appropriate.

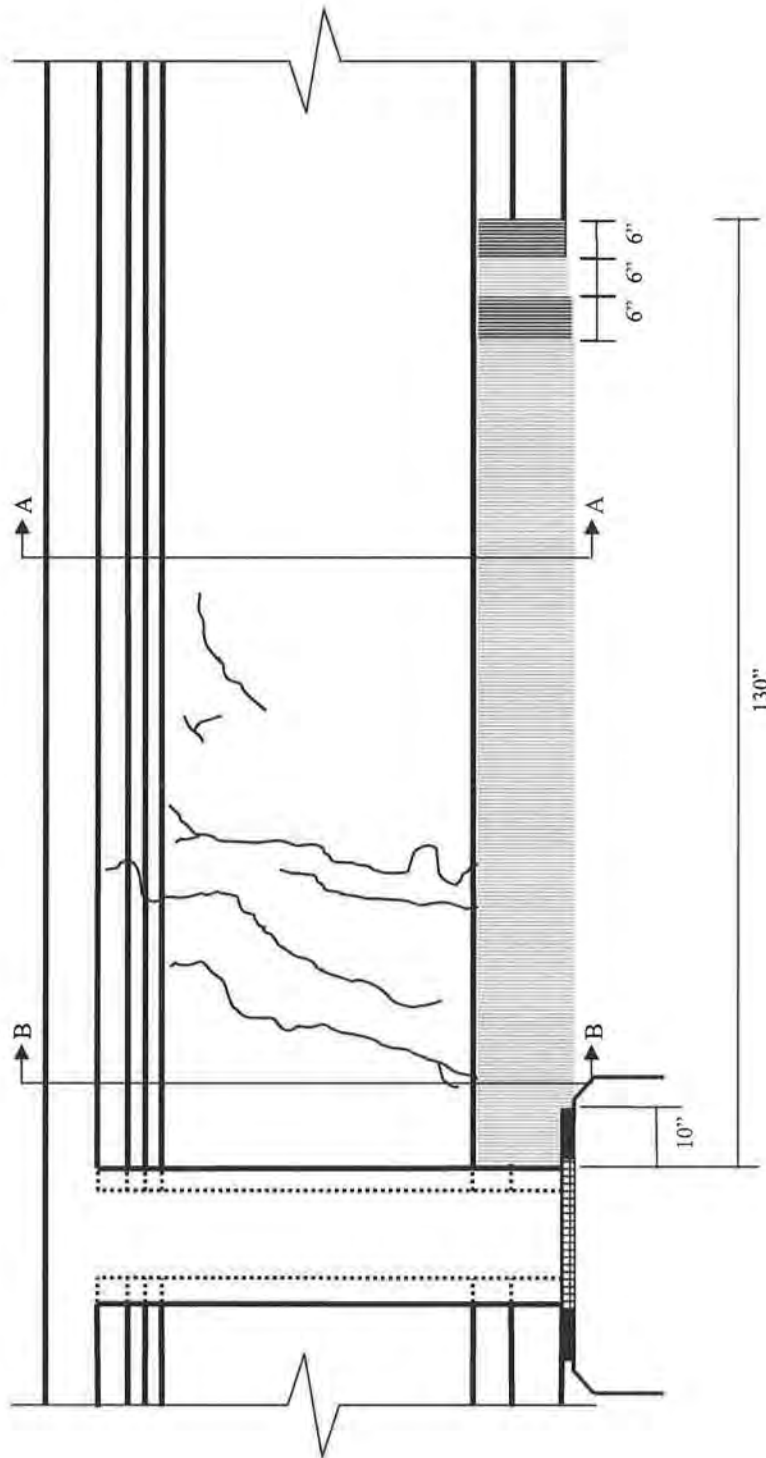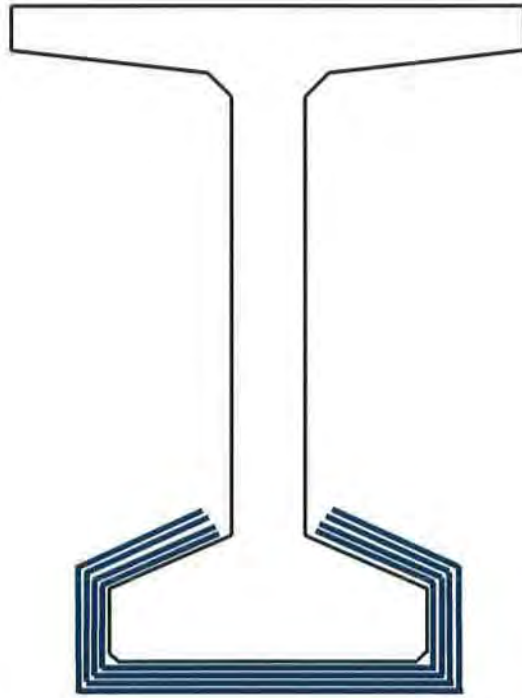Figure 8.1 – Detail of the Longitudinal FRP Configuration

Labels within figure: A, A, B, B, 6", 6", 6", 130", 10"

Figure 8.2 – Detail of the Cross-sectional FRP Configuration at Section A
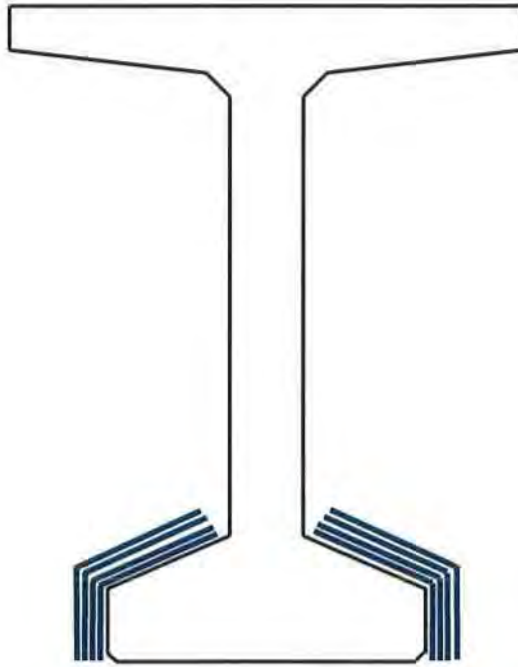
Figure 8.3 – Detail of the Cross-sectional FRP Configuration at Section B

BIBLIOGRAPHY

ACI Committee 318 (2002). *Building Code Requirements for Structural Concrete (ACI 318-02) and Commentary (ACI 318R-02)*. Farmington Hills, MI, American Concrete Institute.

ACI Committee 440 (2002). *Guide for the Design and Construction of Externally Bonded FRP Systems for Strengthening Concrete Structures (ACI 440.2R-02)*. Farmington Hills, MI, American Concrete Institute.

ACI-ASCE Committee 445 (2000). *Recent Approaches to Shear Design of Structural Concrete (ACI 445R-99)*. Farmington Hills, MI, American Concrete Institute.

Alabama Department of Transportation (ALDOT) (1994a). "Summary of Field Survey – I565-45-11.5 A&B." Montgomery, Alabama. ALDOT Maintenance Bureau – Bridge Rating and Load Testing.

Alabama Department of Transportation (ALDOT) (1994b). Interoffice Memorandum, May 3.

Alabama Department of Transportation (ALDOT) (1994c). "Summary of Investigation of I-565-45-11.5 A&B June 14&15 1994." Montgomery, Alabama.

Alabama Department of Transportation (ALDOT) (1994d). "Cracks in Precast Prestressed Bulb Tee Girders on Structure No.'s I-565-45-11.5 A. & B. on I-565 in Huntsville, Alabama." Montgomery, Alabama.

American Association of State Highway and Transportation Officials (2002). *AASHTO LRFD, 2002 Interim Bridge Design Specifications*, Second Edition. Washington, DC, American Association of State Highway and Transportation Officials.

Adhikary, B. B., and H. Mutsuyoshi (2000). "Enhancement of Shear Strength for Reinforced Concrete Beams Using Externally Bonded Fiber-Reinforced Polymer Sheet." ACI Special Publication 193(35): 587-604.

Al-Nahlawi, K. A., and J. K. Wight (1992). "Beam Analysis using Concrete Tensile Strength in Truss Models." *ACI Structural Journal* 89(3): 284-289.

Annaiah, R. H., F. Micelli, and A. Nanni (2001). "Shear Performances of RC Beams Strengthened in Situ with FRP Composites." Composites in Construction 2001 International Conference, Porto, Portugal.

Bakis, C. E., L. C. Bank, V. L. Brown, E. Cosenza, J. F. Davalos, J. J. Lesko, A. Machida, S. H. Rizkalla, and T. C. Triantafillou (2002). "Fiber-Reinforced Polymer Composites for Construction—State-of-the-Art Review." *Journal of Composites for Construction* 6(2): 73-87.

Barnes, R. W., N. H. Burns, and M. E. Kreger (1999). *Development Length of 0.6-Inch Prestressing Strand in Standard I-Shaped Pretensioned Concrete Beams*. Austin, TX, Center for Transportation Research.

Breña, S. F. (2000). *Strengthening of Reinforced Concrete Bridges Using Carbon Fiber Reinforced Polymer Composites*, Dissertation. University of Texas at Austin: 436.

Chaallal, O., M. Shahawy, and M. Hassan (2002). "Performance of Reinforced Concrete T-Girders Strengthened in Shear with Carbon Fiber-Reinforced Polymer Fabric." *ACI Structural Journal* 99(3): 335-342.

Chajes, M. J., T. F. Januszka, D. R. Mertz, T. A. Thomson, and W. W. Finch (1995). "Shear Strengthening of Reinforced-Concrete Beams Using Externally Applied Composite Fabrics." *ACI Structural Journal* 92(3): 295-303.

Colotti, V., and G. Spadea (2001). "Shear Strength of RC Beams Strengthened with Bonded Steel or FRP Plates." *Journal of Structural Engineering* 127(4): 367-373.

De Lorenzis, L., B. Miller, and A. Nanni (2001). "Bond of Fiber-Reinforced Polymer Laminates to Concrete." *ACI Materials Journal* 98(3): 256-264.

Deniaud, C., and J. J. R. Cheng (2001). "Review of Shear Design Methods for Reinforced Concrete Beams Strengthened with Fibre Reinforced Polymer Sheets." *Canadian Journal of Civil Engineering* 28(2): 271-281.

Emmons, P. H. (1993). *Concrete Repair and Maintenance Illustrated*. Kingston, MA, R. S. Means Company, Inc.: 201-204.

Freyermuth, C. L. (1969). "Design of Continuous Highway Bridges with Precast, Prestressed Concrete Girders." *PCI Journal* 14(2): 14-39.

Gao, N. (2003). *Investigation of Cracking in Precast Prestressed Girders Made Continuous for Live Load*, Thesis. Auburn University: 137.

Harmon, T., Y. J. Kim, J. Kardos, T. Johnson, and A. Stark (2003). "Bond of Surface Mounted FRP Reinforcement for Concrete Structures." *ACI Structural Journal* (accepted for publication).

Khalifa, A., W. J. Gold, A. Nanni, and A. Aziz (1998). "Contribution of Externally Bonded FRP to Shear Capacity of RC Flexural Members." *Journal of Composites for Construction* 2(4): 195-202.

Khalifa, A., A. Belarbi, and A. Nanni (2000). "Shear Performance of RC Members Strengthened with Externally Bonded FRP Wraps." 12th World Conference on Earthquake Engineering, Auckland, New Zealand.

Khalifa, A., and A. Nanni (2000). "Improving Shear Capacity of Existing RC T-Section Beams Using CFRP Composites." *Cement & Concrete Composites* 22(3): 165-174.

Lamanna, A. J., L. C. Bank, and D. W. Scott (2001). "Flexural Strengthening of Reinforced Concrete Beams Using Fasteners and Fiber-Reinforced Polymer Strips." *ACI Structural Journal* 98(3): 368-376.

Lees, J. M., A. U. Winistörfer, and U. Meier (2002). "External Prestressed Carbon Fiber-Reinforced Polymer Straps for Shear Enhancement of Concrete." *Journal of Composites for Construction* 6(4): 249-256.

Li, A., J. Assih, and Y. Delmas (2001a). "Shear Strengthening of RC Beams with Externally Bonded CFRP Sheets." *Journal of Structural Engineering* 127(4): 374-380.

Li, A.; C. Diagana; and Y. Delmas (2001b). "CRFP Contribution to Shear Capacity of Strengthened RC Beams." *Engineering Structures* 23(10): 1212-1220.

Ma, Z., X. Huo, M. K. Tadros, and M. Baishya (1998). "Restraint Moments in Precast/Prestressed Concrete Continuous Bridges." *PCI Journal* 43(6): 40-57.

Malek, A. M., and H. Saadatmanesh (1998a). "Analytical Study of Reinforced Concrete Beams Strengthened with Web-Bonded Fiber Reinforced Plastic Plates or Fabrics." *ACI Structural Journal* 95(3): 343-352.

Malek, A. M., and H. Saadatmanesh (1998b). "Ultimate Shear Capacity of Reinforced Concrete Beams Strengthened with Web-Bonded Fiber-Reinforced Plastic Plates." *ACI Structural Journal* 95(4): 391-399.

Micelli, F., R. H. Annaiah, and A. Nanni (2002). "Strengthening of Short Shear Span Reinforced Concrete T Joists with Fiber-Reinforced Plastic Composites." *Journal of Composites for Construction* 6(4): 264-271.

Mirmiran, A., S. Kulkarni, R. Castrodale, R. Miller, and M. Hastak (2001). "Nonlinear Continuity Analysis of Precast, Prestressed Concrete Girders with Cast-in-Place Decks and Diaphragms." *PCI Journal* 46(5): 60-80.

Noppakunwijai, P., N. Jongpitakseel, Z. Ma, S. A. Yehia, and M. K. Tadros (2002). "Pullout Capacity of Non-Prestressed Bent Strands for Prestressed Concrete Girders." *PCI Journal* 47(4): 90-103.

Norris, T., H. Saadatmanesh, and M. R. Ehsani (1997). "Shear and Flexural Strengthening of R/C Beams with Carbon Fiber Sheets." *Journal of Structural Engineering* 123(7): 903-911.

Oesterle, R. G., J. D. Glikin, and S. C. Larson (1989). *Design of Precast Prestressed Bridge Girders Made Continuous*. Skokie, Illinois, Construction Technology Laboratories, Inc.

Pellegrino, C., and C. Modena (2002). "Fiber Reinforced Polymer Shear Strengthening of Reinforced Concrete Beams with Transverse Steel Reinforcement." *Journal of Composites for Construction* 6(2): 104-111.

Russell, B. W., N. H. Burns, and L. G. ZumBrunnen (1994). "Predicting the Bond Behavior of Prestressed Concrete Beams Containing Debonded Strands." *PCI Journal* 39(5): 60-77.

Schlaich, J., K. Schäfer, and M. Jennewein (1987). "Towards a Consistent Design of Structural Concrete." *Journal of the Prestressed Concrete Institute* 32(3): 74-150.

Swamy, R. N., P. Mukhopadyaya, and C. J. Lynsdale (1999). "Strengthening for Shear of RC Beams by External Plate Bonding." *The Structural Engineer* 77(12): 19-30.

Triantafillou, T. C. (1998a). "Composites: A New Possibility for the Shear Strengthening of Concrete, Masonry and Wood." *Composites Science and Technology* 58(8): 1285-1295.

Triantafillou, T. C. (1998b). "Shear Stengthening of Reinforced Concrete Beams Using Epoxy-Bonded FRP Composites." *ACI Structural Journal* 95(2): 107-115.

Triantafillou, T. C., and C. P. Antonopoulos (2000). "Design of Concrete Flexural Members Strengthened in Shear with FRP." *Journal of Composites for Construction* 4(4): 198-205.

Vogel, T., and T. Ulaga (2002). "Strengthening of a Concrete Bridge and Loading to Failure." *Structural Engineering International* 12(2): 105-110.

APPENDIX A: ADHESION TESTS

The experimental method used to evaluate the tensile strength of the concrete was based on recommendations given in the American Society for Testing and Materials (ASTM) specification D 4541 – 95, *Standard Test Method for Pull-Off Strength of Coatings Using Portable Adhesion Testers*. The test method provides a means to evaluate the pull-off strength of a coating or material by applying a direct tensile force to a test surface with a known area. The result is either a failure load, which is used to calculate a tensile strength, or a pass/fail rating based upon the maximum stress applied during the test (ASTM D 4541 – 95 1995). The procedure is described in detail in Section A.1.3. Results of the testing program are presented in Section A.2.

A.1 EXPERIMENTAL EVALUATION OF CONCRETE TENSILE STRENGTH

The recommendations given in ASTM D 4541 – 95 were used to develop a procedure to evaluate the tensile strength of the concrete. The failure load measured during the test was used to determine the pull-off (tensile) strength of the concrete. Some minor changes were made to the ASTM D 4541 – 95 testing procedure to accommodate the specific nature of the adhesion tests on the cracked prestress concrete girders.

If the strength of the adhesive bond was greater than the tensile strength of the concrete, failure occurred through the concrete substrate. This type of failure was desirable because it resulted in a measure of the tensile strength of the concrete to which the external FRP reinforcement will be bonded. If the tensile strength of the concrete exceeded that of the adhesive bond, the failure occurred through the adhesive layer. Such a failure only provided a lower bound estimate of the concrete strength.

Adhesion tests were performed on Girders 3 and 4 of northbound Span 51, which is supported by northbound Bents 51 and 52. Both of the girders chosen are cracked at their continuous ends, though the cracking is not as severe as the cracking found in girders of other spans. Northbound Bent 52 was the best location to perform the adhesion tests because it supported cracked bulb-tee girders and it could be accessed from beneath the structure with the use of scaffolding and a ladder.

A.1.1 Adhesion Testing Equipment

An Elcometer 106 fixed-alignment portable adhesion tester was used for all adhesion tests. A limited review of several different types of adhesion testers is included within ASTM D 4541 – 95, one of which is a fixed-alignment portable adhesion tester. The Elcometer 106 removes high-tensile aluminum test dollies from surface and measures the tensile stress that causes failure. The load is applied to the test dolly by turning the nut on the top of the instrument. For a 1.57 in. (40 mm) diameter test dolly, the Elcometer 106 can apply an evenly distributed tensile stress as high as 800 psi (5.5 MPa). The

168

Elcometer 106 fixed-alignment portable adhesion tester is shown in Figure A.1. A typical 1.57 in. (40 mm) diameter test dolly is shown in Figure A.2.

All adhesion tests were performed on the top surface of the bottom flange of cracked prestressed concrete bulb-tee girders. Adhesion testing on other surfaces of the girder was not considered. Although the adhesion testing procedure described in ASTM D 4541 – 95 may be performed on vertical and inverted surfaces, doing so is very difficult in non-laboratory conditions.

A.1.2 Test Preparation

A visual inspection of the concrete was performed to determine the best location to perform the adhesion tests. The selected surface needed to be free of cracks, voids, and pitting. The selected surface had to be located away from edges and discontinuities as well. Unfortunately, the entire top surface of the bottom flange was mildly honeycombed. Locations for test surfaces had to be selected carefully to ensure that the test dolly would be bonded to sound concrete that was free of pitting and voids.

A power grinder with an abrasive grinding wheel was used to remove debris and protruding surface imperfections. Once an adequate area had been ground and smoothed on the top surface of the bottom flange, a permanent marker was used to mark locations where a hole saw would be used to create test surfaces. A template clamped to the top surface of the bottom flange was used to aid in the creation of test surfaces. A diamond-coated hole saw with a diameter of 1.75 in. (44 mm) was used to create the test surfaces. The groove around the test surface had a width of about 0.125 in. (3.2 mm). The depth of the groove varied, though a depth of 0.25 in. (6.4 mm) was desired. Figures A.3 and A.4 show the abrasive grinding wheel and diamond-coated hole saw used to create the test surface.

After the hole saw had been used to create the test surfaces, each surface was sanded with 120-grit sand paper to remove small surface imperfections. A drinking straw was used to blow away small debris and dust created by grinding, hole sawing, and sanding of the test surface. Each test surface was then cleaned with rubbing alcohol and a coarse brush. A caliper was used to measure the diameter of each test surface. The diameter of each test surface was measure two times so that the area of the test surface could be calculated as though it was elliptical. The equation for the area of an ellipse is given in Equation A.1, where d_1 and d_2 are the major and minor axis diameters.

$$A_{test} = \frac{\pi}{4} d_1 d_2 \qquad \text{Eq. A.1}$$

Once dry, the cleaned test surfaces were coated with Tyfo S epoxy. The two-part Tyfo S epoxy was mixed in a 100/42 ratio, as recommended by the manufacturer. An even coat of the Tyfo S epoxy was applied to each test surface with a foam brush. The Tyfo S epoxy was allowed to cure for 18 hours so that a hardened finish was achieved. Because the test surfaces were on an inclined surface, the Tyfo S epoxy pooled near the bottom of some test surfaces and in the groove around the test surfaces. Upon hardening, the build-up of Tyfo S epoxy was removed from the test surfaces to ensure that the test dollies were bonded to a flat surface. The hardened epoxy finish was then sanded lightly with

120-grit sand paper. Figure A.5 shows five test surfaces that have been coated with a hardened Tyfo S epoxy and lightly sanded. A build-up of Tyfo S epoxy was present on some of the test surfaces shown in Figure A.5, though it is difficult to distinguish them in the figure.

Each test dolly was prepared by lightly sanding the bottom surface with 120-grit sand paper and cleaning with rubbing alcohol to remove all grit and dirt. A two-part high-strength epoxy, Araldite RAPID, was mixed in a 1:1 ratio and applied evenly over the bottom surface of a single test dolly and test surface. Bonding of test dollies to test surfaces had to be done individually because the cure time of the Araldite RAPID epoxy was only ten minutes. The test dolly was placed on the test surface and pressure was applied manually to remove excess epoxy from between the bonded surfaces. Excess epoxy was removed with a cotton swab. After the test dolly had been held in place on the test surface for two minutes, a piece of cardboard was inserted into the groove surrounding the test surface. The purpose of the cardboard was to prevent movement of the test dolly before the Araldite RAPID epoxy was fully cured. The Araldite epoxy was allowed to cure for 22 hours before adhesion tests were performed.

The use of two epoxy adhesives, the Tyfo S and the Araldite RAPID, was necessary to create a bond between the test dolly and the concrete girder that was strong enough to cause a failure through the concrete substrate. The Tyfo S epoxy does not bond well to the test dolly, though it is effective in penetrating the concrete substrate. The Araldite epoxy proved to provide a strong bond between the test dolly and a roughened Tyfo S surface. The ability of these epoxy adhesives to provide a bond with adequate strength was experimentally verified before adhesion tests were performed on the cracked prestressed concrete bulb-tee girders.

A.1.3 Test Procedure

After the Araldite RAPID epoxy had adequately cured, the Elcometer 106 was used to remove the test dollies from the test surfaces. The following procedure was followed for each adhesion test. The procedure was derived from the recommendations given in ASTM D 4541 – 95 and the Elcometer manufacturer specifications.

1. Using 120-grit sand paper, the area around the test dolly was sanded to remove excess epoxy, creating a more uniform and flat surface. Once sanding was completed, the base ring was set in place. The dragging indicator on the Elcometer 106 was reset to zero. Figure A.6 shows the proper base ring orientation.

2. The nut on the top of the Elcometer 106 was loosened, lowering the claw. Once the claw had been lowered to an appropriate level, the Elcometer 106

was positioned such that the top of the test dolly fit into the claw and the three feet of the Elcometer 106 rested on the base ring. The nut was then tightened until the claw engaged the top of the test dolly and a significant torque was required to turn the nut. Figure A.7 shows the Elcometer 106 after engaging a test dolly.

3. Using the ratchet spanner, the nut was slowly turned to increase the force applied to the test dolly. The nut was turned until a failure occurred, or until the maximum capacity of the Elcometer 106 was reached.

4. If a failure had occurred, the test dolly was removed from the claw, put into a sandwich bag, and labeled. The nut was loosened to relieve any load remaining on the spring inside the Elcometer 106.

5. The reading from the dragging indicator and a brief description of the failure were recorded for each test.

A.2 RESULTS OF EXPERIMENTAL EVALUATION OF CONCRETE TENSILE STRENGTH

A total of ten adhesion tests were performed on the cracked prestressed concrete bulb-tee girders. Each test was performed according to the procedure described in Section A1.3. A summary of the data collected during the adhesion tests is given in Table A.1. A brief description of the failure mode of each test is included with the test results.

The majority of the adhesion tests resulted in a failure mode where the failure plane propagated through the adhesive layer and the concrete. A test dolly that has failed in this manner is shown in Figure A.8. Of the eight adhesion tests that resulted in this type of failure, a minimal amount of concrete remained bonded to the test dolly after failure. The amount of concrete that remained bonded to the test dollies varied, though none of the test dollies removed a uniform layer of concrete. The concrete bonded to the test dollies was spotty, very thin, and contained no coarse aggregate.

Table A.1 – Results of Adhesion Tests Performed on Cracked Prestressed Concrete Bulb-tee Girders

Test #	d_1 (in)	d_2 (in)	$A_{ellipse}$ (in^2)	Stress at Failure (psi)	Failure Mode
1	1.530	1.550	1.863	497	Adhesive/Concrete
2	1.550	1.563	1.903	128	Concrete
3	1.544	1.544	1.872	312	Adhesive layer
4	1.517	1.520	1.811	484	Adhesive/Concrete
5	1.490	1.540	1.802	473	Adhesive/Concrete
6	1.535	1.520	1.833	452	Adhesive/Concrete
7	1.550	1.510	1.839	397	Adhesive/Concrete
8	1.520	1.520	1.815	416	Adhesive/Concrete
9	1.440	1.487	1.682	579	Adhesive/Concrete
10	1.530	1.530	1.839	530	Adhesive/Concrete

1 in. = 25.4 mm, 1 psi = 6.895 kPa

Adhesion test #2 resulted in a significantly different failure mode. Failure occurred at a very low applied stress. The failure plane propagated through the concrete, leaving a layer of concrete with a thickness of 0.2 in. (5.1 mm) bonded to the test dolly. The concrete bonded to the test dolly contained coarse aggregate particles, some of which were fractured as a result of the tensile force applied during the adhesion test. Test dolly #2 is shown in Figure A.9.

Adhesion test #3 resulted in a failure plane that propagated through the adhesive layer. A very small amount of epoxy was bonded to the bottom surface of the test dolly after failure. No concrete was removed from the test surface. Gouges and scratches on the bottom surface of the test dolly were exposed after failure. This led to the belief that the failure plane was though the test dolly/epoxy interface, not through the epoxy/epoxy interface.

A limited amount of statistical data from the adhesion test results is presented in Table A.2. The statistics shown have been calculated for a sample of eight test results. The results of adhesion tests #2 and #3 have been omitted, based upon the irregularities in the failure modes and failure stresses of the two tests. According to Section 8.4 of ASTM D 4541 – 95, test results may be omitted if the irregular results are due to experimental causes or are statistical outliers. It is quite likely that experimental errors and irregularities caused the results of adhesion tests #2 and #3 to be different than those of the other eight tests.

Table A.2 – Statistical Data from Adhesion Test Results

	d_1	d_2	$A_{ellipse}$	Stress at Failure
Mean	1.514 in.	1.522 in.	1.810 in^2	478 psi
Standard Deviation	0.0345	0.0191	0.0553	59
Variance	0.00119	0.00036	0.00306	3479
Coefficient of Variation	0.0228	0.0125	0.0306	0.1233

1 in. = 25.4 mm, 1 psi = 6.895 kPa

For the eight adhesion tests that resulted in a typical failure through the concrete and adhesive layer, similar stresses at failure were observed. Stresses at failure ranged from 397 psi (2.7 MPa) to 579 psi (4.0 MPa) and the mean stress at failure was 478 psi (3.3 MPa). Because the failure of the test dollies was controlled by a combined failure of the epoxy adhesive and the concrete paste, the mean stress at failure provides a lower bound value for the tensile strength of the concrete. Thus, a value of 480 psi (3.3 MPa) can be used as a conservative estimate of the tensile strength of the concrete.

Figure A.1 - Elcometer 106 Fixed-alignment Portable Adhesion Tester

Figure A.2 – Typical 1.57-in. Diameter Test Dolly

Figure A.3 – Abrasive Grinding Wheel

Figure A.4 – Diamond-coated Hole Saw

Figure A.5 – Test Surfaces after Application of Tyfo S Epoxy and Light Sanding

Figure A.6 – Orientation of the Base Ring

Figure A.7 – Claw of the Elcometer 106 Engaged with a Typical Test Dolly
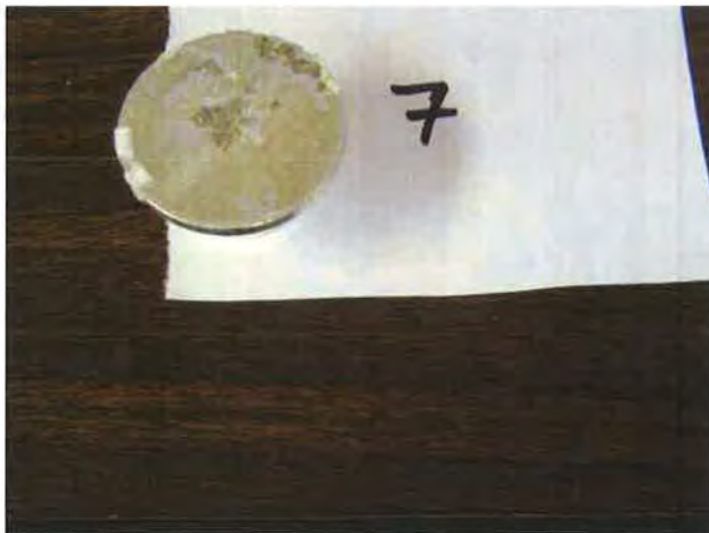
Figure A.8 – Bottom Surface of Test Dolly #7 after Failure

Figure A.9 – Test Dolly #2 after Failure

APPENDIX B: NOTATION

A	Area of the member cross section (in.^{2})
A_c	Area of concrete on the flexural tension side of the member (in.^{2})
A_f	Area of the external FRP reinforcement (in.^{2})
A_{ps}	Cross-sectional area of the prestressing tendons (in.^{2})
A_s	Cross-sectional area of the longitudinal mild steel reinforcement (in.^{2})
A_{test}	Area of the adhesion test surface (in.^{2})
A_v	Cross-sectional area of the vertical mild steel reinforcement (in.^{2})
a	Depth of the rectangular stress block (in.)
$\dfrac{a}{d}$	Shear span to effective depth ratio
b_f	Width of the flange (in.)
b_v	Width of the web, adjusted for the presence of post-tensioning ducts (in.)
b_w	Width of the web (in.)
C_E	Environmental factor for FRP reinforcement
c	Depth to the neutral axis (in.)
DF_{SHEAR}	Distribution factor for shear
DF_{MOMENT}	Distribution factor for moment
d	Effective depth of the cross section, measured from the extreme compression fiber to the centroid of the tension reinforcement (in.)

179

d_d	Diameter of the post-tensioning duct (in.)
d_e	Horizontal distance from exterior web of the exterior girder to the interior edge of the curb or traffic barrier (in.)
d_p	Distance from the extreme compression fiber to the centroid of the prestressing tendons (in.)
d_v	Effective shear depth (in.)
d_1	Diameter of the major axis of an ellipse (in.)
d_2	Diameter of the minor axis of an ellipse (in.)
E_B	Elastic modulus of beam material (ksi)
E_c	Elastic modulus of concrete (ksi)
E_D	Elastic modulus of deck/slab material (ksi)
E_e	Elastic modulus of epoxy (psi)
E_f	Design elastic modulus of FRP (ksi)
E_{fiber}	Elastic modulus of dry fiber (ksi)
E_f^*	Elastic modulus of FRP determined experimentally (ksi)
E_{ps}	Elastic modulus of the prestressing tendons (ksi)
e	Eccentricity of the prestressing tendons (in.), eccentricity of the centroid of a design truck load or design lane load and the centroid of the pattern of girders (in.)
e_g	Distance between the centroid of girder cross section and the deck/slab cross section (in.)
F_e	Effective force in the prestressing tendons after losses (kips)
F_{frp}	Tensile strength of the external FRP reinforcement (kips)
$F_{p,MAX}$	Maximum force that can be developed in the prestressing tendons at cross sections strengthened with external FRP reinforcement (kips)

F_u	Factored ultimate force in a tension tie (kips)
f_e	Specified tensile strength of Epoxy (psi)
f_{fe}	Effective limiting stress in the FRP reinforcement (ksi)
$f_{fiber,MAX}$	Specified tensile strength of dry fibers (ksi)
f_{fu}	Design tensile strength of FRP (ksi)
f_{fu}^*	Ultimate tensile strength of FRP reported by manufacturer (ksi)
f_{pe}	Effective stress in the prestressing tendons after losses (ksi)
f_{ps}	Average maximum stress in the prestressing tendons at the time for which the nominal flexural resistance of the member is required (ksi)
f_{pu}	Specified tensile strength of the prestressing tendons (ksi)
$f_{p,MAX}$	Approximate maximum stress that can be developed in the prestressing tendons at cross sections strengthened with external FRP reinforcement (ksi)
f_y	Yield strength of mild steel reinforcement (ksi)
f_c'	Compressive strength of concrete at 28 days (psi)
G_b	Shear modulus of bond layer (ksi)
g_b	Effective shear stiffness of bond layer (ksi/in.)
h	Depth of member (in.)
I	Moment of inertia (in.^{4})
IF	Impact factor
K_g	Longitudinal stiffness parameter (in.^{4})
L	Clear span length (in.), bonded length of external FRP reinforcement (in.)
l_{crack}	Distance from the end of the girder to the cracked cross section (in.)
l_t	Transfer length (in.)
M_{dead}	Moment due to dead loads (kip-in.)

M_{lane}	Moment due to lane load (kip-in.)
M_n^+	Nominal positive moment capacity (kip-in.)
M_n^-	Nominal negative moment capacity (kip-in.)
M_{truck}	Moment due to truck loads (kip-in.)
M_u	Factored ultimate moment (kip-in.)
N_B	Number of girders
N_L	Number of loaded design lanes
N_u	Factored ultimate axial force (kips)
n	number of plies of external FRP reinforcement
R	Reaction on exterior beam in terms of loaded design lanes
S	Girder spacing (in.)
s	Crack spacing (in.)
T	Minimum required tension capacity of longitudinal reinforcement on the flexural tension side of the member (kips)
T_o	Force per unit width that can be achieved in the external FRP reinforcement (kips/in.)
T_s	Force per unit width of FRP at the non-critical crack (kips/in.)
t_f	Thickness of the external FRP reinforcement (in.)
t_s	Thickness of the deck/slab (in.)
V_c	Shear resistance provided by the concrete (kips)
V_{dead}	Shear due to dead loads (kips)
V_f	Shear resistance provided by external FRP reinforcement (kips)
V_{lane}	Shear due to lane load (kips)
V_n	Nominal shear capacity (kips)

V_p	Vertical portion of the force in the prestressing tendons (kips)
V_s	Shear resistance provided by transverse mild steel reinforcement (kips)
V_{truck}	Shear due to truck loads (kips)
V_u	Factored ultimate shear force (kips)
w_c	Crack width (in.)
X_{ext}	Horizontal distance from centroid of girder pattern to centroid of exterior girder (in.)
x	Horizontal distance from centroid of girder pattern to centroid of an individual girder (in.)
y	Distance from centroid of girder cross section to mid-depth of girder cross section (in.)
α	Angle of inclination of the stirrups, parameter used in calculation of anchorage of external FRP reinforcement (in.$^{-1}$)
β	Factor relating the effect of longitudinal strain on the shear capacity of concrete
β_1	Ratio of the depth of the rectangular stress block to the depth of the neutral axis
$\varepsilon_{e,MAX}$	Specified strain at failure for epoxy (in./in.)
ε_{fe}	Effective limiting strain in the FRP (in./in.)
$\varepsilon_{fiber,MAX}$	Specified strain at failure for dry fiber (in./in.)
ε_{fu}	Design ultimate tensile strain of FRP (in./in.)
ε_{fu}^{*}	Ultimate tensile strain of FRP reported by manufacturer (in./in.)
ε_{ps}	Strain in prestressing tendons (in./in.)
ε_s	Strain in the longitudinal mild steel reinforcement at the ultimate strength limit state (in./in.)
ε_x	Longitudinal strain at mid-depth of the member cross section (in./in.)
ε_y	Yield strain of mild steel reinforcement (in./in.)

θ	Angle of inclination of diagonal compression stresses
κ	Factor used in the calculation of the average maximum stress in the prestressing tendons at the ultimate strength limit state
κ_M	Bond-dependent coefficient for flexure
ρ_f	External FRP reinforcement ratio
ρ_s	Flexural reinforcement ratio
ρ_v	Shear reinforcement ratio
τ_{max}	Maximum allowable stress in the concrete (psi)
ν	Factored shear stress on the cross section (psi)
ϕ	Strength reduction factor
ϕ_a	Strength reduction factor for axial capacity
ϕ_f	Strength reduction factor for flexure
ϕ_s	Strength reduction factor for shear